МИСИС
УНИВЕРСИТЕТ НАУКИ И ТЕХНОЛОГИЙ

СибГИУ
Сибирский государственный индустриальный университет

ISSN 0368-0797
eISSN 2410-2091

ИЗВЕСТИЯ ВЫСШИХ УЧЕБНЫХ ЗАВЕДЕНИЙ ЧЕРНАЯ МЕТАЛЛУРГИЯ

IZVESTIYA. FERROUS METALLURGY

fermet.misis.ru

2024 Том Vol. 67 № No. 3

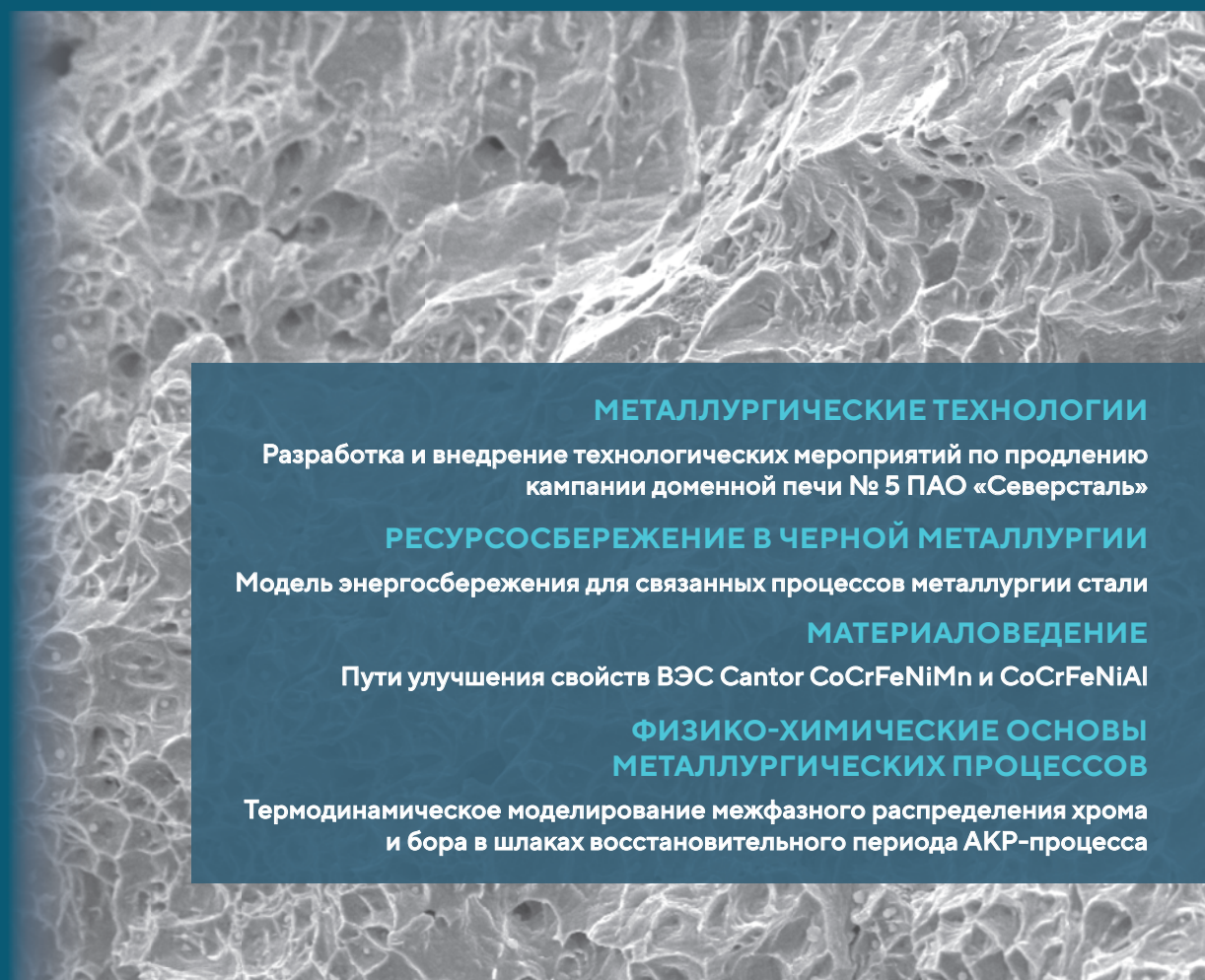

МИСИС УНИВЕРСИТЕТ

СибГИУ
Сибирский государственный индустриальный университет

ISSN 0368-0797
eISSN 2410-2091

ИЗВЕСТИЯ ВЫСШИХ УЧЕБНЫХ ЗАВЕДЕНИЙ ЧЕРНАЯ МЕТАЛЛУРГИЯ

Научно-технический журнал

Издается с января 1958 г. Выпускается 6 раз в год

2024 Том Vol. 67 № No. 3

IZVESTIYA FERROUS METALLURGY

Scientific and Technical Journal

Published since January 1958. Issued 6 times a year

IZVESTIYA FERROUS METALLURGY

www.fermet.misis.ru

ISSN 0368-0797 *(Print)* ISSN 2410-2091 *(Online)*

Alternative title:

Izvestiya vuzov. Chernaya metallurgiya

Founders:

MISIS UNIVERSITY OF SCIENCE AND TECHNOLOGY

SibSIU Siberian State Industrial University

Publisher:

National University of Science and Technology "MISIS"

Editorial Office Address:

in Moscow
4 Leninskii Ave., Moscow 119049, Russian Federation
National University of Science and Technology "MISIS"
Tel.: +7 (495) 638-44-11
E-mail: fermet.misis@mail.ru, ferrous@misis.ru

in Novokuznetsk
42 Kirova Str., Novokuznetsk, Kemerovo Region – Kuzbass
654007, Russian Federation
Siberian State Industrial University
Tel.: +7 (3843) 74-86-28 *E-mail*: redjizvz@sibsiu.ru

In accordance with paragraph 5 of the Rules for the formation of the Higher Attestation Comission list journal "Izvestiya. Ferrous metallurgy" is included in the list of leading peer-reviewed scientific journals, publication in which is taken into account in the defense of candidate and doctoral dissertations, as indexed in internatonal data bases.

Indexed: Scopus, Russian Science Citation Index (RSCI), Research Bible, Chemical Abstracts, OCLC and Google Scholar

Registered in Federal Service for Supervision in the Sphere of Mass Communications **PI number FS77-35456**.

ИЗВЕСТИЯ
ВЫСШИХ УЧЕБНЫХ ЗАВЕДЕНИЙ
ЧЕРНАЯ МЕТАЛЛУРГИЯ

www.fermet.misis.ru

ISSN 0368-0797 *(Print)* ISSN 2410-2091 *(Online)*

Варианты названия:

Известия вузов. Черная металлургия

Izvestiya. Ferrous Metallurgy

Учредители:

МИСИС
УНИВЕРСИТЕТ НАУКИ И ТЕХНОЛОГИЙ

СибГИУ
Сибирский государственный индустриальный университет

Издатель:

Национальный исследовательский технологический университет «МИСИС»

Адреса подразделений редакции:

в Москве
Россия, 119049, Москва, Ленинский просп., д. 4, стр. 1
Национальный исследовательский технологический университет «МИСИС»
Тел.: +7 (495) 638-44-11 *E-mail*: ferrous@misis.ru

в Новокузнецке
Россия, 654007, Новокузнецк,
Кемеровская обл. – Кузбасс, ул. Кирова, зд. 42
Сибирский государственный индустриальный университет
Тел.: +7 (3843) 74-86-28 *E-mail:* redjizvz@sibsiu.ru

В соответствии п. 5 Правил формирования перечня ВАК журнал «Известия вузов. Черная металлургия» входит в перечень ведущих рецензируемых научных журналов и изданий, публикация в которых учитывается при защитах кандидатских и докторских диссертаций как индексируемый в МБД.

Индексирование: Scopus, Russian Science Citation Index (RSCI), Research Bible, Chemical Abstracts, OCLC и Google Scholar

Зарегистрирован Федеральной службой по надзору в сфере связи и массовых коммуникаций **ПИ № ФС77-35456**.

Izvestiya. Ferrous Metallurgy.
2024;67(3)

Известия вузов. Черная металлургия.
2024;67(3)

CONTENTS / СОДЕРЖАНИЕ

METALLURGICAL TECHNOLOGIES

RESOURCE SAVING IN FERROUS METALLURGY

MATERIALS SCIENCE

SUPERDUTY STEEL

МЕТАЛЛУРГИЧЕСКИЕ ТЕХНОЛОГИИ

РЕСУРСОСБЕРЕЖЕНИЕ В ЧЕРНОЙ МЕТАЛЛУРГИИ

МАТЕРИАЛОВЕДЕНИЕ

СТАЛИ ОСОБОГО НАЗНАЧЕНИЯ

CONTENTS *(Continuation)*

СОДЕРЖАНИЕ *(продолжение)*

PHYSICO-CHEMICAL BASICS OF METALLURGICAL PROCESSES

INNOVATIONS IN METALLURGICAL INDUSTRIAL AND LABORATORY EQUIPMENT, TECHNOLOGIES AND MATERIALS

INFORMATION TECHNOLOGIES AND AUTOMATIC CONTROL IN FERROUS METALLURGY

ФИЗИКО-ХИМИЧЕСКИЕ ОСНОВЫ МЕТАЛЛУРГИЧЕСКИХ ПРОЦЕССОВ

ИННОВАЦИИ В МЕТАЛЛУРГИЧЕСКОМ ПРОМЫШЛЕННОМ И ЛАБОРАТОРНОМ ОБОРУДОВАНИИ, ТЕХНОЛОГИЯХ И МАТЕРИАЛАХ

ИНФОРМАЦИОННЫЕ ТЕХНОЛОГИИ И АВТОМАТИЗАЦИЯ В ЧЕРНОЙ МЕТАЛЛУРГИИ

UDC 669.1
DOI 10.17073/0368-0797-2024-3-260-269

Original article
Оригинальная статья

Development and implementation of technological measures to extend the campaign of blast furnace No. 5 of PJSC Severstal

A. A. Kal'ko[1] ✉, E. N. Vinogradov[1], O. A. Kal'ko[2], A. A. Kal'ko[1, 2]

[1] **PJSC Severstal, Cherepovets Steel Mill** (30 Mira Str., Cherepovets, Vologda Region 162608, Russian Federation)
[2] **Cherepovets State University** (5 Lunacharskogo Ave., Cherepovets, Vologda Region 162600, Russian Federation)

✉ aakalko@severstal.com

Abstract. The work presents generalized experience in the development and implementation at PJSC Severstal of technological measures to extend the campaign of blast furnace No. 5. The authors carried out an analysis, identified and described the problem areas, generalized the principles for ensuring the safety of the shaft lining, boshes and metal receiver of the blast furnace. The results of a study of the working space of blast furnace No. 5 in 2006 are also presented. The identified technological factors ensure an increase in duration of the unit campaign. Technological measures are given for: washing the blast furnace hearth, reducing chemical erosion of the carbon blocks of the hearth and flange, forming a protective skull in the blast furnace shaft, special methods for loading solid coke substitutes, and organizing an effective structure of the charge column in the blast furnace. It is necessary to use digital models integrated into the blast furnace expert system for operational control of blast furnace technology. The results of the current blast furnace campaign were compared with previous ones. It was proven that the systematic use of all elements of the developed technology makes it possible to achieve high economic indicators while exceeding the standard duration of the campaign by 1.75 times. Experience in technology development made it possible to increase the furnace campaign duration to 17.46 years, achieve a reduction in specific coke consumption by 15.9 %, and increase the specific consumption of natural gas for cast iron smelting by 46.4 %; reduce the specific carbon consumption for cast iron smelting by 6.3 %.

Keywords: blast furnace, campaign duration, PJSC Severstal, blast-furnace hearth, shaft, toterman, hearth washing, skull formation, specific consumption of natural gas, solid fuel consumption per ton of cast iron, digital model, iron ore materials, coke, CSR

For citation: Kal'ko A.A., Vinogradov E.N., Kal'ko O.A., Kal'ko A.A. Development and implementation of technological measures to extend the campaign of blast furnace No. 5 of PJSC Severstal. *Izvestiya. Ferrous Metallurgy*. 2024;67(3):260–269.
https://doi.org/10.17073/0368-0797-2024-3-260-269

Разработка и внедрение технологических мероприятий по продлению кампании доменной печи № 5 ПАО «Северсталь»

А. А. Калько[1] ✉, Е. Н. Виноградов[1], О. А. Калько[2], А. А. Калько[1, 2]

[1] **ПАО «Северсталь» Череповецкий металлургический комбинат** (Россия, 162608, Вологодская область, Череповец, ул. Мира, 30)
[2] **Череповецкий государственный университет** (Россия, 162600, Вологодская область, Череповец, пр. Луначарского, 5)

✉ aakalko@severstal.com

Аннотация. В работе представлен обобщенный опыт по разработке и внедрению на ПАО «Северсталь» технологических мероприятий по продлению кампании доменной печи № 5. Авторы провели анализ, выявили и описали проблемные зоны, обобщили принципы обеспечения сохранности футеровки шахты, заплечиков и металлоприемника доменной печи. Также представлены результаты исследования рабочего пространства доменной печи № 5 в 2006 г. Выявленные технологические факторы обеспечивают увеличение длительности кампании агрегата. Приведены технологические мероприятия по промывкам горна доменной печи, снижению химической эрозии углеродистых блоков горна и лещади, формированию защитного гарнисажа в шахте доменной печи, особым приемам загрузки твердых заменителей кокса и организации эффективной структуры столба шихты в доменной печи. Для оперативного управления технологией доменной плавки необходимо использовать цифровые модели, объединенные в экспертную систему доменной печи. Авторы провели сравнение результатов текущей кампании доменной печи с предыдущими и доказали, что системное применение всех элементов разработанной

технологии позволяет достигать высоких экономических показателей при превышении нормативной продолжительности кампании в 1,75 раза. Опыт развития технологии позволил увеличить длительность кампании печи до 17,46 лет, достигнуть снижения удельного расхода кокса на 15,9 %, увеличить удельный расход природного газа на выплавку чугуна на 46,4 % и сократить удельный расход углерода на выплавку чугуна на 6,3 %.

Ключевые слова: доменная печь, продолжительность кампании, ПАО «Северсталь», горн, шахта, тотерман, промывка горна, гарнисажеобразование, удельный расход природного газа, расход твердого топлива на тонну чугуна, цифровая модель, железорудные материалы, кокс, показатель CSR

Для цитирования: Калько А.А., Виноградов Е.Н., Калько О.А., Калько А.А. Разработка и внедрение технологических мероприятий по продлению кампании доменной печи № 5 ПАО «Северсталь». *Известия вузов. Черная металлургия*. 2024;67(3):260–269. https://doi.org/10.17073/0368-0797-2024-3-260-269

Introduction

The current development trends of global blast furnace production are aimed, as before, at bringing down the cost of cast iron smelting by reducing coke consumption, enhancing the productivity of blast furnaces (BF) and the duration of their campaign. Increased duration of the campaign, the period between overhauls of the first category above the standard level, enables to reduce the unit cost and boost the competitiveness of the manufacturer in the world market.

This work presents generalized experience in the development and implementation of technological measures aimed at extending the campaign of blast furnace No. 5 at PJSC Severstal. As previously scheduled, on April 1 – 2, 2024, PJSC Severstal performed blowingout of blast furnace No. 5 "Severyanka" with a useful volume of 5500 m^3 and tapped the salamander. The furnace was submitted for the overhaul of the first category. Blowing-out was successful, accident-free, consistent with the developed technological program. The furnace campaign lasted 17.46 years from 20.10.2006 to 02.04.2024 (hereinafter referred to as the current campaign), significantly exceeding the standard service life of blast furnaces with the similar design. Blast furnace No. 5 was first blown in on April 12, 1986 and is currently the largest cast iron production unit in Europe. The current campaign is the third in a row, the first two lasted 9 and 11 years respectively.

Theoretical background

The standard blast furnace campaign in most cases is 12 – 15 years [1; 2], but campaign durations of some furnaces, such as Hamborn No. 9 blast furnace made by ThyssenKrupp Steel Europe, can exceed 22 years [3]. The authors of [4] believe that the key technological factors ensuring the duration of the blast furnace campaign are stability and compliance of charge materials with quality standards, rational slag and blast modes, loading mode parameters ensuring the required distribution of charge components and gas flow, and technologically justified mode of melting products processing. In addition, a number of researchers [5 – 7] note that, to a large extent, durability of the flange and hearth lining, contribute, to a large extent, to achieving long-term safe and accident-free operation of the blast furnace.

The major factors affecting wear of the refractory lining are:

– abrasive effect of liquid cast iron flows;

– chemical effects of cast iron and slag;

– infiltration and thermomechanical stress in the lining [8].

While high quality iron-containing materials are required to ensure a long service life of the blast furnace shaft lining, the service life of the hearth lining is largely determined by the quality of the loaded coke. Wear-resistant hearth structures are currently non-existent [9], but the technologies aimed at extending the life of the furnace lining are continuously improving. The numerous studies were conducted by domestic and foreign researchers on blown-out and cooled blast furnaces to establish the main types of impacts destroying the lining and changes in their intensity along the blast furnace height [10 – 12].

Creation of a stable skull is one of the main measures aimed at ensuring the safety of the shaft lining, boshes and metal receiver of the blast furnace, which contributes to increasing the duration of its campaign.

The gas flow distribution along the blast furnace radius and height is controlled by a purposefully formed zone of enhanced gas permeability, the so-called vent, which can be formed by distribution of ore loads both in the axial zone of the furnace and at the periphery.

Identification of critical areas of blast furnace No. 5 requiring protection based on the results of the previous campaign

Blast furnace No. 5 was shut down for overhaul of the first category at the end of the previous campaign in 2006. After blowing-out of blast furnace No. 5, the samples of refractory lining and skull-forming masses were selected along its height. Fig. 1 features a scheme of the sampling points and the Table presents the chemical composition of the studied material samples.

The analysis of the state of blast furnace No. 5 working space in 2006 revealed the following:

– in the area of cast iron notches, the refractory thickness did not exceed 200 – 250 mm, carbon peripheral blocks of the upper flange located directly under the notches were deformed, cracks and chips emerging in some places;

– significant reduction in the thickness of the shaft lining (the upper rows were 270 – 300 mm thick) and wear of the uncooled part of the shaft were mainly caused by abrasive impact of charge materials and vapors of sublimated alkaline compounds;

– horizontal coolers of the shaft cooled part were mostly deformed and destroyed, only the upper three – four rows were in satisfactory condition;

– boshes in the upper part were mostly open, no traces of skull deposits were noticed on the coolers in this part.

– chemical analysis of the skull samples taken in the furnace hearth revealed the presence of significant amounts of alkali in it, as well as the presence of zinc oxide and even metallic zinc in the high-temperature furnace zone.

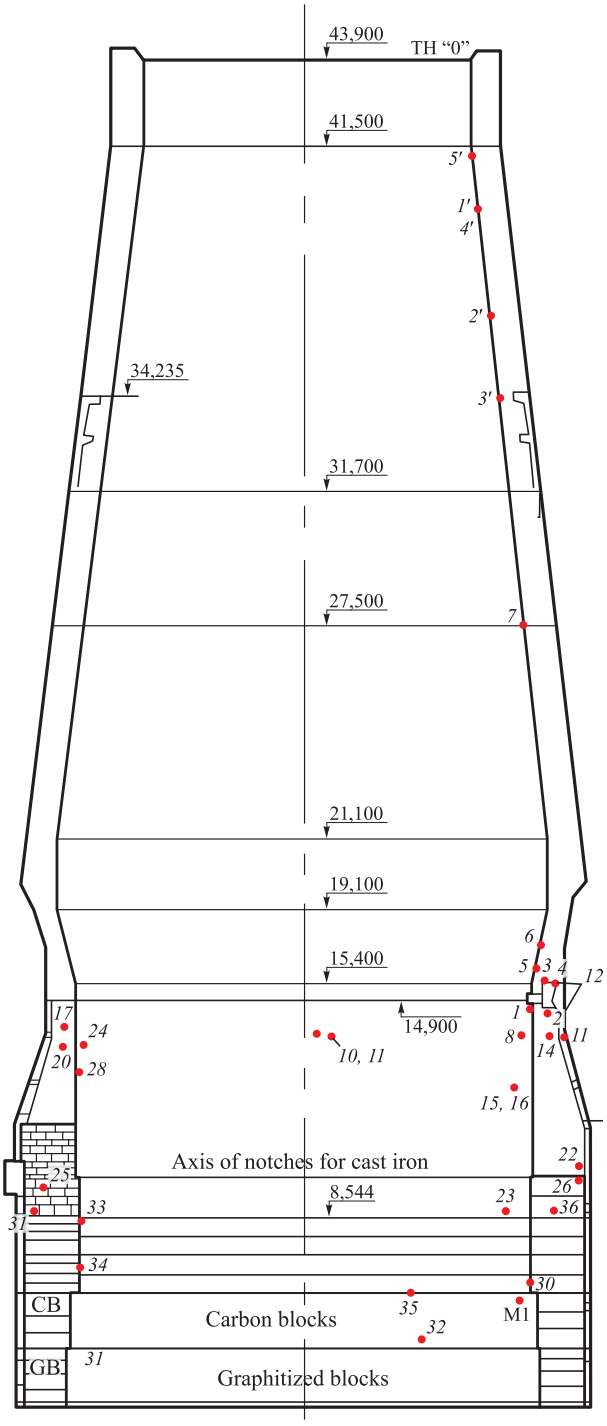

Fig. 1. Location of sampling points for refractory materials and skull from the working space of blast furnace No. 5 after blowing-out of the furnace in 2006

Рис. 1. Расположение точек отбора проб огнеупорных материалов и гарнисажа из рабочего пространства ДП № 5 после выдувки печи в 2006 г.

During the 2006 overhaul, the furnace shell was partially replaced and the lining was replaced completely. The hearth structure was reinforced within the dimensions of the furnace shell. On the steel leveled surface of the furnace bottom, the graphite blocks, 800 mm high, were vertically installed and carbon blocks, 1100 mm high, were vertically placed on them. On the periphery, the blocks were stacked horizontally in the following order: two 400-mm graphite and two 550-mm carbon ones. Above, on the periphery of the furnace, seven rows of ring carbon blocks supplied by NDK were laid. The bottom two rows of those were made of BS-8SM2 grade microporous blocks and the top five rows were made of BS-8SR grade super microporous blocks. The internal volume of the five lower rows was laid with high-aluminous MLLD-62 blocks, 550 mm high, thus the value of the "dead" layer in the hearth increased from 1500 to 2050 mm.

Copper coolers were installed in the under-notch area, three coolers under each notch. The cooling channels were made by drilling holes in the cast and rolled copper plate. A pumping station of chemically treated water was built to supply these twelve coolers. The combined cooling by smooth plate coolers, 120 mm thick, in combination with horizontal 100-mm thick coolers installed in the inner recess, was provided in the furnace belly and shaft at about 65 % of its height. The uncooled portion of the shaft was lined with chamotte.

Thus, in the 2006 – 2024 campaign, the basic technical solutions for the design of blast furnace No. 5 hearth and shaft were retained in the classical form, with necessary adjustments in problem areas based on the experience of the first two campaigns of 1986 – 1995 and 1995 – 2006. To maximize the duration of the current furnace campaign, certain technological measures were applied as a priority.

Chemical composition of the samples of refractory materials and skull extracted during dismantling of the refractory lining of blast furnace No. 5 in 2006

Химический состав проб огнеупорных материалов и гарнисажа, извлеченных при разборе огнеупорной футеровки ДП № 5 в 2006 г.

Place of sampling	Material	Content of chemical compounds, wt. %				
		Fe_2O_3	Al_2O_3	Na_2O	K_2O	ZnO
1′	ShPD – 39 (chamotte engineering domain bricks)	1.34	38.7	–	–	–
2′	ShPD – 42 (chamotte engineering domain bricks)	1.33	43.4	–	–	–
3′	Skull	–	–	0.23	0.81	0.110
4′	ShPD – 42 (chamotte engineering domain bricks)	4.07	38.7	–	–	–
5′	ShPD – 42 (chamotte engineering domain bricks)	1.89	42.8	–	–	–
22	Skull (ChL 3 (cast iron))	–	–	0.22	3.80	30.500
23	Skull	–	–	0.08	0.20	0.045
24	Refractory material	–	–	0.28	0.79	1.200
25	Skull (ChL 2 (cast iron))	–	–	0.07	0.36	40.000
27	Skull (ChL 4 (cast iron))	–	–	0.30	2.70	1.000
29	Skull (ChL 1 (cast iron))	–	–	0.17	0.40	0.035
Place of sampling	Material	Content of chemical elements, wt. %					
		C	S	P	Si	Mn	Zn
M1	Metal in carbon block joints	0.69	0.060	0.057	0.25	0.29	95.00
GB	Graphite block of the first row	98.2	0.450	–	–	–	–

Development and implementation of technological measures aimed at extending the campaign of blast furnace No. 5 in 2006 – 2024

The series of investigations of the 1995 – 2006 campaign results (see the Table, Fig. 1) revealed low residual thicknesses of refractory materials and the absence (or small amount) of protective skull and enabled to determine critical zones of blast furnace No. 5 that require protection and adjustment of smelting technology in the current campaign: the hearth, the bottom part of the shaft and the top of the boshes.

First of all, to increase the durability of the hearth lining, the development of abrasive action of liquid cast iron flows in the near-wall zone should be prevented, i.e., it is necessary to ensure intensive filtration of liquid melting products through the toterman and to achieve good gas permeability in the central furnace zone. In real conditions of blast furnace operation, the toterman porosity can significantly decrease due to fluctuations of coke quality characteristics, water ingress into the hearth from defective elements of the cooling system, localized masses of refractory components of blast furnace charge entering the hearth, even an area can form impermeable for flows of liquid melting products in the hearth, as well as for countercurrent flows of gases and liquids above the tuyere level.

The results of experimental studies at blast furnace No. 9 at the metallurgical plant Krivorozhstal proved that it is possible to form a dense, poorly permeable layer on the toterman's surface [13; 14]. Since this furnace has about the same parameters as blast furnace No. 5 at PJSC Severstal, the experience gained from its operation was taken into account by the authors when the technological process at "Severyanka" was arranged. First of all, the above experience proved that gas permeability in the central furnace zone and the condition of the toterman should be systematically controlled.

It is extremely difficult to control the toterman size in an operating furnace. Temperatures of melting products in the hearth reach 1500 °C and in the tuyere zones, the gas temperature can exceed 2000 °C. In such conditions, physical sounding without bulky equipment is complicated and remote methods are not yet sufficiently developed. To assess the toterman permeability and control its geometry at blast furnaces of PJSC Severstal, a scheme was proposed of systematic probing of the blast furnace hearth during short-term shutdowns for planned preventive maintenance. A metal slice bar, 10 m long, with a diameter of 28 mm, served as a probe. The probe was plunged into the furnace until it became obvious that the front of the slice bar reached the hard-to-penetrate zone. The toterman was probed systematically, at least once a quarter during normal furnace operation and more often if the charge conditions changed or signs of impurity content in the hearth emerged.

To clean the hearth from refractory flux residues and fine coke fractions, technological provisions were deve-

loped for complex washing of the blast furnace hearth. The procedures were proposed for forming a washing portion consisting of a mixture of a sinter, pellets, lump iron ore and converter slag, as well as the mass of this portion depending on the mass of the working portion of iron ore materials. Consumption of charge materials in the washing portion was determined based on obtaining primary slag melt with FeO content in the range from 35 to 55 %, which was calculated by the equation

$$FeO_{psm} = 29.73 - 1.43CaO + 3.27SiO_2 - 10.18MgO + 1.36Al_2O_3 - 0.58FeO,$$

where FeO_{psm} is FeO content in the primary slag melt, %; CaO, SiO_2, MgO, Al_2O_3 and FeO represent the content of these components in the washing feed, %.

The efficiency of the developed procedures for complex washing was controlled by means of toterman probing. Its results showed that systematic washing helped to maintain high level of the coke head permeability. The area of the hard-to-penetrate zone at the tuyere level shrank by 47.8 rel. % compared to the previous (before complex washing) measurements.

In addition to the traditional methods of assessing the condition of the lining based on the data of heat removal by the hearth and flange cooling system and embedded thermocouples installed at different levels, new nondestructive inspection methods were applied in the current campaign. The purpose of the survey was to determine the condition of the refractory materials and the thickness of the residual lining, as well as to detect anomalies in the refractory materials such as cracks, delaminations and unfilled mortar joints in brickwork. The work was carried out using the technique of supersonic sounding using the echo method (AU-E). The scope of the survey included periodic monitoring of the condition of the furnace refractory lining from the metal receiver to the tuyere level, as well as determining the trend of the refractory lining wear in various zones.

To reduce chemical erosion of carbon blocks of the hearth and flange due to non-equilibrium chemical compositions of cast iron, the method was developed to control the technological process through monitoring the ratio of the actual carbon content in cast iron C_f to the saturated content C_s by regulating the flow rate of natural gas blown into the furnace. The indicated C_f/C_s ratio was maintained in the range of 0.92 – 0.98. When the C_f/C_s ratio dropped below 0.92, the natural gas consumption was increased by 2.0 – 10.0 m^3/t of cast iron, and when the C_s/C_s ratio rose above 0.98, the natural gas consumption was reduced by 0.2 – 2.0 m^3/t of cast iron while maintaining the oxygen content in the blast. The applied method enabled to significantly (from 5.8 to 1.4 % of the total number) reduce the number of tappings aggressive to carbon lining. During 12 months of the use of the claimed method, the increment of heat loads on the cooling system coolers in the metal receiver decreased on average twice compared to the previous similar period. The effectiveness of the applied method can also be evaluated by the results of supersonic sounding using the echo method. Its use enabled us to record the fact that the average thickness of the unchanged lining did not alter significantly during 2019 – 2021, probably because the skull layer that protected the underlying lining was preserved. The average thickness of the residual intact lining of the hearth wall measured by the AU-E method was 540 mm or about 21 % of the initial lining thickness.

To ensure self-renewal of the protective skull in the blast furnace shaft, the previously developed method [15] was used, which involves cyclic loading of charge materials, including the skull-forming mixture consisting of iron ore and sinter, which enables to obtain from it the primary slag melt in the amount of 20 – 25 %, the proportion of ferrous oxide in this melt not exceeding 15 %. In addition, the requirements for enhancing the economic efficiency of cast iron smelting made it necessary to develop the methods for industrial use of small substandard fractions of iron ore materials. The mass fraction of 3 – 5 mm of the sinter loaded into the near-wall zone was determined depending on the index of sinter strength during the reduction-heat treatment of its oversize fraction by the following formula

$$M = KM_h \frac{100 - A(100 - R)}{100},$$

where M – mass of undersize fraction of the 3 – 5 mm sinter in the loaded iron ore portion, t; K – empirical coefficient equal to 0.10 – 0.25; M_h – mass of the sinter in the head part of the loaded iron ore portion, t; A – share of the sinter in iron ore portion, units; R – index of the sinter strength during reduction-heat treatment of the sinter oversize fraction, %.

To achieve the given number of closed cycles of the chute, the fraction of the 3 – 5 mm sinter was distributed in the furnace working space using a bell-less top depending on the bulk weight of undersize fractions of iron ore materials.

Due to the need to use cheaper fuel for smelting cast iron, in the second part of the campaign the specific consumption of various solid substitutes for skip coke considerably increased. Both substandard fractions of metallurgical coke (less than 25 mm) and anthracite served this purpose. In the final third of the furnace campaign, an innovative carbon-containing product (ICCP) was additionally used. It was obtained in the process of laminar coking of the coal charge, consisting of 60 – 100 % of coals of one or several grades tentatively suitable for coking.

The results of earlier theoretical studies and industrial experience revealed [16 – 19] that effective replacement of skip coke with various substitutes (natural gas, pulverized coal fuel, anthracite, substandard coke fractions) is only possible if the quality of the bulk of coke and iron ore materials is high. Therefore, to use solid coke substitutes with relatively low-quality characteristics in significant quantities, which includes the charge containing solid fuel with reduced hot strength reaching almost 50 %, special methods of its loading and distribution over the cross-section of the furnace mouth had to be preliminarily developed and applied. The solid fuel with reduced strength before reaction (CSR) was loaded into the intermediate zone of the blast furnace in portions at a distance of 0.1 – 0.5 of the furnace mouth radius from the furnace wall, and the ore load in the axial zone of the furnace mouth was maintained in the range from 0.8 to 3.2 depending on the difference in the index (CSR) of high and low quality solid fuel. Smaller ore load in the furnace axis corresponds to a larger difference of the CSR characteristic for the two solid fuels.

The escalating environmental challenges associated with the climate change and the prospect of carbon regulation call for a continuous search for new ways to reduce CO_2 emissions in the course of steel production [20]. Technologically, in the production chain "blast furnace – converter", carbon dioxide emissions are reduced by cutting the specific consumption of solid carbon fuel for smelting cast iron and increasing the consumption of hydrocarbon coke substitutes blown into the blast furnace.

The approach to building an effective structure of the charge column in the blast furnace had to be reconsidered and a set of procedures was developed to regularly wash the hearth from coke waste and flux residues, maintain a stable self-renewing skull in the lower part of the shaft, effectively distribute various types of solid fuel over the furnace cross-section and develop the technology of ultra-high specific consumption of natural gas during cast iron smelting. As a result, we, on a permanent basis, used the system of charge material distribution over the height and cross-section of blast furnace No. 5, which includes the specified distribution of ore load over the furnace cross-section [21], as well as the cyclic use of axial, prewashing and washing portions, providing a central operating mode of the blast furnace under variable charge and gas blowing conditions [22]. Fig. 2 shows the structure of the charge distribution used on a permanent basis in the working space of blast furnace No. 5. The efficiency of the applied system of charge materials distribution was evaluated during the final third of the current furnace campaign, when, despite significant changes in charge conditions and transition to a technology of high (more than 170 m^3/t of cast iron) specific consumption of natural gas, stable operation of the furnace could be achieved. The presence of protective skull in the lower part of the blast furnace shaft was established when the furnace was disassembled during the overhaul of the first category, and the condition of the horizontal coolers of the furnace shaft cooling system and their recesses, which have not lost their initial geometry, indicates that the cooling system operates under protection of the sufficient layer of stable self-renewing skull.

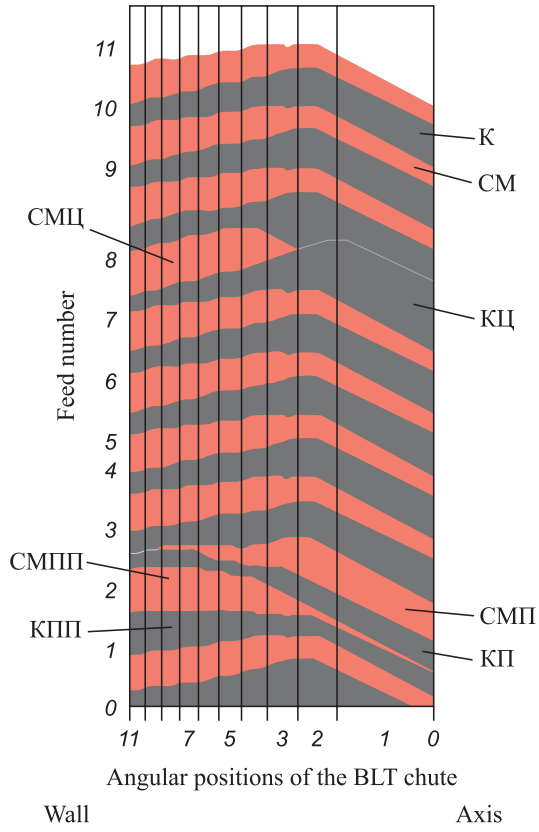

Fig. 2. Structure of the charge column from 11 feeds including axial, pre-washing and washing portions: К – portion of coke, positions of the BLT (Bell Less Top) chute (*9 – 3*); СМ – portion of the iron ore mixture, position of the BLT chute (*11 – 3*); КЦ – central (axial) portion of coke, position of the BLT chute (*8 – 2*); СМЦ – portion of iron ore mixture for feeding with axial coke, position of the BLT chute (*10 – 5*); КПП – pre-washing feed coke, position of the BLT chute (*10 – 3*); СМПП – portion of iron ore mixture of the pre-washing feed, the position of the BLT chute (*11 – 5*); КП – washing feed coke, position of the BLT chute (*9 – 3*); СМП – a portion of the iron ore mixture of the washing feed, the position of the BLT chute (*7 – 3*)

Рис. 2. Структура столба шихты из 11-ти подач, включающая осевые, предпромывочные и промывочные порции: К – рабочая коксовая порция, положения лотка БЗУ (*9 – 3*); СМ – рабочая порция железорудной смеси, положения лотка БЗУ (*11 – 3*); КЦ – центровая (осевая) порция кокса, положения лотка БЗУ (*8 – 2*); СМЦ – порция железорудной смеси для подачи с осевым коксом, положения лотка БЗУ (*10 – 5*); КПП – кокс предпромывочной подачи, положения лотка БЗУ (*10 – 3*); СМПП – порция железорудной смеси предпромывочной подачи, положения лотка БЗУ (*11 – 5*); КП – кокс промывочной подачи, положения лотка БЗУ (*9 – 3*); СМП – порция железорудной смеси промывочной подачи, положения лотка БЗУ (*7 – 3*)

It should be noted that the application of a set of measures aimed at extending the campaign of blast furnace No. 5 under conditions of frequent changes in the quality characteristics of iron ore raw materials, as well as the increased use of solid and gaseous coke substitutes, requires constant monitoring of both the smelting parameters and the effectiveness of the applied technological solutions. At the coke-and-sinter production of PJSC Severstal, this task is solved, among other things, by using operational control of blast-furnace smelting technology involving on-line digital assistants [23], united in a blast furnace expert system (ES). The blast furnace expert system is a proprietary development of PSJC Severstal. It is a system for optimizing, monitoring and managing the cast iron smelting process. It is based on highly efficient technological models, special application software, graphical end-user interfaces and many years of practical experience of domainers.

The task of the blast furnace expert system is to develop controlling technological influencing factors affecting the blast furnace melting process adequate to the current conditions due to unambiguously interpreted results of processing the heterogeneous source data. Thus, to prevent fluctuations in the thermal state of the furnace, related to the inertness of traditional methods of fuel consumption operational control through changing the mass of coke in the feed, a digital model of the melting hourly heat balance is used, as well as monitoring of the specific consumption of solid and blown fuel and a model for calculating the minimum theoretical value of coke consumption. To prevent the phenomenon of spontaneous skull descent, the following models are used: models of skull accumulation, charge materials distribution in the furnace working space, charge descent with controlled feed position in the working space, gas-tuyere model with the estimated oxidation and circulation zones depths. The models of melting products accumulation in the hearth, tapping control and slag viscosity are applied to arrange effective melting products processing. The source data for the above models are the values of technological parameters, chemical compositions of raw materials and melting products, the amount of raw materials and fuel consumed per unit of time, etc., coming into the system and processed automatically, without involving the technical team.

The use of the calculation results, recommendations of the blast furnace expert system enables to reduce the influence of human factor in the evaluation and interpretation of controlled process parameters, thereby decreasing the number of deviations of the blast furnace operation parameters from the optimal range, to achieve the most stable specified chemical composition of melting products and minimum fuel consumption, as well as to minimize the negative impact on the refractory lining of the furnace.

Main production results of blast furnace No. 5 campaign in 2006 – 2024

Due to implementation of the above-mentioned developed technological measures on a permanent basis, the furnace worked in the campaign for 17 years 5 months and 13 days (17.46 years). The standard duration of the campaign was exceeded 1.75 times or by 74.6 %.

During the current campaign, the furnace smelted 75,180,099 tons of cast iron, which is ~1.6 mln tons more than the total cast iron production for the first two campaigns of blast furnace No. 5 (a total of 73,582,218 tons of cast iron were smelted during the previous two campaigns in the periods 12.04.1986 – 03.07.1995 and 26.10.1995 – 19.06.2006).

The productivity and duration of the current campaign increased due to a radical change in blast furnace smelting technology and practically 1.5 times growth in coke replacement with natural gas. Moreover, the negative factors caused by hydrocarbons that are additionally blown into the furnace hearth (reduced theoretical combustion temperature, redistribution of temperatures over the height of the furnace, significant fluctuations in the furnace thermal state, etc.) were successfully compensated by the developed technological measures. The fuel efficiency was improved during the current campaign (hereinafter the comparison is made between the first full year of operation of blast furnace No. 5 after in 2006, it was blown in and in 2024, full capacity was achieved with the final three months of the campaign):

– specific coke consumption was reduced from 417.3 to 351.1 kg/t of cast iron, i.e., by 66.2 kg/t of cast iron or by 15.9 %;

– specific consumption of natural gas for cast iron smelting was increased from 118.0 to 172.7 m^3/t of cast iron, i.e., by 54.7 m^3/t of cast iron or by 46.4 %;

– specific carbon consumption for cast iron smelting, defined as the ratio of total carbon input into the blast furnace with solid and gaseous fuel, as well as with components of iron ore charge to the amount of smelted cast iron was reduced from 428.9 to 401.7 kg/t of cast iron, i.e., by 27.2 kg/t of cast iron or by 6.3 %.

Conclusion

The use of a systematic scientific approach aimed at maximum extension of blast furnace No. 5 campaign based on the analysis of the previous campaigns results, identification of problem areas and ways to improve cast iron smelting technology, development of technological measures taking into account the accumulated experience and prospects for further development enabled to increase the service life of the unit by 1.75 times and achieve its highly efficient operation during the entire 2006 – 2024 campaign.

The results were obtained at the blast furnace of "classical" design without principal capital-intensive changes in refractory lining of the blast furnace shaft and hearth only by developing new methods of maintenance, control and adjustment of cast iron smelting technology.

The system for optimizing, monitoring and managing the cast iron smelting process based on in-house developed digital assistants is the most promising direction for further development. It provides stabilization of smelting results at significant fluctuations of incoming parameters, maximum efficiency of the developed scientific and technological measures during long time spans due to reduction of human factor impact during the process operational control.

References / Список литературы

1. Liu Z., Zhang J., Zuo H.-B., Yang T.-j. Recent progress on long service life design of Chinese blast furnace hearth. *ISIJ International*. 2012;52(10):1713–1723. https://doi.org/10.2355/isijinternational.52.1713
2. Analysis of metal receiver operation in order to increase the duration of blast furnace campaign and its safe operation. *Novosti chernoi metallurgii za rubezhom*. 2003;(4):32–36. (In Russ.).

   Анализ работы металлоприемника с целью увеличения продолжительности кампании доменной печи и безопасной ее эксплуатации. *Новости черной металлургии за рубежом*. 2003;(4):32–36.
3. Ruther P., Peters M. Requirements for a campaign life of more than 20 years at the blast furnace 2 of Thyssen Krupp Steel Europe. *Chernye metally*. 2015;(10):59–66. (In Russ.).

   Рютер П., Петерс М. Условия продления более чем на 20 лет кампании доменной печи № 2 компании Thyssen Krupp Steel Europe. *Черные металлы*. 2015;(10):59–66.
4. Bol'shakov V.I., Ivancha N.G., Nesterov A.S., etc. Development of measures to extend the blast furnace campaign by improving loading technology, slag mode and automated control of blast furnace parameters in conditions of unstable quality of charge materials. In: *Proceedings of the Institute of Electric Welding named after E.O. Paton. Problems of Service Life and Operational Safety of Structures, Structures and Machines*. Dnepropetrovsk: Z.I. Nekrasov Institute of Ferrous Metallurgy, National Academy of Sciences of Ukraine; 2015:628–634.

   Большаков В.И., Иванча Н.Г., Нестеров А.С. и др. Разработка мероприятий по продлению кампании доменных печей путем усовершенствования технологии загрузки, шлакового режима и автоматизированного контроля параметров доменной плавки в условиях нестабильности качества шихтовых материалов. *В сборнике научных статей Института электросварки им. Е.О. Патона: Проблемы ресурса и безопасности эксплуатации конструкций, сооружений и машин*. Днепропетровск: ИЧМ им. З.И. Некрасова НАН Украины; 2015:628–634.
5. Mozharenko N.M., Kanaev V.V., Panchokha G.V. Influence of smelting technology on lining of metal receiver of blast furnaces. *Metallurgicheskaya i gornorudnaya promyshlennost'*. 2003;(5):5–8. (In Russ.).

   Можаренко Н.М., Канаев В.В., Панчоха Г.В. Влияние технологии плавки на футеровку металлоприемника доменных печей. Metallurgical and mining industry. *Металлургическая и горнорудная промышленность*. 2003;(5):5–8.
6. Kurunov I.F., Loginov V.N., Tikhonov D.N. Methods of extending a blast-furnace campaign. *Metallurgist*. 2006;50:605–613. https://doi.org/10.1007/s11015-006-0131-5

   Курунов И.Ф., Логинов В.Н., Тихонов Д.Н. Методы продления кампании доменной печи. *Металлург*. 2006;(12):34–39.
7. The influence of blast furnace productivity on duration of its campaign. *Novosti chernoi metallurgii za rubezhom*. 2005;(1):21–24. (In Russ.).

   Влияние производительности доменной печи на продолжительность ее кампании. *Новости черной металлургии за рубежом*. 2005;(1):21–24.
8. Shul'te M., Klima R., Ringel' D., Foss M. Monitoring the wear of blast furnace hearth using heat flow sensors. *Chernye metally*. 1998;(4):17–22. (In Russ.).

   Шульте М., Клима Р., Рингель Д., Фосс М. Контроль износа горна доменной печи с помощью датчиков теплового потока. *Черные металлы*. 1998;(4):17–22.
9. Koval'ski V., Lyungen Kh.B., Shtrikker K.P. Durability of blast furnaces: current level, development and company development measures. *Chernye metally*. 1999;(9):26–35. (In Russ.).

   Ковальски В., Люнген Х.Б., Штриккер К.П. Стойкость доменных печей: современный уровень, развитие и мероприятия по развитию компании. *Черные металлы*. 1999;(9):26–35.
10. Kaplun L.I., Malygin A.V., Onorin O.P., Parkhachev A.V. Construction and Design of Blast Furnaces: Tutorial. Ekaterinburg: URFU; 2016:217. (In Russ.).

    Каплун Л.И., Малыгин А.В., Онорин О.П., Пархачев А.В. Устройство и проектирование доменных печей: Учебное пособие. Екатеринбург: УрФУ; 2016:217.
11. Bliznyukov A.S., Feshchenko S.A., Kurunov I.F., etc. Study of the blast furnace hearth lining. Report 1. *Ferrous Metallurgy. Bulletin of Scientific, Technical and Economic Information*. 2010;(9):31–36. (In Russ.).

    Близнюков А.С., Фещенко С.А., Курунов И.Ф. и др. Исследование футеровки горна доменной печи. Сообщение 1. *Черная металлургия. Бюллетень научно-технической и экономической информации*. 2010;(9):31–36.
12. Bol'shakov V.I., Mozharenko N.M., Murav'eva I.G. Ensuring the safety and integrity of blast furnace linings during blowing-down and blowing-in. *Metall i lit'e Ukrainy*. 2009;(7–8):75–80. (In Russ.).

    Большаков В.И., Можаренко Н.М., Муравьева И.Г. Обеспечение безопасности и сохранности футеровки доменных печей при выдувке и задувке. *Металл и литье Украины*. 2009;(7–8):75–80.
13. Bol'shakov V. I., Gladkov N. A., Murav'eva I. G., etc. The structure of the lower part of the charge column and the role of its elements in the organization of smelting processes. In: *Proceedings of IFM. Fundamental and Applied Problems of Ferrous Metallurgy*. 2004;(8):112–119. (In Russ.).

    Большаков В.И., Гладков Н.А., Муравьева И.Г. и др. Структура нижней части столба шихты и роль ее элементов в организации процессов плавки. *Сборник научных*

трудов ИЧМ. Фундаментальные и прикладные проблемы черной металлургии. 2004;(8):112–119.

14. Bol'shakov V.I., Buzoverya M.T., Stromenko V.A., etc. Experimental study of gas sampling machines and a 5000m^3 blast furnace shaft. In: *Intensification of Blast Furnace Processes and Development of Large-Volume Furnaces*. Moscow: Metallurgiya; 1980;(7):75–80. (In Russ.).

Большаков В.И., Бузоверя М.Т., Строменко В.А. и др. Экспериментальное исследование машин для отбора проб газа и шахты доменной печи объемом 5000 м^3. В сборнике: *Интенсификация процессов доменной плавки и освоение печей большого объема*. Москва: Металлургия; 1980;(7):75–80.

15. Loginov V.N., Sukhanov M.YU.., Gurkin M.A., Vasil'ev L.E., Karimov M.M., Bol'shakov V.I., Nesterov A.S., Mozharenko N.M., Yakushev V.S. Method for creating a protective skull in a blast furnace shaft. Patent RF no. 2251575. MPK C21B 5/00. *Byulleten' izobretenii*. 2005;(13). (In Russ.).

Пат. 2251575 RU. Способ создания защитного гарнисажа в шахте доменной печи / Логинов В.Н., Суханов М.Ю., Гуркин М.А., Васильев Л.Е., Каримов М.М., Большаков В.И., Нестеров А.С., Можаренко Н.М., Якушев В.С.; заявлено 21.04.2004; опубликовано 10.05.2005. Бюллетень № 13.

16. Yaroshevskii S.L. Iron Smelting using Pulverized Coal Fuel. Moscow: Metallurgiya; 1988:166. (In Russ.).

Ярошевский С.Л. Выплавка чугуна с применением пылеугольного топлива. Москва: Металлургия; 1988:166.

17. Leittsel' D., Khunger I., Kryuger V., etc. Processes during injection of coal dust into a blast furnace. *Chernye metally*. 1999;(5):20–28. (In Russ.).

Лейтцель Д., Хунгер Й., Крюгер В. и др. Процессы при вдувании угольных пылей в доменную печь. *Черные металлы*. 1999;(5):20–28.

18. Chizhikov V.M., Bachinin A.A., Nesterenko S.V. Viscosity of heterogeneous slags containing fuel. *Izvestiya. Ferrous Metallurgy*. 1987;30(5):145–146. (In Russ.).

Чижиков В.М., Бачинин А.А., Нестеренко С.В. Вязкость гетерогенных шлаков, содержащих топливо. *Известия вузов. Черная металлургия*.1987;30(5):145–146.

19. Lyalyuk V.P., Tovarovskii I.G., Demchuk D.A., etc. Anthracite and Thermoanthracite in Blast Furnace Charge. Dnepropetrovsk: Porogi; 2008:245. (In Russ.).

Лялюк В.П., Товаровский И.Г., Демчук Д.А. и др. Антрацит и термоантрацит в шихте доменной плавки. Днепропетровск: Пороги; 2008:245.

20. Roginenko S.A., Shevelev L.N. The Paris Agreement and Russian metallurgy: time to reduce risks and stimulate energy saving. *Stal'*. 2018;(12):61–66. (In Russ.).

Рогиненко С.А., Шевелев Л.Н. Парижское соглашение и Российская металлургия: время снижать риски и стимулировать энергосбережение. *Сталь*. 2018;(12):61–66.

21. Vinogradov E.N., Kal'ko A.A., Volkov E.A., Zavodchikov M.V. Method of blast furnace smelting. Patent RF no. 2709318. MPK C21B 5/00. *Byulleten' izobretenii*. 2019;(34). (In Russ.).

Пат. 2709318 RU. Способ ведения доменной плавки / Виноградов Е.Н., Калько А.А., Волков Е.А., Заводчиков М.В.; заявлено 24.04.2019; опубликовано 17.12.2019. Бюллетень № 34.

22. Kal'ko A.A., Volkov E.A., Karimov M.M., Terebov A.L. Method of loading washing and working feeds into a blast furnace. Patent RF no. 2786283. MPK C21B 3/00. *Byulleten' izobretenii*. 2022;(35). (In Russ.).

Пат. 2786283 RU. Способ загрузки промывочных и рабочих подач в доменную печь / Калько А.А., Волков Е.А., Каримов М.М., Теребов А.Л.; заявлено 01.03.2022; опубликовано 19.12.2022. Бюллетень № 35.

23. Vinogradov E.N., Kal'ko A.A., Chikinov S.V., Volkov E.A., Kal'ko O.A. Development and implementation of coke substitution technology with natural gas to reduce solid fuel consumption at the classic blast furnaces of PJSC Severstal. *Metallurg*. 2024;(1):11–16. (In Russ.).

Виноградов Е.Н., Калько А.А., Чикинов С.В., Волков Е.А., Калько О.А. Разработка и внедрение технологии замещения кокса природным газом для снижения расхода твердого топлива на классических доменных печах ПАО «Северсталь». *Металлург*. 2024;(1):11–16.

Information about the Authors / Сведения об авторах

Andrei A. Kal'ko, *Head of Technological Development Center Upstream,* PJSC Severstal, Cherepovets Steel Mill
E-mail: aakalko@severstal.com

Evgenii N. Vinogradov, *Deputy General Director of Production – General Director Severstal Russian Steel Division and Mining Assets,* PJSC Severstal, Cherepovets Steel Mill
E-mail: envinogradov@severstal.com

Oksana A. Kal'ko, *Cand. Sci. (Eng.), Assist. Prof. of the Chair of Chemical Technologies,* Cherepovets State University
ORCID: 0000-0001-8158-5626
E-mail: oakalko@chsu.ru

Aleksei A. Kal'ko, *Gas Operator of Blast Furnace,* PJSC Severstal, Cherepovets Steel Mill; *MA Student of the Chair "Metallurgy, Mechanical Engineering and Technological Equipment",* Cherepovets State University
E-mail: akalko@chsu.ru

Андрей Александрович Калько, *руководитель центра технологического развития Upstream,* ПАО «Северсталь» Череповецкий металлургический комбинат
E-mail: aakalko@severstal.com

Евгений Николаевич Виноградов, *заместитель генерального директора по производству – генеральный директор дивизиона «Северсталь Российская Сталь» и ресурсных активов,* ПАО «Северсталь» Череповецкий металлургический комбинат
E-mail: envinogradov@severstal.com

Оксана Александровна Калько, *к.т.н., доцент кафедры химических технологий,* Череповецкий государственный университет
ORCID: 0000-0001-8158-5626
E-mail: oakalko@chsu.ru

Алексей Андреевич Калько, *газовщик доменной печи,* ПАО «Северсталь» Череповецкий металлургический комбинат; *магистрант кафедры металлургии, машиностроения и технологического оборудования,* Череповецкий государственный университет
E-mail: akalko@chsu.ru

Contribution of the Authors / Вклад авторов

A. A. Kal'ko – analysis of the results of previous campaigns, identification of problem areas, development of measures to increase the durability of the blast furnace hearth lining and organize an effective charge column structure in the blast furnace.
E. N. Vinogradov – analysis of the results of previous campaigns, identification of problem areas, development of measures to increase the durability of the blast furnace shaft lining and special techniques for loading solid coke substitutes.
O. A. Kal'ko – analysis of the results of previous campaigns, determination of the physical and chemical principles of obtaining melts of a given composition.
A. A. Kal'ko – analysis of the results of previous and current campaigns, comparative calculations of the specific carbon consumption for cast iron smelting during different periods of blast furnace operation.

А. А. Калько – анализ результатов предыдущих кампаний, определение проблемных зон, разработка мероприятий по повышению стойкости футеровки горна доменной печи и организации эффективной структуры столба шихты в доменной печи.
Е. Н. Виноградов – анализ результатов предыдущих кампаний, определение проблемных зон, разработка мероприятий по повышению стойкости футеровки шахты доменной печи и особых приемов загрузки твердых заменителей кокса.
О. А. Калько – анализ результатов предыдущих кампаний, определение физико-химических закономерностей получения расплавов заданного состава.
А. А. Калько – анализ результатов предыдущих и текущей кампаний, сравнительные расчеты удельного расхода углерода на выплавку чугуна в различные периоды работы доменной печи.

Received 23.04.2024
Revised 24.05.2024
Accepted 28.05.2024

Поступила в редакцию 23.04.2024
После доработки 24.05.2024
Принята к публикации 28.05.2024

RESOURCE SAVING IN FERROUS METALLURGY / **РЕСУРСОСБЕРЕЖЕНИЕ В ЧЕРНОЙ МЕТАЛЛУРГИИ**

UDC 658.51
DOI 10.17073/0368-0797-2024-3-270-282

Original article
Оригинальная статья

Energy saving model for related processes in steelmaking

W. Wang[1], S. Li[1, 2], W. Xu[1],
O. A. Chikova[2] ✉, Y. Zhang[1, 2]

[1] **Institute of Thermal Energy Engineering, North China University of Water Resources and Electric Power** (36 North Third Ring Str., Zhengzhou 450011, China)
[2] **Ural Federal University named after the first President of Russia B.N. Yeltsin** (19 Mira Str., Yekaterinburg 620002, Russian Federation)

✉ chik63@mail.ru

Abstract. In the development of advanced energy saving technologies in the metallurgical industry, a comprehensive approach to managing energy flows is crucial. This article presents an in-depth analysis of the steelmaking and metallurgical industry in China and Russia, focusing on the evolution and current shortcomings of energy saving methods in metallurgical processes. The authors thoroughly analyze various technological processes, including sintering, coking, pellet production, iron production in blast furnaces, steel production in oxygen converters and electric arc furnaces, as well as steel rolling, identifying significant potential for enhancing energy efficiency and reducing harmful emissions. The main outcome of the research is the development of structural models of technological processes based on the concept of energy saving "temperature matching, cascade utilization, and global linkage", covering key stages of steelmaking. These models provide detailed descriptions of the role and interrelation of each process within the complete metallurgical cycle and combine into a comprehensive structural model of steelmaking technological process. The model includes not only specific operations and characteristics of each stage but also explains how these processes interact and depend on each other, forming an integrated and interconnected system of metallurgical production. This model encompasses comprehensive temperature-pressure and production links, providing a theoretical basis for the development of mathematical models of energy saving and the design of corresponding computer applications. The structural model of steelmaking technological process is important for understanding and optimizing the entire process of metallurgical production, contributing to its energy and ecological efficiency.

Keywords: steelmaking, process energy saving, linked energy saving, thermal coupling, pressure coupling, cascading energy use, production process modeling

Acknowledgements: This paper was supported by the Program for Innovative Research Team (in Science and Technology) at the University of Henan Province (grant No. 224200510022).

For citation: Wang W., Li S., Xu W., Chikova O.A., Zhang Y. Energy saving model for related processes in steelmaking. *Izvestiya. Ferrous Metallurgy*. 2024;67(3):270–282. https://doi.org/10.17073/0368-0797-2024-3-270-282

Модель энергосбережения для связанных процессов металлургии стали

В. Ванг[1], Ш. Ли[1, 2], В. Ху[1],
О. А. Чикова[2] ✉, И. Чжан[1, 2]

[1] **Институт теплоэнергетики, Северо-Китайский университет водных ресурсов и электроэнергетики** (Китай, 450011, Чжэнчжоу, ул. Северное Третье кольцо, 36)
[2] **Уральский федеральный университет имени первого Президента России Б.Н. Ельцина** (Россия, 620002, Екатеринбург, ул. Мира, 19)

✉ chik63@mail.ru

Аннотация. При разработке передовых технологий энергосбережения металлургической промышленности ключевое значение имеет комплексный подход к управлению энергетическими потоками. В данной работе проведен глубокий анализ металлургических отраслей Китая и России с акцентом на эволюцию и текущие недостатки методов экономии энергии в металлургических процессах. Авторы подробно проанализировали различные технологические процессы, включая агломерацию, коксование, производство окатышей, чугуна

в доменных печах, стали в кислородных конвертерах и электродуговых печах, а также прокатку стали. При этом выявляется значительный потенциал для повышения эффективности использования энергии и сокращения вредных выбросов. Основным результатом исследования является разработка структурных моделей технологических процессов на основе концепции энергосбережения «соответствия температур, каскадного использования и глобальной связи», охватывающих ключевые этапы производства стали. Эти модели подробно описывают роль и взаимосвязь каждого процесса в рамках полного металлургического цикла и объединяются в комплексную структурную модель технологического процесса производства стали. Модель включает в себя не только конкретные операции и характеристики каждого этапа, но и объясняет, как эти процессы взаимодействуют и зависят друг от друга, формируя целостную и взаимосвязанную систему металлургического производства. Эта модель включает в себя комплексные связи по температуре, давлению и отрасли производства, обеспечивая теоретическую основу для развития математических моделей энергосбережения и разработки соответствующих компьютерных приложений. Структурная модель технологического процесса производства стали имеет важное значение для понимания и оптимизации всего процесса металлургического производства, способствует повышению его энергетической и экологической эффективности.

Ключевые слова: металлургия стали, энергосбережение процессов, связанное энергосбережение, тепловая связь, связь по давлению, каскадное использование энергии, моделирование производственных процессов

Благодарности: Исследование выполнено при поддержке программы Инновационной исследовательской группы (в области науки и технологий) Университетом провинции Хэнань (грант № 224200510022).

Для цитирования: Ванг В., Ли Ш., Ху В., Чикова О.А., Чжан И. Модель энергосбережения для связанных процессов металлургии стали. *Известия вузов. Черная металлургия*. 2024;67(3):270–282. https://doi.org/10.17073/0368-0797-2024-3-270-282

Introduction

Steelmaking is the key sector of China's national economy, it determines the development of major industries and the state's competitiveness in world markets. In 2017, the volume of steel produced by China three times exceeded that manufactured by the US, Russia and Japan combined. Steel has propelled China's shipbuilding and automobile industries to the top of the global market [1]. Steelmaking is characterized by long production cycles and high energy consumption. Meanwhile, steel production is a dangerous source of atmospheric pollution by off gases and solid emissions, which contain various toxic substances. Energy saving and emission reduction in steelmaking are crucial for China's national economy [2]. Back in 2014, Chinese President Xi Jinping formulated the main principles of China's new energy strategy FROCSV (*Four Revolutions and One Cooperation Strategic Vision*), including the energy consumption reform that involves energy efficiency improvement [1]. China's iron and steel industry has made significant progress in enhancing energy efficiency – the average intensity of total energy consumption at major steel plants has decreased. An evaluation framework has been developed to quantify the energy and environmental benefits (i.e., CO_2 and air-pollutants emission reduction and water savings) associated with 36 energy-efficiency measures [3]. The key topic of the 2011 – 2025 research on energy savings is the synergistic operation of material and energy flows [4] based on the energy saving model for China's iron and steel industry IECUA (*Industrial Energy Conservation Uncertainty Analysis*) [5].

At present, Russia actively uses modern energy- and resource-saving environmentally friendly technologies in steel production, so the analysis of the Chinese researchers' experience in this matter is especially important [6]. Low energy consuming metallurgical technologies (continuous casting of steel, evaporative cooling, etc.) are introduced [7]. The technology of dry granulation of slag using its physical heat developed by Russian metallurgical scientists is applied at metallurgical plants in China [8]. An energy-efficient environmentally friendly technology of injecting hot reducing gases into the blast furnace (blast furnace gas recycling) has been developed and introduced [9]. There are only two routes of steel production: blast furnace – basic oxygen furnace (BF – BOF) and electric arc furnace (EAF) [10]. China and Russia use the BF – BOF route as their main route of steel production [11], so our countries can share their best practices. In China, energy efficiency (EI) in steel production is achieved by applying energy-saving and secondary energy-recovery technologies such as:

– use of waste heat and LDG;

– comprehensive utilization of steelmaking waste [11];

– widespread use of energy-saving technologies reducing emissions CO_2 [12].

On the BF – BOF route, material and energy flows are closely linked, enabling the iron-containing materials and energy to move and transform [13]. Chinese scientists have developed structural models of energy flows within the IDDD+N concept (*Integration of the processes, Differentiation of the demand, Diversification of the supply, Decentralization of the grid, and Network of multi-energy flows*) aimed at optimizing the energy use, integrating the technological processes and decentralizing the production management [14]. The structural model of energy flows includes systems for heat conversion, utilization, and recovery, as well as energy buffering and storage. In fact, metallurgical plants produce and consume energy at the same time: BFs consume coal and produce coke and coke oven gas (COG), BOFs consume electricity and oxygen and produce Linz-Donawitz Gas (LDG) [15], i.e., they are prosumers [16]. Mathematical modeling enables to conduct a quantitative study of structural models for energy saving [10; 17], in particular, the specialized soft-

ware METSIM and SYSCAD provides for calculating the heat/material balance [18]. The authors of [19; 20] note that structural models of energy flows should take into account the interactions and synergy between material and energy flows. Recently, the concept of smart steel manufacturing as part of Industry 4.0 built on cyber-physical systems (CPS) has become popular [21 – 24]. Decarbonization of the metallurgical industry is a pressing task [25], researchers are currently focused on developing carbon capture and storage (CCS) technologies [26].

Chinese scientists have created a conceptual model linking the material, energy and emission flows along the BF – BOF route, including byproduct cokemaking, sinter production and iron founding, where by-product gases are used as fuel, the surplus being transferred to power plants for energy generation [27]. The model involves macro-grid control of the steel production process considering the interrelation of the material, energy and information flows to achieve "minimum" emissions, as well as of energy and materials consumption [28]. Lu Zhongwu proposed the concept of linked saving of energy and materials for the metallurgical industry [29]. Based on the phenomenological model of substance (iron) flow in the technological cycle of steel production, a system of equations was obtained to calculate the indexes of substance flow and the relationship between them [30]. Yin Ruiyu proposed a series of measures of energy-saving and emission reduction based on the mechanism of ferrogenious flow and carbon energy flow system. His concept involves "buying coal only, not electricity or fuel" and achieving "zero emissions" of by-product gases and other energy mediums [31]. Yin Ruiyu established a dynamic integration for the "mass – energy – time – space – information" during the steel manufacturing process based on analyzing the basic elements and characteristics of the processes [32]. Yongqi Sun, Zuotai Zhang developed a blast furnace slags (BFS) and steel slags (SS) disposal model based on the integration of heat recovery and material recycling and crystallization control of the slags [33]. A mind map of the integration of material and energy flows at steel plants was developed [34]. The paper [35] presents an analytical review of publications on decarbonization of iron and steel industry in the context of financial, organizational and behavioral aspects. Numerous works by Chinese researchers on the interrelation of material and energy flows for the sintering process are noteworthy [36 – 38]. The exergy analysis in steelmaking serves as a theoretical basis for energy saving because exergy accounting of energy and material flows provides an integrated measure of resources, products and wastes at different aggregation levels, from single unit operations and upstream production steps to steel plants and production routes, and exergy indicators can be easily linked to techno-economic ones [39].

Russia has also adopted a similar energy saving model for linked steelmaking processes, which includes the following combined energy saving methods for metallurgical processes: enhancing the blast furnace productivity by implementing the technologies of injecting hot reducing gas and replacing quality ores with siderite ore concentrate (SOC); using CO_2 washed from the blast furnace gas in refrigerating equipment; full recovery of LDG heat for SOC roasting [40].

Research methodology

The integration of several scientific approaches – systematic, analytical and comparative – forms the theoretical and methodological basis of the conceptual model of energy saving for the linked processes of steelmaking. It enabled us to explore the main aspects of the problem and the tasks set, to reveal new trends of energy saving for the linked processes of steelmaking and quality indicators of energy saving. We used the methods of theoretical and methodological analysis (comparative, retrospective, and model), comparative analysis of scientific literature, methods for systematizing the authors' experience in the energy saving organization to identify the main trends in the development of the concept of "linked processes" in the context of energy and materials saving management and environmental safety in the steelmaking industry.

We conducted a conceptual study of the methods of linked reduction of energy consumption in steel production processes based on the principle of cascading energy use and analysis of the causes of energy consumption surges. To enhance energy efficiency, new methods for network energy distribution and coupled energy reduction in steel production processes are proposed. The objective of the work is to develop temperature, pressure and industry coupling models for energy saving in linked steelmaking processes based on the principles of "correspondence of temperatures, cascading use and global coupling". We developed structural models of technological processes of sintering, coking, pellet manufacture, cast iron production in a blast furnace, iron production in a BOF and an electric furnace, and steel rolling combined into a structural model of steelmaking technological process.

Research results

We will consider sintering and coking processes as study objects. The structural model of sintering (Fig. 1) includes a sintering machine, a cooler, as well as crushing, screening and mixing equipment. The iron-containing material is turned into sinter, which is sent to the blast furnace after cooling. High temperature off gases are used to recover the residual heat. The structural model of the coking process (Fig. 2) includes formation of coke

column and quenching technologies. The input materials are turned into red hot coke, which is sent after cooling to the hopper or returned to the raw material cycle. COG and off gases, as well as hot nitrogen from the coke quenching process, are directed to heat recovery and energy saving.

Our study objects are the processes of pellet and cast iron production. The structural model of pellet production (Fig. 3) includes a stirrer, a granulator, a sorting device, a chain lattice conveyor, a circulating furnace and a cooler. Green pellets are formed from the powdered concentrate and binders and, after sintering and cooling, are sent to the blast furnace or returned for processing. The cold exhaust air is used for energy saving. The structural model of the cast iron production (Fig. 4) includes a blast furnace and an air heater. A blast furnace produces cast iron from sinter, coke, pellets and lump iron ore with the addition of air. Off gases and slag are used for further recovery and energy saving.

For the purpose of the study, let us consider the processes of steelmaking in a BOf and in an electric furnace. The structural model of steel production in a BOF (Fig. 5) includes cast iron pretreatment equipment, a BOF, a ladle for steel transfer, a secondary treatment unit and a ladle for pouring steel. Output materials include steel, slag, LDG and dust. The waste is used for heat and energy recovery. The structural model of steel production in an electric furnace (Fig. 6) includes cast iron pretreatment equipment, an electric furnace, a ladle for transfer, a secondary treatment unit and a ladle for pouring. The input and output materials are similar to the converter process. The waste is also used for heat and energy recovery.

As an object of study, let us consider the process of steel rolling and create a structural model of this technological process (Fig. 7). The main equipment of the rolling process includes continuous casting machines, heating furnaces, hot and cold rolling mills. In the steel rolling process model, the input materials include steel, oxygen, water, lubricants, refractory materials, gas and combustion air. The input materials first pass through a continuous casting machine where they are solidified and cast into cast blanks. Then, after heating in the furnace, the blanks are sent to various rolling shops for processing into products of various types (profiles, rods, rails, seamless pipes, sheets or strips). In this case, off gases generated in the heating furnaces are considered in the structural model (Fig. 8) as a direction of leaving the operational framework of the rolling process for residual heat recovery and energy saving.

At the final stage, the structural models of technological processes of sintering, coking, pellet manufacture, cast iron production in a blast furnace, iron production in a BOf and an electric furnace, and steel rolling were combined into a structural model of the steelmaking technological process (Fig. 8).

Using the basic principles of linked energy saving, cascading energy use and loss minimization, we proposed the models of thermal coupling, pressure coupling and

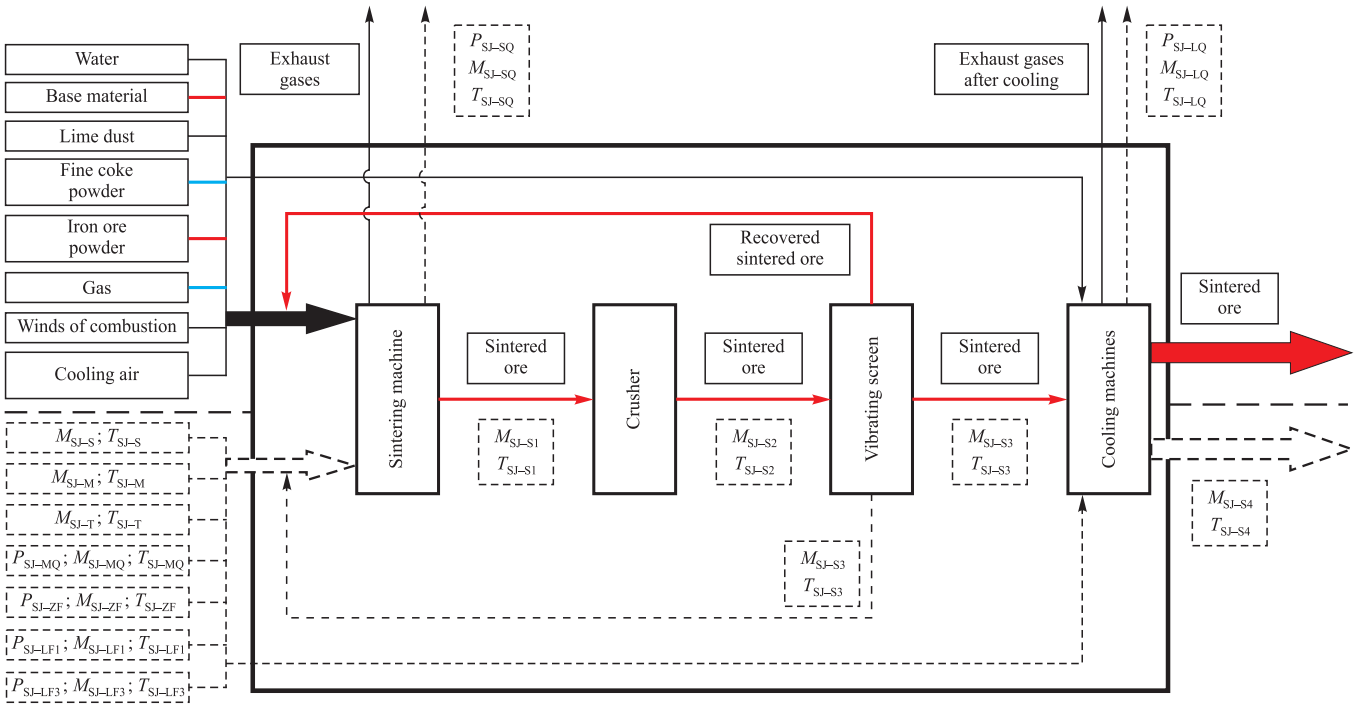

Fig. 1. Model of sintering process

Рис. 1. Модель процесса агломерации

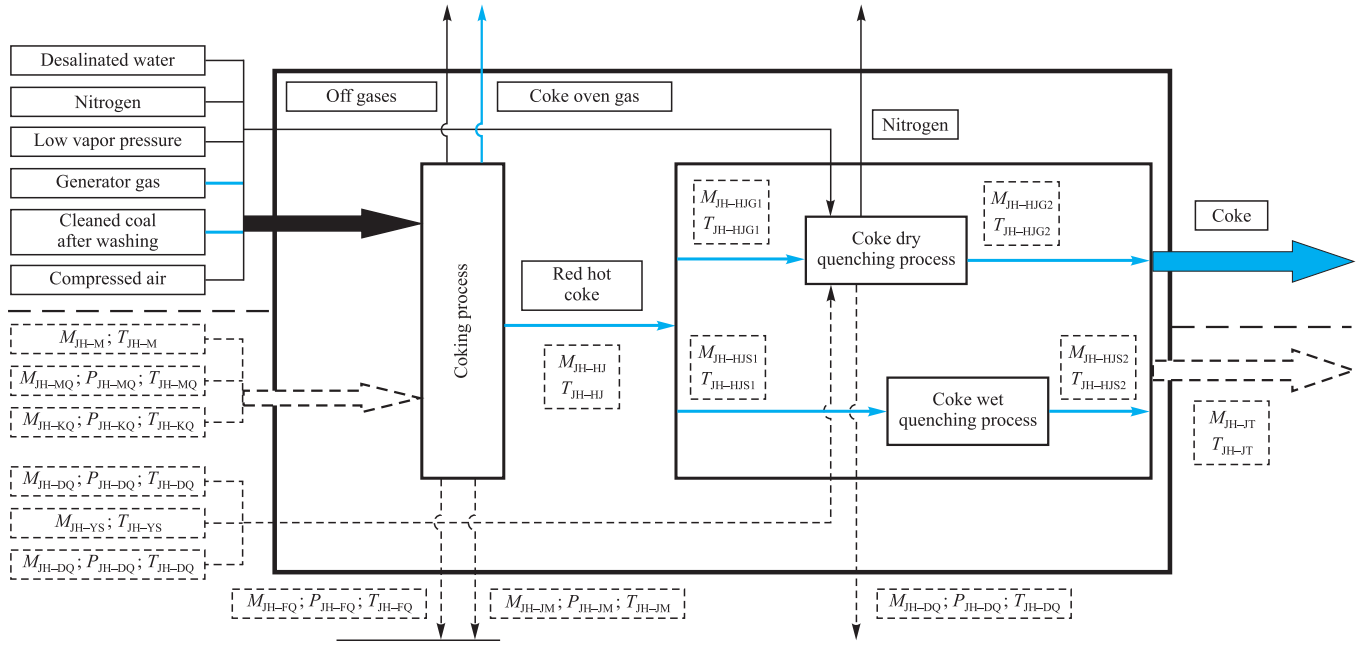

Fig. 2. Model of coking process

Рис. 2. Модель процесса коксования

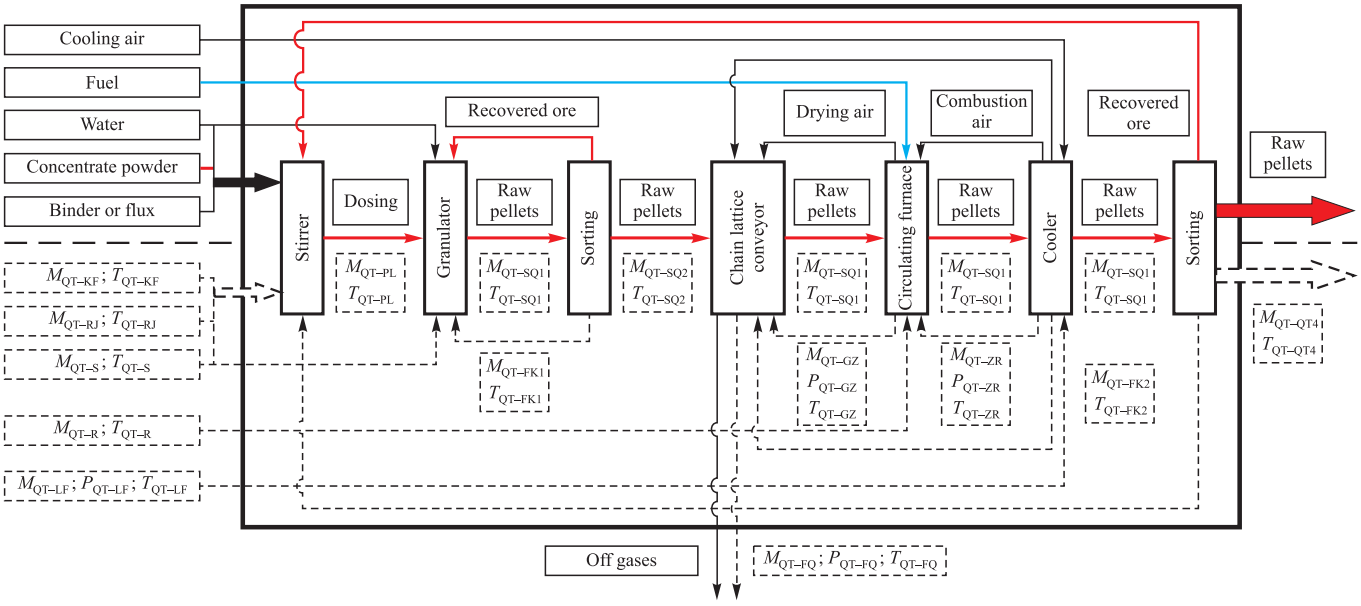

Fig. 3. Model of pellet production

Рис. 3. Модель процесса производства окатышей

inter-branch coupling for separate technological processes of steelmaking – sintering, coking, pellet manufacturing, cast iron production in a blast furnace, iron production in a BOF and an electric furnace, and steel rolling (Fig. 8). Thermal coupling means linking the process where excessive heat is produced to the processes that consume heat in order to provide the best match between heat production and consumption in each process, thereby reducing dependence on external heat sources and enhancing energy efficiency throughout the metallurgical process. In pressure-coupled processes, the excessive pressure produced is transferred to processes with suitable pressure in order to achieve the best possible match between heat energy supply and consumption in each process and thereby reduce pressure supply from external sources and enhance the energy efficiency of the entire metallurgical process. Industry coupling involves linking surplus materials and energy in steel production to customers in other industries where they can be applied to improve materials and energy efficiency. Energy saving through indus-

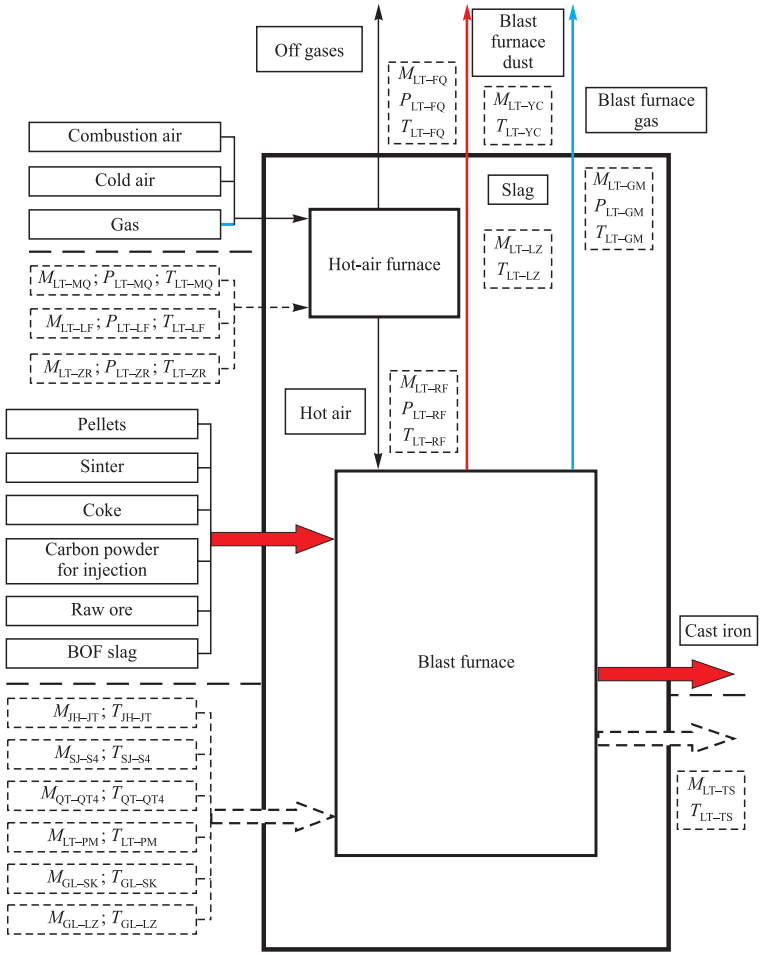

Fig. 4. Model of iron production

Рис. 4. Модель процесса производства чугуна

try coupling is realized by transferring excessive materials and energy of the metallurgical process to related industries, establishing a link between the metallurgical industry and other industries to ensure the interrelation of materials and energy supply in order to enhance the efficiency of the materials and energy use.

Discussion of the research results

This paper presents a conceptual structural model of temperature, pressure and industry coupling for energy saving in linked steelmaking processes. The model is based on the principles of temperature matching, cascading use, and global coupling. In contrast to the matrix model of the interrelation of material, energy and emission flows for the ferrous metallurgy enterprise [26], the presented model is universal in relation to individual technological processes of ferrous metallurgy, it reflects thermal, pressure and industry coupling and allows for an optimized steel production process based on material and energy saving and emission reduction. Lu Zhongwu [28; 29] investigated the effect of logistics on energy and iron consumption during steel production. He found that taking iron-containing materials out of the production process causes an increase in energy and iron consumption per 1 ton of material. Circulation of iron-containing materials within the same process or between processes does not affect the iron consumption per 1 ton, but results in increased energy consumption per 1 ton of material. Consequently, circulation of iron-containing materials should be minimized as much as possible, which is reflected in the modeling rules. Lu Zhongwu [30] used Lagrange and Euler methods to describe fluid flow. He also explained a material flow tracking model based on the iron flow diagram in the life cycle of steel products, which provided a reference for creating and optimizing downstream metallurgical processes. Yin Ruiyu [31] described the behavior models of iron and carbon-energy flows during steel production. He analyzed the potential for energy saving and emission reduction in the steel industry, optimization of metallurgical processes being one of the effective methods. Yin Ruiyu [32] proposed a theoretical approach to creating a new generation of steelmaking processes based on the interaction and synergy of materials, energy and information flows during the metallurgical process. Based on the research of the material and

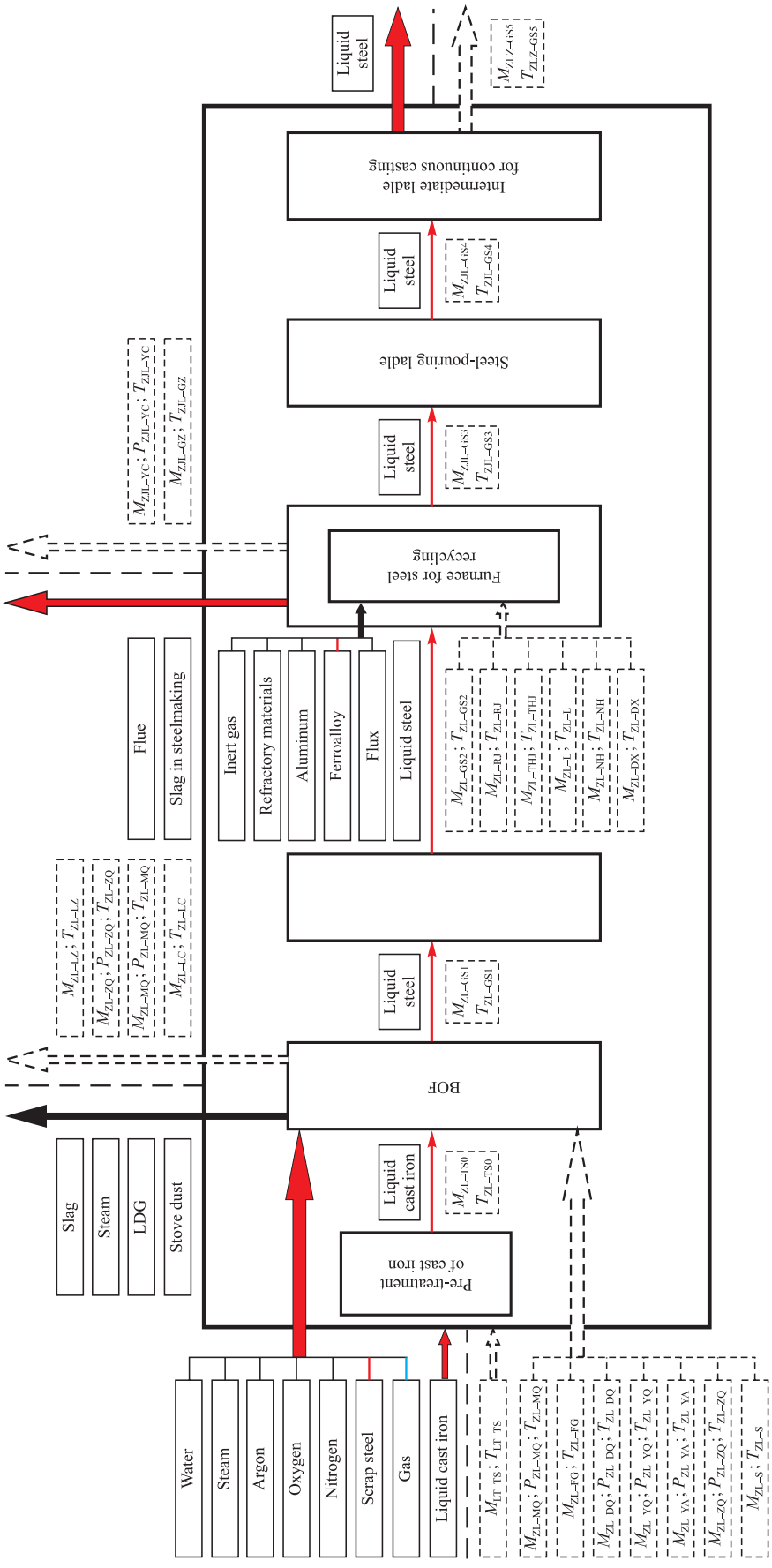

Fig. 5. Model of steelmaking in a converter

Рис. 5. Модель процесса производства стали в конвертере

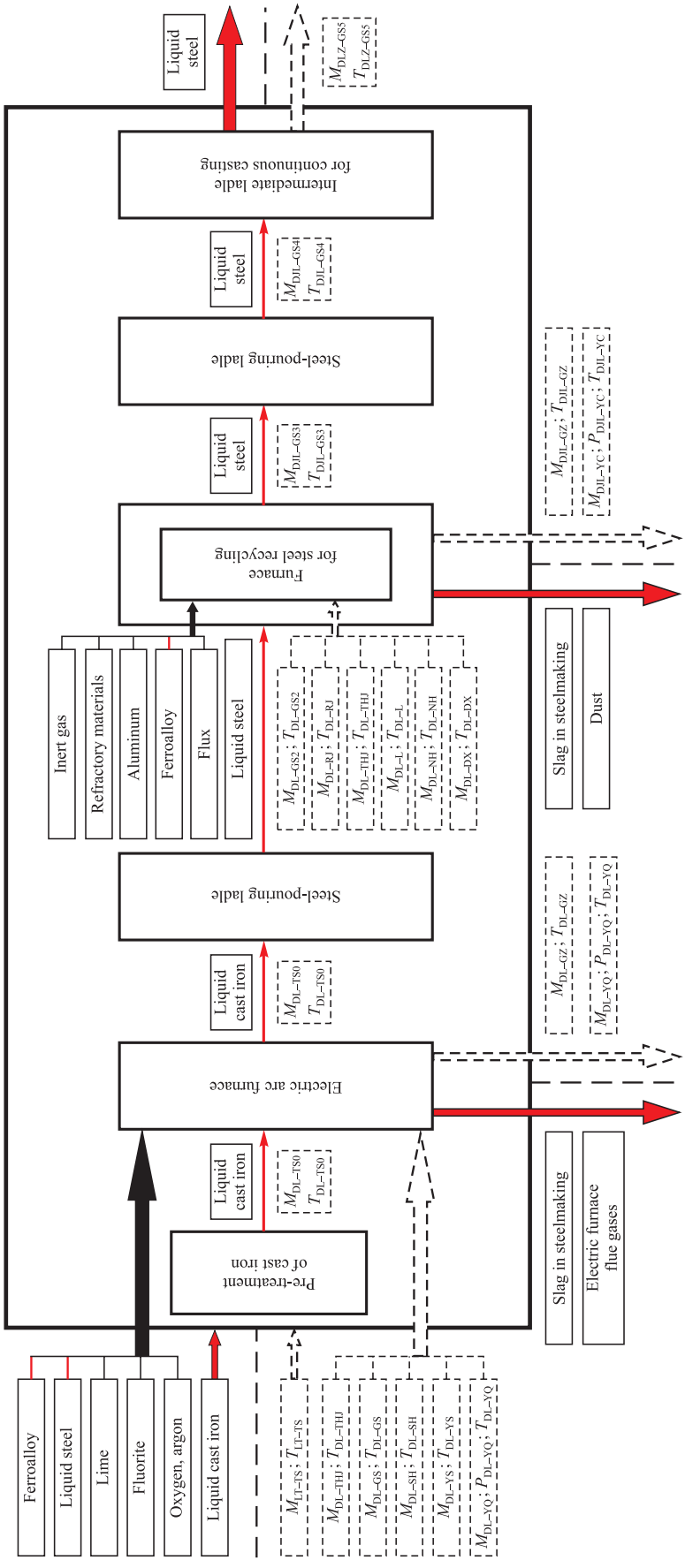

Fig. 6. Model of steelmaking in an electric furnice

Рис. 6. Модель процесса производства стали в электрической печи

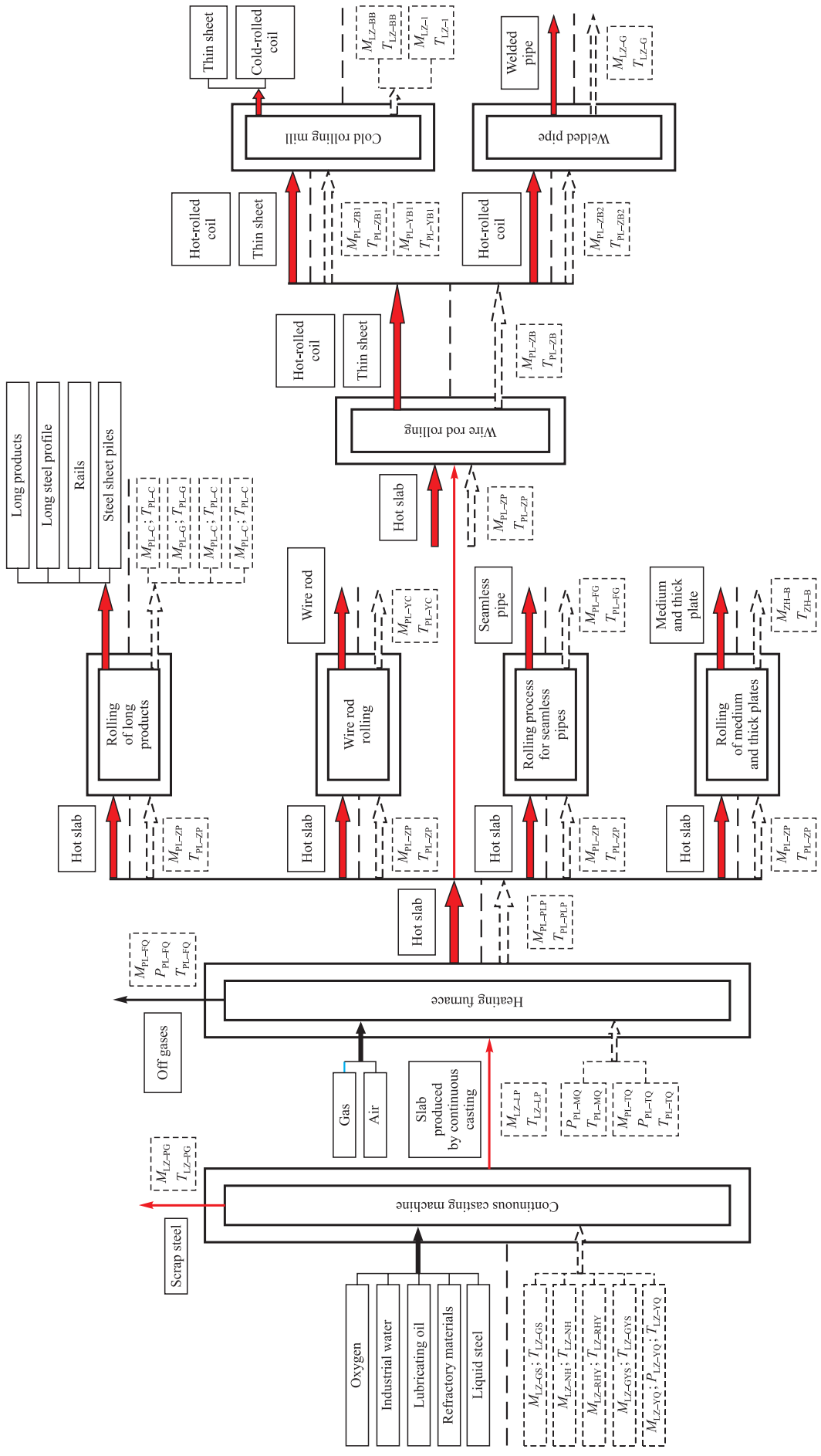

Fig. 7. Model of steel rolling process

Рис. 7. Модель процесса прокатки стали

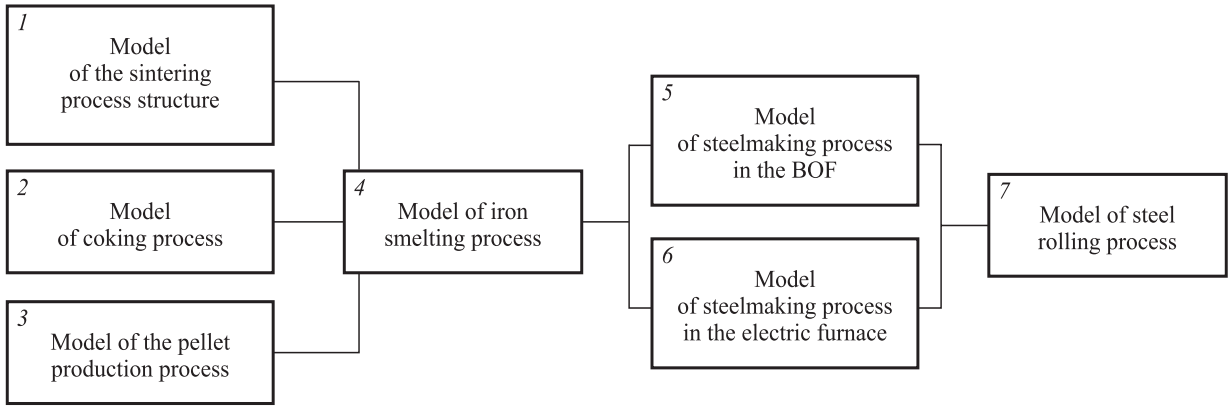

Fig. 8. Structural model of technological process of steelmaking:
1 – 7 – detailed diagrams of technological processes models in Figs. *1 – 7*

Рис. 8. Структурная модель технологического процесса производства стали:
1 – 7 – подробные схемы моделей технологических процессов на рис. *1 – 7*

energy flows in steel making processes, combined with the rules of metallurgical process modeling and the real conditions of metallurgical engineering, we developed a technique for designating the material and energy flows and created a structural model of the whole metallurgical production process. In addition to considering material and energy flows, this model includes coupled pressure and temperature conversion and industry integration. The mode takes into account the individual metallurgical processes and emphasizes the interaction between them, which greatly improves energy saving and emission reduction. The qualitative description of a similar energy saving model for linked steelmaking processes in Russia was presented, which includes a number of combined energy-saving methods for metallurgical processes [40].

Conclusions

The paper investigates the key energy saving aspects and trends in steelmaking in both China and Russia. The analysis of various processes, including sintering, coking, pellet manufacturing, cast iron production in a blast furnace, iron production in a BOf and/or an electric furnace, and steel rolling, revealed significant potential for enhancing energy efficiency and reducing emissions.

The main finding of this study is that minimum energy and material consumption, as well as emission reductions, can be achieved by creating a new concept of coupling energy saving with the technological process: “temperature matching, cascading use, and global coupling.” The linked processes in steelmaking are complex processes of continuous and discrete changes in energy and material flows. The model of interrelation of material and energy flows is a restrained model of linked process nodes for ensuring energy and material savings and monitoring emissions. We developed structural models of technological processes covering the key stages of the steelmaking process, including sintering, coking, pellet manufacturing, cast iron production in a blast furnace, iron production in a BOf and an electric furnace, and steel rolling. These models provide detailed descriptions of the role and interrelations of each process within the complete metallurgical cycle and combine into a structural model of steelmaking technological process. The structural model of steel production process reflects the system of interrelations of all metallurgical production stages. Not only does it include the specific operations and characteristics of each stage, but also explains how these processes interact and depend on each other, forming an integrated and interconnected system of metallurgical production. The structural model of steelmaking process is important for understanding and optimizing the entire process of metallurgical production, contributing to its energy and ecological efficiency.

References / Список литературы

1. Zhong C., Zhao Q. Energy efficiency management in China’s steel industry. *StudNet*. 2021;4(5). (In Russ.).
Чжун Ч., Чжао Ц. Управление энергоэффективностью в черной металлургии Китая. *StudNet*. 2021;4(5).
2. Cai J.J., Sun W.Q. Systems energy conservation and scientific energy utilization of iron and steel industry in China. *Iron and Steel*. 2012;47(5):1–8.
3. Ma D., Chen W., Xu T. Quantify the energy and environmental benefits of implementing energy-efficiency measures in China’s iron and steel production. *Future Cities and Environment*. 2015;1:1–7. https://doi.org/10.1186/s40984-015-0005-8
4. Sun W.Q., Cai J.J., Zhu Y. Advances in energy conservation of China steel industry. *The Scientific World Journal*. 2013;2013(2):247035. https://doi.org/10.1155/2013/247035
5. Wen Z.G., Wang Y.H., Zhang C.K., Zhang X.L. Uncertainty analysis of industrial energy conservation management in

China's iron and steel industry. *Journal of Environmental Management*. 2018;225:205–214. https://doi.org/10.1016/j.jenvman.2018.07.096

6. Chernobrovin V.P. Ferrous metallurgy in Russia in dynamics (1970–2018). *Vestnik Yuzhno-Ural'skogo gosudarstvennogo universiteta. Seriya: Metallurgiya*. 2020;20(1): 7–17. (In Russ.).

   Чернобровин В.П. Черная металлургия России в динамике (1970–2018 гг.). *Вестник Южно-Уральского государственного университета. Серия: Металлургия*. 2020; 20(1):7–17.
7. Druzhinin G.M., Zainullin L.A., Kazyaev M.D., Spirin N.A., Yaroshenko Yu.G., Gubinskii M.V. Main directions of resource and energy saving in ferrous metallurgy. In: *Creative Heritage of V.E. Grum-Grzhimailo: History, Current State, Future. Proceedings of the Int. Sci. and Pract. Conf. Vol. 1*. Yekaterinburg: UrFU; 2014:205–212. (In Russ.).

   Дружинин Г.М., Зайнуллин Л.А., Казяев М.Д., Спирин Н.А., Ярошенко Ю.Г., Губинский М.В. Основные направления ресурсоэнегосбережения в черной металлургии. В кн.: *Творческое наследие В.Е. Грум-Гржимайло: история, современное состояние, будущее. Сборник докладов Международной научно-практической конференции. Том 1*. Екатеринбург: Уральский федеральный университет имени первого Президента России Б.Н. Ельцина; 2014:205–212.
8. Zajnullin L.A., Druzhinin G.M., Butkarev A.A. Innovative developments of JSC "VNIIMT" for energy saving and ecology in metallurgy. In: *Creative Heritage of V.E. Grum-Grzhimailo: History, Current State, Future. Proceedings of the Int. Sci. and Pract. Conf. Vol. 1*. Yekaterinburg: UrFU; 2014:235–240. (In Russ.).

   Зайнуллин Л.А., Дружинин Г.М., Буткарев А.А. Инновационные разработки ОАО «ВНИИМТ» для энергосбережения и экологии в металлургии. В кн.: *Творческое наследие В.Е. Грум-Гржимайло: история, современное состояние, будущее. Сборник докладов Международной научно-практической конференции. Том 1*. Екатеринбург: Уральский федеральный университет имени первого Президента России Б.Н. Ельцина; 2014:235–240.
9. Shevelev L.N., Brodov A.A. Energy saving, increasing energy efficiency and reducing greenhouse gas emissions in the Russian ferrous metallurgy. *Ferrous Metallurgy. Bulletin of Scientific, Technical and Economic Information*. 2018;1(2):3–6. (In Russ.).

   Шевелев Л.Н., Бродов А.А. Энергосбережение, повышение энергоэффективности и снижение выбросов парниковых газов в черной металлургии России. *Черная металлургия. Бюллетень научно-технической и экономической информации*. 2018;1(2):3–6.
10. Sun W.Q., Wang Q., Zhou Y., Wu J.Z. Material and energy flows of the iron and steel industry: Status quo, challenges, and perspectives. *Applied Energy*. 2020;268:114946. https://doi.org/10.1016/j.apenergy.2020.114946
11. He K., Wang L., Li X.Y. Review of the energy consumption and production structure of China's steel industry: Current situation and future development. *Metals*. 2020;10(3):302. https://doi.org/10.3390/met10030302
12. Wang P., Morten R., Yang Y., Feng K.S., Kara S., Hauschild M., Chen W.Q. Efficiency stagnation in global steel production urges joint supply- and demand-side mitigation efforts. *Nature Communications*. 2021;12(1):2066. https://doi.org/10.1038/s41467-021-22245-6
13. Yin R.Y. Theory and Methods of Metallurgical Process Integration. Academic Press; 2016:336.
14. Yang L., Li Z., Hu H., Zou Y., Feng Z., Chen W., Chen F., Wang S., Guo Y. Evaluation of energy utilization efficiency and optimal energy matching model of EAF steelmaking based on association rule mining. *Metals*. 2024;14(4):458. https://doi.org/10.3390/met14040458
15. Jović M., Laković M., Banjac M. Improving the energy efficiency of a 110 MW thermal power plant by low-cost modification of the cooling system. *Energy Environ*. 2018;29(2): 245–259. https://doi.org/10.1177/0958305X17747
16. Zhou Y., Wu J., Long C. Evaluation of peer-to-peer energy sharing mechanisms based on a multiagent simulation framework. *Applied Energy*. 2018;222:993–1022. https://doi.org/10.1016/j.apenergy.2018.02.089
17. Valsalam R., Krishnan N., Muralidharen V. Energy management and control system for integrated steel plants. In: *National Convention on Computerisation and Automation in Steel Industry*. 1996;2:59–83.
18. Zhao Q.Y., Zhang T.A., Lv G.Z., Zhu X.F., Liu Y. Application of process simulation software METSIM in metallurgy. *TELKOMNIKA*. 2012;10(8):2202–2208.
19. Yu Q.B., Lu Z.W., Cai J.J. Calculating method for influence of material flow on energy consumption in steel manufacturing process. *Journal of Iron and Steel Research International*. 2007;14(2):46–51. https://doi.org/10.1016/S1006-706X(07)60026-0
20. Na H., Du T., Sun W., He J., Sun J., Yuan Y., etc. Review of evaluation methodologies and influencing factors for energy efficiency of the iron and steel industry. *International Journal of Energy Research*. 2019;43(11):5659–5677. https://doi.org/10.1002/er.4623
21. Cicconi P., Russo A.C., Germani M., Prist M., Pallotta E., Monteriù A. Cyber–physical system integration for industry 4.0: Modelling and simulation of an induction heating process for aluminum-steel molds in footwear soles manufacturing. In: *2017 IEEE 3rd Int. Forum on Research and Technologies for Society and Industry*. Modena: IEEE; 2017:1–6.
22. Haag S., Anderl R. Digital twin – Proof of concept. *Manufacturing Letters*. 2018;15(B):64–66. https://doi.org/10.1016/j.mfglet.2018.02.006
23. Zhao H.T., Jiang P., Chen Z., Ezeh C.I., Hong Y.D., Guo Y.S., Zheng C.H., Hrvoje D., Gao X., Wu T. Improvement of fuel sources and energy products flexibility in coal power plants via energy–cyber–physical–systems approach. *Applied Energy*. 2019;254:113554. https://doi.org/10.1016/j.apenergy.2019.113554
24. Al-Wakeel A., Wu J., Jenkins N. State estimation of medium voltage distribution networks using smart meter measurements. *Applied Energy*. 2016;184:207–218. https://doi.org/10.1016/j.apenergy.2016.10.010
25. Gao C., Gao W., Song K., Na H., Tian F., Zhang S. Spatial and temporal dynamics of air-pollutant emission inventory of steel industry in China: A bottom-up approach. *Resources, Conservation & Recycling*. 2019;143:184–200. https://doi.org/10.1016/j.resconrec.2018.12.032
26. Griffin P.W., Hammond G.P. Industrial energy use and carbon emissions reduction in the iron and steel sector: A UK

perspective. *Applied Energy*. 2019;249:109–125. https://doi.org/10.1016/j.apenergy.2019.04.148

27. Sun W.Q., Wang Q., Zheng Z., Cai J.J. Material–energy–emission nexus in the integrated iron and steel industry. *Energy Conversion and Management*. 2020;213:112828. https://doi.org/10.1016/j.enconman.2020.112828

28. Lu Z.-W., Cai J.-J., Yu Q.-B. The influences of materials flow in steel manufacturing process on its energy intensity. *Acta Metallurgica Sinica(China)*. 2000;36(4):370–378.

29. Lu Z.-W., Dai T. Influence of material flow in steel manufacturing process on energy consumption and metal yield. *Iron and Steel*. 2005;(4):1–7.

30. Lu Z.-W. The following-observing method for substance flow analysis. *Engineering Science*. 2006;8(1):18–25.

31. Yin R.Y. The energy flow behavior and energy flow network in steel manufacturing process. *Journal of Engineering Studies*. 2010;2(1):1–4.

32. Yin R.Y. Theory and Methods of Metallurgical Process Integration. Academic Press; 2016:336.

33. Sun Y.Q., Zhang Z.T. Disposal of high-temperature slags: A review of integration of heat recovery and material recycling. *Metallurgical and Materials Transactions E*. 2016;3:114–122. https://doi.org/10.1007/s40553-016-0075-z

34. Gu Y., Liu W., Wang B., Tian B., Yang X., Pan C. Analysis and prediction of energy, environmental and economic potentials in the iron and steel industry of China. *Processes*. 2023;11(12):3258. https://doi.org/10.3390/pr11123258

35. Jinsoo K., Benjamin K.S., Morgan B., Steve G., Junghwan L., Minyoung Y., Jordy L. Decarbonizing the iron and steel industry: A systematic review of sociotechnical systems, technological innovations, and policy options. *Energy Research & Social Science*. 2022;89:102565. https://doi.org/10.1016/j.erss.2022.102565

36. Jia F.R., Wang E.G., He J.C., Dong H., Zhao Y.D. Waste heat recovery and utilization during sintering process. *Industrial Heating*. 2014;43(4):45–48.

37. Yang B., Chen L.G., Shen X., Qin X.Y., Sun F.R. Current status and case study on sintering process waste heat recovery and utilization in China. *Research on Iron and Steel*. 2014;42(4):54–57.

38. Liu W.C., Cai J.J., Dong H., Zhang Q., Qi G.C. Thermodynamic analysis on the effective recovery and utilization of sinter waste heat. *China Metallurgy*. 2013;23(2):15–20.

39. Costa M.M., Schaeffer R., Worrell E. Exergy accounting of energy and materials flows in steel production systems. *Energy*. 2001;26(4):363–384. https://doi.org/10.1016/S0360-5442(01)00004-4

40. Sergeev P.A., Neshporenko E.G. Analysis of the effective use of energy-saving technologies at a metallurgical enterprise. *Sovremennye innovatsii*. 2015;(2(2)):27–30. (In Russ.).

Сергеев П.А., Нешпоренко Е.Г. Анализ эффективного использования энергосберегающих технологий металлургического предприятия. *Современные инновации*. 2015;(2(2)):27–30.

Information about the Authors / Сведения об авторах

Weishu Wang, *Dr. Sci. (Energy Sci. and Engineering Thermophysics), Prof. of the Chair of Power Engineering and Engineering Thermophysics,* Institute of Thermal Energy Engineering, North China University of Water Resources and Electric Power
ORCID: 0000-0002-5523-7254
E-mail: wangweishu@ncwu.edu.cn

Shuailong Li, *Master of Thermal Power Engineering,* Institute of Thermal Energy Engineering, North China University of Water Resources and Electric Power; *Student,* Ural Federal University named after the first President of Russia B.N. Yeltsin
ORCID: 0009-0003-4237-8941
E-mail: shuailun.li@urfu.me

Weihui Xu, *Master of Nuclear Engineering and Technology, Assist. Prof. of the Chair of Nuclear Engineering and Technology,* Institute of Thermal Energy Engineering, North China University of Water Resources and Electric Power
ORCID: 0000-0002-1143-9268
E-mail: xuweihui@ncwu.edu.cn

Ol'ga A. Chikova, *Dr. Sci. (Phys.–Math.), Prof. of the Chair of Physics,* Ural Federal University named after the first President of Russia B.N. Yeltsin
ORCID: 0000-0002-3347-9148
E-mail: chik63@mail.ru

Yimeng Zhang, *Senior Lecturer of the Chair of Architecture,* Institute of Thermal Energy Engineering, North China University of Water Resources and Electric Power; *Master of Architecture,* Ural Federal University named after the first President of Russia B.N. Yeltsin
ORCID: 0009-0002-7271-0143
E-mail: zhangyimeng@ncwu.edu.cn

Вейшу Ванг, *доктор энергетических наук и технической теплофизики, профессор кафедры энергетики и технической теплофизики,* Институт теплоэнергетики, Северо-Китайский университет водных ресурсов и электроэнергетики
ORCID: 0000-0002-5523-7254
E-mail: wangweishu@ncwu.edu.cn

Шайлун Ли, *магистр теплоэнергетики,* Институт теплоэнергетики, Северо-Китайский университет водных ресурсов и электроэнергетики; *студент,* Уральский федеральный университет имени первого Президента России Б.Н. Ельцина
ORCID: 0009-0003-4237-8941
E-mail: shuailun.li@urfu.me

Вейхой Ху, *магистр ядерной техники и ядерных технологий, доцент кафедры ядерной техники и технологий,* Институт теплоэнергетики, Северо-Китайский университет водных ресурсов и электроэнергетики
ORCID: 0000-0002-1143-9268
E-mail: xuweihui@ncwu.edu.cn

Ольга Анатольевна Чикова, *д.ф.-м.н., профессор кафедры физики,* Уральский федеральный университет имени первого Президента России Б.Н. Ельцина
ORCID: 0000-0002-3347-9148
E-mail: chik63@mail.ru

Имэн Чжан, *старший преподаватель кафедры архитектуры,* Институт теплоэнергетики, Северо-Китайский университет водных ресурсов и электроэнергетики; *магистр архитектуры,* Уральский федеральный университет имени первого Президента России Б.Н. Ельцина
ORCID: 0009-0002-7271-0143
E-mail: zhangyimeng@ncwu.edu.cn

Contribution of the Authors

W. Wang – conceptualization, methodology, scientific guidance, supervision.
S. Li – software, methodology, data analysis, writing the draft, conceptualization.

W. Xu – writing and editing the text.

O. A. Chikova – writing and editing the text, scientific guidance.

Y. Zhang – writing and editing the text.

Вклад авторов

В. Ванг – концептуализация, методология, научное руководство, наблюдение.
Ш. Ли – программное обеспечение, методология, обработка данных, написание первоначального текста статьи, концептуализация.
В. Ху – написание, рецензирование и редактирование текста статьи.
О. А. Чикова – написание, рецензирование и редактирование текста статьи; научное руководство.
И. Чжан – написание и редактирование текста статьи.

Received 20.09.2023
Revised 07.03.2024
Accepted 28.03.2024

Поступила в редакцию 20.09.2023
После доработки 07.03.2024
Принята к публикации 28.03.2024

MATERIALS SCIENCE / МАТЕРИАЛОВЕДЕНИЕ

UDC 536.425:539.25:539.351
DOI 10.17073/0368-0797-2024-3-283-292

Review article
Обзорная статья

Ways to improve the properties of high-entropy alloys Cantor CoCrFeNiMn and CoCrFeNiAl

V. E. Gromov, S. V. Konovalov, M. O. Efimov, I. A. Panchenko, V. V. Shlyarov

Siberian State Industrial University (42 Kirova Str., Novokuznetsk, Kemerovo Region – Kuzbass 654007, Russian Federation)

gromov@physics.sibsiu.ru

Abstract. Created one of the first and studied more than 20 years ago, high-entropy five-component alloys CoCrFeNiMn (Cantor alloy) and CoCrFeNiAl still attract the attention of researchers in the field of physical materials science due to their possible application in various industries because of their successful combination of strength and plastic properties. To date, a large amount of experimental materials has been accumulated on the ways to control the properties of these alloys. This article reviews the publications of domestic and foreign authors in two areas of improving the properties of these alloys: alloying, precipitation and heat treatment, and the use of CALPHAD phase diagrams. In the first direction, the role of alloying with B, Al, V, Si, Nb is analyzed; γ and γ′ nanoprecipitations, various modes of thermal and deformation processing. It was concluded that it is necessary to conduct experiments on the alloying of HEAs with Zr and Nb, which have proven themselves well in hardening steels. Creation and modification of the properties of five-component HEAs is possible using the CALPHAD computer programs developed for calculating state diagrams. The results of publications on the thermodynamic description of five-component alloys analyzed in the article are confirmed by comparing the phase diagrams with the available experimental data. In one of the analyzed works on the phase formation of five-component HEAs consisting of Co, Cr, Fe, Ni, Al, Mn, Cu, 2436 compositions were considered, which made it possible to determine 1761 variants of reliable prediction of the formation of bcc/B2 and fcc phases, bypassing amorphous phases and intermetallic compounds, thereby designing a certain level of mechanical properties. It is shown that the design of a new generation of HEAs is possible based on calculation of the CALPHAD phase diagrams.

Keywords: high-entropy alloys, CoCrFeNiMn, CoCrFeNiAl, alloying, hardening, heat treatment, CALPHAD

Acknowledgements: The work was supported by the Russian Science Foundation, grant No. 23-49-00015.

For citation: Gromov V.E., Konovalov S.V., Efimov M.O., Panchenko I.A., Shlyarov V.V. Ways to improve the properties of high-entropy alloys Cantor CoCrFeNiMn and CoCrFeNiAl. *Izvestiya. Ferrous Metallurgy*. 2024;67(3):283–292.
https://doi.org/10.17073/0368-0797-2024-3-283-292

Пути улучшения свойств ВЭС Cantor CoCrFeNiMn и CoCrFeNiAl

В. Е. Громов, С. В. Коновалов, М. О. Ефимов, И. А. Панченко, В. В. Шляров

Сибирский государственный индустриальный университет (Россия, 654007, Кемеровская обл. – Кузбасс, Новокузнецк, ул. Кирова, 42)

gromov@physics.sibsiu.ru

Аннотация. Созданные одними из первых и исследованные более 20 лет назад высокоэнтропийные пятикомпонентные сплавы CoCrFeNiMn (сплав Cantor) и CoCrFeNiAl по-прежнему привлекают внимание исследователей в области физического материаловедения из-за возможности их применения в различных отраслях промышленности благодаря удачному сочетанию прочностных и пластических свойств. К настоящему времени накоплен большой экспериментальный материал по управлению свойствами этих сплавов. В настоящей работе выполнен обзор публикаций отечественных и зарубежных авторов по двум направлениям улучшения свойств этих сплавов: легированием, выделениями и термообработкой и использованием фазовых диаграмм CALPHAD. По первому направлению проанализирована роль легирования бором, алюминием, ванадием, кремнием, ниобием; γ- и γ′-нановыделениями, различными режимами термической и деформационной обработки. Сделан вывод о необходимости проведения экспериментов по легированию ВЭС Zr и Nb, хорошо зарекомендовавших себя в упрочнении сталей. Создание и модифицирование свойств пятикомпонентных ВЭС возможно при использовании компьютерных программ CALPHAD, разработанных для расчета диаграмм состояния. Проанализированные в статье результаты публи-

каций по термодинамическому описанию пятикомпонентных сплавов подтверждены сравнением фазовых диаграмм с имеющимися экспериментальными данными. В одной из анализируемых работ по фазообразованию пятикомпонентных состоящих из Co, Cr, Fe, Ni, Al, Mn, Cu ВЭС рассмотрено 2436 композиций, позволивших определить 1761 вариант надежного прогнозирования образования ОЦК/B2 и ГЦК фаз, минуя аморфные фазы и интерметаллиды, тем самым конструируя определенный уровень механических свойств. Показано, что на основе расчета фазовых диаграмм CALPHAD возможен дизайн нового поколения ВЭС.

Ключевые слова: высокоэнтропийные сплавы, легирование, упрочнение, термообработка, программа CALPHAD

Благодарности: Работа выполнена при поддержке гранта Российского научного фонда 23-49-00015.

Для цитирования: Громов В.Е., Коновалов С.В., Ефимов М.О., Панченко И.А., Шляров В.В. Пути улучшения свойств ВЭС Cantor CoCrFeNiMn и CoCrFeNiAl. *Известия вузов. Черная металлургия*. 2024;67(3):283–292.
https://doi.org/10.17073/0368-0797-2024-3-283-292

Introduction

Created in the early 21st century, a new class of metallic materials known as high-entropy alloys (HEAs) has attracted the attention of researchers in the field of physical materials science due to their superior properties compared to conventional alloys [1 – 5]. Among the first five-component HEAs studied were the CoCrFeNiMn (Cantor alloy) and CoCrFeNiAl HEAs [5 – 10], which exhibit a successful combination of strength and plasticity.

Discussion on improving the mechanical and operational properties of these HEAs began shortly after their creation and continues actively to this day. Reviews [11 – 14] have analyzed methods for enhancing the mechanical properties of the CoCrFeNiAl and CoCrFeNiMn HEAs, considering their potential industrial applications. Approaches to solving this problem include grain boundary strengthening [10], solid solution strengthening, creating a nanocrystalline state, strengthening through precipitates, partial amorphization, surface strengthening treatments, developing new production methods for HEAs [14 – 19], ultrasonic treatment [20], and the formation of structure gradients [21]. These methods can significantly expand the application areas of these HEAs. Based on the analysis of experimental results, it has been noted [22] that there are several hundred five-component HEAs containing over 40 different elements. All HEAs are conventionally divided into nine families: *1* – transition 3*d*-metals Al, Co, Cr, Fe, Ni, Mn, Cu, Ti; *2* – refractory metals Hf, Mo, Nb, Ta, Ti, V, W, Zr; *3* – Al, Be, Li, Mn, Se, Sn, Ti, Zn; *4* – transition 4*f*-metals Dy, Gd, Lu, Tb, Tm, Y; *5* – bronzes and brasses; *6* – Ag, Au, Co, Cr, Cu, Ni, Pd, Pt, Rh, Ru with catalytic properties; *7* – high-entropy metallic glasses of the $Fe_{26.7}Co_{26.7}Ni_{26.7}Si_9B_{11}$ type; *8* – high-entropy borides, carbides, nitrides, oxides, silicides; *9* – HEA films and coatings.

Due to the extensive volume of information, the authors limited their analysis to experimental works from the last three years on strengthening and modifying the properties of CoCrFeNiMn and CoCrFeNiAl HEAs, as well as those with similar compositions using CALPHAD. The second research approach involved analyzing works on predicting the composition of HEAs with specific high functional properties using CALPHAD software developed for phase diagram calculations [23 – 26]. These calculations are often combined with experimental verification of the created materials at the final stage known as *integrated computational materials engineering – ICME*. It is believed that this approach can lead to further progress in creating HEAs with desired industrial properties [22]. The need for such analysis is justified by the fact that the most detailed examination of the properties and prospects of HEAs was conducted 3 – 4 years ago [27 – 29], which is a significant period given the pace of publication activity.

In the past 2 – 3 years, there has been an exponential growth in the number of publications dedicated to high-entropy alloys (HEAs) CoCrFeNiAl and CoCrFeNiMn. Consequently, there is a need to identify and analyze the most promising directions for predicting ways to improve the mechanical and operational properties of these HEAs, which is the objective of this work.

Results and discussion

For Cantor CoCrFeNiMn and CoCrFeNiAl alloys, the main approaches to solving the fundamental problem of solid-state physics – improving their mechanical properties – can be identified as follows: analysis of heat treatment, plastic deformation, and external influences; quantum mechanical calculations of crystalline and electronic structure; computer simulation; and the use of phase diagram calculations (CALPHAD), among others [22].

Improvement of mechanical properties of HEAs by alloying, precipitation, and heat treatment

The first approach involves searching for patterns among a large amount of fresh experimental data and forming criteria for improving the strength and plastic properties of HEAs.

Optimally, in terms of strengthening effect for Cantor alloys with FCC and BCC lattices, is vanadium. This is due to its atomic size: it is large for BCC alloys and small

for FCC alloys. There is both quantitative and qualitative evidence for this across a large number of alloys. According to the authors of a study, the optimum concentration of vanadium should be approximately 25 at. %.

By varying the annealing temperature conditions (720 h at 800 °C), it is possible to achieve the precipitation of an FCC phase enriched with chromium and a sigma (σ) phase in the Cantor alloy with manganese content of 10 – 15 and 25 – 30 at. %, respectively. These precipitates do not have an orientation relationship with the BCC matrix. Comparisons with a calculated phase diagram based on a thermodynamic database confirmed the stability prediction of the BCC phase but did not predict the stability of the σ and FCC phases [11; 12; 22]. Microhardness measurements showed that the precipitation of the σ phase significantly strengthens the $CoCrFeMnNi_{2-x}$ (x = 1.25; 1.50) alloy. The obtained results serve as a basis for the development of the composition and heat treatment of the Cantor alloy.

In recent years, attempts have also been made to improve the mechanical properties of the Cantor alloy through alloying with various elements. In a study by Japanese researchers, the role of titanium and silicon in the phase equilibrium and changes in the mechanical properties of the equiatomic Cantor alloy was analyzed. It was shown that titanium stabilizes the σ phase, A12, and C14 Laves phases, while silicon stabilizes the A13 phase. Phase relationships were presented as projections on the isothermal cross section of (CoFeMnNi)-C_{2-x} at 1000 °C of the Cantor alloy. Mechanical tests showed an increase in ultimate strength and yield strength with the addition of titanium and silicon, with the effect of titanium additives being more significant. This may be attributed to the different deformation strengthening of the Cantor alloy with these additives.

In a brief overview, it is not possible to provide a comprehensive analysis of the state of the problem of improving the properties of even two HEAs, but the main trends and approaches can be noted based on the review of the most significant recent publications.

One of the most discussed issues in strengthening these equiatomic alloys is the role of γ and γ′ nanoscale precipitates. In [32], a series of $Ni_{60-x}Co_xCr_{10}Fe_{10}Al_{18}Mo_2$ HEAs (x = 30; 20; 10; 0) with enhanced strength and plastic properties was presented. Increasing the nickel concentration and decreasing the cobalt concentration resulted in the formation of a BCC phase with γ′ particles within it. In the as-cast state, the $Ni_{60}Cr_{10}Fe_{10}Al_{18}Mo_2$ alloy with BCC/γ′ + B2 phase structure exhibited very high values of $\sigma_{0.2}$ (831 MPa).

A systematic study was conducted on the influence of temperature (660 – 960 °C) and time (1 – 48 h) of aging on the mechanical properties of niobium-containing HEAs such as $CoCrNi_{1.5}Nb_{0.2}$. It was observed that aging at 660 °C led to the formation of nanoscale γ″ precipitates with a DO22 superlattice, which strengthened the HEAs through a dislocation slip mechanism [33]. The ultimate strength and yield strength increased with increasing aging time, resulting in an increase in the volume fraction and size of γ″ precipitates, while the elongation decreased. Aging at 860 and 960 °C for 1 h resulted in the formation of semi-coherent ε precipitates with a DO19 structure, changing the strengthening mechanism to the Orowan one.

For the design of microstructure and corresponding properties of nearly equiatomic HEAs such as AlCoCrFeNi, the development of next-generation dispersion-strengthened alloys, a template based on an FCC matrix reinforced with ordered B2 precipitates, was proposed [34]. Using thermodynamic modeling of $Al_{0.5}$CoCrFeNi HEA solutions, isothermal solid-state aging was performed to precipitate fine-scale intragranular B2 phases. Previous studies by these authors have already analyzed the positive role of the B2 phase in ultimate strength and deformation strengthening. In this work, the positive influence of the fine-scale B2 phase on wear resistance and dynamic compression was noted. The yield stress at a true strain of 0.02 % increased more than two times from 670 to 1350 MPa, and the compressive strength increased by 20 % from 1160 to 1500 MPa. Moreover, the wear resistance increased more than fivefold. This result is considered exceptionally important within the proposed approach to improving mechanical properties.

The role of boron in increasing the strength of steel and wear resistance of overlay coatings by forming high-hardness compounds is well-known in classical metallurgy. However, the number of studies on the influence of boron on the structural-phase state and mechanical properties of five-component HEAs is extremely limited. In [35], this gap was addressed for $CoCrFeNiCuB_x$ (x = 0 – 5 at. %) samples obtained by two-stage sintering and vacuum arc melting, using modern methods of physical materials science. It was shown that HEAs based on an FCC matrix contain dendritic phase with a high content of FeCrCoNi and interdendritic phase with a high content of copper. The hardness increased to 337 HV with increasing boron content. At 3 at. % B, the maximum strength of 1900 MPa was achieved in bending tests with good ductility.

In the creation and investigation of strengthening new HEAs, the role of heat treatment is more important than ever. This is demonstrated in [36], where a sample was fabricated using the combined method of cable-pulse arc additive manufacturing (CCW-AAM), and the evolution of microstructure and mechanical properties of the dual-phase CoCrFeNiAl alloy (FCC + ordered B2 phase) was studied during an 8 h heat treatment. At 600 °C, the formation of a large amount of chromium-

rich σ-phase was observed in the B2 matrix, and nanoscale ordered L12 phase was observed in the FCC matrix, resulting in an increase in hardness from 338 to 420 HV, yield strength from 654 to 810 MPa, and ultimate strength from 876 to 1115 MPa, while the elongation decreased from 3.11 to 2.46 %. With an increase in heat treatment temperature to 800 °C, the size of the σ-phase particles increased, and the L12 phase transformed into a B2 phase with high AlNi content. The tensile properties remained unchanged, but the elongation increased by 176 %. Heat treatment at 1000 °C led to significant coarsening of the dissolved σ-phase in the B2 matrix and rod-like precipitates of B2, resulting in strengthening of the alloy. Hardness (308 HV) and yield strength (542 MPa) noticeably decreased, but the elongation increased significantly to 14.2 %. Analysis of these results suggests the potential for creating CoCrFeNiAl HEAs with a combination of high mechanical properties and control over the physical nature of these properties through heat treatment conditions.

One attractive strategy for creating multicomponent cast HEAs is the separation (and/or precipitation) induced by decreasing the configurational entropy during cooling and solidification, as proposed in [37]. It has been noted that the presence of copper in alloys similar to the Cantor alloy expands the phase separation (and precipitation) due to the high positive enthalpy of mixing between copper and various transition metals. It has been suggested that reducing the enthalpy of mixing through the separation of the copper-enriched phase from the Co – Cr or Fe– Cr enriched phases induces two- or three-phase structures. Previous work by the authors of [37] has shown that the hierarchically structured $CrFeNiMn_{0.5}Cu_{0.5}$ HEA exhibited an excellent combination of strength and ductility (1.02 GPa, 28 %), suggesting its potential for industrial applications. However, the deformation mechanisms of this cast alloy with micro- and nano-precipitates are not yet fully understood.

Dispersion strengthening and quasi-linear deformation strengthening in the cast $CoCrCu_{1.5}MnNi$ HEA provide an excellent combination of yield strength and ductility at both room temperature (431.5 MPa, 55 %) and cryogenic conditions (600 MPa, 67 %) [37]. This alloy has a dual FCC phase structure with dendritic regions enriched in Co – Cr and interdendritic regions enriched in Cu – Mn. These regions contain submicron and nanoscale precipitates, respectively, due to the reduced solubility of elements in the two phases. The nature of the quasi-linear deformation strengthening is associated with the accumulation of dislocation-related defects, packing defects, and twins induced by deformation.

The design of the eutectic $AlCoCrFeNi_{2.1}$ HEA is considered in [38] based on the analysis of mechanical properties and mechanisms of cold and hot deformation. This HEA has a typical eutectic microstructure and consists of an FCC phase and eutectic B2 phases with nanoscale precipitates. The yield strength and elongation are 1.2 GPa and 22.8 %, respectively. At –196 °C, the yield strength is 857 MPa, the ultimate strength is 1.48 GPa, and the elongation is ~20 %. This good ductility may be related to the transformation of the L12 phase into a disordered solid solution phase during low-temperature deformation. At high temperatures, the strengthening of the nanoscale B2 and L12 phases occurs through the Orowan mechanism and dislocation cutting. It is noted that the plate-like structure in the as-cast state transformed into a fine equiaxed structure, resulting in improved strength and ductility. The authors considered the construction of HEAs comprehensively from four perspectives. The first method was based on the phase diagram and its modeling, where CoCrFeNi was considered as one of the elements in pseudo-binary eutectic alloys. The second method considered the enthalpy of mixing in multi-component alloys, with $AlCoCrFeNi_{2.1}$ as a reference. Elements with a large negative enthalpy of mixing, such as zirconium, niobium, and hafnium, were selected to replace aluminum. The third method considered valence electrons. The fourth approach focused on creating HEAs without cobalt due to its weak influence on microstructure and phase composition. The importance of the results in [38] lies in the necessity of considering all four perspectives when designing eutectic HEAs with superior properties.

A new paradigm of low-cost Cantor HEA development was proposed in [39]. The strategy of designing super-strong and ductile multi-component BCC alloys involves introducing the so-called “local chemical order” controlled by interstitials and created through simple thermomechanical processing. In the experimental multi-component CoCrFeMnNi alloy, processed by partial recrystallization annealing, a high density of thin racks containing domains of close and medium order predominates. These racks develop from flat dislocation slip bands caused by the internal close order of the alloy during prior cold deformation. In the multicomponent metastable alloy $Fe_{30}Mn_{30}Co_{10}Cr_{10}$ (at. %) with reduced content of expensive nickel and cobalt (compared to the Cantor alloy), the local chemical order consisted of forming heterostructures with non-recrystallized grains with thin racks and a small amount of recrystallized submicron-sized grains with nanonitrides. Due to the strengthening effect of racks, the local chemical order provides an ultra-high yield strength of 1.34 GPa, and deformation twinning contributes to a relative elongation of 13.9 %. The universality of the design strategy is confirmed in multi-component austenitic steel. Using the example of the CoCrNiMnAl HEA, it is shown that one way to achieve a good combination of strength and ductility is by changing the chemical composition. In HEA without iron, this is largely determined by

the absence of brittle σ-phase. Based on thermodynamic predictions, three single-phase BCC HEAs were proposed: $Co_{25}Ni_{30}Mn_{30}Cr_{10}Al_{15}$, $Co_{30}Ni_{25}Mn_{30}Cr_{10}Al_{15}$, and $Co_{30}Ni_{30}Mn_{25}Cr_{10}Al_{15}$, which do not contain the σ-phase. It is shown that the addition of a minimal amount of aluminum provides a strengthening effect due to the formation of a controlled amount of NiAl-B2 precipitates in the microstructure. The alloys, subjected to intensive cold rolling with subsequent short annealing at 1000 °C, achieved high strength values without loss of ductility. The $Co_{30}Ni_{25}Mn_{30}Cr_{10}Al_{15}$ high-entropy alloy, with low defect packing energy, fine grain size, a large volume fraction of twinning, and the formation of small-scale precipitates, represents a HEA with the best combination of strength and ductility.

In summary, considering the publications on the strengthening of five-component HEAs, it can be noted that the number of articles on all HEA families strengthened by vanadium, zirconium, and niobium is limited [41; 42]. From works on classical metallurgy dedicated to studying the effect of microalloying on the properties of steels, the positive role of vanadium, zirconium, and niobium in strengthening, such as in pearlitic steels, is well known. This suggests the need to clarify their role in HEA strengthening, which should become a priority area for further research. Breakthrough achievements can be expected in this field.

Using CALPHAD software

According to its chemical composition, the equiatomic Cantor alloy is expensive for practical applications. In [43], an analysis of alloys with a composition of $Co_{10}Cr_{12}Fe_{43}Mn_{18}Ni_{17}$ was conducted using CALPHAD (Calculation Phase Diagram) software, revealing a cost 40 % lower than that of the equiatomic Cantor alloy. Although these alloys had reduced strength compared to the equiatomic BCC structure at room temperature, they exhibited significantly higher strength at 873 K. This can be largely attributed to deformation twinning due to low defect energy in packing at room temperature. The Labusch model was used to calculate the "softening" effect in the solid solution strengthening of the Cantor alloy. Such calculations allow for the development of an algorithm for designing alloys with specific mechanical properties.

The attempt to automate the evaluation of the kinetic database for BCC equiatomic HEAs seems justified. The development of accurate kinetic databases through parameterization of composition and temperature-dependent atomic mobilities is necessary for correcting multicomponent calculations and CALPHAD modeling. Using the example of the CoCrFeNiMn HEA, an automated evaluation procedure is proposed, which includes storing raw data and evaluation results, automatic weighting, parameter selection, and re-evaluation. The proposed software, written in Python, only uses diffusion indicator data for clear separation of thermodynamic and kinetic data. The created database is valid for the entire composition range of five-component HEAs.

Based on experimental data, the authors of [45] were able to obtain a polynomial equation for strength (hardness) for BCC HEAs containing 4 – 5 elements of the Cantor alloy system. An important conclusion of the study is that as the iron content increases, the strength of the five-component Cantor alloy decreases. This is due to a decrease in the shear modulus with decreasing iron concentration. The role of mixing enthalpy and electron concentration is also important. It is shown that the strength in Cantor alloys increases with decreasing mixing enthalpy and increasing concentration of valence electrons. This is particularly important for controlling mechanical properties, as it allows for purposefully increasing or decreasing their values.

The CALPHAD thermodynamic calculation program can be very useful for the development of new CoCrFeNiMn HEAs with increased strength. Computerized thermodynamic prediction of phase equilibria is the basis for this, as mechanical properties are largely determined by the phase composition of alloys. This task is quite complex due to the incomplete description of ternary systems. In [46], a successful attempt was made to develop a self-consistent thermodynamic description of the five-component Cantor alloy system by completing the description for all triple subsystems and making new thermodynamic assessments for CoCrNi and CoCrMn.

The reliability of the developed thermodynamic description of the five-component Cantor alloy is confirmed by comparing the calculated vertical sections of the five-component phase diagram with available experimental data. This provides a basis for higher-order thermodynamic descriptions of systems with various additional elements.

To improve the strength characteristics of the Cantor alloy, various alloying elements have been and are being introduced [47 – 52]. When designing a new Cantor alloy, it is necessary to consider the possibility of forming intermetallic σ- and B2-phases [53 – 55]. The influence of alloying elements on phase stability is very complex, and their individual contributions to a multi-component alloy like Cantor are small, which makes reliable prediction difficult.

The way forward lies in considering the simultaneous influence of various alloying elements. This can be achieved within the framework of CALPHAD (Calculation of Phase Diagram) [56]. Commercial databases (TCHEA and PanHEA) do not allow for the reproduction of experimental vertical sections of five-element

HEAs and, consequently, cannot adequately predict phase equilibrium between FCC, BCC, and σ-phases. To achieve this, thermodynamic descriptions are needed for all binary and ternary systems. Unfortunately, for most multicomponent HEAs, these have not been developed. According to publications, alloying of HEAs is carried out over a wide range of concentrations, which highlights the importance of developing thermodynamic descriptions for all ternary systems that significantly impact the prediction of phase equilibrium.

The most detailed analysis of phase formation in five-component HEAs consisting of cobalt, chromium, iron, nickel, manganese, aluminum, and copper was conducted in a particular study [57]. A total of 2436 compositions were considered, of which CALPHAD selected 1761 variants for reliable prediction of FCC/B2 and BCC phase formation, excluding the amorphous phase and intermetallics. It was shown that thermodynamic calculations and experimental data closely matched. As the atomic size difference between elements increases, more FCC/B2 phase alloys are formed compared to HEAs with BCC structures. It was found that the concentration of valence electrons is the most important parameter for predicting FCC/B2, BCC, and FCC/B2 + BCC phases. These results are crucial for designing HEAs with specific structures and, consequently, properties.

A new approach to creating five-element eutectic HEAs is proposed in [58]. It is based on the possibility of using composite phase diagrams and the mixing entropy of two- and three-component eutectic alloys in the development of new HEAs. The search for such HEAs is justified, as five-component eutectic HEAs demonstrate a successful combination of high strength and plastic properties [59 – 62] due to their lamellar composite microstructures.

Reliable phase diagrams for five-element alloys are clearly insufficient, so the approach proposed in [58] looks promising. This is confirmed by experimental results in creating eutectic alloys in the AlCoCrFeNi and CoCrFeNiTi systems.

To develop new HEAs with high yield strength, a method combining CALPHAD phase diagram calculations, electronegativity differences, and machine learning [63] is proposed. In the first stage, this method allows avoiding the formation of undesirable brittle phases. Following the trend of creating new HEAs, points with high yield strength and elemental ranges are identified

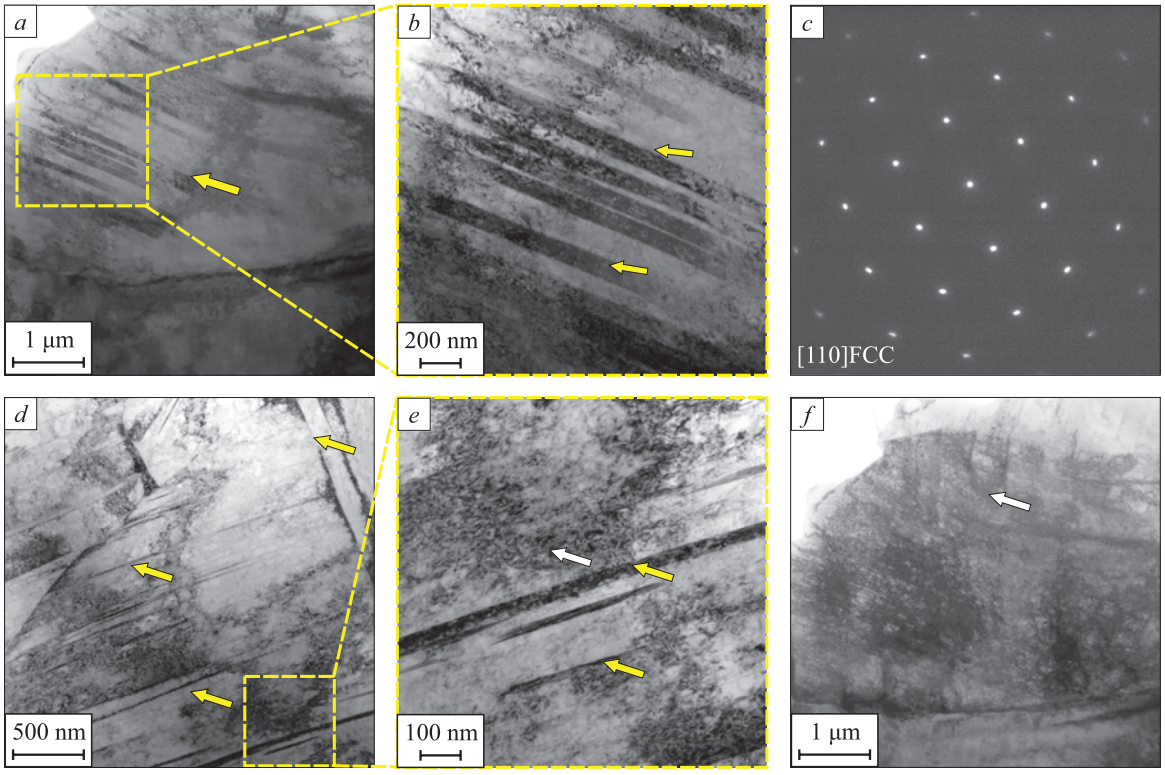

TEM images of the destroyed alloy $Co_{14}Cr_{30}Ni_{50}Mo_6$ [63]:
a, *b* – images of shear bands in a light field and corresponding diffraction patterns of the selected area;
d, *e* – interaction of dislocations with shear bands; *f* – light field, images of a tangle dislocation substructure in another grain

ПЭМ-изображения разрушенного сплава $Co_{14}Cr_{30}Ni_{50}Mo_6$ [63]:
a, *b* – изображения полос сдвига в светлом поле и соответствующие дифракционные картины выбранной области;
d, *e* – взаимодействие дислокаций с полосами сдвига;
f – светлое поле, изображения клубковой дислокационной субструктуры в другом зерне

in the single-phase region. Additionally, if the content of molybdenum and iron is 6 and 0 at. % respectively, the ranges for nickel and cobalt are expanded. The next step is the experimental verification of the developed alloy. It is shown that the yield strength of the single-phase $Co_{14}Cr_{30}Ni_{50}Mo_6$ HEA with a grain size of 17.1 μm was 472 MPa with an electronegativity difference of 0.136. The high ductility and deformation strengthening ability of the alloy are due to the high density of dislocation slip bands and their interaction. The distance between slip bands is about 100 nm (refer to Figure, *b*). The contrast from the slip bands is darker than the FCC matrix, and the presence of high-density dislocation tangles in the slip bands (refer to Figure, *f*). indicates intensive deformation.

For the aerospace industry, the $Al_{10}Co_{19}Cr_{16}Fe_{20}Ni_{35}$ HEA, obtained in the cast state, homogenized at 1200 °C for 8 h, and subjected to step annealing at (24 h) and 590 °C (120 h) [64], can be useful. This provided an FCC matrix microstructure with B2 precipitates and chromium-enriched carbide. The design of this HEA was based on CALPHAD phase diagram calculations. Mechanical testing showed an excellent combination of strength and ductility: the yield strength was 470 MPa, the ultimate strength was 790 MPa, and the elongation was 48 %. The results of this study vividly demonstrate the possibilities of creating next-generation HEAs based on phase diagrams.

Conclusions

Due to the large number of publications accumulated on various directions for improving the mechanical properties of the CoCrFeNiMn (Cantor alloy) and CoCrFeNiAl HEAs, an analysis of works from the last three years on alloying, strengthening by precipitations, heat treatment, and the use of CALPHAD phase diagrams has been carried out.

References / Список литературы

1. Yeh J.W. Recent progress in high-entropy alloys. *Annales de Chimie – Science des Matériaux*. 2006;31(6):633–648. http://dx.doi.org/10.3166/acsm.31.633-648
2. Ma L.-S., Fu G.-L., Tian F.-C., Zhang T.-Y. Recent progress in high-entropy alloys. *Advanced Materials Research*. 2013;631-632:227–232. https://doi.org/10.4028/www.scientific.net/AMR.631-632.227
3. Zhang Y., Zuo T.T., Tang Z., Gao M.C., Dahmen K.A., Liaw P.K., Lu Z.P. Microstructures and properties of high-entropy alloys. *Progress in Materials Science*. 2014;61:1–93. https://doi.org/10.1016/j.pmatsci.2013.10.001
4. Cantor B., Chang I.T.H., Knight P., Vincent A.J.B. Microstructural development in equiatomic multicomponent alloys. *Materials Science and Engineering: A*. 2004;375-377:213–218. https://doi.org/10.1016/j.msea.2003.10.257
5. George E.P., Curtin W.A., Tasan C.C. High entropy alloys: A focused review of mechanical properties and deformation mechanisms. *Acta Materialia*. 2020;188:435–474. https://doi.org/10.1016/j.actamat.2019.12.015
6. Osintsev K.A., Konovalov S.V., Glezer A.M., Gromov V.E., Ivanov Yu.F., Panchenko I.A., Sundeev R.V. Research on the structure of $Al_{2.1}Co_{0.3}Cr_{0.5}FeNi_{2.1}$ high-entropy alloy at submicro- and nano-scale levels. *Materials Letters*. 2021;294:129717. https://doi.org/10.1016/j.matlet.2021.129717
7. Li Z., Zhao S., Ritchie R.O., Meyers M.A. Mechanical properties of high-entropy alloys with emphasis on face-centered cubic alloys. *Progress in Materials Science*. 2019;102:296–345. https://doi.org/10.1016/j.pmatsci.2018.12.003
8. Cantor B., Chang I.T.H., Knight P., Vincent A.J.B. Microstructural development in equiatomic multicomponent alloys. *Materials Science and Engineering: A*. 2004;375-377:213–218. https://doi.org/10.1016/j.msea.2003.10.257
9. Otto F., Dlouhy A., Somsen C., Bei H., Eggeler G., George E.P. The influences of temperature and microstructure on the tensile properties of a CoCrFeMnNi high-entropy alloy. *Acta Materialia*. 2013;61(15):5743–5755. https://doi.org/10.1016/j.actamat.2013.06.018
10. Schuh B., Mendez-Martin F., Volker B., George E.P., Clemens H., Pippan R., Hohenwarter A. Mechanical properties, microstructure and thermal stability of a nanocrystalline CoCrFeMnNi high-entropy alloy after severe plastic deformation. *Acta Materialia*. 2015;96:258–268. https://doi.org/10.1016/j.actamat.2015.06.025
11. Gromov V.E., Konovalov S.V., Ivanov Yu.F., Osintsev K.A. Structure and Properties of High-Entropy Alloys. Springer, Advanced structured materials; 2021:110.
12. Gromov V.E., Ivanov Yu.F., Osintsev K.A., Shlyarova Yu.A., Panchenko I.A. Structure and Properties of High-Entropy Alloys. Moscow: RuScience; 2021:203.
13. Osintsev K.A., Gromov V.E., Konovalov S.V., Ivanov Yu.F., Panchenko I.A. High-entropy alloys: Structure, mechanical properties, deformation mechanisms and application. *Izvestiya. Ferrous Metallurgy*. 2021;64(4):249–258. (In Russ.). https://doi.org/10.17073/0368-0797-2021-4-249-258

Осинцев К.А., Громов В.Е., Коновалов С.В., Иванов Ю.Ф., Панченко И.А. Высокоэнтропийные сплавы: структура, механические свойства, механизмы деформации и применение. *Известия вузов. Черная металлургия*. 2021;64(4):249–258. https://doi.org/10.17073/0368-0797-2021-4-249-258
14. Gromov V.E., Rubannikova Yu.A., Konovalov S.V., Osintsev K.A., Vorob'ev S.V. Generation of increased mechanical properties of Cantor high-entropy alloy. *Izvestiya. Ferrous Metallurgy*. 2021;64(8):599–605. (In Russ.). https://doi.org/10.17073/0368-0797-2021-8-599-605

Громов В.Е., Рубанникова Ю.А., Коновалов С.В., Осинцев К.А., Воробьёв С.В. Формирование улучшенных механических свойств высокоэнтропийного сплава Cantor. *Известия вузов. Черная металлургия*. 2021; 64(8):599–605. https://doi.org/10.17073/0368-0797-2021-8-599-605
15. Coury F.G., Kaufman M., Clarke A.J. Solid-solution strengthening in refractory high entropy alloys. *Acta Materialia*. 2019;175:66–81. https://doi.org/10.1016/j.actamat.2019.06.006
16. Ikeda Y., Tanaka I., Neugebauer J., Kormann F. Impact of interstitial C on phase stability and stacking-fault energy of the CrMnFeCoNi high-entropy alloy. *Physical Review*

Materials. 2019;3:113603. https://doi.org/10.1103/PhysRevMaterials.3.113603

17. Li F., Zhao H., Yue Y., Yang Z., Zhang Y., Gou L. Dual-phase super-strong and elastic ceramic. *ACS Nano*. 2019;13(4): 4191–4198. https://doi.org/10.1021/acsnano.8b09195
18. Li Z., Kormann F., Grabowski B., Neugebauer J., Raabe D. Ab initio assisted design of quinary dual-phase high-entropy alloys with transformation-induced plasticity. *Acta Materialia*. 2017;136:262–270. https://doi.org/10.1016/j.actamat.2017.07.023
19. Gromov V.E., Ivanov Yu.F., Glezer A.M., Konovalov S.V., Alsaraeva K.V. Structural evolution of silumin treated with a high-intensity pulse electron beam and subsequent fatigue loading up to failure. *Bulletin of the Russian Academy of Sciences. Physics*. 2015;79(9):1169–1172. https://doi.org/10.3103/S1062873815090087
20. Listyawan T.A., Lee H., Park N., Lee U. Microstructure and mechanical properties of CoCrFeMnNi high entropy alloy with ultrasonic nanocrystal surface modification process. *Journal of Materials Science and Technology*. 2020;57: 123–130. https://doi.org/10.1016/j.jmst.2020.02.083
21. Guo L., Wu W., Ni S., Yuan Z., Cao Y., Wang Z., Song M. Strengthening the $FeCoCrNiMo_{0.15}$ HEA by gradient structure. *Journal of Alloys and Compounds*. 2020;841:155688. https://doi.org/10.1016/j.jallcom.2020.155688
22. Rogachev A.S. Structure, stability and properties of high entropy alloys. *Fizika metallov i metallovedenie*. 2020; 121(8):807–841. (In Russ.). https://doi.org/10.31857/S0015323020080094

    Рогачев А.С. Структура, стабильность и свойства высокоэнтропийных сплавов. *Физика металлов и металловедение*. 2020;121(8):807–841. https://doi.org/10.31857/S0015323020080094
23. Raturi A., Aditya C.J., Gurao N.P., Biswak K. ICME approach to explore equiatomic and non-equiatomic single phase BCC refractory high entropy alloys. *Journal of Alloys and Compounds*. 2019;806:587–595. https://doi.org/10.1016/j.jallcom.2019.06.387
24. Senkov O.N., Zhang C., Pilchak A.L., Payton E.J., Woodward C., Zhang F. CALPHAD-aided development of quaternary multi-principal element refractory alloys based on NbTiZr. *Journal of Alloys and Compounds*. 2019;783: 729–742. https://doi.org/10.1016/j.jallcom.2018.12.325
25. Menou E., Tancret F., Toda-Caraballo I., Ramstein G., Castany P., Bertrand E., Gautier N., Rivera Díaz-Del-Castillo P.E.J. Computational design of light and strong high entropy alloys (HEA): Obtainment of an extremely high specific solid solution hardening. *Scripta Materialia*. 2018;156:120–123. https://doi.org/10.1016/j.scriptamat.2018.07.024
26. Tapia A.J.S.E, Yim D., Kim H.S., Lee B.-J. An approach for screening single phase high-entropy alloys using an in-house thermodynamic database. *Intermetallics*. 2018;101:56–63. https://doi.org/10.1016/j.intermet.2018.07.009
27. Alaneme K.K., Bodunrin M.O., Oke S.R. Processing, alloy composition and phase transition effect on the mechanical and corrosion properties of high entropy alloys: a review. *Journal of Materials Research and Technology*. 2016;5(4):384–393. https://doi.org/10.1016/j.jmrt.2016.03.004
28. Murty B.S., Yeh J.W., Ranganathan S., Bhattacharjee P.P. High-Entropy Alloys. 2nd ed. Amsterdam: Elsevier; 2019:374.
29. Zhang Y. High-Entropy Materials. A Brief Introduction. Singapore: Springer Nature; 2019:159.
30. Yin B., Maresca F., Curtin W.A. Vanadium is an optimal element for strengthening in both fcc and bcc high-entropy alloys. *Acta Materialia*. 2020;188:486–491. https://doi.org/10.1016/j.actamat.2020.01.062
31. Yamanaka S., Ikeda Ki., Miura S. The effect of titanium and silicon addition on phase equilibrium and mechanical properties of CoCrFeMnNi-based high entropy alloy. *Journal of Materials Research*. 2021;36:2056–2070. https://doi.org/10.1557/s43578-021-00251-0
32. Jia Y., Wang Z., Wu Q., He F., Li J., Wang J. Enhancing the yield strength of Ni-Co-Cr-Fe-Al as-cast hypoeutectic high-entropy alloys by introducing γ′ precipitation. *Materials Science and Engineering: A*. 2022;858:144190. https://doi.org/10.1016/j.msea.2022.144190
33. Zhou H., Lin Y., Chen F., Shen Q. Effect of precipitation behavior on mechanical properties of a Nb-containing CoCrNi-based high-entropy alloy. *Metals and Materials International*. 2023;29:674–692. https://doi.org/10.1007/s12540-022-01265-x
34. Gwalani B., Torgerson T., Dasari S., Jagetia A., Nartu M.S.K.K.Y., Gangireddy S., Pole M., Wang T., Scharf T.W., Banerjee R. Influence of fine-scale B2 precipitation on dynamic compression and wear properties in hypoeutectic $Al_{0.5}CoCrFeNi$ high-entropy alloy. *Journal of Alloys and Compounds*. 2021;853:157126. https://doi.org/10.1016/j.jallcom.2020.157126
35. Algan Şimşek İ.B., Arık M.N., Talaş Ş., Kurt A. The effect of B addition on the microstructural and mechanical properties of FeNiCoCrCu high entropy alloys. *Metallurgical and Materials Transactions A*. 2021;52:1749–1758. https://doi.org/10.1007/s11661-021-06186-9
36. Shen Q., Kong X., Chen X. Significant transitions of microstructure and mechanical properties in additively manufactured Al-Co-Cr-Fe-Ni high-entropy alloy under heat treatment. *Materials Science and Engineering: A*. 2021;815:141257. https://doi.org/10.1016/j.msea.2021.141257
37. Shim S.H., Pouraliakbar H., Lee B.J., Kim Y.K., Rizi M.S., Hong S.I. Strengthening and deformation behavior of as-cast $CoCrCu_{1.5}MnNi$ high entropy alloy with micro-/nanoscale precipitation. *Materials Science and Engineering: A*. 2022;853:143729. https://doi.org/10.1016/j.msea.2022.143729
38. Xie X., Li N., Liu W., Huang S., He X., Yu Q., Xiong H., Wang E., Hou X. Research progress of refractory high entropy alloys: A review. *Chinese Journal of Mechanical Engineering*. 2022;35:142. https://doi.org/10.1186/s10033-022-00814-0
39. He Z., Guo Y., Sun L., Yan H.-L., Guan X., Jiang S., Shen Y., Yin W., Zhao X., Li Z., Jia N. Interstitial-driven local chemical order enables ultrastrong face-centered cubic multicomponent alloys. *Acta Materialia*. 2023;243:118495. https://doi.org/10.1016/j.actamat.2022.118495
40. Mehranpour M.S., Shahmir X., Kim H.S. Microstructure tailoring by manipulating chemical composition in novel CoNiMnCrAl high-entropy alloys. *Journal of Alloys and Compounds*. 2023;944:169207. https://doi.org/10.1016/j.jallcom.2023.169207
41. Knieps M.S., Messe O.M.D.M., Barriobero-Vila P., Hecht U. Advanced characterization of two novel Fe-rich high

entropy alloys developed for laser powder bed fusion in the Al-Co-Cr-Fe-Ni-Zr system. *Materialia*. 2022;26:101615. https://doi.org/10.1016/j.mtla.2022.101615

42. Abbasi E., Dehghani K. Phase prediction and microstructure of centrifugally cast non-equiatomic Co-Cr-Fe-Mn-Ni(Nb,C) high entropy alloys. *Journal of Alloys and Compounds*. 2019;783:292–299. https://doi.org/10.1016/j.jallcom.2018.12.329

43. Conway P.L.J., Klaver T.P.C., Steggo J., Ghassemali E. High entropy alloys towards industrial applications: High-throughput screening and experimental investigation. *Materials Science and Engineering: A*. 2022;830:142297. https://doi.org/10.1016/j.msea.2021.142297

44. Abrahams K., Zomorodpoosh S., Khorasgani A., Roslyakova I., Steinbach I., Kundin J. Automated assessment of a kinetic database for fcc Co-Cr-Fe-Mn-Ni high entropy alloys. *Modelling and Simulation in Materials Science and Engineering*. 2021;29:055007. https://doi.org/10.1088/1361-651X/abf62b

45. Shafiei A. Simple approach to model the strength of solid-solution high entropy alloys in Co-Cr-Fe-Mn-Ni system. *Strength of Materials*. 2022;54:705–716. https://doi.org/10.1007/s11223-022-00448-6

46. Do H.-S., Choi W.-M., Lee B.-J. A thermodynamic description for the Co–Cr–Fe–Mn–Ni system. *Journal of Materials Science*. 2022;57:1373–1389. https://doi.org/10.1007/s10853-021-06604-8

47. Li Z., Pradeep K.G., Deng Y., Raabe D., Tasan C.C. Metastable high-entropy dual-phase alloys overcome the strength–ductility trade-off. *Nature*. 2016;534:227–230. https://doi.org/10.1038/nature17981

48. Gao N., Lu D.H., Zhao Y.Y., Liu X.W., Liu G.H., Wu Y., Liu G., Fan Z.T., Lu Z.P., George E.P. Strengthening of a CrMnFeCoNi high-entropy alloy by carbide precipitation. *Journal of Alloys and Compounds*. 2019;792:1028–1035. https://doi.org/10.1016/j.jallcom.2019.04.121

49. Wang Z., Baker I., Guo W., Poplawsky J.D. The effect of carbon on the microstructures, mechanical properties, and deformation mechanisms of thermo-mechanically treated $Fe_{40.4}Ni_{11.3}Mn_{34.8}Al_{7.5}Cr_6$ high entropy alloys. *Acta Materialia*. 2017;126:346–360. https://doi.org/10.1016/j.actamat.2016.12.074

50. Peng H., Hu L., Li L., Gao J., Zhang Q. On the correlation between $L1_2$ nanoparticles and mechanical properties of $(NiCo)_{52+2x}(AlTi)_{4+2x}Fe_{29-4x}Cr15$ (x=0–4) high-entropy alloys. *Journal of Alloys and Compounds*. 2020;817:152750. https://doi.org/10.1016/j.jallcom.2019.152750

51. Jo Y.H., Jung S., Choi W.-M., Sohn S.S., Kim H.S., Lee B.-J., Kim N.J., Lee S. Cryogenic strength improvement by utilizing room-temperature deformation twinning in a partially recrystallized VCrMnFeCoNi high-entropy alloy. *Nature Communications*. 2017;8:15719. https://doi.org/10.1038/ncomms15719

52. Lu Y., Dong Y., Guo S., Jiang L., Kang H., Wang T., Wen B., Wang Z., Jie J., Cao Z., Ruan H., Li T. A promising new class of high-temperature alloys: Eutectic high-entropy alloys. *Scientific Reports*. 2014;4:6200. https://doi.org/10.1038/srep06200

53. Zhang Y., Chen Z., Cao D., Zhang J., Zhang P., Tao Q., Yang X. Concurrence of spinodal decomposition and nano-phase precipitation in a multi-component AlCoCrCuFeNi high-entropy alloy. *Journal of Materials Research and Technology*. 2019;8(1):726–736. https://doi.org/10.1016/j.jmrt.2018.04.020

54. Otto F., Dlouhý A., Pradeep K.G., Kuběnová M., Raabe D., Eggeler G., George E.P. Decomposition of the single-phase high-entropy alloy CrMnFeCoNi after prolonged anneals at intermediate temperatures. *Acta Materialia*. 2016;112:40–52. https://doi.org/10.1016/j.actamat.2016.04.005

55. Stepanov N.D., Shaysultanov D.G., Ozerov M.S., Zherebtsov S.V., Salishchev G.A. Second phase formation in the CoCrFeNiMn high entropy alloy after recrystallization annealing. *Materials Letters*. 2016;185:1–4. https://doi.org/10.1016/j.matlet.2016.08.088

56. Lukas H.L., Fries S.G., Sundman B. Computational Thermodynamics: The Calphad Method. Cambridge: Cambridge University Press; 2007:313. https://doi.org/10.1017/CBO9780511804137

57. Wang C., Zhong W., Zhao J. Insights on phase formation from thermodynamic calculations and machine learning of 2436 experimentally measured high entropy alloys. *Journal of Alloys and Compounds*. 2022;915:165173. https://doi.org/10.1016/j.jallcom.2022.165173

58. Shafiei A. Design of Eutectic high entropy alloys. *Metallurgical and Materials Transactions A*. 2022;53:4329-4361. https://doi.org/10.1007/s11661-022-06831-x

59. Gao X., Lu Y., Zhang B., Liang N., Wu G., Sha G., Liu J., Zhao Y. Microstructural origins of high strength and high ductility in an $AlCoCrFeNi_{2.1}$ eutectic high-entropy alloy. *Acta Materialia*. 2017;141:59–66. https://doi.org/10.1016/j.actamat.2017.07.041

60. Wani I.S., Bhattacharjee T., Sheikh S., Bhattacharjee P.P., Guo S., Tsuji N. Tailoring nanostructures and mechanical properties of $AlCoCrFeNi_{2.1}$ eutectic high entropy alloy using thermo-mechanical processing. *Materials Science and Engineering: A*. 2016;675:99–109. https://doi.org/10.1016/j.msea.2016.08.048

61. Zhang P.C., Zhai B., Wang H.P. Effect of microstructure, strain rate, and elevated temperature on the compression property of Fe-Co-Ni-Cr-Zr alloy. *Metallurgical and Materials Transactions A*. 2023;54:346–357. https://doi.org/10.1007/s11661-022-06887-9

62. Wu M., Wang S., Huang H., Shu D., Sun B. CALPHAD aided eutectic high-entropy alloy design. *Materials Letters*. 2020;262:127175. https://doi.org/10.1016/j.matlet.2019.127175

63. Yan J., Song Z., Fang W., He X., Chang R., Huang S., Huang J., Yu H., Yin F. Composition design of high yield strength points in single-phase Co-Cr-Fe-Ni-Mo multi-principal element alloys system based on electronegativity, thermodynamic calculations, and machine learning. *Tungsten*. 2023;5:169–178. https://doi.org/10.1007/s42864-021-00129-y

64. Yen S., Liu Y., Chu S., Chang C., Lin S., Tsai M. B2-strengthened Al-Co-Cr-Fe-Ni high entropy alloy with high ductility. *Materials Letters*. 2022;325:132928. https://doi.org/10.1016/j.matlet.2022.132828

Information about the Authors

Viktor E. Gromov, *Dr. Sci. (Phys.-Math.), Prof., Head of the Chair of Science named after V.M. Finkel',* Siberian State Industrial University
ORCID: 0000-0002-5147-5343
E-mail: gromov@physics.sibsiu.ru

Sergei V. Konovalov, *Dr. Sci. (Eng.), Prof., Vice-Rector for Research and Innovation,* Siberian State Industrial University
ORCID: 0000-0003-4809-8660
E-mail: konovserg@gmail.com

Mikhail O. Efimov, *Candidates for a degree of Cand. Sci. (Eng.) of the Chair of Science named after V.M. Finkel',* Siberian State Industrial University
ORCID: 0000-0002-4890-3730
E-mail: moefimov@mail.ru

Irina A. Panchenko, *Cand. Sci. (Eng.), Head of the Laboratory of Electron Microscopy and Image Processing,* Siberian State Industrial University
ORCID: 0000-0002-1631-9644
E-mail: i.r.i.ss@yandex.ru

Vitaly V. Shlyarov, *Postgraduate of the Chair of Science named after V.M. Finkel', Research Associate of the Laboratory of Electron Microscopy and Image Processing,* Siberian State Industrial University
ORCID: 0000-0001-8130-648X
E-mail: shlyarov@mail.ru

Сведения об авторах

Виктор Евгеньевич Громов, *д.ф.-м.н., профессор, заведующий кафедрой естественнонаучных дисциплин им. профессора В.М. Финкеля,* Сибирский государственный индустриальный университет
ORCID: 0000-0002-5147-5343
E-mail: gromov@physics.sibsiu.ru

Сергей Валерьевич Коновалов, *д.т.н., профессор, проректор по научной и инновационной деятельности,* Сибирский государственный индустриальный университет
ORCID: 0000-0003-4809-8660
E-mail: konovserg@gmail.com

Михаил Олегович Ефимов, *соискатель степени к.т.н. кафедры естественнонаучных дисциплин им. профессора В.М. Финкеля,* Сибирский государственный индустриальный университет
ORCID: 0000-0002-4890-3730
E-mail: moefimov@mail.ru

Ирина Алексеевна Панченко, *к.т.н., заведующий лабораторией электронной микроскопии и обработки изображений,* Сибирский государственный индустриальный университет
ORCID: 0000-0002-1631-9644
E-mail: i.r.i.ss@yandex.ru

Виталий Владиславович Шляров, *аспирант кафедры естественнонаучных дисциплин им. профессора В.М. Финкеля, научный сотрудник лаборатории электронной микроскопии и обработки изображений,* Сибирский государственный индустриальный университет
ORCID: 0000-0001-8130-648X
E-mail: shlyarov@mail.ru

Contribution of the Authors

V. E. Gromov – analysis of the works of foreign authors on strengthening of CoCrFeNiMn and CoCrFeNiAl HEAs by alloying.
S. V. Konovalov – analysis of the works of foreign authors on strengthening of CoCrFeNiMn and CoCrFeNiAl HEAs based on CALPHAD programs.
M. O. Efimov – analysis of drawings and EM images in the works of foreign authors on strengthening of HEAs by alloying.

I. A. Panchenko – analysis of drawings and EM images in the works of foreign authors on strengthening of HEAs based on CALPHAD programs.
V. V. Shlyarov – design of the article, discussion of the results.

Вклад авторов

В. Е. Громов – анализ работ зарубежных авторов по упрочнению CoCrFeNiMn и CoCrFeNiAl ВЭС путем легирования.
С. В. Коновалов – анализ работ зарубежных авторов по упрочнению CoCrFeNiMn и CoCrFeNiAl ВЭС на основе программ CALPHAD.

М. О. Ефимов – анализ рисунков и электронных микроскопических изображений в работах зарубежных авторов по упрочнению ВЭС путем легирования.
И. А. Панченко – анализ рисунков и электронных микроскопических изображений в работах зарубежных авторов по упрочнению ВЭС на основе программ CALPHAD.
В. В. Шляров – оформление статьи, обсуждение результатов.

Received 10.05.2023
Revised 25.12.2023
Accepted 29.03.2024

Поступила в редакцию 10.05.2023
После доработки 25.12.2023
Принята к публикации 29.03.2024

MATERIALS SCIENCE / МАТЕРИАЛОВЕДЕНИЕ

UDC 621.791.011
DOI 10.17073/0368-0797-2024-3-293-302

Original article
Оригинальная статья

Calculations of phase composition of austenitic high-nitrogen welding wire and study of a welded joint made from it

V. S. Kostina ✉, **M. V. Kostina, D. V. Zinoveev, A. E. Kudryashov**

Baikov Institute of Metallurgy and Materials Science, Russian Academy of Sciences (49 Leninskii Ave., Moscow 119991, Russian Federation)

✉ vskostina@yandex.ru

Abstract. The processability of a material is directly related to the possibility of its production, operation and maintainability. One of the most important indicators of the processability of any metal is weldability. Austenitic steels with a high nitrogen content proved themselves as high-strength, corrosion- and cold-resistant materials, but the issue of their weldability is still not fully understood. The lack of welding filler materials on the market specifically designed for welding high-nitrogen steels is the primary obstacle to solving this problem. Thus, the goal of the work was to develop and obtain a laboratory sample of high-nitrogen welding wire. Based on calculations of nitrogen solubility and the phase composition of the weld metal, the chemical composition of Cr–Mn–Ni–Mo–V,N steel was selected for this wire. A defect-free ingot with 0.57 % N was obtained, and wire with a nitrogen content of 0.57 wt. % was produced using hot plastic deformation and drawing methods. Testing of this wire to obtain a welded joint of austenitic cast steel, close to it in chemical composition, with the welding process carried out according to the developed technological recommendations, made it possible to obtain a defect-free welded joint without loss of nitrogen in the weld metal. With a microhardness of the base metal of 252 HV_{50}, due to the alloying of the welding wire steel with nitrogen and vanadium, the metal of the weld and fusion line had a high microhardness (278 and 273 HV_{50}, respectively), significantly exceeding the microhardness of Cr–Ni cast austenite. The metal of the welded joint has high strength (0.9 of the base metal strength) and high impact toughness. The fracture of impact samples is characterized by a dimple structure characteristic of viscous materials. According to the obtained results, the new welding wire showed itself to be a promising material for welding austenitic high-nitrogen steels.

Keywords: high-nitrogen steel, welded joint, manual arc welding, high-nitrogen welding wire, mechanical properties, impact strength, fractography

Acknowledgements: The work was supported by the President, grant No. MK-1100.2022.4.

For citation: Kostina V.S., Kostina M.V., Zinoveev D.V., Kudryashov A.E. Calculations of the phase composition of austenitic high-nitrogen welding wire and study of a welded joint made from it. *Izvestiya. Ferrous Metallurgy*. 2024;67(3):293–302.
https://doi.org/10.17073/0368-0797-2024-3-293-302

Расчеты фазового состава аустенитной высокоазотистой сварочной проволоки и исследование выполненного из нее сварного соединения

В. С. Костина ✉, **М. В. Костина, Д. В. Зиновеев, А. Э. Кудряшов**

Институт металлургии и материаловедения им. А.А. Байкова РАН (Россия, 119991, Москва, Ленинский пр., 49)

✉ vskostina@yandex.ru

Аннотация. Технологичность материала напрямую связана с возможностью его производства, эксплуатации и ремонтопригодности. Одним из важнейших показателей технологичности металла является свариваемость. Аустенитные стали с высоким содержанием азота проявили себя как высокопрочные, коррозионно- и хладостойкие материалы, однако вопрос их свариваемости до сих пор раскрыт не до конца. Отсутствие на рынке сварочных присадочных материалов, специально разработанных для сварки высокоазотистых сталей, первостепенная преграда перед решением обозначенной проблемы. В связи с этим целью данной работы является разработка и получение лабораторного образца высокоазотистой сварочной проволоки. На основе проведенных расчетов растворимости азота и фазового состава металла шва выбран химический состав Cr–Mn–Ni–Mo–V,N стали для этой проволоки. Получен бездефектный слиток с 0,57 % N и методами горячей пластической деформации и волочения изготовлена проволока с содержанием 0,57 мас. % N. Опробование этой проволоки для получения сварного соединения аустенитной литейной стали, близкой к ней по химическому составу, с проведением

процесса сварки по разработанным технологическим рекомендациям, позволило получить бездефектное сварное соединение без потери азота в металле шва. При микротвердости основного металла 252 HV_{50}, благодаря легированию стали сварочной проволоки азотом и ванадием металл сварного шва и линии сплавления имел высокую микротвердость (278 и 273 HV_{50} соответственно), заметно превышающую микротвердость Cr–Ni литого аустенита. Металл сварного соединения характеризовался высокой прочностью (0,9 от прочности основного металла) и высокой ударной вязкостью. Излому ударных образцов присуще характерное для вязких материалов ямочное строение. По результатам исследования новая сварочная проволока показала себя как перспективный материал для сварки аустенитных высокоазотистых сталей.

Ключевые слова: высокоазотистая сталь, сварное соединение, ручная дуговая сварка, высокоазотистая сварочная проволока, механические свойства, ударная вязкость, фрактография

Благодарности: Работа выполнена при финансовой поддержке гранта Президента МК-1100.2022.4.

Для цитирования: Костина В.С., Костина М.В., Зиновеев Д.В., Кудряшов А.Э. Расчеты фазового состава аустенитной высокоазотистой сварочной проволоки и исследование выполненного из нее сварного соединения. *Известия вузов. Черная металлургия*. 2024;67(3):293–302. https://doi.org/10.17073/0368-0797-2024-3-293-302

Introduction

Due to the combination of properties, austenitic high-nitrogen steels can be used in mechanical engineering, instrumentation technology, medicine, oil and gas industry, for everyday necessities, etc. The practical application of such steels implies good processability, including weldability. While welding austenitic steels with high concentration of nitrogen (0.4 – 0.6 %), it is recommended to use the welding filler with the increased concentration of this element. It is difficult to obtain high quality welded joints of such steels as the welding filler materials developed specifically for welding high-nitrogen steels are not available in the market [1; 2]. Until recently, filler materials for welding this type of steel were chosen based on the following principles.

1. The Fe–Cr–Ni–Mo welding filler was used. In some cases, they contain small amounts of manganese and 0.10 – 0.25 % of nitrogen[1] [3; 4]. In this case, for the welding material to retain its austenitic structure, the nickel concentration in it should be significantly (~2 times) increased (compared to common stainless steels) [5; 6]. Also, for the same purpose, the carbon concentration may be slightly increased [7 – 10]. This option is most feasible in practice, but it has a number of disadvantages:

– the steel strength reduces due to the lack of solid-solution hardening with nitrogen;

– the balance shifts towards ferrite formation.

In some cases, a certain amount of nitrogen gas [11 – 14] or nitride-containing powder [15] are added to the shielding gas to increase the nitrogen content in the weld metal during welding. Addition of nitrogen in the properly calculated concentration during the welding process results in decreased ferrite amount, enhanced ductility and corrosion resistance [16 – 19].

2. Ni-based welding filler materials originally developed for welding heat-resistant steels can be used [4; 20]. They are characterized by high performance properties, but contain a large number of expensive alloying elements: 55 – 68 % Ni and 2.5 – 16 % Mo. When high-nickel fillers are used, low welding current should be applied for welding so that the high-nitrogen base metal is not mixed with the filler metal. Otherwise, the mixing zone will be depleted of nitrogen due to the high concentration of nickel, which reduces nitrogen solubility [21], thus making its zone the most vulnerable area of the welded joint [22].

3. The metal with the chemical composition similar or identical to that of the base metal can be used as the filler, this option is called autogenous TIG welding [23]. The advantage of this method is that the concentration of nitrogen in the welding filler is as high as that in the base metal, therefore, the welded joint can be expected to be quite strong. However, this option cannot be used on an industrial scale if thin base metal rods are applied for autogenous TIG welding, as many welding processes involve automatic wire feeding.

Recently, the issue of selecting welding filler materials for welding high-nitrogen steels has attracted special attention. A number of research groups have reported the development of welding wire samples with high-nitrogen content [17; 19; 24].

The authors of [24] developed three samples of experimental Cr–Mn–Ni welding wires with a nitrogen content of 0.15; 0.6 and 0.9 %. Welded joints of 22Cr–16Mn–2Ni–0.75N high-nitrogen steel were obtained using the developed wires in argon shielding gas. During the welding process, the resulting degassing of nitrogen in the molten wire droplets led to reduction in nitrogen content in the weld hard metal. As a result, some amount of ferrite was formed in the metal of welds obtained using wires with a nitrogen content of 0.6 and 0.9 %, which led to a drop in the impact strength of welded joints. At the same time, porosity was revealed in the metal of the weld with the highest nitrogen content, which negatively affected the strength of the welded

[1] https://www-eng.lbl.gov/~shuman/NEXT/MATERIALS&COMPONENTS/ss-weld_manual_avesta.pdf

joint. The welded joint with 0.15 % N had an austenitic structure, however, due to the low nitrogen concentration, its strength characteristics were the lowest.

In the study [17], welded joints of 22Cr–2Ni–16Mn–0.75N steel were obtained by arc welding using the 20Cr–2Mo–18Mn–0.6N filler. To prevent the risks of losing nitrogen from the welding wire, the Ar–N_2–CO_2 mixture was used as the shielding gas. It was found that as the CO_2 content increases, so does the nitrogen content in the weld metal, which results in enhanced strength and impact strength of the welded joint. The addition of N_2 gas (up to 7 %) also boosted the nitrogen content in the weld metal. During automatic arc welding described in [19], welded joints of 21Cr–Ni–17Mn–4Mo–0.8N steel were obtained in a shielding gas mixture of 93.5 % Ar + 5 % N_2 + 1.5 % O_2 while experimental 21Cr–2Ni–17Mn–2Mo–0.78N welding wire was used. The wire feed speed and voltage were varied. It was found that a low wire feed speed (3 – 8 m/min) at moderate arc voltage (up to 20 V) is preferable to ensure a stable welding process. The use of high welding speeds and higher voltages resulted in wire metal scattering and smoke in the arc burning area.

Having analyzed the reasons behind the difficulties hampering the development of a suitable high-nitrogen welding wire, we can emphasize the following. When designing a wire, it is important to take into account the chemical composition, post-weld microstructure formed by the welding wire metal and the weld crystallization mode. All of these factors can affect the wire manufacturing technology. The higher the nitrogen content of the wire metal, the more metal degassing will occur during the welding process. Accordingly, ingots obtained by smelting under nitrogen pressure are not suitable for this purpose. When developing the wire chemical composition, it is also important to take into account the content of alloying elements that tend to form hard and brittle nitrides during welding, such as Cr, Nb and V. In addition, the stacking fault energy enhances with increasing nitrogen content, which may create difficulties for welding wire drawing from steel with high nitrogen content.

Given this, the objectives of this work include developing the chemical composition of welding wire with high nitrogen content, predicting the phase composition of weld metal in Thermo-Calc, obtaining a wire laboratory sample and studying the properties of welded joints fabricated using the developed welding wire.

Materials and methods

As the study object, we used welded joints obtained by manual argon arc welding of austenitic steel, grade 05Kh21AG15N8MFL, with a nitrogen content of ~0.6 wt. %, 20 mm thick, in an argon environment. After smelting, the steel was subjected to homogenizing annealing at 1200 °C for 3 h followed by cooling in water. The chemical composition of the base metal is presented in Table 1.

The welded joints were obtained based on the technological recommendations developed by the authors [25] using the following welding parameters: welding current of 100 – 120 A; arc voltage of 9 V; and welding speed of 3 m/h. According to the recommendations, air cooling was performed after each layer of deposited metal.

The welding wire with high nitrogen content, 1.2 mm in diameter, developed and obtained at IMET RAS was used as a welding filler material [26]. To select the chemical composition of Cr–Ni–Mn–Mo–N welding wire, we performed:

– thermodynamic calculations of nitrogen [N] solubility [27]

$$\lg[N] = -560/T - 1{,}06 - 2600/T - \{0.39(-0.048([Cr] + 0.5[Mn] - 2.45[C] - 0.9[Si] - 0.23[Ni] + 0.27[Mo] + 2.04[V] - 0.12[Cu] - 0.15[S] - [P] + 0.41[W]) + 3.5\cdot10^{-4}([Cr] + 0.5[Mn] - 2.45[C] - 0.9[Si] - 0.23[Ni] + 0.27[Mo] + 2.04[V] - 0.12[Cu] - 0.15[S] - [P] + 0.41[W])^2\} + (700/T - 0.37); \quad (1)$$

– calculations of the phase composition using Schaeffler diagram based on estimated nitrogen concentrations under the following condition:

$$Ni_{eq}/Cr_{eq} > 0.8, \quad (2)$$

where the values of nickel and chromium equivalents were calculated by the following formulas

$$Ni'_{eq} = Ni + 0.1Mn - 0.01Mn^2 + 18N + 30C, \quad (3)$$

$$Cr'_{eq} = Cr + 1.5Mo + 0.48Si + 2.3V + 1.75Nb; \quad (4)$$

– ensuring corrosion resistance:

$$PREN = \%\,Cr + 3.3\,\%\,Mo + 16\,\%\,N \geq 31. \quad (5)$$

Phase composition calculations of the weld metal were performed using thermodynamic values from the TCFE 7.0 database in Thermo-Calc. The initial parameters in thermodynamic modeling were the concentrations of the system components (chemical composition), temperature and pressure. The calculations were

Table 1. **Grade chemical composition of the base metal**

Таблица 1. **Марочный химический состав основного металла**

Base metal	Chemical composition, wt. % (Fe and impurities – the rest)									
	N	Cr	Ni	Mn	Mo	Si	V	C	S	P
						maximum				
05Kh21AG15N8MFL	maximum 0.6	21 – 22	7.7 – 9.0	15 – 16	1 – 2	0.2	0.3	0.04	0.008	0.012

performed at normal atmospheric pressure in the temperature range from 600 to 1200 °C.

Fabricating the sections and revealing the microstructure. The samples were pressed into bakelite on an Opal 400 hot mounting press, then successively ground on a Saphir 250 grinder and polished on a cloth using emulsion. Polished samples of welded joints were subjected to etching in the reagent: 2 parts of HCl + 1 part of HNO_3 + 1 part of glycerin.

Optical microscopy. The microstructure was studied using an Olympus GX51 light microscope.

Ferritometry. The ferrite content was measured by the magnetometric method using an MVP-2M multifunctional eddy current tester. The ferritic phase content range can be measured from 0 to 25 %; limit of permissible basic error of the ferritic phase: $0.05(1 + X_\varphi)$, where X_φ is the measured value of the ferritic phase, %.

Microhardness. Microhardness of different zones of welded joints was measured according to GOST 9450 – 76 on a Volpert 402MVD hardness meter at a load of 50 g, with the sample being held under this load for 10 s. A tetrahedral diamond pyramid was used as an indenter. The microindentation hardness number was determined by the formula

$$HV = \frac{F}{S} = \frac{0.102 \cdot 2F \cdot \sin d/2}{d^2} = 0.189\frac{F}{d^2}, \qquad (6)$$

where F is the load, N; d is the diagonal of impression, mm.

Mechanical properties were determined on the samples of the base metal and the resulting welded joints, in which the weld was located in the center of the cut sample.

Tensile tests were conducted according to GOST 1497 – 84 on an Instron 3382 testing machine. Proportional cylindrical samples, type IV, No. 7 were used. The test was performed at a speed of 1 mm/min in all cases, at room temperature.

Impact bending tests were conducted according to GOST 9454 – 78 on an Amsler RKP 450 (Zwick/Roell) impact testing machine at 20 °C. We used the samples defined in GOST 9454 – 78 with a *V*-concentrator. The maximum pendulum impact energy is 300 J.

Raster electronic microscopy. Fractographic analysis of samples after destruction was carried out on a LEO-1420 scanning electron microscope with an Oxford Instruments microscope for micro *X*-ray spectral analysis (MXSA).

Results and discussion

Development of chemical composition and production of welding wire

The high-nitrogen welding wire was developed based on Fe–Cr–Mn steel alloyed with interstitial elements – nitrogen (~0.5 %) and carbon, substitution elements – nickel and molybdenum, which ensured an austenitic structure, high strength, corrosion and cold resistance[2] [4]. Based on the calculations by formulas (1) – (5) we selected the chemical composition of the welding wire (Table 2).

Due to the melting of Cr–Ni–Mn–Mo–N wires during welding, the volatile elements – nitrogen and manganese – can partially escape from the weld metal. The objective of this work is to evaluate the thermodynamically equilibrium phase composition of weld metal depending on the content of nitrogen and manganese using the Thermo-Calc software for plotting temperature sections of phase diagrams.

Fig. 1 shows the plotted phase diagrams for the composition of the new welding wire with variable nitrogen and manganese content. The dotted line indicates the amount of nitrogen and manganese contained in the weld wire metal of the calculated composition (Table 2).

In the steel of this chemical composition, in equilibrium conditions when the temperature drops to ~700 °C and nitrogen concentration decreases to 0.5 %, the undesirable *Z*-phase (Cr, V)N can be separated from austenite, in addition to CrN nitrides, $Me_{23}C_6$ carbides and σ-phase (Fig. 1, *a*). However, according to [28], the *Z*-phase is formed in case of long thermal soak in heat-resistant steels. Taking into account that welding is a non-equilibrium process in which each pass of the welding arc is accompanied by melting of a small area of the welded metal edge and melting of the welding wire of a small diameter

[2] Refer to: Ibid.

Table 2. **Grade chemical composition of the welding wire metal**

Таблица 2. **Марочный химический состав металла сварочной проволоки**

Welding wire	Chemical composition, wt. % (Fe and impurities – the rest)										[N], %	Ni_{eq}/Cr_{eq}	PREN
	N	Cr	Ni	Mn	Mo	Si	V	C	S	P			
						maximum							
Sv-0.57N	maximum 0.57	21 – 23	7.8 – 8.3	14 – 16	0.5 – 1.5	0.5	0.2	0.06	0.007	0.013	0.57	0.73	32

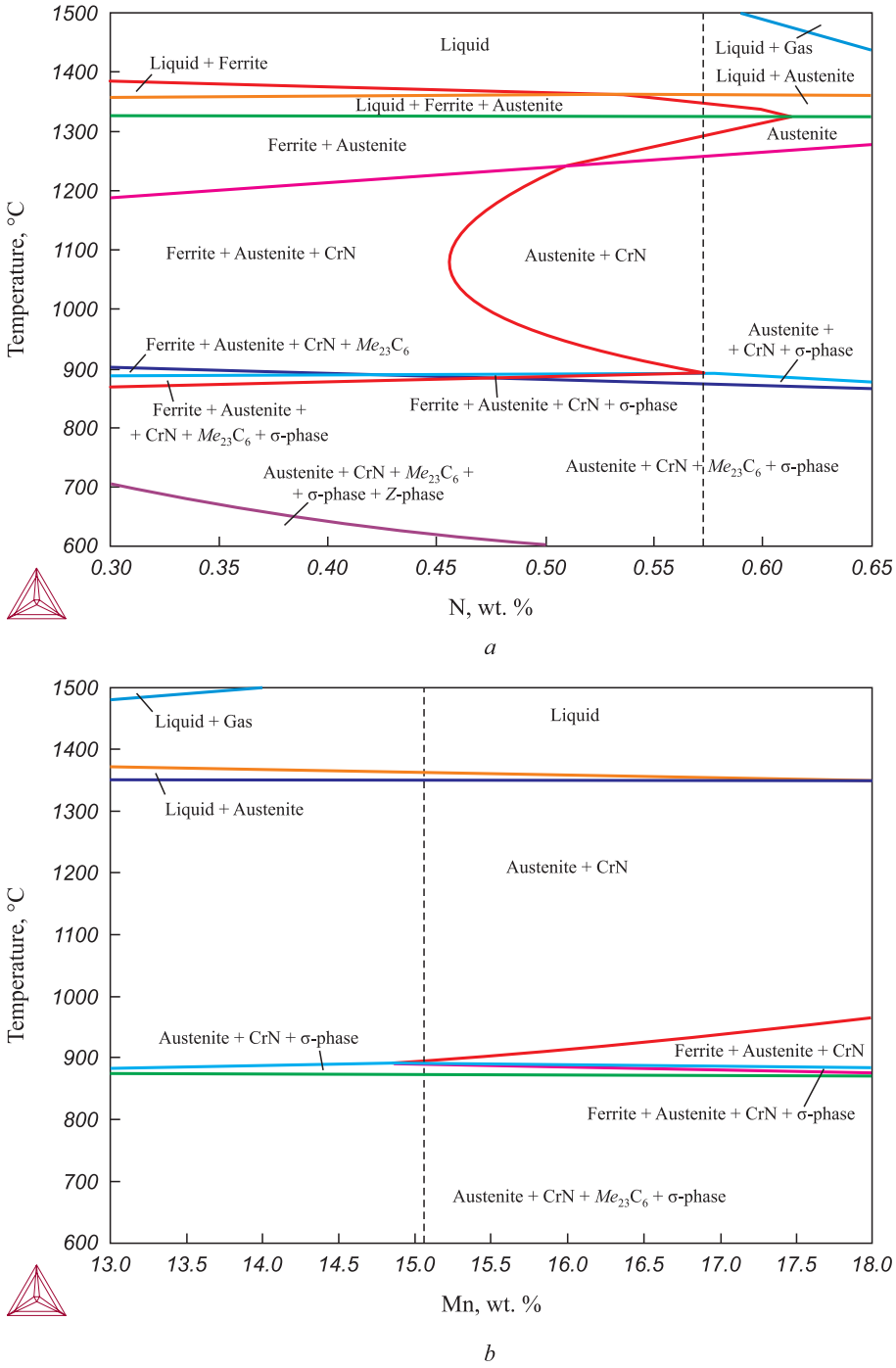

Fig. 1. Calculations of thermodynamically equilibrium phase composition of welding wire Sv-0.57N depending on the content in it of nitrogen (at 15.1 % Mn) (*a*) and manganese (at 0.57 % N) (*b*)

Рис. 1. Расчеты термодинамически равновесного фазового состава сварочной проволоки Св-0,57N в зависимости от содержания в ней азота при концентрации 15,1 % Mn (*a*) и марганца при концентрации 0,57 % азота (*b*)

(~1.2 mm), followed by cooling, undesirable *Z*-phase or σ-phase are not likely to emerge in the weld metal zone, fusion zone or heat affected zone of the welded product.

According to the calculated data presented in Fig. 1, *b*, some possible reduction of manganese concentration during welding cannot lead to negative changes of the phase composition, the latter should remain austenitic.

Welding wire manufacturing involved the following process steps: smelting of steel with the given chemical composition in an open induction furnace with the addition of nitrided ferroalloys; homogenization of the cast structure at 1200 °C; rolling with preheating at 1100 °C; rotary forging and wire drawing.

Microstructure

The examination in the optical light microscope did not reveal any pores, cracks or non-welds (Fig. 2). The authors of [24] present a general view of welded joints studied using the microscope of low magnification. When welding wire with 0.9 % nitrogen content was used, pores in the weld metal were observed with the naked eye.

The microstructure of the base metal, 05Kh21AG15N8MFL cast steel, is characterized by large grains of austenite, 200 – 700 μm in size (Fig. 2, *a*). The weld metal structure includes small grains elongated in the direction of crystallization (Fig. 2, *b*). A number of ferrite grains are observed in each of the weld zones. The ferritometry test revealed that the volume content of ferrite does not exceed 0.27.

Comparing the data obtained by calculations of the phase diagram presented in Fig. 1 and microstructure images, it is important to point out that optical microscopy did not confirm the presence of $Me_{23}C_6$ carbides and σ-phase in the obtained welded joints.

The high-temperature welding process can adversely affect the heat affected zone of the weld. Thus, for example, the works [29; 30] showed that large particles of Cr_2N nitrides were released in the heat affected zone, which led to reduction in corrosion resistance. However, large nitride particles were not detected in the studied welded joints, obviously due to the use of low weld heat input.

The nitrogen content in the weld metal amounted to 0.58 %, apparently due to the transfer of nitrogen from the base metal (with 0.6 % N) into the welding bath during welding. Such high nitrogen assimilation was achieved by following the technological recommendations for welding high-nitrogen steels [25]. In the previously discussed work [24], when multi-pass argon-arc welding and welding wires with 0.6 and 0.9 % N were used, as in this case, the nitrogen content in the weld metal was 0.54 and 0.64 %, respectively. In [17], even the addition of 5 % N_2 to the shielding gas did not help to keep all the nitrogen contained in the filler metal (0.6 %), and its value in the weld metal amounted to 0.58 %.

Mechanical properties

The weld samples for tensile and impact bending tests were cut so that the weld metal was centered on the test samples. Fig. 3 presents the histogram that demonstrates high properties in the "yield strength – tensile strength – impact strength" combination of welded joints of cast high-nitrogen steel. As a comparison, the paper [31] indicates the following mechanical properties of the 05Kh21AG15N8MFL cast steel sample after homogenization annealing at 1200 °C, 4 h: $\sigma_{0.2}$ = 407 MPa, σ_u = 674 MPa, KCU = 209 J/cm^2. Consequently, the welded joints of high-nitrogen steel investigated in this study, obtained using the developed welding material and based on the formulated technological recommendations, are practically equal in strength

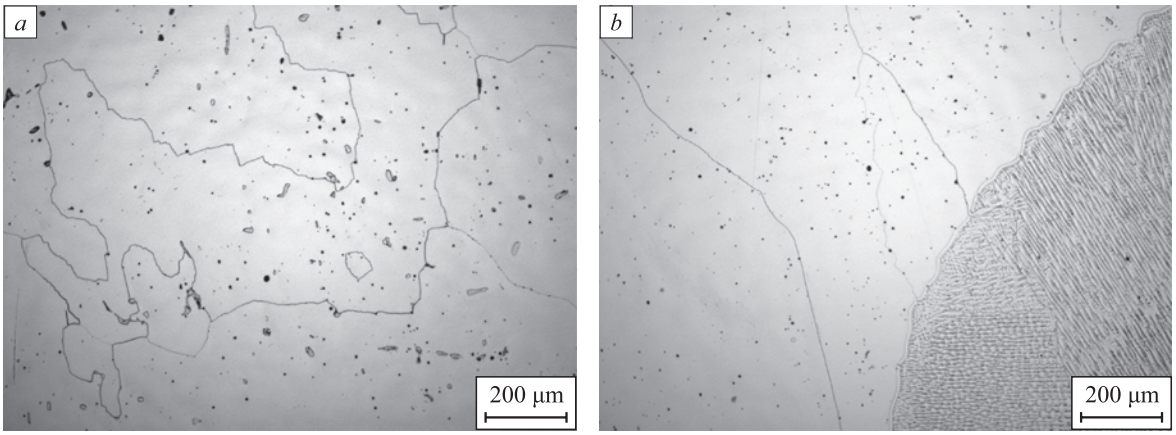

Fig. 2. Microstructure of base cast metal (*a*) and welded joint (*b*)

Рис. 2. Микроструктура основного литого металла (*a*) и сварного соединения (*b*)

to the base metal without welding (90 % of the strength of the base metal).

Microhardness values measured in different zones of the welded joint (Fig. 4) are consistent with the grain size in each of the research areas. Among other things, the lowest hardness values are typical for the base metal with the coarse-grained cast austenitic structure. The microhardness in the fusion zone and weld metal is higher as boundaries of small grains formed in the weld metal contribute to the hardening.

The fracture morphology of the samples after impact tests indicates ductile dimpled fracture pattern (Fig. 5). Large dimples contribute to enhancing plastic properties[3]. The steels have high impact strength when, with

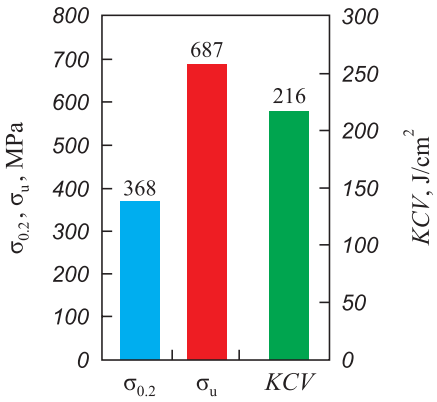

Fig. 3. Mechanical properties of the samples of welded joints of high-nitrogen austenitic steel

Рис. 3. Механические свойства образцов сварных соединений высокоазотистой аустенитной стали

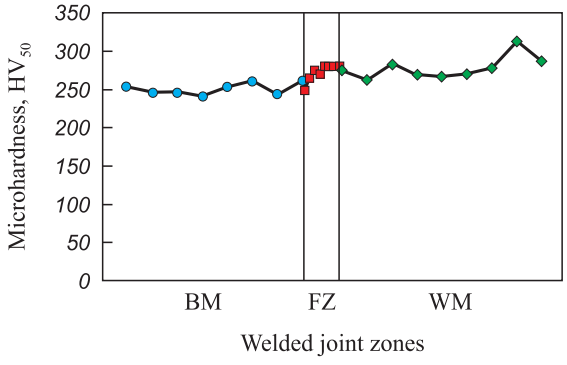

Fig. 4. Microhardness in each zone of the welded joint: BM – base metal, FZ – fusion zone, WM – weld metal

Рис. 4. Микротвердость в каждой из зон сварного соединения: BM – основной металл; FZ – зона сплавления; WM – металл шва

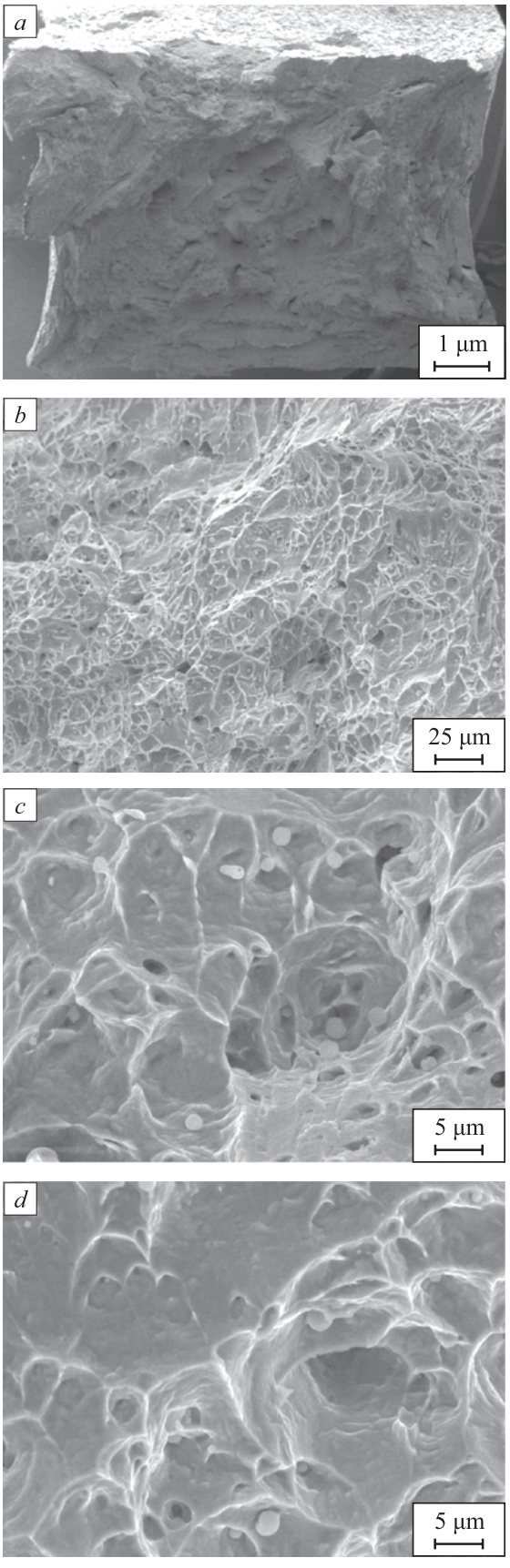

Fig. 5. Fractography of the samples of welded joints after impact tests

Рис. 5. Фрактография образцов сварных соединений после испытаний на ударную вязкость

[3] S.L. Gorobchenko, Y.S. Krivtsov, A.K. Andreev, Yu.P. Solntsev Competitiveness of reinforcement castings beyond impact strength or application of a new comprehensive method to validate the reliability of austenitic steels for cryogenic valves. TPA. *Pipeline Valves & Equipment, International Magazine* [Electronic resource]. URL: http://www.valverus.info/popular/3219-konkurentosposobnost-armaturnogo-litya.html

a large number of small-sized dimples, the largest area in the fracture is covered by dimples, minimum 10 – 15 μm in size, with globular inclusions not exceeding 8 μm. Another indication of high metal ductility is the depth and plasticity of the dimples themselves, the serpentine sliding on their walls and the absence of the dimples fracturing[4] – these are the features observed in the fracture (Fig. 5, *c*, *d*).

Discussing the strength characteristics achieved in this experiment, the following observations can be made. The strength level of a welded joint is determined by its weakest section. The authors tested this wire while welding cast austenitic steel, which is considered to be high strength among cast austenitic steels (the standard yield strength value of austenitic steels of the Fe – 18Cr – 10Ni system does not exceed 200 MPa). When the same wire is used for welding hot-wrought metal of the same composition, the properties of the welded joint should be higher. For example, in [24], welding filler with 0.6 % N was used to obtain a welded joint of high-nitrogen deformed steel. Accordingly, the tensile strength σ_u = 912 MPa was reached, while the impact strength was expectedly lower, *KCV* = 110 J/cm^2. This level of properties was obtained as the base metal structure was reinforced by deformation.

The welded joint obtained using a welding filler with 0.78 % N, during welding n the shielding gas atmosphere (87 % Ar – 6.5 % N_2 – 6.5 % CO_2), also demonstrated high mechanical properties characteristic of deformed high-nitrogen metal: σ_u = 956 MPa, *KCV* = 132 J/cm^2 [17].

Conclusions

We calculated the phase composition of steel of the selected composition Fe – Cr – Mn – Ni – Mo – V, N while varying the content of manganese and nitrogen, which can volatilize during welding. The study showed that the selected nitrogen-containing welding wire should have an austenitic structure.

Sv-0.57N welding wire was manufactured from the steel melted in laboratory conditions using hot plastic deformation and drawing methods. Testing of this wire to obtain a welded joint of austenitic cast steel 05Kh21AG15N8MFL ~0.6 % N, with the argon-arc welding carried out based on the developed technological recommendations, enabled to obtain a defect-free welded joint without loss of nitrogen in the weld metal.

The welded joint metal is characterized by high strength (0.9 of the base metal strength) and high impact strength, while the fracture has a dimpled structure characteristic of ductile materials. The new welding wire Sv-0.57N may be regarded as a promising material for welding austenitic high-nitrogen steels.

[4] Refer to: Ibid.

References / Список литературы

1. Wang X., Tian J., Li S., He P., Fang N., Wen G. Weldability of high nitrogen steels: A review. *Reviews on Advanced Materials Science*. 2023;62(20220325):1–17. https://doi.org/10.1515/rams-2022-0325
2. Du Toit M. Filler metal selection for welding a high nitrogen stainless steel. *Journal of Materials Engineering and Performance*. 2002;11(3):306–312. https://doi.org/10.1361/105994902770344123
3. Bishokov R.V., Baryshnikov A.P., Gezha V.V., Mel'nikov P.V. Welding materials and technologies of high strength steels. *Voprosy materialovedeniya*. 2014;2(78):128–137. (In Russ.).
   Бишоков Р.В., Барышников А.П., Гежа В.В., Мельников П.В. Сварочные материалы и технологии сварки высокопрочных сталей. *Вопросы материаловедения*. 2014;2(78):128–137.
4. Harzenmoser M. Welding of high nitrogen steels. *Materials and Manufacturing Processes*. 2004;19(1):75–86. https://doi.org/10.1081/AMP-120027503
5. Du Toit M. The microstructure and mechanical properties of Cromanite welds. *Journal of the South African Institute of Mining and Metallurgy*. 1999;99(6):333–339.
6. Mohammed R., Reddy G.M., Rao K.S. Effect of filler wire composition on microstructure and pitting corrosion of nickel free high nitrogen stainless steel GTA welds. *Transactions of the Indian Institute of Metals*. 2016;69(10):1919–1927. https://doi.org/10.1007/s12666-016-0851-6
7. Fomina O.V. Creation of technological principles for controlling the structure and physical and mechanical properties of high-strength austenitic nitrogen-containing steel: Dr. Tech. Sci. Diss. St. Petersburg; 2018:433. (In Russ.).
   Фомина О.В. Создание технологических принципов управления структурой и физико-механическими свойствами высокопрочной аустенитной азотсодержащей стали: Диссертация … доктора технических наук. Санкт-Петербург; 2018:433.
8. Mohammed R., Madhusudhan R.G., Rao K.S. Welding of nickel free high nitrogen stainless steel: Microstructure and mechanical properties. *Defence Technology*. 2017;13:59–71. https://doi.org/10.1016/j.dt.2016.06.003
9. Liu Z., Fan C., Yang C., Zhu Ming, Hua Z., Lin S., Wang L. Investigation of the weldability of dissimilar joint between high nitrogen steel and low alloy steel by comparing filler metals. *Materials Today Communications*. 2023;35:105551. https://doi.org/10.1016/j.mtcomm.2023.105551
10. Kumar N., Arora N., Goel S.K., Goel D.B. A comparative study of microstructure and mechanical properties of 21-4-N steel weld joints using different filler materials. *Materials Today Proceedings*. 2018;5(9):17089–17096. https://doi.org/10.1016/j.matpr.2018.04.116
11. Kokawa H. Nitrogen absorption and desorption by steels during arc and laser welding. *Welding International*. 2004;18(4):277–287. https://doi.org/10.1533/wint.2004.3235
12. Du Toit M., Pistorius P.C. Nitrogen control during the autogenous ARC welding of stainless steel. *Welding in the World*. 2003;47(9–10):30–43. https://doi.org/10.1007/BF03266398
13. Huang H.-Y. Effects of shielding gas composition and activating flux on GTAW weldments. *Materials & Design*. 2009;30(7):2404–2409. https://doi.org/10.1016/j.matdes.2008.10.024
14. Kah P., Martikainen J. Influence of shielding gases in the welding of metals. *The International Journal of Advanced*

Manufacturing Technology. 2013;64:1411–1421. https://doi.org/10.1007/s00170-012-4111-6

15. Liu Z., Fan C., Chen C., Ming Z., Liu A., Yang C., Lin S., Wang L. Optimization of the microstructure and mechanical properties of the high nitrogen stainless steel weld by adding nitrides to the molten pool. *Journal of Manufacturing Processes*. 2020; 49:355–364. https://doi.org/10.1016/j.jmapro.2019.12.017
16. Zhao L., Tian Z., Peng Y., Qi Y., Wang Y. Influence of nitrogen and heat input on weld metal of gas tungsten arc welded high nitrogen steel. *Journal of Iron and Steel Research, International*. 2007;14(5):259–262. https://doi.org/10.1016/S1006-706X(08)60090-4
17. Liu Z., Fan C., Ming Z., Chen C., Yang C., Lin S., Wang L. Optimization of shielding gas composition in high nitrogen stainless steel gas metal arc welding. *Journal of Manufacturing Processes*. 2020;58:19–29. https://doi.org/10.1016/j.jmapro.2020.08.001
18. Qiang W., Wang K. Shielding gas effects on double-sided synchronous autogenous GTA weldability of high nitrogen austenitic stainless steel. *Journal of Manufacturing Processes*. 2017; 250:169–181. https://doi.org/10.1016/j.jmatprotec.2017.07.021
19. Yang D., Xiong H., Huang Y., Yan D., Li D., Peng Y., Wang K. Droplet transfer behavior and weld formation of gas metal arc welding for high nitrogen austenitic stainless steel. *Journal of Manufacturing Processes*. 2021;65:491–501. https://doi.org/10.1016/j.jmapro.2021.03.048
20. Zhang Y., Jing H., Xu L., Han Y., Zhao L., Xiao B. Microstructure and mechanical performance of welded joint between a novel heat-resistant steel and Inconel 617 weld metal. *Materials Characterization*. 2018;139:279–292. https://doi.org/10.1016/j.matchar.2018.03.012
21. Pehlke R.D., Elliott J.F. Solubility of nitrogen in liquid iron alloys. *Transactions of the Metallurgical Society of AIME*. 1960;218(6):1088–1101.
22. Bonnefois B., Coudreuse L., Charles J. A-TIG welding of high nitrogen alloyed stainless steels: a metallurgically high-performance welding process. *Welding International*. 2004;18(3):208–212. https://doi.org/10.1533/wint.2004.3226
23. Bannykh O.A., Blinov V.M., Kostina M.V., Blinov E.V., Zvereva T.N. Study of the weldability of high-nitrogen corrosion-resistant austenitic steels of the X22AG16N8M type. *Metally*. 2007;(4):51–67. (In Russ.).

    Банных О.А., Блинов В.М., Костина М.В., Блинов Е.В., Зверева Т.Н. Исследование свариваемости высокоазотистых коррозионностойких аустенитных сталей типа Х22АГ16Н8М. *Металлы*. 2007;(4):51–67.
24. Liu Z., Fan C., Chen C., Ming Z., Yang C., Lin S., Wang L. Design and evaluation of nitrogen-rich welding wires for high nitrogen stainless steel. *Journal of Materials Processing Technology*. 2021;288:116885. https://doi.org/10.1016/j.jmatprotec.2020.116885
25. Kostina V.S. Research and development of technological fundamentals for welding high-nitrogen corrosion-resistant Cr-Ni-Mn-Mo austenitic steels: Cand. Tech. Sci. Diss. Moscow: IMET RAS; 2020:181. (In Russ.).

    Костина В.С. Исследование и развитие технологических основ сварки высокоазотистых коррозионностойких Cr-Ni-Mn-Mo аустенитных сталей: Диссертация … кандидата технических наук. Москва: ИМЕТ РАН; 2020:181.
26. Kostina V.S., Kostina M.V., Dormidontov N.A., Muradyan S.O. Welding wire with high nitrogen content. Patent for invention 2768949 C1, 25.03.2022. Application No. 2021110801 dated 16.04.2021. Publ. 25.03.2022. (In Russ.).

    Сварочная проволока с высоким содержанием азота. Костина В.С., Костина М.В., Дормидонтов Н.А., Мурадян С.О. / Патент на изобретение 2768949 С1, 25.03.2022. Заявка № 2021110801 от 16.04.2021. Дата публикации: 25.03.2022.
27. Rigina L.G., Vasiliev Ya.M., Dub V.S., etc. Alloying steel with nitrogen. *Elektrometallurgiya*. 2005;(2):14–21. (In Russ.).

    Ригина Л.Г., Васильев Я.М., Дуб В.С. и др. Легирование стали азотом. *Электрометаллургия*. 2005;(2):14–21.
28. Mohammed R., Reddy G.M., Rao K.S. Microstructure and pitting corrosion of shielded metal arc welded high nitrogen stainless steel. *Defence Technology*. 2015;11(3):237–243. https://doi.org/10.1016/j.dt.2015.04.002
29. Ogawa M., Hiraoka K., Katada Y., Sagara M., Tsukamoto S. Chromium nitride precipitation behavior in weld heat-affected zone of high nitrogen stainless steel. *ISIJ International*. 2002;42(12):1391–1398. https://doi.org/10.2355/isijinternational.42.1391
30. Moon J., Ha H.-Y., Lee T.-H., Lee C. Different aspect of pitting corrosion and interphase corrosion in the weld heat-affected zone of high-nitrogen Fe-18Cr-10Mn-N steel. *Materials Chemistry and Physics*. 2013;142(2-3):556–563. https://doi.org/10.1016/j.matchemphys.2013.07.052
31. Muradyan S.O. Structure and properties of casting corrosion-resistant steel alloyed with nitrogen: Cand. Tech. Sci. Diss. Moscow; 2016:132. (In Russ.).

    Мурадян С.О. Структура и свойства литейной коррозионностойкой стали, легированной азотом: Диссертация … кандидата технических наук. Москва; 2016:132.

Information about the Authors / Сведения об авторах

Valentina S. Kostina, *Cand. Sci. (Eng.), Junior Researcher of the Laboratory "Physicochemistry and Mechanics of Metallic Materials",* Baikov Institute of Metallurgy and Materials Science, Russian Academy of Sciences
ORCID: 0000-0001-7956-499X
E-mail: vskostina@yandex.ru

Mariya V. Kostina, *Dr. Sci. (Eng.), Assist. Prof., Senior Researcher, Head of the Laboratory "Physicochemistry and Mechanics of Metallic Materials",* Baikov Institute of Metallurgy and Materials Science, Russian Academy of Sciences
ORCID: 0000-0002-2136-5792
E-mail: mvk@imet.ac.ru

Валентина Сергеевна Костина, *к.т.н., младший научный сотрудник лаборатории физикохимии и механики металлических материалов,* Институт металлургии и материаловедения им. А.А. Байкова РАН
ORCID: 0000-0001-7956-499X
E-mail: vskostina@yandex.ru

Мария Владимировна Костина, *д.т.н., доцент, ведущий научный сотрудник, заведующий лабораторией физикохимии и механики металлических материалов,* Институт металлургии и материаловедения им. А.А. Байкова РАН
ORCID: 0000-0002-2136-5792
E-mail: mvk@imet.ac.ru

Dmitrii V. Zinoveev, *Cand. Sci. (Eng.), Junior Researcher of the Laboratory "Physicochemistry and Technology of Iron Ore Processing", Baikov Institute of Metallurgy and Materials Science, Russian Academy of Sciences*
ORCID: 0000-0003-4520-4659
E-mail: zinoveevimet@yandex.ru

Aleksandr E. Kudryashov, *Research Engineer,* Baikov Institute of Metallurgy and Materials Science, Russian Academy of Sciences
E-mail: al.kudriashov@mail.ru

Дмитрий Викторович Зиновеев, *к.т.н., младший научный сотрудник лаборатории физикохимии и технологии переработки железорудного сырья,* Институт металлургии и материаловедения им. А.А. Байкова РАН
ORCID: 0000-0003-4520-4659
E-mail: zinoveevimet@yandex.ru

Александр Эдуардович Кудряшов, *инженер-исследователь,* Институт металлургии и материаловедения им. А.А. Байкова РАН
E-mail: al.kudriashov@mail.ru

Contribution of the Authors

V. S. Kostina – conducting the research, writing the text, processing the results.
M. V. Kostina – finalization of the text, correction of conclusions.
D. V. Zinoveev – carrying out calculations of the phase composition.
A. E. Kudryashov – study of the structure of welded joints.

Вклад авторов

В. С. Костина – проведение исследований, подготовка текста статьи, обработка результатов.
М. В. Костина – доработка текста, корректировка выводов.
Д. В. Зиновеев – проведение расчетов фазового состава.
А. Э. Кудряшов – исследование структуры сварных соединений.

Received 14.12.2023
Revised 18.01.2024
Accepted 28.02.2024

Поступила в редакцию 14.12.2023
После доработки 18.01.2024
Принята к публикации 28.02.2024

MATERIALS SCIENCE / МАТЕРИАЛОВЕДЕНИЕ

UDC 621.791.927.5
DOI 10.17073/0368-0797-2024-3-303-310

Original article
Оригинальная статья

Effect of heat treatment on structure of austenitic steel 07Cr25Ni13 obtained by WAAM

M. S. Anosov, S. A. Sorokina, M. A. Chernigin, Yu. S. Mordovina

R.E. Alekseev Nizhny Novgorod State Technical University (24 Minina Str., Nizhny Novgorod 603022, Russian Federation)

honeybadger52@yandex.ru

Abstract. Currently, the use of additive technologies in industry is becoming more promising. The intensification of development of 3D technologies leads to the need for a more thorough study of the structure and properties of metals obtained by this method. In this paper, the effect of heat treatment on structure of the metal deposited by Wire Arc Additive Manufacturing (WAAM) is considered. The paper describes the effect of quenching at various temperatures and annealing on the structure of austenitic steel 07Cr25Ni13. As a result of the work, it was found that during metal deposition, crystallization occurs according to the FA type with the formation of a coarse dendritic structure with mainly skeletal and vermicular morphology, consisting of δ- and σ-phases. It is noted that quenching at 1070 °C practically does not change the metal structure. Despite the fact that quenching at elevated temperatures (1100 °C) leads to partial dissolution and spheroidization of the dendrites released during surfacing, there are no cardinal structural changes. The most complete dissolution of the dendritic component occurs during quenching at 1150 °C. The structure after this procedure is predominantly austenitic, remains of the dendritic component are represented by small spherical inclusions. The steel structure after annealing (1150 °C) practically does not differ from the structure obtained after quenching at the same temperature. A significant increase in grain size, typical for austenitic steels, is not observed in this case. Based on the structure obtained after heat treatment, the most promising treatment options for future physico-mechanical properties are quenching and annealing at 1150 °C.

Keywords: austenitic steel 07Cr25Ni13, additive technologies, WAAM, steel structure formation, δ-ferrite, quenching, annealing

Acknowledgements: The research was supported by the Russian Science Foundation, grant No. 22-79-00095 “Development of scientific and technological foundations for structure formation of structural materials obtained by additive electric arc manufacturing for the mechanical properties formation during fatigue using artificial intelligence approaches”.

For citation: Anosov M.S., Sorokina S.A., Chernigin M.A., Mordovina Yu.S. Effect of heat treatment on structure of austenitic steel 07Cr25Ni13 obtained by WAAM. *Izvestiya. Ferrous Metallurgy*. 2024;67(3):303–310. https://doi.org/10.17073/0368-0797-2024-3-303-310

Влияние термообработки на структуру аустенитной стали 07Х25Н13, полученной методом аддитивного выращивания WAAM

М. С. Аносов, С. А. Сорокина, М. А. Чернигин, Ю. С. Мордовина

Нижегородский государственный технический университет им. Р.Е. Алексеева (Россия, 603022, Нижний Новгород, ул. Минина, 24)

honeybadger52@yandex.ru

Аннотация. В настоящее время все более перспективным является применение аддитивных технологий в промышленности. Интенсификация развития 3D-технологий приводит к необходимости более тщательного изучения структуры и свойств металлов, получаемых данным методом. В работе рассматривается влияние термообработки (ТО) на структуру наплавляемого методом электродуговой наплавки (WAAM) металла. Изучено влияние закалки при различных температурах и отжига на структуру аустенитной стали 07Х25Н13. Установлено, что при наплавке металла происходит кристаллизация по типу ФА с образованием грубой дендритной структуры со скелетной и вермикулярной морфологией и состоящей из δ- и σ-фаз. Закалка при температуре 1070 °С практически не изменяет структуру металла. При повышенных температурах (1100 °С) закалка приводит к частичному растворению и сфероидизации выделившихся при наплавке дендритов, однако кардинальных структурных изменений не происходит. Наиболее полное растворение дендритной составляющей происходит во время закалки при температуре 1150 °С. Структура после данной ТО преимущественно аустенитная, остатки дендритной составляющей представлены мелкими сферическими включениями. Структура стали после отжига (1150 °С) практически не отличается от получаемой после закалки при той же температуре. Значительного увеличения размера зерен, характерного для аустенитных сталей, в данном случае не наблюдается. Исходя из структуры, получаемой после ТО,

наиболее перспективными для будущих физико-механических свойств вариантами обработки являются закалка и отжиг при температуре 1150 °С.

Ключевые слова: аустенитная сталь 07Х25Н13, аддитивные технологии, WAAM, структурообразование стали, δ-феррит, закалка, отжиг

Благодарности: Исследование выполнено при поддержке гранта Российского научного фонда № 22-79-00095 «Разработка научно-технологических основ структурообразования конструкционных материалов, полученных путем аддитивного электродугового выращивания для формирования механических свойств при усталости с использованием подходов искусственного интеллекта».

Для цитирования: Аносов М.С., Сорокина С.А., Чернигин М.А., Мордовина Ю.С. Влияние термообработки на структуру аустенитной стали 07Х25Н13, полученной методом аддитивного выращивания WAAM. *Известия вузов. Черная металлургия*. 2024;67(3):303–310. https://doi.org/10.17073/0368-0797-2024-3-303-310

Introduction

Currently, austenitic steels are widely used in the chemical, oil, and food industries, as well as in the production of medical and nuclear power plant equipment [1]. A number of industries in the modern world can hardly exist without austenitic corrosion-resistant steels. This type of material possesses unique properties, such as high corrosion resistance in acid and alkaline environments of varying corrosive strength, as well as paramagnetism. The combination of physical and mechanical properties is achieved not only through alloying with significant amounts of chromium, nickel, magnesium, and other elements but also through maintaining a homogeneous austenitic structure throughout the product's entire service life [2].

Currently, additive technologies are becoming increasingly promising for industry as they reduce the total cost of products, especially in single and small batch production. The rapid development of 3D printing technologies necessitates a thorough investigation of the mechanical properties, structure, and chemical composition of metals produced by these methods. To date, the main methods of metal 3D printing are layer-by-layer powder fusion (selective laser sintering, SLM), laser powder deposition (laser engineered net shaping, LENS/direct metal deposition, DMD), and electric arc deposition (wire arc additive manufacturing, WAAM) [3]. WAAM 3D printing, which we used for this study, is the most productive and technologically simple [4; 5].

The advantages of additive manufacturing methods are as follows:

– the process of obtaining products can be fully automatized;

– when products are manufactured of expensive materials, such as titanium and nickel alloys, the material consumption is considerably reduced;

– small batch production, unprofitable when using traditional production methods, becomes cost-efficient [6 – 8].

SLM technology enables the manufacture of complex products by laser melting of metal powder using CAD models. At the powder melting point, the energy density is higher compared to other electric arc processes (e.g., welding), but lower than in the case of laser exposure [9]. The main problem of parts produced by the SLM method is relatively high surface roughness, which reduces fatigue resistance by increasing stress concentration on the sample surface [10].

Laser powder deposition is the process of overlay welding performed by fusing the powdered material layer onto the substrate. The laser beam creates a molten bath into which the powdered metal is introduced. The metal melts and solidifies in the bath to form metallic bonds with the substrate. During the surfacing process, the powdered metal is automatically fed from the feed system to the substrate, which is lowered to the height equal to the thickness of the layer to be deposited. However, it should be noted that the laser deposition method does not ensure reproducibility of the chemical composition and mechanical properties of the final products [11; 12], which is a significant disadvantage of this technology.

WAAM technology is a relatively new additive growth method that emerged in the 1990s. It includes depositing a common welding wire, widely available commercially, onto the substrate, resulting in a finished part. Compared to conventional manufacturing, WAAM can reduce manufacturing time by 40 – 60 % and post-processing time by 15 – 20 %, depending on the size of the part. For example, the use of this technology for manufacturing airplane landing gear stiffeners results in about 78 % raw material savings compared to conventional production [13]. Metals with good weldability can potentially be used for the WAAM process, and so far, researchers have successfully applied this method to fabricate parts from Ti [13], Al [14], steel [15], and Ni [16] based alloys.

In the additive growth process, the surfaced metal is in a liquid state and is subsequently subjected to multiple cycles of high-temperature heating, including to temperatures above critical. As a result, the microstructure of the surfaced metal differs from that of metal produced by conventional technologies, and consequently, the physicochemical and strength properties of the metal may also differ from those of rolled material.

Table 1. **Chemical composition of the studied material**

Таблица 1. **Химический состав исследованного материала**

Material	Content of chemical elements, %								
	C	Si	Mn	Cr	Ni	Mo	Ti	S	P
GOST 2246	<0.09	0.5 – 1.0	1.0 – 2.0	23.0 – 26.0	12.0 – 14.0	not regulated	not regulated	<0.018	<0.025
ER309LSI	0.016	0.7	1.9	23.3	13.7	0.1	0	0.004	0.019

An increasing number of foreign studies are investigating the application of additive technologies in industry. However, in Russia, these methods are developing locally and are not yet widespread. In addition to reducing the cost of small-batch products from austenitic steels, which are currently quite popular, additive technologies can also contribute to the advancement of Russian science.

The objective of this study is to explore the effect of heat treatment modes on the structure of austenitic steel 07Cr25Ni13 obtained by additive growth using the WAAM method.

Materials and methods

The research was conducted using metastable austenitic steel 07Cr25Ni13 obtained by the WAAM method. The samples for investigating the deposited metal were produced on a specialized bench for additive arc surfacing [17]. Surfacing was performed with the following parameters: $I = 120$ A; $U = 24$ V; $v = 350$ mm/min. A shielding gas mixture of 98 % Ar and 2 % CO_2 was used. The samples for metallographic studies were cut from the obtained blanks using waterjet cutting followed by milling. ER309LSI welding wire was used as the initial material for surfacing. The chemical composition of the wire is presented Table 1.

The metal surfacing process can result in the loss of alloying elements. The chemical composition of the surfaced metal was determined using a Foundry-Master optical emission analyzer.

The structural affiliation of the deposited material to the austenitic class was derived from the Scheffler diagram. According to the literature data [15 – 20], the phase composition obtained after surfacing depends on the Cr_{eq} and Ni_{eq} ratio and can be specified from the Scheffler diagram.

We know from the literature sources [18 – 23] that phase transformations during crystallization and the final phase composition depend on the Cr_{eq}/Ni_{eq} ratio and are divided into the following types:

- A (<1.25): $L – (L + \gamma) – \gamma$;
- AF (1.25 ≪ 1,48): $L – (L + \gamma) – (L + \gamma + \delta) – (\gamma + \delta)$;
- FA (1.48 ≪ 1,95): $L – (L + \delta) – (L + \delta + \gamma) – (\delta + \gamma)$;
- F (>1.95): $L – (L + \delta) – (\delta + \gamma)$.

These equivalents were determined using the following formulas

$$Cr_{eq} = Cr + Mo + 1.5Si + 0.5Nb + 2Ti; \quad (1)$$

$$Ni_{eq} = Ni + 30C + 0.5Mn. \quad (2)$$

Metallographic studies were performed in cross section relative to the surfacing direction at magnifications of 100 and 200, and the milled surface of the samples was also examined. The metallographic sections were prepared following the standard procedure – the samples were sanded mechanically using the sandpaper of different grits and polished with pastes. The solution consisting of 5 cm^3 HNO_3, 50 cm^3 HCl and 50 cm^3 H_2O was used as a chemical etching reagent.

To investigate the impact of heat treatment on the structure of the samples, we performed quenching in three modes followed by metal annealing. The heat treatment parameters are presented in Table 2.

Table 2. **Modes of the samples heat treatment**

Таблица 2. **Режимы термообработки образцов**

Mode number	Heating temperature, °C	Holding time, min	Cooling medium
1	1070	30	Air
2	1100	60	Air
3	1150	60	Air
4	1150	60	Furnace

Results and discussion

The study of the chemical composition of the surfaced metal revealed the decrease in the content of all alloying elements (AE), except silicon. The diminishing AE concentration is typical for metal welding and smelting processes due to their losses. The increased wire content in the surfaced metal compared to the original wire can be attributed to the heterogeneity of its chemical composition along its length. It should be noted that as the steel

Table 3. **Chemical composition of the surfaced metal**

Таблица 3. **Химический состав наплавленного металла**

Material	Content of chemical elements, %								
	C	Si	Mn	Cr	Ni	Mo	Ti	S	P
ER309LSI	0.016	0.700	1.90	23.3	13.7	0.100	0	0.004	0.0190
Surfaced metal	0.018	0.820	1.75	23.2	13.4	0.036	0	0.005	0.0114

chemical composition changed after surfacing, the AE content variations did not exceed the permissible limit (in accordance with GOST 2246 – 70). The final composition of the surfaced metal is presented in Table 3.

Chromium and nickel equivalents are calculated by the formulas (1), (2): Cr_{eq} – 23.2578; Ni_{eq} – 14.815. The Cr_{eq}/Ni_{eq} ratio is 1.57, hence, in this case the transformations during crystallization can be described by the FA mode (the Cr_{eq}/Ni_{eq} ratio exceeds 1.48). The approximate ferrite content in the surfaced metal can be determined from the Scheffler diagram (Fig. 1).

Based on the above diagram, the approximate content of δ-ferrite in the metal after surfacing is about 7.5 %, which is consistent with the theoretical data [24].

We studied the cross direction relative to the metal surfacing axis based on the microstructural analysis of the samples before and after the heat treatment. Fig. 2 shows the structure of the surfaced metal prior to heat treatment.

The dendrites are oriented normal to the surface of the laser track due to the direction of heat removal. The dendrites located deep within the surfaced metal have a more developed boundary structure. The dendritic structure refinement on the laser track surface can be put down to the supply of additional thermal energy as the next metal layer is deposited. In general, the structure of the surfaced metal is similar to the microstructure resulting from the crystallization of austenitic steel.

It was noted in [25] that the dendrites formed during surfacing may include δ-ferrite and σ-phase. Fig. 3, *b* shows that δ-ferrite has mainly skeletal and vermicular morphology. Surfacing of AISI 316L [25] and AISI 316 [26] steel resulted in a similar structure. The interdendritic space is filled with γ-phase (austenite).

Austenitization according to mode *1* (1070 °C, 30 min) did not result in visible changes in the grain structure, which is indicative of insufficient holding time

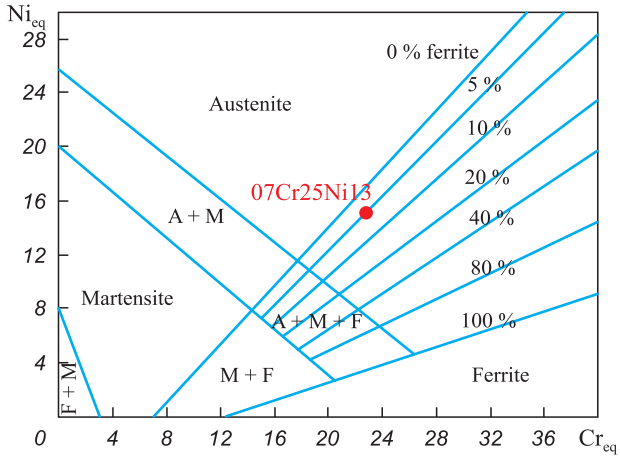

Fig. 1. Location of steel 07Cr25Ni13 on the Scheffler diagram

Рис. 1. Расположение стали 07Х25Н13 на диаграмме Шеффлера

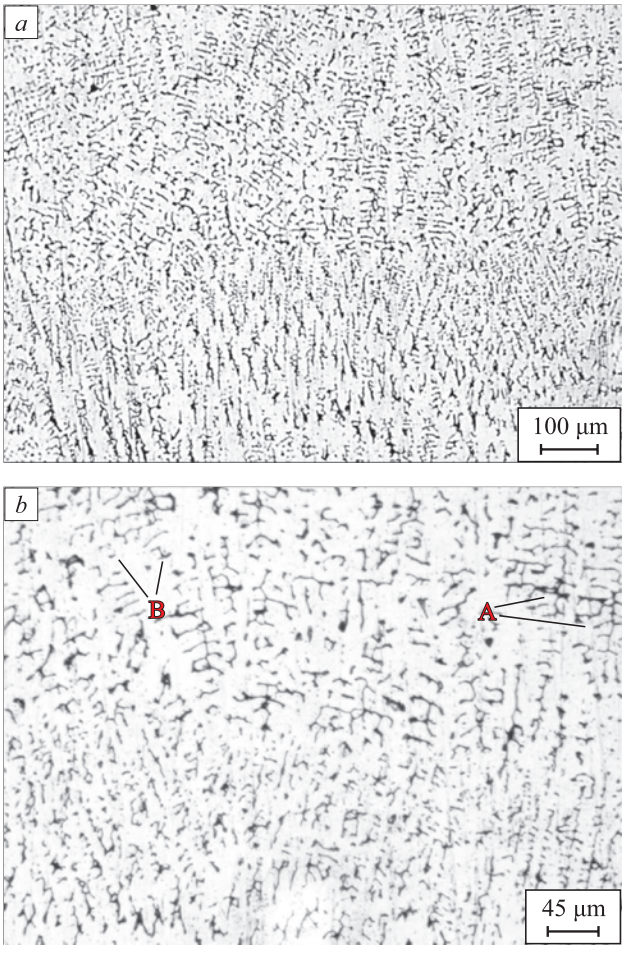

Fig. 2. Structure of the sample after surfacing: ×100 (*a*); ×200 (*b*)

Рис. 2. Структура образца после наплавки: ×100 (*a*); ×200 (*b*)

or temperature or both during austenitization (Fig. 3). It should be noted that the overall etchability of the samples increased.

The grain boundaries only begin to emerge in the structure after heat treatment according to mode *1*, which is also indicative of insufficient holding at the austenitization temperature (Fig. 3). The dendritic structure does not decrease, which indirectly shows that the content of δ- and σ-phases did not reduce. The δ-ferrite morphology does not significantly change.

We performed quenching using mode *2* (1100 °C, 60 min) to study the effect of increased austenitization temperature and holding time. Fig. 4 shows the sample microstructure in the direction transverse to the surfacing axis after heat treatment according to mode *2*.

In the micrographs of the sample after austenitization at 1100 °C, the grains formed can be seen more clearly. The dendrite size generally decreases compared to the microstructure after surfacing and treatment according to mode *1*. This effect indicates more complete diffusion processes during austenitization. Spheroidization of dendritic components is observed, their general orientation remaining the same. The percentage of δ-ferrite and σ-phase should significantly decrease after this treatment.

After quenching according to mode *3* (1150 °C, 60 min), grain boundaries and austenite twins are clearly visible in the metal structure (Fig. 5). The dendritic structure dissolved almost completely; the dendrites that failed to do so are represented by small spheroidal inclusions.

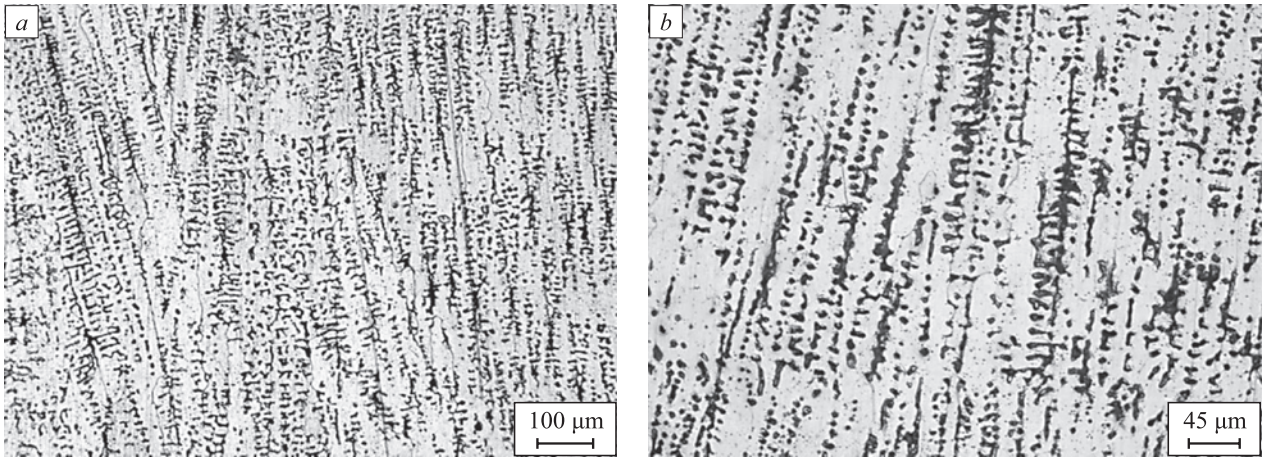

Fig. 3. Structure of the sample after quenching according to mode *1*:
×100 (*a*); ×200 (*b*)

Рис. 3. Структура образца после закалки по режиму *1*:
×100 (*a*); ×200 (*b*)

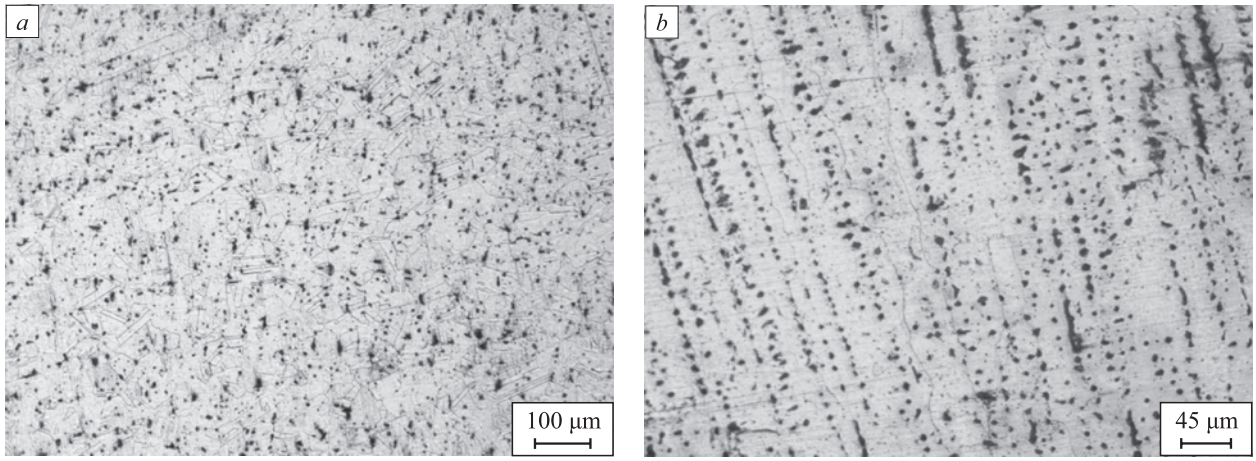

Fig. 4. Structure of the sample after quenching according to mode *2*:
×100 (*a*); ×200 (*b*)

Рис. 4. Структура образца после закалки по режиму *2*:
×100 (*a*); ×200 (*b*)

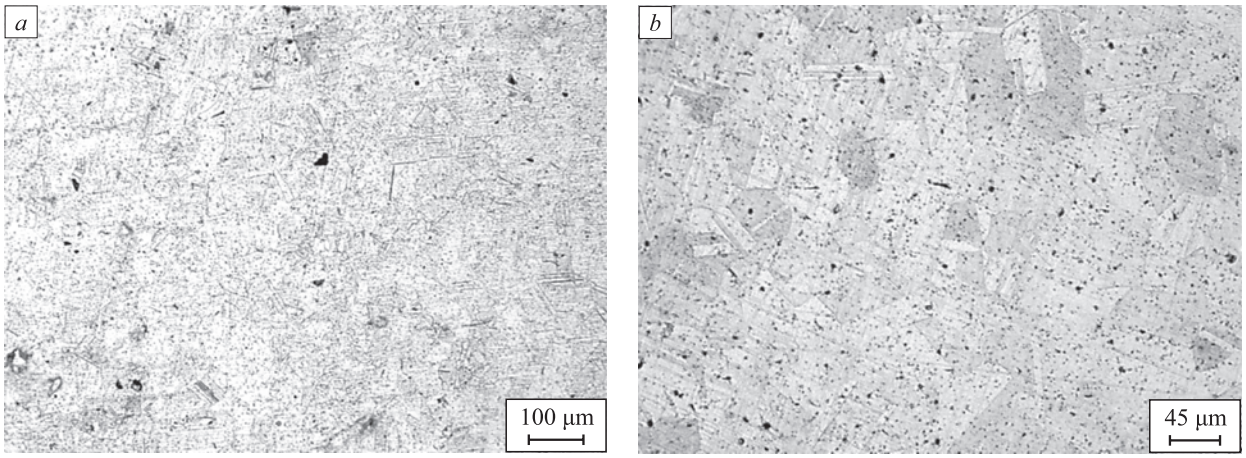

Fig. 5. Structure of the sample after quenching according to mode *3*:
×100 (*a*); ×200 (*b*)

Рис. 5. Структура образца после закалки по режиму *3*:
×100 (*а*); ×200 (*b*)

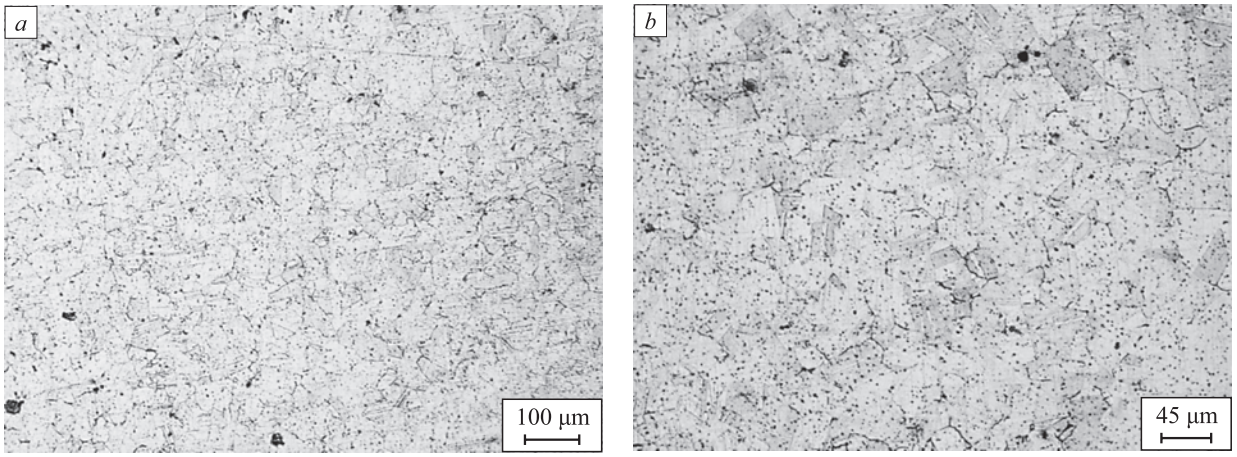

Fig. 6. Structure of the sample after annealing according to mode *4*:
×100 (*a*); ×200 (*b*)

Рис. 6. Структура образца после отжига по режиму *4*:
×100 (*а*); ×200 (*b*)

Mode *4* (1150 °C, 60 min) enables more complete dissolution of the remaining dendrites because at such metal temperatures, the diffusion is active for a longer time. The austenitic structure of the metal with characteristic twins is clearly visible (Fig. 6).

It should be noted that after annealing according to mode *4*, there is no significant grain increase compared to quenching at the same temperature and holding time.

Conclusions

It is found that after WAAM surfacing, steel 07Cr25Ni13 forms a rough dendritic structure, which may consist of δ-ferrite and σ-phase. The post-deposition structure features δ-ferrite of skeletal and vermicular morphology, with the interdendritic space filled with γ-phase. The phase composition of the deposited material is consistent with that determined from the Scheffler diagram.

Austenitization at 1070 °C with a 30 min holding time practically does not change the structure of the deposited metal. After aging the samples at 1100 °C for 60 min, we can clearly see the formation of austenitic grains and a reduction in dendrite size. Thus, structural-phase transformations in steel 07Cr25Ni13 require heating to temperatures above 1100 °C during heat treatment.

Quenching according to mode *3* (1150 °C, 60 min) results in almost complete dissolution of dendrites. The remaining undissolved dendrites appear as small spheroidized particles.

The metal structure after heat treatment according to mode *4* (1150 °C, 60 min, furnace cooling) is prac-

tically the same as that of the metal quenched from the same temperature. A significant increase in grain size, typical for austenitic steels, is not observed in this case.

In terms of potential physical and mechanical properties, heat treatment modes *3* and *4* proved to be the most favorable.

References / Список литературы

1. Chernigin M.A., Sorokina S.A., Vorobyev R.A. Study of the microstructure of metastable austenitic chromium manganese steel 14Kh15G9ND by optical and electron microscopy. *Industrial Laboratory. Diagnostics of Materials*. 2023;89(4):38–44. (In Russ.).
https://doi.org/10.26896/1028-6861-2023-89-4-38-44

   Чернигин М.А., Сорокина С.А., Воробьев Р.А. Исследование микроструктуры метастабильной аустенитной хромомарганцевой стали 14Х15Г9НД методами оптической и электронной микроскопии. *Заводская лаборатория. Диагностика материалов*. 2023;89(4):38–44.
https://doi.org/10.26896/1028-6861-2023-89-4-38-44
2. Sorokina S.A., Vorob'ev R.A., Gorshunov M.G., Chernigin M.A. Use of chromium-manganese corrosion-resistant steel in district heating network applications. *Metal Science and Heat Treatment*. 2023;65(3–4):159–166.
https://doi.org/ 10.1007/s11041-023-00908-z

   Сорокина С.А., Воробьев Р.А., Горшунов М.Г., Чернигин М.А. Опыт использования хромомарганцевой коррозионно-стойкой стали для эксплуатации в системе горячего водоснабжения (ГВС). *Металловедение и термическая обработка металлов*. 2023;3(813):32–39.
https://doi.org/10.30906/mitom.2023.3.32-39
3. Li J.L.Z., Alkahari M.R., Rosli N.A.B., Hasan R., Sudin M.N., Ramli F.R. Review of wire arc additive manufacturing for 3D metal printing. *International Journal of Automation Technology*. 2019;13(3):346–353.
https://doi.org/10.20965/ijat.2019.p0346
4. Ding D., Pan Z., Cuiuri D., Li H. Wire-feed additive manufacturing of metal components: technologies, developments and future interests. *The International Journal of Advanced Manufacturing Technology*. 2015;81:465–481.
https://doi.org/10.1007/s00170-015-7077-3
5. Wu B., Pan Z., Ding D., Cuiuri D., Li H., Xu J., Norrish J. A review of the wire arc additive manufacturing of metals: Properties, defects and quality improvement. *Journal of Manufacturing Processes*. 2018;35:127–139.
https://doi.org/10.1016/j.jmapro.2018.08.001
6. Oskolkov A.A., Matveev E.V., Bezukladnikov I.I., Trushnikov D.N., Krotova E.L. Advanced technologies for additive manufacturing of metal product. *Bulletin PNRPU. Mechanical engineering, materials science*. 2018;20(3):90–105. (In Russ.). https://doi.org/10.15593/2224-9877/2018.3.11

   Осколков А.А., Матвеев Е.В., Безукладников И.И., Трушников Д.Н., Кротова Е.Л. Передовые технологии аддитивного производства металлических изделий. *Вестник Пермского национального исследовательского политехнического университета. Машиностроение, материаловедение*. 2018;20(3):90–105.
https://doi.org/10.15593/2224-9877/2018.3.11
7. Cunningham C.R., Wikshåland S., Xu F., Kemakolam N., Shokrani A., Dhokia V., Newman S.T. Cost modelling and sensitivity analysis of wire and arc additive manufacturing. *Procedia Manufacturing*. 2017:11:650–657.
https://doi.org/10.1016/j.promfg.2017.07.163
8. Pant H., Arora A., Gopakumar G.S., Chadha U., Saeidi A., Patterson A.E. Applications of wire arc additive manufacturing (WAAM) for aerospace component manufacturing. *The International Journal of Advanced Manufacturing Technology*. 2023;127:4995–5011.
https://doi.org/10.1007/s00170-023-11623-7
9. Wang F., Williams S., Rush M. Morphology investigation on direct current pulsed gas tungsten arc welded additive layer manufactured Ti6Al4V alloy. *The International Journal of Advanced Manufacturing Technology*. 2011;57: 597–603. https://doi.org/10.1007/s00170-011-3299-1
10. Ahmadkhaniha D., Möller H., Zanella C. Studying the microstructural effect of selective laser melting and electropolishing on the performance of maraging steel. *Journal of Materials Engineering and Performance*. 2021;30:6588–6605.
https://doi.org/10.1007/s11665-021-05927-6
11. Beese A.M., Carroll B.E. Review of mechanical properties of Ti–6Al–4V made by laser-based additive manufacturing using powder feedstock. *JOM*. 2016;68:724–734.
https://doi.org/10.1007/s11837-015-1759-z
12. Kirka M.M., Lee Y., Greeley D.A., Okello A., Goin M.J., Pearce M.T., Dehoff R.R. Strategy for texture management in metals additive manufacturing. *JOM*. 2017;69:523–531.
https://doi.org/10.1007/s11837-017-2264-3
13. Williams S.W., Martina F., Addison A.C., Ding J., Pardal G., Colegrove P. Wire + arc additive manufacturing. *Materials Science and Technology*. 2016;32(7):641–647.
https://doi.org/10.1179/1743284715Y.0000000073
14. Gu J., Ding J., Williams S.W., Gu H., Bai J., Zhai Y., Ma P. The strengthening effect of inter-layer cold working and post-deposition heat treatment on the additively manufactured Al–6.3Cu alloy. *Materials Science and Engineering: A*. 2016;651:18–26. https://doi.org/10.1016/j.msea.2015.10.101
15. Nannan G., Ming L. Additive manufacturing: Technology, applications and research needs. *Frontiers of Mechanical Engineering*. 2013;8:215–243.
https://doi.org/10.1007/s11465-013-0248-8
16. Xu F., Lv Y., Liu Y., Shu F., He P., Xu B. Microstructural evolution and mechanical properties of Inconel 625 alloy during pulsed plasma arc deposition process. *Journal of Material Science and Technology*. 2013;29(5):480–488.
https://doi.org/10.1016/j.jmst.2013.02.010
17. Kabaldin Y.G., Shatagin D.A., Anosov M.S., Kolchin P.V., Kiselev A.V. Diagnostics of 3D printing on a CNC machine by machine learning. *Russian Engineering Research*. 2021;41(4):320–324.
https://doi.org/10.36652/0042-4633-2021-1-55-59
18. Fetisov G. P., Karpman M. G., etc. Materials Science and Technology of Metals. Moscow: Vysshaya shkola; 2002:638.

   Фетисов Г. П., Карпман М. Г. и др. Материаловедение и технология металлов. Москва: Высшая школа; 2002:638.
19. Suuatala N., Takalo T., Moisio T. The relationship between solidification and microstructure in austenitic and austenitic-ferritic stainless steel welds. *Metallurgical and Materials Transactions A*. 1979;10:512–514.
https://doi.org/10.1007/BF02697081

20. Kim Y.H., Kim D.G., Sung J.H., Kim I.S., Ko D.E., Kang N.H., Hong H.U., Park J.H., Lee H.W. Influences of Cr/Ni equivalent ratios of filler wires on pitting corrosion and ductility-dip cracking of AISI 316l weld metals. *Metals and Materials International*. 2011;17:151–155. https://doi.org/10.1007/s12540-011-0221-1

21. Jacob G. Prediction of solidification phases in Cr-Ni stainless steel alloys manufactured by laser based powder bed fusion process. *NIST Advanced Manufacturing Series (NIST AMS)*. 2018;100–114:1–38. https://doi.org/10.6028/NIST.AMS.100-14

22. Olson D.L. Prediction of austenitic weld metal microstructure and properties. *Welding Research Supplement*. 1985;64:281–295.

23. Sindo K. Welding Metallurgy. 2nd ed. New York: Willey; 2003.

24. Astafurov S., Astafurova E. Phase composition of austenitic stainless steels in additive manufacturing: A review. *Metals*. 2021;11(7):1052. https://doi.org/10.3390/met11071052

25. Chen X., Li J., Cheng X., He B., Wang H., Huang Z. Microstructure and mechanical properties of the austenitic stainless steel 316L fabricated by gas metal arc additive manufacturing. *Materials Science and Engineering: A*. 2017;703:567–577. https://doi.org/10.1016/j.msea.2017.05.024

26. Gürol U., Kocaman E., Dilibal S., Koçak M. A comparative study on the microstructure, mechanical properties, wear and corrosion behaviors of SS 316 austenitic stainless steels manufactured by casting and WAAM technologies. *CIRP Journal of Manufacturing Science and Technology*. 2023;47:215–227. https://doi.org/10.1016/j.cirpj.2023.10.005

Information about the Authors

Maksim S. Anosov, *Cand. Sci. (Eng.), Assist. Prof. of the Chair "Technology and Equipment Engineering",* R.E. Alekseev Nizhny Novgorod State Technical University
E-mail: anosov-maksim@list.ru

Svetlana A. Sorokina, *Cand. Sci. (Eng.), Assist. Prof. of the Chair "Materials Science, Technology of Materials and Heat Treatment of Metals",* R.E. Alekseev Nizhny Novgorod State Technical University
E-mail: rihhi@yandex.ru

Mikhail A. Chernigin, *Postgraduate of the Chair "Technology and Equipment Engineering",* R.E. Alekseev Nizhny Novgorod State Technical University
E-mail: honeybadger52@yandex.ru

Yuliya S. Mordovina, *Engineer of the Chair "Technology and Equipment Engineering", Postgraduate,* R.E. Alekseev Nizhny Novgorod State Technical University
E-mail: ips4@nntu.ru

Сведения об авторах

Максим Сергеевич Аносов, *к.т.н., доцент кафедры «Технология и оборудование машиностроения»,* Нижегородский государственный технический университет им. Р.Е. Алексеева
E-mail: anosov-maksim@list.ru

Светлана Александровна Сорокина, *к.т.н., доцент кафедры «Материаловедение, технологии материалов и термическая обработка металлов»,* Нижегородский государственный технический университет им. Р.Е. Алексеева
E-mail: rihhi@yandex.ru

Михаил Алексеевич Чернигин, *аспирант кафедры «Технология и оборудование машиностроения»,* Нижегородский государственный технический университет им. Р.Е. Алексеева
E-mail: honeybadger52@yandex.ru

Юлия Сергеевна Мордовина, *инженер кафедры «Технология и оборудование машиностроения», аспирант,* Нижегородский государственный технический университет им. Р.Е. Алексеева
E-mail: ips4@nntu.ru

Contribution of the Authors

M. S. Anosov – planning of experimental research, conducting welding of experimental samples, scientific guidance.

S. A. Sorokina – scientific guidance, metallographic analysis, editing of the article.
M. A. Chernigin – metallographic analysis, mechanical processing of the samples, chemical analysis of ingots after surfacing, thermal treatment of the samples, editing of the article.
Yu. S. Mordovina – metallographic analysis, analysis of changes in the alloy chemical composition, design and editing of the article.

Вклад авторов

М. С. Аносов – составление плана экспериментального исследования, проведение наплавки экспериментальных образцов, научное руководство.
С. А. Сорокина – научное руководство, металлографический анализ, редактирование статьи.
М. А. Чернигин – металлографический анализ, механическая обработка образцов, химический анализ заготовок после наплавки, термическая обработка образцов, редактирование статьи.
Ю. С. Мордовина – металлографический анализ, анализ изменения химического состава сплава, оформление и редактирование статьи.

Received 27.02.2024
Revised 11.03.2024
Accepted 28.03.2024

Поступила в редакцию 27.02.2024
После доработки 11.03.2024
Принята к публикации 28.03.2024

МАТЕРИАЛОВЕДЕНИЕ / MATERIALS SCIENCE

УДК 621.039.53
DOI 10.17073/0368-0797-2024-3-311-317

Оригинальная статья
Original article

Миграция границ зерен и изменение механических свойств сплава Fe – 10Ni – 20Cr при радиационном облучении

Д. С. Крыжевич, **А. В. Корчуганов**, **К. П. Зольников**

Институт физики прочности и материаловедения Сибирского отделения РАН (Россия, 634055, Томск, пр. Академический, 2/4)

kryzhev@ispms.ru

Аннотация. Проведено молекулярно-динамическое изучение механизмов миграции наклонных симметричных границ ∑5(210)[001] и ∑5(310)[001] в бикристаллических образцах Fe – 10Ni – 20Cr при радиационном облучении. Плотность радиационных дефектов растет достаточно быстро вплоть до дозы ~0,02 сна и затем выходит на насыщение. Это обусловлено уравновешиванием скоростей генерации и аннигиляции радиационных дефектов. Показано, что на ранней стадии облучения границы зерен начинали стохастически отклоняться от исходных положений вследствие взаимодействия с каскадами атомных смещений и поглощения дефектов структуры. В процессе облучения область границ зерен утолщалась и становилась шероховатой. С ростом дозы облучения увеличивались размеры кластеров точечных дефектов (тетраэдов дефектов упаковки и дислокационных петель). Взаимодействие с крупными кластерами точечных дефектов привело к образованию изгибов на изначально плоских поверхностях границ зерен. При малых расстояниях между границами высокая движущая сила между изогнутыми поверхностями существенно увеличивала скорости сближения границ зерен. Показано, что средние скорости миграции границ зерен до их непосредственного взаимодействия друг с другом составляли примерно 0,8 м/с. В результате сближения границы зерен аннигилировали, потенциальная энергия образца скачкообразно уменьшилась, и зерна объединились. Для аннигиляции границ зерен ∑5(310)[001] потребовалась в два раза большая доза облучения по сравнению с границей зерен ∑5(210)[001]. Непосредственное взаимодействие границ зерен друг с другом скачкообразно увеличивает скорости их миграции из-за возникновения движущей силы со стороны изогнутых участков поверхностей границ зерен. Изучено влияние дозы радиационного облучения на особенности деформационного поведения образцов при одноосных растяжениях. Показано, что с ростом дозы облучения предел упругости быстро понижается и выходит на насыщение при дозе облучения ~0,01 сна.

Ключевые слова: молекулярная динамика, радиационные дефекты, дефект упаковки, облучение, одноосное растяжение, Fe – 10Ni – 20Cr, миграция межзеренных границ

Благодарности: Работа выполнена при финансовой поддержке гранта РНФ № 23-29-0062.

Для цитирования: Крыжевич Д.С., Корчуганов А.В., Зольников К.П. Миграция границ зерен и изменение механических свойств сплава Fe – 10Ni – 20Cr при радиационном облучении. *Известия вузов. Черная металлургия*. 2024;67(3):311–317. https://doi.org/10.17073/0368-0797-2024-3-311-317

Grain boundary migration and mechanical properties altering in Fe – 10Ni – 20Cr alloy under irradiation

D. S. Kryzhevich, **A. V. Korchuganov**, **K. P. Zolnikov**

Institute of Strength Physics and Materials Science, Siberian Branch of the Russian Academy of Sciences (2/4 Akademicheskii Ave., Tomsk 634021, Russian Federation)

kryzhev@ispms.ru

Abstract. Mechanisms of ∑5(210)[001] and ∑5(310)[001] symmetrical tilt grain boundaries migration in bicrystall Fe – 10Ni – 20Cr samples under irradiation were investigated by means of molecular dynamics method. The density of radiation defects grows quite quickly up to a dose of ~0.02 dpa and then reaches saturation. This is due to balancing of the radiation defects generation and annihilation rates. It is shown that at the early stage of irradiation, grain boundaries began to deviate stochastically from their initial positions due to interaction with cascades of atomic displacements and absorption of structural defects. During irradiation, the grain boundary region thickened and became rough. With an increase in the radiation dose, size of the clusters of point defects (tetrahedrons of stacking faults and dislocation loops) increased. Interaction with large clusters of point defects led to the formation of bends on initially flat surfaces of grain boundaries. At small distances between the boundaries, the high driving force between

the curved surfaces of grain boundaries significantly increased the rates of their approach. The average migration rates of grain boundaries before their direct interaction with each other were approximately 0.8 m/s. As a result of their approach, the grain boundaries were annihilated, the potential energy of the sample decreased abruptly, and the grains merged. The annihilation of ∑5(310)[001] grain boundaries required twice the radiation dose compared to the ∑5(210)[001] grain boundaries. The direct interaction of grain boundaries with each other abruptly increased the velocity of their migration due to the emergence initiation of a driving force from the curved sections of the grain boundary surfaces. Influence of the radiation dose on deformation behavior features of the samples under uniaxial strains was studied. With an increase in the radiation dose, the elastic limit decreased rapidly and reached saturation at an irradiation dose of ~0.01 dpa.

Keywords: molecular dynamics, radiation defects, stacking fault, irradiation, uniaxial tension, Fe – 10Ni – 20Cr, grain boundary migration

Acknowledgements: The work was supported by the Russian Science Foundation, grant No. 23-29-0062.

For citation: Kryzhevich D.S., Korchuganov A.V., Zolnikov K.P. Grain boundary migration and mechanical properties altering in Fe – 10Ni – 20Cr alloy under irradiation. *Izvestiya. Ferrous Metallurgy*. 2024;67(3):311–317. https://doi.org/10.17073/0368-0797-2024-3-311-317

Introduction

One of effective ways to enhance radiation resistance of materials is to form various kinds of interfaces [1 – 3]. The interfaces such as grain boundaries can accumulate a considerable part of defects generated during irradiation. Irradiation of nanocrystalline Ni and Cu samples showed that their grain boundaries are the main sink for radiation defects, which significantly reduces the density of structural defects compared to coarse-grained analogs [4]. The authors of [5] applied the molecular dynamic approach to show that grain boundaries actively absorb interstitials generated by atomic displacement cascades, and a significant number of vacancies remain in the bulk. Later, the excessive interstitials leave the grain boundaries, returning to the bulk where they enhance the recombination with vacancies. The experimental study of the ion-irradiated nanocrystalline gold revealed thermal instability of the generated defects caused by a high density of grain boundaries [6]. The works [7; 8] investigated the peculiarities of grain boundaries interaction with radiation defects at the microscopic level. It is noted that grain boundaries segregate in their region their own interstitials, which are characterized by higher mobility compared to vacancies and pores. However, the issues related to the grain boundaries absorbing defects with low mobility require additional research.

High-temperature heating of materials in the nuclear reactor zone significantly accelerates the recrystallization process based on the migration of boundaries [9; 10]. To contain this process, it is important to investigate the mechanisms of interaction of radiation-induced structural defects with moving grain boundaries. The grain boundary migration controls the evolution of the materials microstructure. The driving forces behind grain boundary migration can have different physical nature, which can be related to the anisotropy of elastic energy, inhomogeneous density of defects and impurities, temperature gradient, and curvature of the grain boundary surface [11]. These driving forces are often considered in experimental and numerical studies of grain boundary migration and recrystallization of polycrystalline materials [12 – 14].

Bicrystalline samples are a reasonable alternative for investigating the behavior features of individual grain boundaries under various types of external influences, both in experiments and in simulations [15 – 18]. In the absence of external influences and internal energy gradients, the migration of grain boundaries has the nature of random walk [18]. The effect of irradiation on the mobility of grain boundaries is a scientific challenge, which should be addressed to reveal the mechanisms of radiation-stimulated grain growth.

We investigated the mechanisms of grain boundary migration in bicrystal Fe – 10Ni – 20Cr samples with ∑5(210)[001] and ∑5(310)[001] symmetrical tilt grain boundaries during irradiation and also the effect of radiation dose on the nucleation and development of plasticity in these samples under uniaxial tension.

Research method

The simulated Fe – 10Ni – 20Cr alloy samples contained two ∑5(210)[001] or ∑5(310)[001] symmetrical tilt grain boundaries and were parallelepiped-shaped with ribs sized at 12×24×12 nm. The gamma-surface minimization algorithm [19] was used to determine the optimal configuration of the grain boundary. The initial temperature of the samples was 950 K. The interatomic interaction in the material was described by the many-body potential, which enables to correctly simulate atomic displacement cascades in the sample [20]. The atoms velocity distribution in the initial samples corresponded to the Maxwell distribution, and their initial direction was set using a random number generator. To speed up the calculation, the integration step was changed dynamically, the maximum atom displacement not exceeding 0.5 pm. The integration step for given loading conditions and temperature varied between $2 \cdot 10^{-18}$ and $3 \cdot 10^{-16}$ s. To simulate irradiation, a sequence of atomic displacement cascades was generated in the samples with the primary knocked-on atom energy of 10 keV. The primary knocked-on atom and the initial direction of its displacement were chosen using a random number generator. The primary knocked-on atom was always an iron atom. To estimate the accu-

mulated radiation dose in the approximation of NRT theory, the threshold displacement energy was set equal to 40 eV, which is commonly used for iron and iron-based alloys [21]. After generation of the atomic displacement cascade, the system was relaxed for 10 ps and cooled by the thermostat to the initial temperature for 5 ps before generation of the next atomic displacement cascade. Mechanical loading was set by tension perpendicular to the grain boundary plane at a constant velocity of 5 m/s by scaling the atomic coordinates and the size of the simulated cell. As for the other directions, the system was deformed so that zero pressure could be maintained in each of these directions. Periodic boundary conditions were modeled in all directions. The simulation was performed using the LAMMPS computational package [22]. To identify local structural changes in the loaded sample, the Common Neighbor Analysis pattern for each atom was used [23]. The OVITo software was used to visualize the structure of simulated crystallites [24].

Calculation results

With the onset of irradiation, the simulated sample starts accumulating radiation-induced damage of the structure. The number of radiation defects grows quite rapidly up to a dose of ~0.02 dpa and at this value the radiation defect density reaches saturation. During irradiation, the growth of the potential energy of interatomic interaction gradually slows down (Fig. 1). At doses higher than 0.02 dpa, the rates of generation and annihilation of radiation defects equalize and the curves in Fig. 1 reach saturation. During irradiation, the grain boundaries grow thicker, and their initially flat surfaces develop roughness and curves. Fig. 2 presents the results of calculations

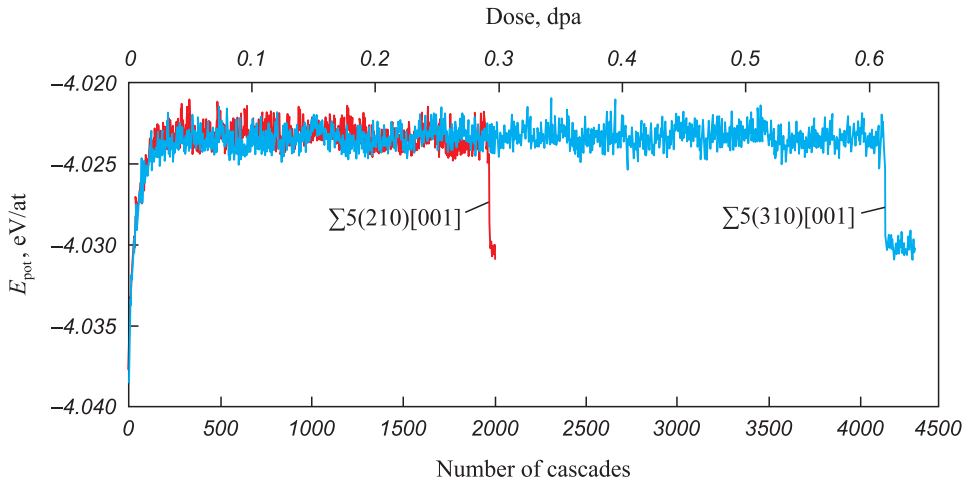

Fig. 1. Potential energy vs radiation dose for the samples with different grain boundaries

Рис. 1. Изменение потенциальной энергии образцов с различными границами зерен в зависимости от дозы облучения

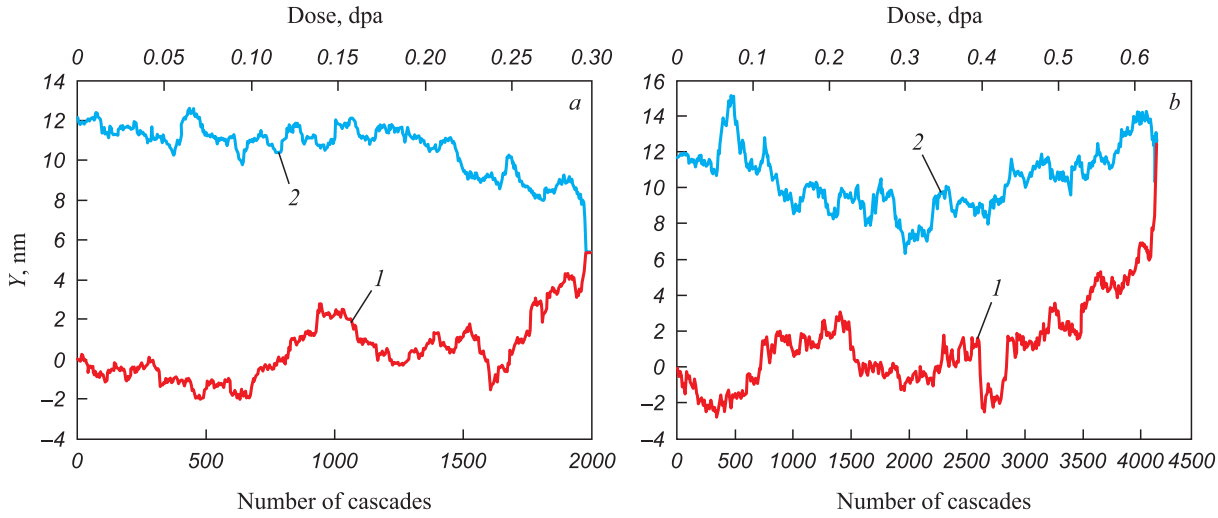

Fig. 2. ∑5[210](001) (*1*) and ∑5[310](001) (*2*) grain boundary location vs radiation dose

Рис. 2. Изменение положения границ зерен ∑5[210](001) (*1*) и ∑5(310)[001] (*2*) в зависимости от дозы облучения

of grain boundary positions in the simulated bicrystals. We can clearly see that the grain boundary movement is of a stick-slip nature. In addition, the curves presented in Fig. 2 feature irradiation intervals when grain boundaries moved both towards each other and in the opposite direction. At the same time, the trend towards their mutual approach is obvious. The impact of such processes as the generation and development of atomic displacement cascades, the cascades distance from grain boundaries, thermally activated defect diffusion, and the interaction of grain boundaries with various radiation defects in the structure, on the migration of grain boundaries accounts for these features [25].

The evolution of the unirradiated sample for more than 200 ns at a temperature of 950 K shows that the grain boundaries do not shift. This indicates that the rate of thermally activated migration of grain boundaries in the sample is significantly lower than that of the radiation-stimulated one. Irradiation of the sample causes radiation-stimulated migration of grain boundaries, during which their structure changes, which can be clearly seen in Fig. 3. The structure of the grain boundaries alters due to the interaction and absorption of various radiation defects. Fig. 3 shows the structure of grain boundaries and large clusters at different radiation doses. The majority of large clusters represent tetrahedrons of stacking faults. At a radiation dose of 0.129 dpa (Fig. 3, *a*), grain boundaries slightly shifted from the initial position, but their initially flat surfaces locally curved due to the interaction with large clusters located nearby. Fig. 2, *a* shows that the distance between the boundaries could both increase and decrease during irradiation. The direction of grain boundary displacement was determined by attraction to large clusters formed randomly on one

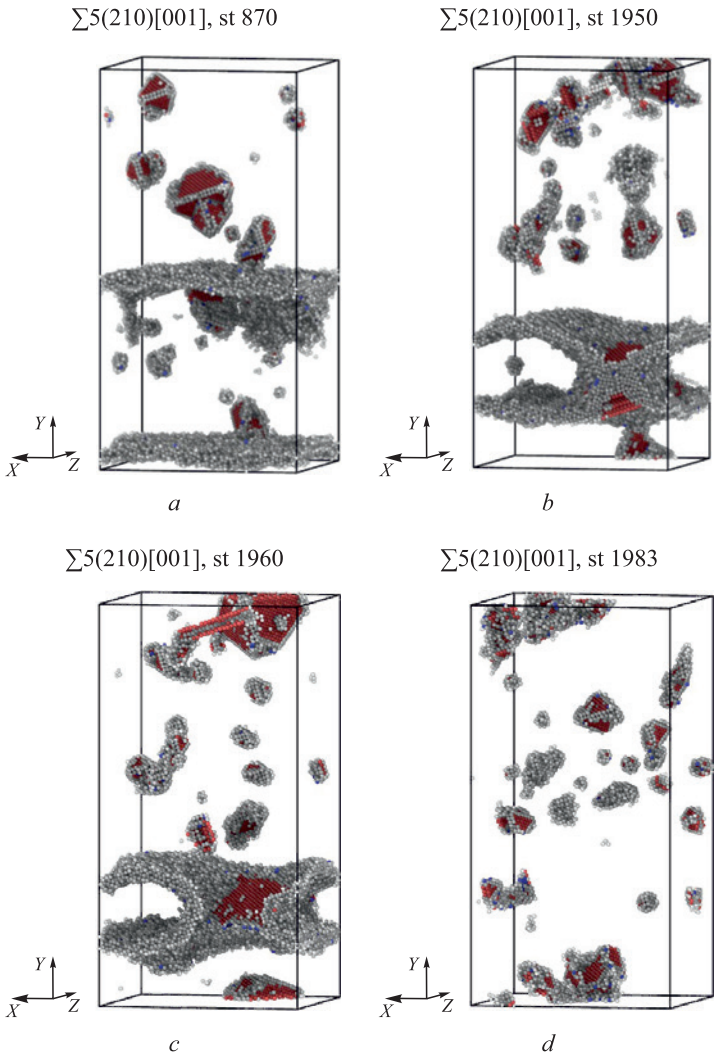

Fig. 3. ∑5[210](001) grain boundary and radiation defects for different radiation doses
(atoms with hcp and uncertain local structure are marked in red and grey, respectively; other atoms are invisible)

Рис. 3. Границы зерен ∑5(210)[001] и радиационные дефекты для различных доз облучения
(красным и серым цветами показаны атомы с ГПУ и неопределенной структурой
ближайшего окружения соответственно, остальные атомы невидимы)

or the other side of the grain boundary surface. Note that elastic forces acting between the clusters of point defects and grain boundaries account for mutual attraction between them [26]. At a radiation dose of 0.290 dpa, the surfaces of the grain boundaries curved locally toward each other due to the joint attraction to a large cluster formed in the region between the grain boundaries (Fig. 3, *b*). The distance between the curved surfaces became sufficient for the grain boundaries to interact and rapidly approach each other (Fig. 3, *c*). The calculations showed that the average migration rates of grain boundaries before their direct interaction with each other were approximately 0.8 m/s. The interaction of the curved surface regions boosted the rate of the grain boundary migration by about an order of magnitude. After the grain boundaries approached and merged, they annihilated (Fig. 3, *d*), which caused a drastic fall in the potential energy of the simulated sample (Fig. 1).

The calculations showed that the mechanisms of grain boundary migration changed during irradiation. Thus, at an early stage, up to a radiation dose of about ~0.01 dpa, grain boundaries increased their mobility compared to unirradiated ones due to the interaction with atomic displacement cascades and absorption of radiation defects. At this stage, migration manifested by chaotic oscillations of grain boundary surfaces. As the radiation dose increased, larger and larger clusters began to form in the sample, interaction with which led to accelerated migration of grain boundaries. At the same time, the migration rate of grain boundaries accelerated and they shifted further relative to their initial positions. In this interval of radiation doses, the grain boundary migration transformed from chaotic oscillations of local surface areas into displacement of surfaces as a whole. As a result, the grain boundaries deviated significantly from their initial positions. When the distance between grain boundaries became less than 4 nm, the grains began to interact directly with each other. At the same time, the rate of their migration spiked due to the high driving force from the curved surfaces of grain boundaries. A bicrystal with ∑5(310)[001] grain boundaries behaves similarly under irradiation. However, in this case, twice the radiation dose was required for grain boundary annihilation (Fig. 2).

We investigated the behavior features of samples irradiated to different doses under uniaxial tension. The calculations showed that the mechanical properties of the sample, to a large extent, depend on the radiation dose, which determines the degree of the sample radiation-induced damage. The deformation behavior showed the following general trend: the growth of the radiation dose was accompanied by rather rapid decrease in the samples elastic limit (Fig. 4, *a*), the value of which reaches saturation at doses exceeding 0.01 dpa (Fig. 4, *b*). At the given radiation dose, the density and sizes of the formed radiation defects minimized the value of energy barriers for the emergence and propagation of stacking faults – the main carriers of plastic deformation in the simulated material. Note that the elastic limit reaches saturation at a lower radiation dose than that at which the processes of generation and annihilation of radiation defects reach balance. Deviations from the elastic limit average value at higher radiation doses were caused by peculiarities of the internal structural changes, primarily related to changes in the configuration and distribution of the large clusters and dislocation loops. These changes in the defect system were stochastic in nature (Fig. 4, *b*).

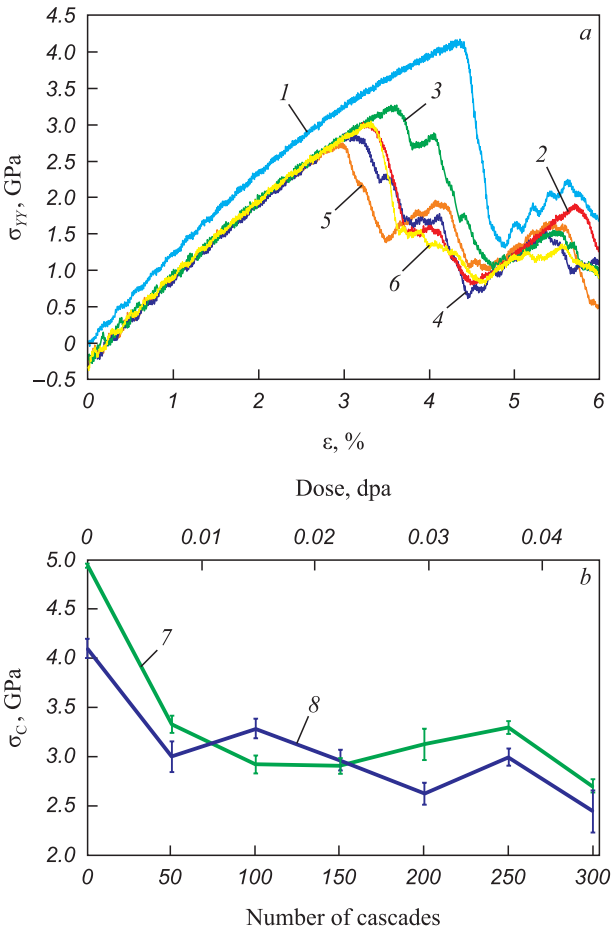

Fig. 4. Stress-strain dependence under uniaxial tension for different radiation doses for the sample with the ∑5(210)[001] grain boundary (*a*). Elastic limits vs radiation dose for samples with different types of grain boundaries (*b*):
1 – before radiation;
2 – 6 – 10, 50, 100, 150 and 250 cascades, respectively;
7 – ∑5(310)[001] ; *8* – ∑5(210)[001]

Рис. 4. Зависимости напряжений от величины деформации при одноосном растяжении для различных доз облучения образцов с границами зерен ∑5(210)[001] (*a*); зависимость предела упругости от дозы облучения для образцов с различными границами зерен (*b*):
1 – до облучения;
2 – 6 – 10, 50, 100, 150 и 250 каскадов соответственно;
7 – ∑5(310)[001] ; *8* – ∑5(210)[001]

Conclusions

The simulation results showed that the migration mechanisms of symmetrical tilt grain boundaries in Fe – 10Ni – 20Cr bicrystal change during irradiation. At low radiation doses, the migration of grain boundaries is manifested by stochastic deviations from the initial positions. This is attributed to the interaction of grain boundaries with atomic displacement cascades and absorption of mobile defects in the structure. Higher radiation doses cause formation of large clusters, interaction with which boosts the migration rate of grain boundaries and enhances local curvature of their surface. The driving force behind the migration of grain boundaries is their elastic interaction with large clusters. As the radiation dose increases further, grain boundaries tend to approach each other even more, which results in their annihilation. The migration rate spikes when the boundaries start interacting with each other. The driving force behind the migration is attributed to the strong mutual attraction between the nearby curved regions of the grain boundaries.

The calculations showed that the elastic limit of the simulated alloy drops rather rapidly, as the radiation dose grows up to 0.01 dpa, and then reaches saturation. With further irradiation, the elastic limit slightly deviates from the mean value. It is found that the elastic limit reaches saturation at a lower radiation dose than that at which the density of surviving radiation defects reaches saturation. This is because the lower radiation dose minimizes energy barriers required for the nucleation and development of plastic deformation in the material under study.

References / Список литературы

1. Zhang X., Hattar K., Chen Y., Shao L., Li J., Sun C., Yu K., Li N., Taheri M.L., Wang H., Wang J., Nastasi M. Radiation damage in nanostructured materials. *Progress in Materials Science*. 2018;96:217–321. https://doi.org/10.1016/j.pmatsci.2018.03.002
2. Grimes R.W., Konings R.J.M., Edwards L. Greater tolerance for nuclear materials. *Nature Materials*. 2008;7:683–685. https://doi.org/10.1038/nmat2266
3. Ackland G. Controlling radiation damage. *Science*. 2010; 327(5973):1587–1588. https://doi.org/10.1126/science.1188088
4. Nita N., Schaeublin R., Victoria M. Impact of irradiation on the microstructure of nanocrystalline materials. *Journal of Nuclear Materials*. 2004;329–333B:953–957. https://doi.org/10.1016/j.jnucmat.2004.04.058
5. Bai X.-M., Voter A.F., Hoagland R.G., Nastasi M., Uberuaga B.P. Efficient annealing of radiation damage near grain boundaries via interstitial emission. *Science*. 2010; 327(5973):1631–1634. https://doi.org/10.1126/science.1183723
6. Chimi Y., Iwase A., Ishikawa N., Kobiyama M., Inami T., Okuda S. Accumulation and recovery of defects in ion-irradiated nanocrystalline gold. *Journal of Nuclear Materials*. 2001;297(3):355–357. https://doi.org/10.1016/S0022-3115(01)00629-8
7. Bai X.-M., Uberuaga B.P. The influence of grain boundaries on radiation-induced point defect production in materials: A review of atomistic studies. *JOM*. 2013;65:360–373. https://doi.org/10.1007/s11837-012-0544-5
8. Beyerlein I.J., Demkowicz M.J., Misra A., Uberuaga B.P. Defect-interface interactions. *Progress in Materials Science*. 2015;74:125–210. https://doi.org/10.1016/j.pmatsci.2015.02.001
9. Li Y.H., Wang L., Li B., E J.C., Zhao F.P., Zhu J., Luo S.N. Thermally driven grain boundary migration and melting in Cu. *The Journal of Chemical Physics*. 2015;142(5):054706. https://doi.org/10.1063/1.4907272
10. Chen K., Han J., Srolovitz D.J. On the temperature dependence of grain boundary mobility. *Acta Materialia*. 2020; 194:412–421. https://doi.org/10.1016/j.actamat.2020.04.057
11. Gottstein G., Shvindlerman L.S. Grain Boundary Migration in Metals. CRC Press; 2009:711. https://doi.org/10.1201/9781420054361
12. Rupert T.J., Gianola D.S., Gan Y., Hemker K.J. Experimental observations of stress-driven grain boundary migration. *Science*. 2009;326(5960):1686–1690. https://doi.org/10.1126/science.1178226
13. Zhang H., Upmanyu M., Srolovitz D.J. Curvature driven grain boundary migration in aluminum: molecular dynamics simulations. *Acta Materialia*. 2005;53(1):79–86. https://doi.org/10.1016/j.actamat.2004.09.004
14. Tonks M., Millett P., Cai W., Wolf D. Analysis of the elastic strain energy driving force for grain boundary migration using phase field simulation. *Scripta Materialia*. 2010; 63(11):1049–1052. https://doi.org/10.1016/j.scriptamat.2010.07.034
15. Cahn J.W., Mishin Y., Suzuki A. Coupling grain boundary motion to shear deformation. *Acta Materialia*. 2006; 54(19):4953–4975. https://doi.org/10.1016/j.actamat.2006.08.004
16. Zhang H., Mendelev M.I., Srolovitz D.J. Computer simulation of the elastically driven migration of a flat grain boundary. *Acta Materialia*. 2004;52(9):2569–2576. https://doi.org/10.1016/j.actamat.2004.02.005
17. Yu W.S., Demkowicz M.J. Non-coherent Cu grain boundaries driven by continuous vacancy loading. *Journal of Materials Science*. 2015;50:4047–4065. https://doi.org/10.1007/s10853-015-8961-9
18. Olmsted D.L., Holm E.A., Foiles S.M. Survey of computed grain boundary properties in face-centered cubic metals – II: Grain boundary mobility. *Acta Materialia*. 2009; 57(13): 3704–3713. https://doi.org/10.1016/j.actamat.2009.04.015
19. Mishin Y., Farkas D. Atomistic simulation of [001] symmetrical tilt grain boundaries in NiAl. *Philosophical Magazine A*. 1998;78(1):29–56. https://doi.org/10.1080/014186198253679
20. Béland L.K., Tamm A., Mu S., Samolyuk G.D., Osetsky Y.N., Aabloo A., Klintenberg M., Caro A., Stoller R.E. Accurate classical short-range forces for the study of collision cascades in Fe–Ni–Cr. *Computer Physics Communication*. 2017;219:11–19. https://doi.org/10.1016/j.cpc.2017.05.001
21. Stoller R.E., Toloczko M.B., Was G.S., Certain A.G., Dwaraknath S., Garner F.A. On the use of SRIM for computing radiation damage exposure. *Nuclear Instruments and*

Methods in Physics Research. Section B. 2013;310:75–80. https://doi.org/10.1016/j.nimb.2013.05.008

22. Plimpton S. Fast parallel algorithms for short-range molecular dynamics. *Journal of Computational Physics*. 1995; 117(1):1–19. https://doi.org/10.1006/jcph.1995.1039

23. Honeycutt J.D., Andersen H.C. Molecular dynamics study of melting and freezing of small Lennard-Jones clusters. *Journal of Physical Chemistry*. 1987;91(19):4950–4963. https://doi.org/10.1021/j100303a014

24. Stukowski A. Visualization and analysis of atomistic simulation data with OVITo – the Open Visualization Tool. *Modelling and Simulation in Materials Science and Engineering*. 2010;18:015012. https://doi.org/10.1088/0965-0393/18/1/015012

25. Jin M., Cao P., Short M.P. Mechanisms of grain boundary migration and growth in nanocrystalline metals under irradiation. *Scripta Materialia*. 2019;163:66–70. https://doi.org/10.1016/j.scriptamat.2018.12.038

26. Jin M., Cao P., Yip S., Short M.P. Radiation damage reduction by grain-boundary biased defect migration in nanocrystalline Cu. *Acta Materialia*. 2018;155:410–417. https://doi.org/10.1016/j.actamat.2018.05.071

Information about the Authors / Сведения об авторах

Dmitrii S. Kryzhevich, *Cand. Sci. (Phys.-Math.), Research Associate of the Laboratory of Computer-Aided Design of Materials,* Institute of Strength Physics and Materials Science, Siberian Branch of the Russian Academy of Sciences
ORCID: 0000-0002-1423-3724
E-mail: kryzhev@ispms.ru

Aleksandr V. Korchuganov, *Cand. Sci. (Phys.-Math.), Research Associate of the Laboratory of Computer-Aided Design of Materials,* Institute of Strength Physics and Materials Science, Siberian Branch of the Russian Academy of Sciences
ORCID: 0000-0002-3765-5911
E-mail: avkor@ispms.ru

Konstantin P. Zolnikov, *Dr. Sci. (Phys.-Math.), Chief Researcher of the Laboratory of Computer-Aided Design of Materials,* Institute of Strength Physics and Materials Science, Siberian Branch of the Russian Academy of Sciences
ORCID: 0000-0001-8988-1040
E-mail: kost@ispms.ru

Дмитрий Сергеевич Крыжевич, *к.ф.-м.н., научный сотрудник лаборатории компьютерного конструирования материалов,* Институт физики прочности и материаловедения Сибирского отделения РАН
ORCID: 0000-0002-1423-3724
E-mail: kryzhev@ispms.ru

Александр Вячеславович Корчуганов, *к.ф.-м.н., научный сотрудник лаборатории компьютерного конструирования материалов,* Институт физики прочности и материаловедения Сибирского отделения РАН
ORCID: 0000-0002-3765-5911
E-mail: avkor@ispms.ru

Константин Петрович Зольников, *д.ф.-м.н., главный научный сотрудник лаборатории компьютерного конструирования материалов,* Институт физики прочности и материаловедения Сибирского отделения РАН
ORCID: 0000-0001-8988-1040
E-mail: kost@ispms.ru

Contribution of the Authors / Вклад авторов

D. S. Kryzhevich – writing the text, planning and performing experiments.
A. V. Korchuganov – writing of the sections Introduction and Methods, performing experiments.
K. P. Zolnikov – writing the text, planning experiments, analysis and selection of literary sources.

Д. С. Крыжевич – написание основного текста статьи, планирование и проведение экспериментов.
А. В. Корчуганов – написание введения, описание методов исследования, проведение экспериментов.
К. П. Зольников – написание основного текста статьи, планирование экспериментов, анализ и подбор литературных источников.

Received 15.11.2023
Revised 18.11.2023
Accepted 28.03.2024

Поступила в редакцию 15.11.2023
После доработки 18.11.2023
Принята к публикации 28.03.2024

MATERIALS SCIENCE / МАТЕРИАЛОВЕДЕНИЕ

UDC 621.785.532
DOI 10.17073/0368-0797-2024-3-318-324

Original article
Оригинальная статья

NITROGEN DIFFUSION ALONG THE LAYER BOUNDARIES AFTER NITRIDING OF MULTILAYER MATERIALS

K. B. Polikevich[1], A. L. Petelin[1, 2], A. I. Plokhikh[1], L. P. Fomina[3]

[1] **Bauman Moscow State Technical University** (5/1 Baumanskaya 2-ya Str., Moscow 105005, Russian Federation)
[2] **National University of Science and Technology "MISIS"** (4 Leninskii Ave., Moscow 119049, Russian Federation)
[3] **Industrial Complex "Salyut", JSC "United Engine Corporation"** (16/2 Budennogo Ave., Moscow 105118, Russian Federation)

polikevich94@mail.ru

Abstract. Diffusion processes play a key role in formation of the structures of new materials and technological processes of strengthening heat treatments, since diffusion is the reason for redistribution of substances in solids. An urgent task is to develop technologically advanced and effective methods for strengthening materials in order to improve their performance properties. There is an increasing need to improve chemical heat treatment methods, which directly affects the wear resistance of working surfaces, and, consequently, the product service life. Near-surface volumes experience increased loads, so the formation of high-strength layers becomes an important task. Quite a few methods of surface hardening are known, among which carburization, nitriding, nitrocarburization and others are widely used. The most interesting is nitriding, since it increases hardness, strength, fatigue limit, and heat resistance. However, despite the proper advantages, nitriding has a number of disadvantages, including the holding duration and small thickness of diffusion layers. The solution is related to intensification of the technological process by increasing the nitriding temperature, activating the nitriding media or directly the parts surface. All these solutions are aimed at accelerating diffusion processes, both in grain volume and along grain boundaries, the velocity along which is many times higher than the velocity of volumetric diffusion. It may be effective to use a new type of structural metal materials with a multilayer structure of hundreds of layers, with thicknesses in the micron and submicron ranges separated by large angular boundaries. The results of metallographic studies showed the effect of the steel layers interchange in the multilayer metal material on diffusion depth after chemical heat treatment. The authors proposed an accelerate diffusion model of diffusible element along the layer boundaries.

Keywords: multilayer metal materials, chemical heat treatment, nitriding, layer boundaries, diffusion

For citation: Polikevich K.B., Petelin A.L., Plokhikh A.I., Fomina L.P. Nitrogen diffusion along the layer boundaries after nitriding of multilayer materials. *Izvestiya. Ferrous Metallurgy*. 2024;67(3):318–324. https://doi.org/10.17073/0368-0797-2024-3-318-324

ДИФФУЗИЯ АЗОТА ПО ГРАНИЦАМ СЛОЕВ ПРИ АЗОТИРОВАНИИ МНОГОСЛОЙНЫХ МАТЕРИАЛОВ

К. Б. Поликевич[1], А. Л. Петелин[1, 2], А. И. Плохих[1], Л. П. Фомина[3]

[1] **Московский государственный технический университет им. Н.Э. Баумана** (Россия, 105005, Москва, 2-я Бауманская ул., 5/1)
[2] **Национальный исследовательский технологический университет «МИСИС»** (Россия, 119049, Москва, Ленинский пр., 4)
[3] **Производственный комплекс «Салют» АО «Объединенная двигателестроительная корпорация»** (Россия, 105118, Москва, пр. Буденного, 16, кор. 2)

polikevich94@mail.ru

Аннотация. Диффузионные процессы играют ключевую роль в формировании структур новых материалов и технологических процессов упрочняющих термических обработок, так как именно благодаря диффузии происходит перераспределение вещества в твердых телах. Актуальной задачей является разработка технологичных и эффективных методов упрочнения материалов в целях повышения их эксплуатационных свойств. Возрастает потребность в усовершенствовании методов химико-термической обработки, что напрямую влияет на износостойкость рабочих поверхностей, а, следовательно, и на ресурс изделия. Приповерхностные объемы испытывают повышенные нагрузки, поэтому важной задачей является формирование высокопрочных слоев. Известно достаточно много методов поверхностного упрочнения, среди которых широкое применение получили цементация, азотирование, нитроцементация и др. Наиболее перспективным является азотирование, поскольку при этом происходит повышение твердости, прочности, предела усталости, жаростойкости. Однако при должных достоинствах азотирование имеет ряд недостатков, среди которых длительность выдержки и малая толщина диффузионных слоев. Поэтому разработка методик, позволяющих интенсифицировать рассматриваемый процесс, также является актуальной задачей. Традиционно, решение связано с интенсификацией технологического процесса путем повышения температуры азотирования, активации

сред азотирования или непосредственно поверхности деталей. Все эти решения направлены на ускорение процессов диффузии как по объему зерна, так и по межзеренным границам, скорость по которым многократно превосходит скорость объемной диффузии. Учитывая это, эффективным может оказаться использование нового типа конструкционных металлических материалов с многослойным строением из сотен слоев с толщинами микронного и субмикронного диапазона, разделенными между собой большими угловыми границами. В работе приведены результаты металлографического исследования, показывающие влияние чередования слоев сталей в многослойных металлических материалах на глубину диффузии при проведении химико-термической обработки азотированием. Предложена модель ускоренного проникновения диффундирующего элемента по границам слоев.

Ключевые слова: многослойные материалы, химико-термическая обработка, азотирование, границы слоев, диффузия

Для цитирования: Поликевич К.Б., Петелин А.Л., Плохих А.И., Фомина Л.П. Диффузия азота по границам слоев при азотировании многослойных материалов. *Известия вузов. Черная металлургия*. 2024;67(3):318–324. https://doi.org/10.17073/0368-0797-2024-3-318-324

Introduction

Currently various mechanical wood treatments by milling are widely used. The main unit of a router is the cutter. There are numerous cutters of different designs and geometries, but, in each case, they should be characterized by high strength and wear resistance, which can be achieved by chemical heat treatment [1]. The multilayer materials used after nitriding for manufacturing cutters can enable to enhance tool durability, preserve tool geometry, increase tool life, and improve processing performance due to a significantly hardened layer. Fig. 1 shows an example of such a cutter.

Additionally, multilayer materials can be used to manufacture gear wheels that also operate under wear (Fig. 2).

This structure can be obtained if steels with different crystalline structure are included in the initial composition [2 – 4]. The developed technological route (Fig. 3) enables to produce sheet billets, 2 to 10 mm thick [5].

The material microstructure has a multilayer laminar structure with the layers, 100 to 0.8 μm thick. At the same time, the layers are characterized by crystallographic disorientation from 15 to 20°, which corresponds to the large-angle grain boundaries in the initial steels (Fig. 4) [6; 7].

The works [8; 9] show that with an appropriate choice of steels included in the initial composite billet, the multilayer structure is preserved up to the temperature of 1000 °C, which corresponds to the temperature of hot

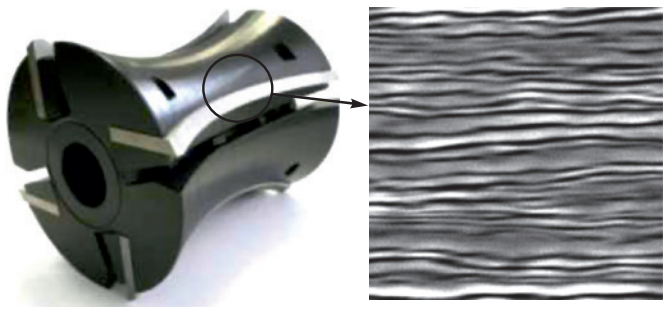

Fig. 1. Layout of a cutter from a multilayer material

Рис. 1. Схема фрезы из многослойного материала

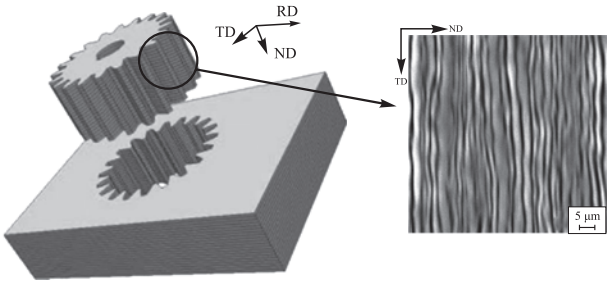

Fig. 2. Scheme of manufacturing a gear wheel from a multilayer material

Рис. 2. Схема изготовления зубчатого колеса из многослойного материала

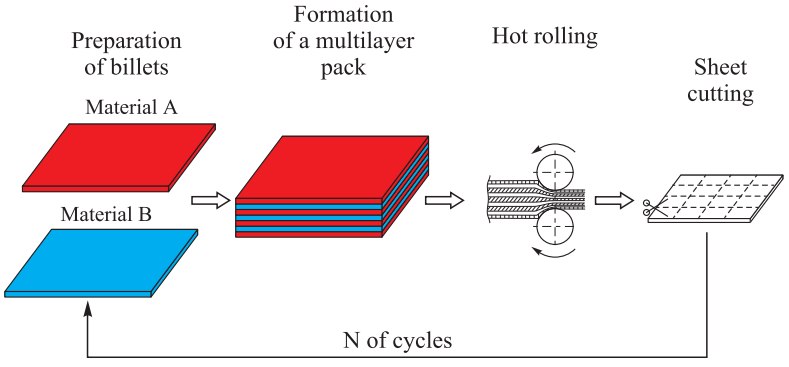

Fig. 3. Scheme of technological route

Рис. 3. Схема технологического маршрута

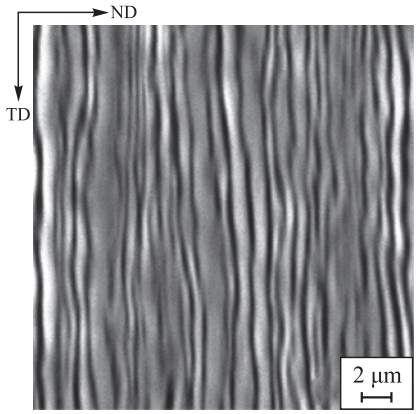

Fig. 4. Typical microstructure of cross section of a multilayer material (composition based on steels AISI420 and AISI304)

Рис. 4. Типичная микроструктура поперечного сечения многослойного материала (композиция из сталей 08Х18Н10 и 40Х13)

pack rolling. In this case, the cross-section of the sheet billets has a structural orientation ready for chemical heat treatment (Fig. 5).

Preliminary evaluation of nitriding the multilayer composition that includes AISI304 and AISI430 steels showed that the nitriding depth in the multilayer material is greater than its depth in AISI304 steel which is hard to nitride. The reason behind the increased thickness of the nitrided layer in multilayer materials may be the accelerated diffusion of nitrogen along the layer boundaries with subsequent saturation of layer volumes from their boundaries as from the diffusing element sources [10].

To thoroughly investigate the resulting effect, we used model compositions of multilayer materials containing steels of different compositions (grades). The following study objects were selected for nitriding: composites consisting of 1008 and AISI304 steels, as well as W108 and AISI304 steels. After hot pack rolling, we obtained 10-mm thick samples with 100 layers, the single layer being 100 μm thick.

The samples of these compositions were nitrided, the nitriding surfaces being in all cases perpendicular to the rolling directions used to produce the multilayer samples. Nitriding was performed in the gas atmosphere containing 20 – 40 % ammonia dissociation products. We used two nitriding conditions with the following temperature and time parameters: 540 °C for 45 h and 580 °C for 25 h. To study the structure of the resulting nitrided layers and to determine their geometric characteristics, we prepared sections with the surfaces perpendicular to the rolling direction and parallel to the direction of nitrogen diffusion penetration that occurred in the course of nitriding (Fig. 6).

Fig. 7 shows the general view of diffusion profiles formed during nitriding for AISI304 and 1008 (*a*), AISI304 and W108 (*b*) compositions obtained after nitriding at 540 °C for 45 h.

The micrographs show the concentration profile of diffusing nitrogen in AISI304 steel with a considerable nitrogen penetration depth (and a long nitrogen diffusion path, respectively) along the layer boundaries of the multilayer material. Inside the AISI304 component layer, for both cases, the nitrogen penetration distance shrinks with increasing distance from the interlayer boundary. The smallest depth of nitrogen penetration is about 100 μm from the outer surface of the samples and midway between the layers of neighboring components (midway between the layers of 1008 steel (*a*) and W108 steel (*b*)) inside the layer of AISI304 steel. This indicates that the source of nitrogen penetration into the volume of AISI304 steel during nitriding is the interface between the layers of the material. The diffusion along these boundaries occurs faster than that through the layer of AISI304 steel from the outer surface.

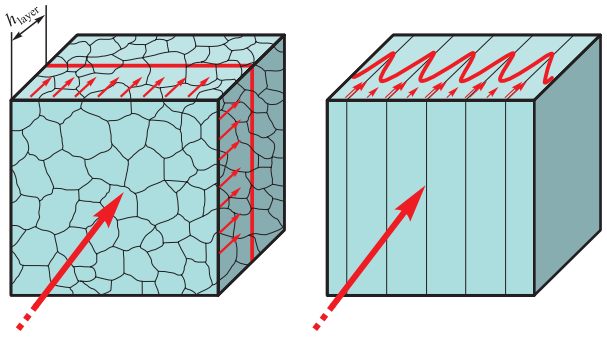

Fig. 5. Scheme of polyhedral and laminar structure of structural metallic materials indicating diffusion profiles. Arrows indicate the direction of diffuser flow

Рис. 5. Схема полиэдрического и ламинарного строения конструкционных металлических материалов с указанием диффузионных профилей. Стрелками указано направление потока диффузанта

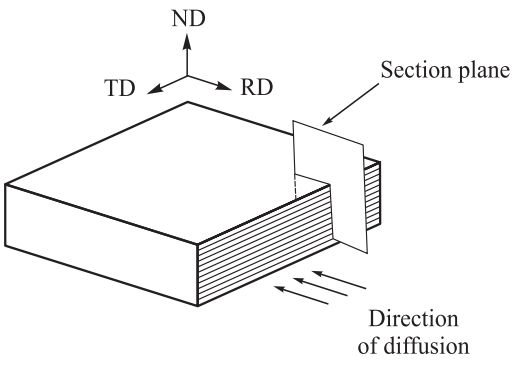

Fig. 6. Scheme of sample cutting for metallographic analysis

Рис. 6. Схема вырезки образцов для проведения металлографического анализа

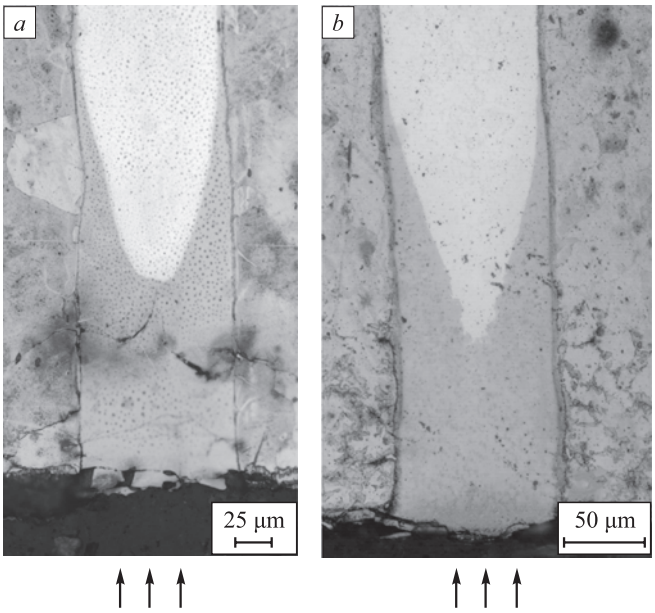

Fig. 7. Microstructure of nitrided layer of composition based on steels: AISI304 and 1008 (*a*), AISI304 and W108 (*b*). Arrows indicate the direction of nitrogen diffusion flow

Рис. 7. Микроструктура азотированного слоя композиций 08Х18Н10 + 08кп (*a*) и 08Х18Н10 + У8 (*b*). Стрелками указано направление диффузионного потока азота

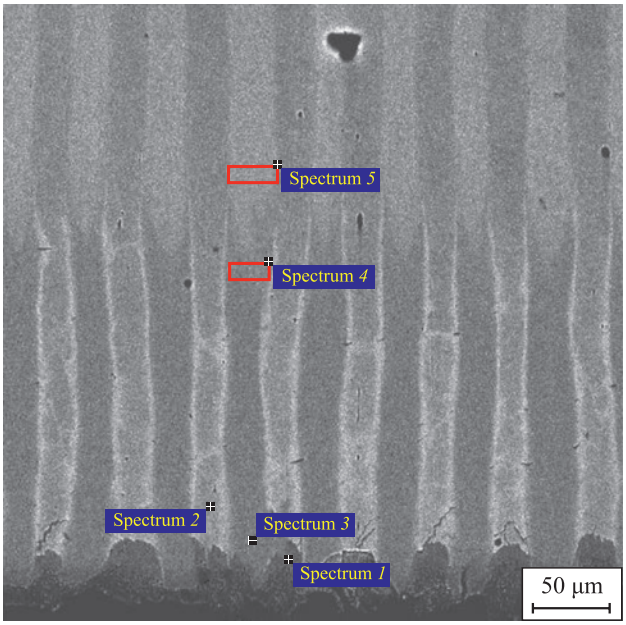

Spectrum	Content, wt. %					
	N	Si	Cr	Mn	Fe	Ni
1	4.53	0	0.63	0.42	94.42	0
2	0	0	0.63	0.46	98.68	0.24
3	4.62	0.57	18.20	1.73	67.43	7.45
4	4.24	0.44	17.48	1.74	68.61	7.49
5	0	0.57	18.10	1.67	72.09	7.57

Fig. 8. Results of qualitative MRS analysis of the diffusion layer of composition based on steels W108 and AISI304

Рис. 8. Результаты качественного МРС анализа диффузионного слоя композиции У8 + 08Х18Н10

Nitrogen penetration into the layers of 1008 and W108 steels at this depth from the nitriding surface was not detected. This is proved by the results of electron microscopy and *X*-ray spectral analysis. There is practically no volume diffusion of nitrogen in 1008 and W108 steels due to low solubility of nitrogen in α-iron (maximum 0.1 wt. %), which is the main pathway of nitrogen diffusion in the ferrite phase [11]. The second reason inhibiting nitrogen movement in 1008 steel is the surface nitride formation consisting of nitrides (Fe_2N), which is also proved by the results of electron microscopy (Fig. 8).

Thus, it can be concluded that the nitriding process in multilayer materials of this type occurs due to the fast nitrogen diffusion along the layer boundaries [12; 13].

It can be assumed that simultaneously nitrogen atoms migrate inside the AISI304 steel perpendicular to the interlayer boundary, which can be considered as an extended source of nitrogen diffusion. This steel is an austenitic grade steel and the solubility of nitrogen in austenite (γ-iron) is about 2.8 wt. %, therefore, diffusion saturation of AISI304 layers with nitrogen is possible. According to literature data [14], the diffusion coefficient of nitrogen in γ-iron at temperatures ranging from 500 to 600 °C is determined by the following equation

$$D_\gamma = 4.6 \cdot 10^{-5} \exp\left(-\frac{108{,}474}{RT}\right), \text{ m}^2/\text{s}. \quad (1)$$

We used the Fisher model for calculating diffusion along grain boundaries in metallic samples to determine the diffusion permeability of layer boundaries of the multilayer material [15 – 18]. According to this model, the product of the diffusion coefficient D_b along the grain boundary (layer boundaries in this case) and the boundary thickness δ, that is value of $s\delta D_b$, can be calculated by the formula [19]

$$s\delta D_b = (\pi t)^{1/2} D_\gamma^{3/2} \text{ctg}^2\theta, \quad (2)$$

where θ is the angle at the top of the component concentration profile (Fig. 7), which passes into the phase (layer) volume from the grain (layer) boundary; s is the ratio of boundary enrichment with atoms of the diffusing component, which can be estimated based on the dependence proposed in [20]:

$$sx_0 = 6.2 \pm 4.5, \quad (3)$$

where x_0 is the volumetric concentration of the impurity in mole fractions.

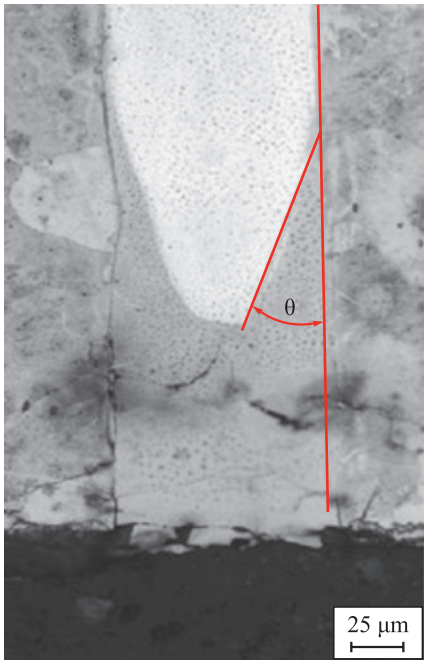

Fig. 9. Concentration angle θ for determining the diffusion coefficient in a multilayer material

Рис. 9. Концентрационный угол θ для определения диффузионной проницаемости слоевых границ в многослойном материале

If we assume that the enrichment of layer boundaries is mainly determined by the ferrite phase, since in accordance with the phase diagram it has the smallest Fe–N concentration of nitrogen, according to formula (3), the value of enrichment of layer boundaries shall equal $s = 5 \cdot 10^3$.

It should be noted that the formula (2) is suitable for describing diffusion along the layer boundary when the diffusive removal of the component (nitrogen in this case) from the boundary into the bulk is one-sided – volume diffusion occurs only towards the layers of AISI304 steel. The experimental data shows that there is no diffusion of nitrogen toward the layers of 1008 steel (Fig. 10, *a*) or W108 steel (Fig. 10, *b*).

The values of angles θ required to calculate the diffusion coefficient D_b along the layer boundaries were determined by analyzing micrographs of cross-sections of multilayer samples of both compositions after nitriding using two processing modes.

For the 1008 + AISI304 composition, Fig. 8, *a* shows the method for measuring these angles when nitriding is performed at 540 °C for 45 h and Fig. 10, *b* – when the operating parameters are 580 °C and 25 h.

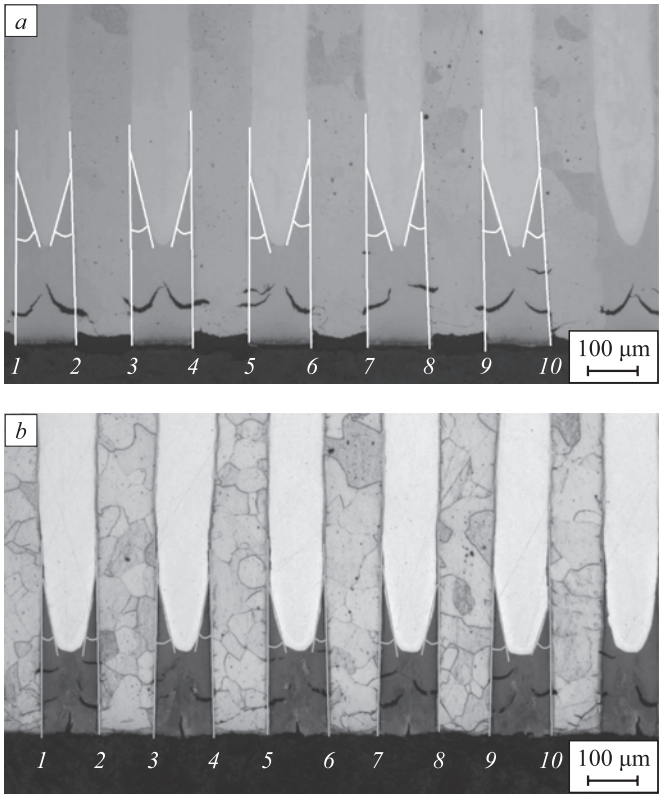

Fig. 10. Determination of the angles θ for calculating the product of δ and D_b for the composition based on steels 1008 and AISI304 after nitriding: t = 540 °C, 45 h (*a*); t = 580 °C, 25 h (*b*)

Рис. 10. Определение углов θ для расчета произведения δ D_b для композиции 08кп + 08Х18Н10 после азотирования при 540 °С, 45 ч (*a*); 580 °С, 25 ч (*b*)

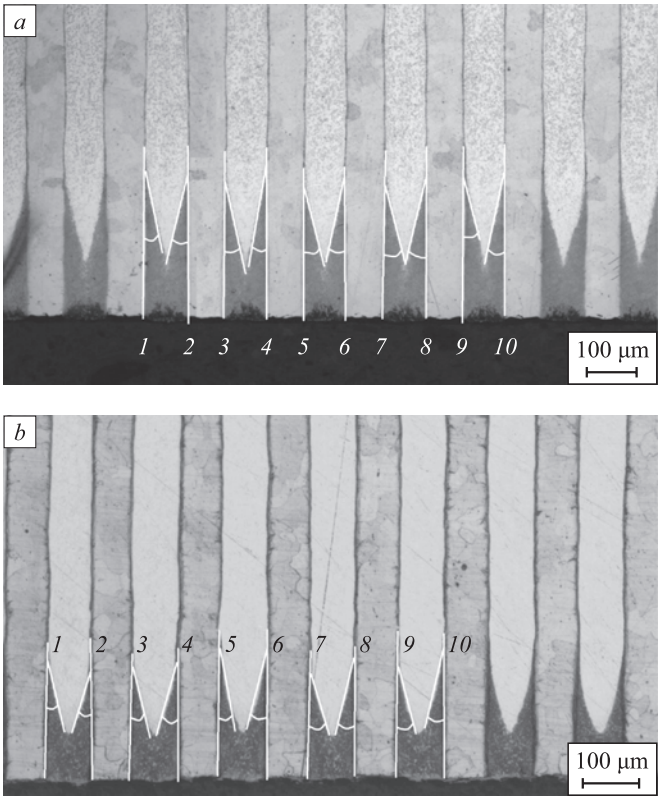

Fig. 11. Determination of the angles θ for calculating the product of δ and D_b for the composition based on steels W108 and AISI304 after nitriding: t = 540 °C, 45 h (*a*); t = 580 °C, 25 h (*b*)

Рис. 11. Определение углов θ для расчета произведения δ D_b для композиции У8 + 08Х18Н10 после азотирования при 540 °С, 45 ч (*a*); 580 °С, 25 ч (*b*)

Nitrogen diffusion coefficients along the layer boundaries D_b, m²/s

Коэффициенты диффузии азота по границам слоев D_b, м²/с

Composition	Nitriding mode	
	540 °C, 45 h	580 °C, 25 h
1008 + AISI304	$1.9 \cdot 10^{-8}$	$8.1 \cdot 10^{-8}$
W108 + AISI304	$4.3 \cdot 10^{-8}$	$15.9 \cdot 10^{-8}$

For the W108 + AISI304 composition, the similar procedure is shown in Fig. 11.

The Table presents the diffusion coefficients of nitrogen atoms along the layer boundaries for 1008 + AISI304 and W108 + AISI304 multilayer compositions obtained by analyzing experimental data as nitriding of these materials samples was investigated. The calculation assumes that the layer boundaries thickness δ is 10^{-9} m.

Conclusions

The experimental study of nitriding the samples of multilayer metallic materials with alternating layers of two different steel grades revealed that the main mechanism behind the process is mass transfer (diffusion) of nitrogen atoms along the boundaries of the material layers.

The analysis of experimental data obtained while investigating cross sections of surface layers of two compositions of multilayer materials after nitriding using two modes enabled us to obtain the estimated values of nitrogen diffusion coefficients D_b along layer boundaries. The D_b values were 10^4 times higher than the volume diffusion coefficient of nitrogen in AISI304 steel under the same conditions.

The study showed that the nitriding depth in both multilayer compositions increased due to fast diffusion penetration of nitrogen atoms along the layer boundaries of multilayer materials.

References / Список литературы

1. Lakhtin Yu.M., Kogan Ya.D., Shpis G.I., Bemer Z. Theory and Technology of Nitriding. Moscow: Metallurgiya; 1991:320.

   Лахтин Я.М., Коган Я.Д., Шпис Г.И., Бемер З. Теория и технология азотирования. Москва: Металлургия; 1991:320.
2. Huang B., Ishihara K.N., Shingu P.H. Preparation of high strength bulk nano-scale Fe/Cu multilayers by repeated pressing-rolling. *Materials Science Letters*. 2001;20:1669–1670. https://doi.org/10.1023/A:1012465117652
3. Yoshioka T., Yasuda M., Miyamura H., Kikuchi S., Tokumitsu K. Structure of Fe-Ag super-laminates fabricated by repeated rolling and mechanically alloyed Fe-Ag powder. *Materials Science Forum*. 2002;386–388:503–508. https://doi.org/10.4028/www.scientific.net/MSF.386-388.503
4. Saito Y., Utsunomiya H., Tsuji N., Sakai T. Novel ultra-high straining process for bulk materials development of the accumulative roll-bonding (ARB) process. *Acta Materialia*. 1999;47(2):579–583. https://doi.org/10.1016/S1359-6454(98)00365-6
5. Torizuka S. Present trend of the development of ultrafine-grained steels and its technology transfer. *Materia Japan*. 2006;45(6):438–443.
6. Kolesnikov A.G., Plokhikh A.I., Shinkarev A.S., Mironova M.O. Multilayer steel composition rolling peculiarities. *Blanking Productions in Mechanical Engineering*. 2013;(8):39–42.
7. Kolesnikov A.G., Plokhikh A.I., Komisarchuk Yu.S., Mikhal'tsevich I.Yu. A study of special features of formation of submicro- and nanosize structure in multilayer materials by the method of hot rolling. *MiTOM*. 2010;(6):44–49.

   Колесников А.Г., Плохих А.И., Комисарчук Ю.С., Михальцевич И.Ю. Исследование особенностей формирования субмикро- и наноразмерной структуры в многослойных материалах методом горячей прокатки. *MuTOM*. 2010;(6):44–49.
8. Tabatchikova T.I., Plokhikh A.I., Yakovlev I.L., Klyueva S.Yu. Structure and properties of a steel-based multilayer material produced by hot pack rolling. *The Physics of Metals and Metallography*. 2013;114(7):580–592.

   Табатчикова Т.И., Плохих А.И., Яковлев И.Л., Клюева С.Ю. Структура и свойства многослойного материала на основе сталей, полученного методом горячей пакетной прокатки. *Физика металлов и металловедение*. 2013;114(7):633–646.
9. Aryulin S.B., Khalipov I.V. Preparation of multilayer composite materials by hot rolling. *Zagotovitel'nye proizvodstva v mashinostroenii*. 2013;(7):31–35.

   Арюлин С.Б., Халипов И.В. Получение многослойных композиционных материалов методом горячей прокатки. *Заготовительные производства в машиностроении*. 2013;(7):31–35.
10. Plokhikh A.I. On the possibility of using metallic materials for machine parts hardened by chemical heat treatment. *Izvestiya Volgogradskogo gosudarstvennogo tekhnicheskogo universiteta*. 2013;(6(109)):13–17.

    Плохих А.И. О возможности применения многослойных металлических материалов для деталей машин упрочняемых ХТО. *Известия Волгоградского государственного технического университета*. 2013;(6(109)):13–17.
11. Bannykh O.A., Budberg P.B., Alisova S.P. State Diagrams of Binary and Multicomponent Systems Based on Iron. Moscow: Metallurgiya; 1986:224.

    Банных О.А., Будберг П.Б., Алисова С.П. Диаграммы состояния двойных и многокомпонентных систем на основе железа. Москва: Металлургия; 1986:224.
12. Polikevich K.B., Plokhikh A.I. Study of the process of nitriding in multilayer materials based on steel. *IOP Conference Series: Materials Science and Engineering*. 2019;683:012048. https://doi.org/10.1088/1757-899X/683/1/012048
13. Petelin A.L., Plokhikh A.I., Novikov A.A. The model of the layer boundary diffusion in multilayer materials. *Defect and Diffusion Forum*. 2015;363:142–147. https://doi.org/10.4028/www.scientific.net/DDF.363.142

14. Fedorov A.A. Diffusion of nitrogen in stainless steel. In: *Technical Sciences in Russia and Abroad: Materials of the 3rd Sci. Conf. (Moscow, July 2014.)*. Moscow: Buki-Vedi; 2014:85-88. Available at URL: https://moluch.ru/conf/tech/archive/90/5561/ (accessed: 07.10.2024).

Федоров А.А. Диффузия азота в нержавеющей стали. Технические науки в России и за рубежом: *Материалы III Международной научной конференции (Москва, июль 2014 г.)*. Москва: Буки-Веди; 2014:85–88. URL: https://moluch.ru/conf/tech/archive/90/5561/ (дата обращения: 07.10.2024).

15. Bokshtein B.S., Kopetskii Ch.V., Shvindlerman L.S. Thermodynamics and Kinetics of Grain Boundaries in Metals. Moscow: Metallurgiya; 1986:224.

Бокштейн Б.С., Копецкий Ч.В., Швиндлерман Л.С. Термодинамика и кинетика границ зерен в металлах. Москва: Металлургия; 1986:224.

16. Boksteyn B.S., Nikolskiy G.S., Smirnov A.N. Grain boundary segregation of antimony in alloys of the cooper-antimony system. *The Physics of Metals and Metallography*. 1995;72:142–146.

17. Bokstein B.S., Straumal B.B. Diffusion in materials science and technology. In: *Diffusive Spreading in Nature, Technology and Society*. Springer, Cham; 2018:261–275. https://doi.org/10.1007/978-3-319-67798-9_13

18. Kaur I., Mishin Y., Gust W. Fundamentals of Grain and Interphase Boundary Diffusion. 3rd ed. John Wiley & Sons; 1995:536.

19. Mishin Y., Herzig Chr. Grain boundary diffusion: recent progress and future research. *Materials Science and Engineering: A*. 1999;260(1–2):55–71. https://doi.org/10.1016/S0921-5093(98)00978-2

20. Hondros E.D., Seah M.P. Segregation to interfaces. *International Metals Reviews*. 1977;22(1):262–301.

Information about the Authors / Сведения об авторах

Kseniya B. Polikevich, *Senior Lecturer of the Chair "Materials Science",* Bauman Moscow State Technical University
E-mail: polikevich94@mail.ru

Aleksandr L. Petelin, *Dr. Sci. (Phys.–Math.), Prof.,* Bauman Moscow State Technical University; *Prof. of the Chair of Physical Chemistry,* National University of Science and Technology "MISIS"
E-mail: alexander-petelin@yandex.ru

Andrei I. Plokhikh, *Cand. Sci. (Eng.), Assist. Prof. of the Chair "Materials Science",* Bauman Moscow State Technical University
E-mail: plokhikh@bmstu.ru

Lyudmila P. Fomina, *Cand. Sci. (Eng.), Assist. Prof.,* Industrial Complex "Salyut", JSC "United Engine Corporation"
E-mail: fominalp@yandex.ru

Ксения Борисовна Поликевич, *старший преподаватель кафедры «Материаловедение»,* Московский государственный технический университет им. Н.Э. Баумана
E-mail: polikevich94@mail.ru

Александр Львович Петелин, *д.ф-м.н., профессор,* Московский государственный технический университет им. Н.Э. Баумана; *профессор кафедры физической химии,* Национальный исследовательский технологический университет «МИСИС»
E-mail: alexander-petelin@yandex.ru

Андрей Иванович Плохих, *к.т.н., доцент кафедры «Материаловедение»,* Московский государственный технический университет им. Н.Э. Баумана
E-mail: plokhikh@bmstu.ru

Людмила Петровна Фомина, *к.т.н, доцент,* Производственный комплекс «Салют» АО «Объединенная двигателестроительная корпорация»
E-mail: fominalp@yandex.ru

Contribution of the Authors / Вклад авторов

K. B. Polikevich – literary review, selection and preparation of the research objects.
A. L. Petelin – development of a mathematical model and determination of diffusion coefficients for the research objects.

A. I. Plokhikh – statement of the problem, development of the research concept.
L. P. Fomina – carrying out the technological process of nitriding on the studied compositions.

К. Б. Поликевич – анализ литературы, подбор и подготовка объектов исследования.
А. Л. Петелин – разработка математической модели и определение коэффициентов диффузии для рассматриваемых объектов исследования.
А. И. Плохих – постановка проблемы, разработка концепции исследования.
Л. П. Фомина – проведение технологического процесса азотирования на исследуемых композициях.

Received 30.06.2023
Revised 04.02.2024
Accepted 28.03.2023

Поступила в редакцию 30.06.2023
После доработки 04.02.2024
Принята к публикации 28.03.2024

MATERIALS SCIENCE / МАТЕРИАЛОВЕДЕНИЕ

UDC 539.213:669.017
DOI 10.17073/0368-0797-2024-3-325-331

Original article
Оригинальная статья

Kinetics of deformation fronts during serrated Lüders deformation in α-iron at high temperature

D. V. Orlova ✉, **V. I. Danilov, V. V. Gorbatenko, L. V. Danilova, A. V. Bochkareva**

Institute of Strength Physics and Materials Science, Siberian Branch of the Russian Academy of Sciences (2/4 Akademicheskii Ave., Tomsk 634055, Russian Federation)

✉ dvo@ispms.ru

Abstract. At room temperature, the deformation of most bcc metals, which contain a small amount of interstitial elements, is accompanied by the formation of a Lüders band and its monotonic propagation over the tensile yield area. Within the framework of the autowave concept, front of the Lüders band is a switching autowave, which realizes the transition from a metastable elastically deformable state to a stable plastically deformable state. However, in the temperature range of blue brittleness of mild steels of 423 – 510 K, when the interaction of atoms of the dissolved substance with mobile dislocations takes place, propagation of the Lüders band is accompanied by a discrete flow. The patterns of propagation of the Chernov-Lüders fronts in ARMCO iron in the temperature range from 296 to 503 K and strain rates from $6.67 \cdot 10^{-6}$ to $3.7 \cdot 10^{-2}$ s^{-1} are considered in this paper. It was established that under these conditions both monotonic and discrete kinetics of front movement can be realized. Regardless of the movement nature, the Lüders deformation and width of the front remain unchanged throughout the entire process. The local strain rate at the front depends on magnitude of the effective stress, and with monotonic kinetics it increases with stress according to an exponential law, and with discrete kinetics it increases according to a linear law. This difference is due to different autowave modes that are formed in this case. The autowave of localized plasticity switching corresponds to monotonic kinetics, and the autowave of excitation – to discrete kinetics.

Keywords: Chernov-Lüders deformation, deformation front, local strain rate, autowave, localized plasticity

Acknowledgements: The work was performed within the framework of the state task of the Institute of Strength Physics and Materials Science, Siberian Branch of the Russian Academy of Science, subject No. FWRW-2021-0011.

For citation: Orlova D.V., Danilov V.I., Gorbatenko V.V., Danilova L.V., Bochkareva A.V. Kinetics of deformation fronts during serrated Lüders deformation in α-iron at high temperature. *Izvestiya. Ferrous Metallurgy*. 2024;67(3):325–331.
https://doi.org/10.17073/0368-0797-2024-3-325-331

Особенности кинетики деформационных фронтов при скачкообразной деформации Людерса в α-железе при повышенной температуре

Д. В. Орлова ✉, **В. И. Данилов, В. В. Горбатенко, Л. В. Данилова, А. В. Бочкарева**

Институт физики прочности и материаловедения Сибирского отделения РАН (Россия, 634055, Томск, пр. Академический, 2/4)

✉ dvo@ispms.ru

Аннотация. При комнатной температуре деформация большинства ОЦК-металлов, которые содержат небольшое количество элементов внедрения, сопровождается образованием полосы Людерса и ее монотонным распространением на площадке текучести при растяжении. В рамках автоволновой концепции фронт полосы Людерса является автоволной переключения, которая реализует переход из метастабильного упруго деформируемого в стабильное пластически деформируемое состояние. Однако в температурном интервале синеломкости мягких сталей 423 – 510 К, когда имеет место взаимодействие атомов растворенного вещества с подвижными дислокациями, распространение полосы Людерса сопровождается прерывистым течением. В настоящей работе рассмотрены закономерности распространения фронтов Чернова-Людерса в АРМКО-железе в интервале температур от 296 до 503 К и скоростей деформирования от $6{,}67 \cdot 10^{-6}$ до $3{,}7 \cdot 10^{-2}$ $с^{-1}$. Установлено, что в этих условиях может реализовываться как монотонная, так и дискретная кинетика движения фронтов.

Независимо от характера движения, деформация Людерса и ширина фронта в течение всего процесса остаются неизменными. Локальная скорость деформации на фронте зависит от величины действующего напряжения, причем при монотонной кинетике она возрастает с напряжением по степенному закону, а при дискретной – по линейному закону. Данное различие обусловлено разными автоволновыми модами, которые при этом формируются. Монотонной кинетике соответствует автоволна переключения локализованной пластичности, а дискретной – автоволна возбуждения.

Ключевые слова: деформация Чернова-Людерса, фронты локализованной деформации, локальная скорость деформации, автоволны, локализованная пластичность

Благодарности: Работа выполнена в рамках государственного задания Института физики прочности и материаловедения Сибирского отделения РАН, тема номер FWRW-2021-0011.

Для цитирования: Орлова Д.В., Данилов В.И., Горбатенко В.В., Данилова Л.В., Бочкарева А.В. Особенности кинетики деформационных фронтов при скачкообразной деформации Людерса в α-железе при повышенной температуре. *Известия вузов. Черная металлургия*. 2024;67(3):325–331. https://doi.org/10.17073/0368-0797-2024-3-325-331

Introduction

At room temperature, deformation of most BCC metals containing small amounts of interstitial elements is accompanied by the formation of a Chernov–Lüders band, which propagates monotonically across the yield plateau during tension [1 – 4]. The propagation behavior of the Lüders band can vary depending on grain size, temperature, applied stress, and strain rate. The band expands uniformly across the yield plateau, with all deformation concentrated at its boundaries, or deformation fronts, at any given moment. The velocities of front movement are proportional to the velocity imposed by the loading device. According to the autowave concept [5 – 7], the Chernov–Lüders band front represents an autowave switch that transitions from a metastable elastically deformable state to a stable plastically deformable state [8; 9]. However, within the blue brittleness temperature range for mild steels (423 – 510 K) [10 – 12], where dislocation movement is influenced by dynamic strain aging, the propagation of the Lüders band is characterized by discrete flow. In [13], it was established that within the temperature range of 393 – 503 K in ARMCO iron, the stationary kinetics of Lüders front movement is replaced by serrated behavior. The temperature at which Lüders deformation becomes serrated increases with increasing deformation rate. On the serrated yield plateau, the discretely propagating Lüders band front represents an autowave of localized plasticity excitation. Notably, front movement in this case only occurs during the stress relaxation process associated with serration. This raises a question about the nature of dependence of the local deformation rate in front region on the applied stress during the serrated process.

This study is dedicated to establishing the kinetic regularities of deformation front propagation during serrated Lüders deformation in α-iron at elevated temperatures.

Materials and methods

The material used for the study was ARMCO iron with the following composition (wt. %): C 0.025; Si 0.05; Cu 0.05; Mn 0.035; S 0.025; P 0.015; Fe – remainder. Test samples in the form of double-sided blades were laser-cut from hot-rolled sheet with a thickness of 1.5 mm. The working area of the sample was 50×10 mm. To standardize the stress and structural states before testing, the samples were annealed in a vacuum according to the following regime: 1233 K for 1 h, followed by cooling with the furnace to room temperature.

The prepared samples were subjected to uniaxial tension using an LFM-125 testing machine at speeds ranging from 0.02 to 10 mm/min. Tests were conducted at temperatures ranging from 296 to 503 K. The STE-12H furnace (Walter + Bai) with independent temperature control in three zones was used. The sample temperature was measured using three thermocouples installed along the sample axis at a distance of 20 mm from each other.

Analysis of the kinetics of Lüders deformation fronts was performed using digital image correlation [14; 15] and digital statistical speckle photography [16; 17]. To form the speckle structure, the sample was illuminated with coherent light from a semiconductor laser (635 nm, 15.0 mW). The sample images were captured using a Point Grey FL3-GE-50S5MC digital video camera with a resolution of 2448×2048 pixels at a frame rate of 2 to 25 fps, depending on the stretching speed. Chronograms [18] were constructed from the obtained data arrays, which allowed for the identification of Lüders band nucleation regions and determination of the kinetic characteristics of their fronts.

Results and discussion

Fig. 1 shows the yield plateaus of the stress-strain curves of ARMCO iron obtained at room temperature and elevated temperatures. At room temperature, the strain curve exhibits a typical tooth and smooth yield plateau characteristic of low-carbon steels. At a test temperature of 423 K and a deformation rate of $6.67 \cdot 10^{-5}$ s^{-1}, periodic stress jumps occur on the yield plateau.

It is known that at temperatures below 393 K, ARMCO iron exhibits normal strain rate sensitivity, meaning that

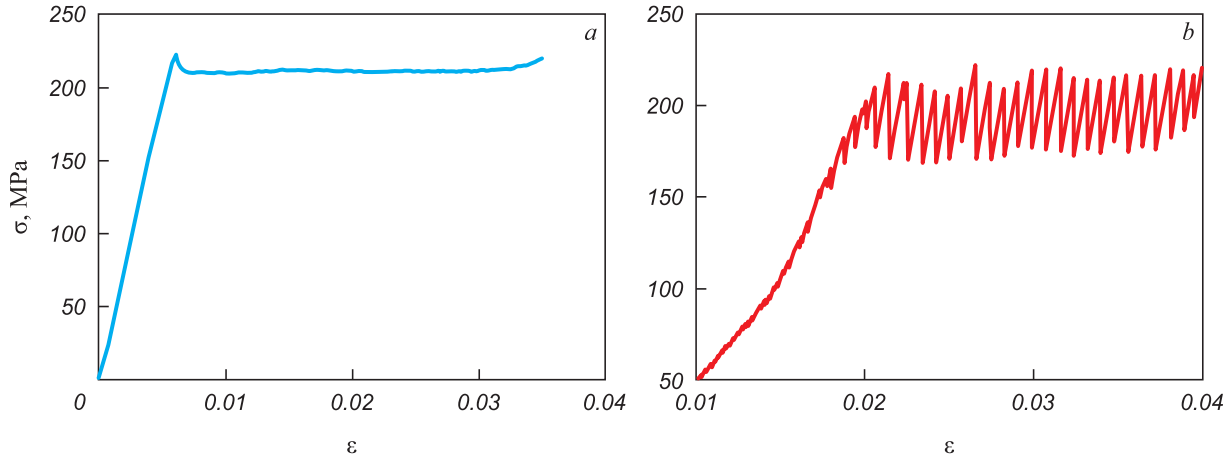

Fig. 1. Yield plateau in α-iron samples at $T = 295$ K, $\dot{\varepsilon} = 6.67 \cdot 10^{-5}$ s^{-1} (*a*) and $T = 423$ K, $\dot{\varepsilon} = 6.67 \cdot 10^{-5}$ s^{-1} (*b*)

Рис. 1. Площадка текучести образцов α-железа при $T = 295$ К, $\dot{\varepsilon} = 6{,}67 \cdot 10^{-5}$ с$^{-1}$ (*a*) и $T = 423$ К, $\dot{\varepsilon} = 6{,}67 \cdot 10^{-5}$ с$^{-1}$ (*b*)

the yield stress on the yield plateau (lower yield strength $\sigma_y^{(l)}$) increases with increasing deformation rate and decrease with increasing temperature [19]. As shown in Fig. 2, *a*, at room temperature, the lower yield strength increases non-linearly with increasing deformation rate.

Studies in the temperature region of the serrated development of the Lueders strain have shown that with increasing deformation rate, the amplitude of stress jumps decreases, while the stress level $\sigma_y^{(l)}$ at which the drop occurs remains constant (Fig. 2, *b*). Thus, in the temperature range of serrated flow, the strain rate sensitivity of the lower yield strength is absent. At the same time, the stress at the onset of the jump (upper yield strength $\sigma_y^{(u)}$) monotonically decreases with increasing deformation rate.

Studies on the nature of deformation localization using digital statistical speckle photography identified that fronts of localized plastic deformation form and move both on the smooth (Fig. 3, *a*) and serrated (Fig. 3, *b*) yield plateaus. However, in the former case, the front moves monotonically at a constant velocity V_f, while in the latter case, it moves discretely, only during the stress drop in the serration process.

Based on the fact that the deformation front passes through the entire length of the sample L during the observed yield plateau Δt, then $L = V_f \Delta t$. During this time, the sample undergoes elongation expressed as $\Delta L = V_d \Delta t$ (where V_d is the deformation rate set by the loading device). Therefore, the deformation acquired by the sample on the yield plateau can be represented as

$$\varepsilon_L = \frac{\Delta L}{L} = \frac{V_d}{V_f}. \qquad (1)$$

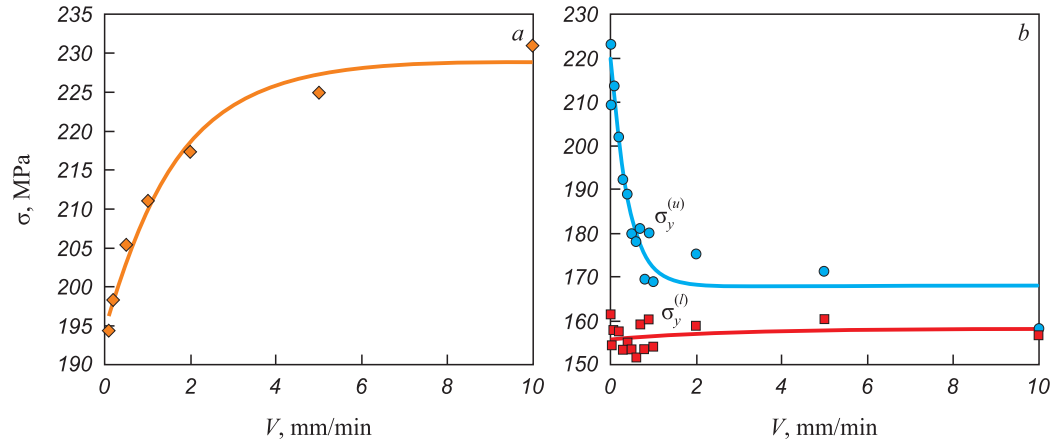

Fig. 2. Strain rate dependence of the lower yield strength at $T = 295$ K (*a*) and strain rate dependence of the lower (■) and upper (●) yield strength at $T = 423$ K (*b*)

Рис. 2. Скоростная зависимость нижнего предела текучести при $T = 295$ К (*a*) и скоростная зависимость нижнего (■) и верхнего (●) предела текучести при $T = 423$ К (*b*)

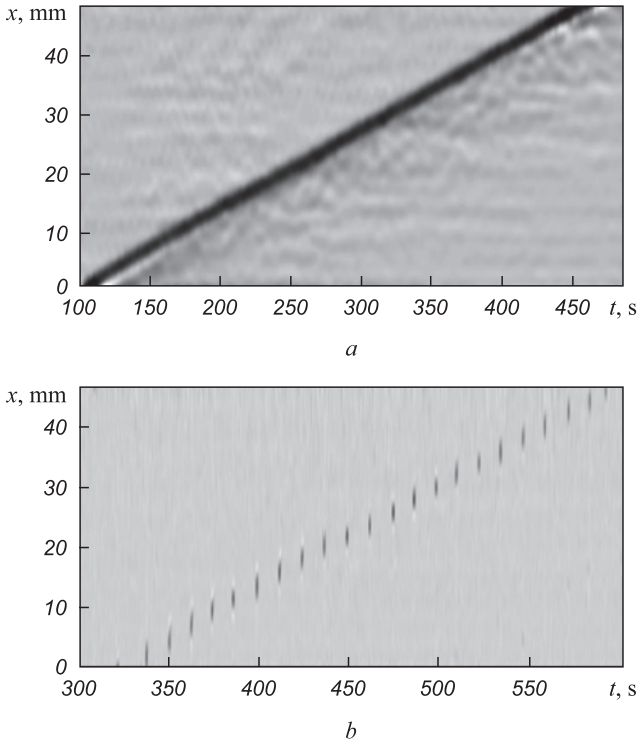

Fig. 3. Chronograms of deformation fronts movement on yield plateaus at strain rate of $6.67 \cdot 10^{-5}$ s^{-1} and temperatures 293 K (*a*) and 423 K (*b*)

Рис. 3. Хронограммы движения деформационных фронтов на площадках текучести при скорости растяжения $6{,}67 \cdot 10^{-5}$ $с^{-1}$ и температурах 293 K (*a*) и 423 K (*b*)

From this, it follows that the front velocity and deformation rate are interrelated by the equation $V_d = \varepsilon_L V_f$. If this relationship is normalized by the front width δ, then the relative deformation velocity is expressed as

$$\dot{\varepsilon} = \frac{V_d}{\delta} = \varepsilon_L \frac{V_f}{\delta} = \frac{\varepsilon_L}{t_f}, \qquad (2)$$

where t_f is the time of front motion during a jump at a certain velocity V_f.

Thus, the relative deformation velocity $\dot{\varepsilon}$ and front velocity V_f must be linearly related if the deformation ε_L at any given time is constant and concentrated at the front. Furthermore, for this equation to hold, the width of the deformation front δ during motion must also remain constant.

To test the first postulate of ε_L constancy, measurements of marker displacements on the surface of the sample were conducted during deformation on a serrated yield plateau. Markers were applied to the surface of the sample in three rows, spaced 100 μm apart, using a PMT-3M microhardness tester. Two series of images of these markers were then taken before and after deformation using a NEOPHOT-21 optical microscope. Measurements of the distance between the centers of two adjacent markers before deformation (l) and after deformation (l_1) allowed for the determination of the displacement of each marker $\Delta l = l_1 - l$, thus obtaining the displacement field $\Delta l(x)$ (where x is the marker coordinate). By numerically differentiating this field, the local deformation at each point was calculated as $\varepsilon_L = \Delta l / l$. Fig. 4 shows the distribution of ε_L along the length of the sample. The application of the hypothesis of a normally distributed population [20] showed that changes in ε_L are random in nature, with the magnitude being considered constant and its average value being $\varepsilon_L = 0.0184 \pm 0.0003$.

As stated in [17], when using the digital statistical speckle photography method to visualize deformation fronts, the brightness of the front image is proportional to the deformation within it. From this, the average width of the front δ can be determined. Measurements for fronts moving during all jumps (Figs. 1, *b* and 3, *b*) showed that their width is constant and equal to 105 ± 7 μm. Thus, the second postulate of front width constancy is also fulfilled, and equation (2) can be used to investigate the relationship between local deformation rate and stress in the during a jump.

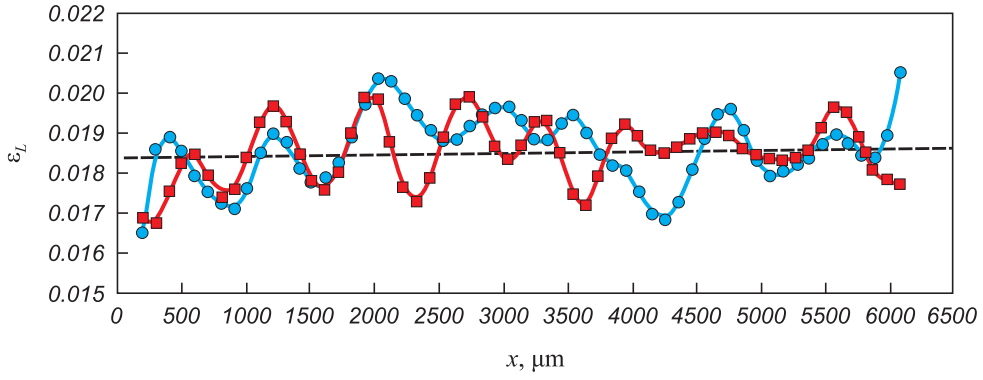

Fig. 4. Dependence of local deformation ε_L on yield plateau on the position of markers x

Рис. 4. Зависимость локальной деформации ε_L на площадке текучести от положения маркеров x

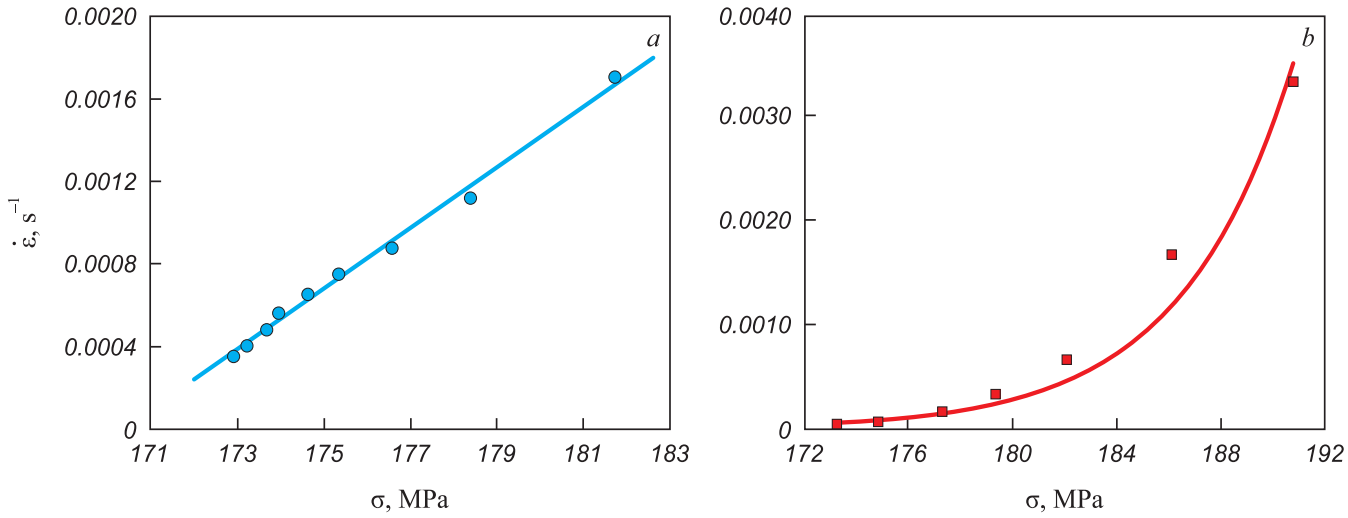

Fig. 5. Change of strain rate during serrated movement of the front (*a*) and change in deformation rate during monotonic movement of the front (*b*)

Рис. 5. Изменение скорости деформации при скачкообразном движении фронта (*a*) и изменение скорости деформации при монотонном движении фронта (*b*)

Fig. 5, *a* shows this dependence. It can be seen that $\dot{\varepsilon}$ increases linearly with increasing stress. The correlation coefficient of the interpolating relationship is $\rho = 0.99$. On the other hand, in the case of a monotonically moving front, based on the correlation relationship (Fig. 2) and equations (1) and (2), the strain rates at the front can be calculated for each $\sigma_y^{(l)}$ (Fig. 5, *b*). It is evident that it cannot be interpolated by a linear function. In other words, the strain rates in the monotonically moving front and the serrated moving front react differently to changes in the stress state.

The reason for this difference may be the change in the deformation autowave mode from the autowave of switching to the autowave of excitation. In [13], it is shown that the kinetics of Lüders front motion in ARMCO iron is indeed controlled by the effect of dynamic strain aging, i.e., the delay time t_w of mobile dislocations at barriers overcome by thermally activated processes, and the time t_a of carbon impurity deposition on these dislocations. At temperatures below 393 K, when $t_a \gg t_w$, front moves monotonically and represents an autowave of localized plasticity switching. In this case, the local strain rate increases non-linearly with stress according to a parabolic law. The discrete nature of the deformation front movement occurs under temperature-rate conditions where t_w and t_a are comparable. The serrated moving deformation front represents an autowave of localized plasticity excitation. In this case, the local strain rate depends linearly on the applied stress.

Conclusion

The deformation accumulated on the serrated yield plateau in α-iron is constant. Under these conditions, the width of the front is also a constant in the first approximation.

The local strain rate during the monotonic movement of the front (296 – 393 K) increases with stress according to a power law. In the case of serrated Lüders deformation (393 – 503 K), the local strain rate is directly proportional to the applied stress.

The difference in front kinetics is determined by the reaction characteristics of active deformable media to external mechanical action and is controlled by the effect of dynamic strain aging.

References / Список литературы

1. Hall E.O. Yield Point Phenomena in Metals and Alloys. New York: Plenum Press; 1970:296.
2. Seeger A., Frank W. Non Linear Phenomena in Materials Science. New York: Trans. Tech. Publ.; 1988:125–137.
3. Fridel J. Dislocations. Oxford – London – Edinburg – N. Y. – Paris – Frankfurt: Pergamon Press; 1964:576.
4. Cottrell A.H. Dislocation and Plastic Flow in Crystals. New York: Oxford Univ. Press.; 1953:223.
5. Zuev L.B. Using a crystal as a universal generator of localized plastic flow autowaves. *Bulletin of the Russian Academy of Sciences: Physics*. 2014;78(10):957–964. https://doi.org/10.3103/S1062873814100256
6. Zuev L.B., Barannikova S.A., Danilov V.I., Gorbatenko V.V. Plasticity: from crystal lattice to macroscopic phenomena. *Progress in Physics of Metals*. 2021;22(1):3–57. https://doi.org/10.15407/ufm.22.01.003
7. Krinsky V.I. Self-Organization: Autowaves and Structures Far from Equilibrium. Berlin: Springer-Verlag; 1984:270.
8. Danilov V.I., Gorbatenko V.V., Danilova L.V. Kinetics of Lüders deformation as an autowave process. *Izvestiya. Ferrous Metallurgy*. 2022;65(4):261–267. (In Russ.). https://doi.org/10.17073/0368-0797-2022-4-261-267

Данилов В.И., Горбатенко В.В., Данилова Л.В. Кинетика деформации Людерса как автоволнового процесса. *Известия вузов. Черная металлургия*. 2022;65(4):261–267. https://doi.org/10.17073/0368-0797-2022-4-261-267

9. Zuev L.B., Danilov V.I., Danilova L.V. Gorbatenko V.V. Deformable material as a nonlinear active medium. *Izvestiya vuzov. Fizika*. 2022;65(2):89–97. (In Russ.). https://doi.org/10.17223/00213411/65/2/89

   Зуев Л.Б., Данилов В.И., Данилова Л.В. Горбатенко В.В. Деформируемый материал как нелинейная активная среда. *Известия вузов. Физика*. 2022;65(2):89–97. https://doi.org/10.17223/00213411/65/2/89
10. Babich V.K., Gul' Yu.P., Dolzhenkov I.E. Strain aging of steel. Moscow: Metallurgiya; 1972:320. (In Russ.).

    Бабич В.К., Гуль Ю.П., Долженков И.Е. Деформационное старение стали. Москва: Металлургия; 1972:320.
11. Liu W., Lian J. Stress-state dependence of dynamic strain aging: Thermal hardening and blue brittleness. *International Journal of Minerals, Metallurgy and Materials*. 2021;28(5):854–866. https://doi.org/10.1007/s12613-021-2250-1
12. Prokhorov A., Vshivkov A., Plekhov O., Kashaev N., Fomin F., Ozerov M., Zherebtsov S. The effect of LSP on the structure evolution and self-heating of ARMCO-iron under cyclic loading. *Metals*. 2021;11(8):119. https://doi.org/10.3390/met11081198
13. Danilov V.I., Orlova D.V., Gorbatenko V.V., Danilova L.V. Effect of temperature on the kinetics of localized plasticity autowaves in Lüders deformation. *Metals*. 2023;13(4):773. https://doi.org/10.3390/met13040773
14. Sutton M.A. Digital Image Correlation for Shape and Deformation Measurements. Springer Handbooks. Boston MA: Springer; 2008:1100.
15. Briers J.D., Webster S. Quasi real-time digital version of single-exposure speckle photography for full-field monitoring of velocity or flow fields. *Optics Communication*. 1995;116(1-3): 36–42. https://doi.org/10.1016/0030-4018(95)00042-7
16. Erbeck R., Merzkirch W. Speckle photographic measurements of turbulence in an air stream with fluctuating temperature. *Experiments in Fluids*. 1988;6(2):89–93. https://doi.org/10.1007/BF00196458
17. Zuev L.B., Gorbatenko V.V., Pavlichev K.V. Elaboration of speckle photography techniques for plastic flow analyses. *Measurement Science and Technology*. 2010;21(5):054014. http://dx.doi.org/10.1088/0957-0233/21/5/054014
18. Sun H.B., Yoshida F., Ohmori M., Ma X. Effect of strain rate on Lüders band propagating velocity and Lüders strain for annealed mild steel under uniaxial tension. *Materials Letters*. 2003;57(29):4535–4539. https://doi.org/10.1016/S0167-577X(03)00358-6
19. Estrin Yu., Kubin L.P. Plastic instabilities: phenomenology and theory. *Materials Science and Engineering: A*. 1991;137: 125–134. https://doi.org/10.1016/0921-5093(91)90326-I
20. Zazhigaev L.S., Kish'yan A.A., Romannikov Yu.I. Methods for Planning and Processing the Results of a Physical Experiment. Moscow: Atomizdat; 1978:232.

    Зажигаев Л.С., Кишьян А.А., Романников Ю.И. Методы планирования и обработки результатов физического эксперимента. Москва: Атомиздат; 1978:232.

Сведения об авторах / Information about the Authors

Дина Владимировна Орлова, *к.ф.-м.н., научный сотрудник лаборатории физики прочности,* Институт физики прочности и материаловедения Сибирского отделения РАН
ORCID: 0000-0003-0068-2542
E-mail: dvo@ispms.ru

Владимир Иванович Данилов, *д.ф.-м.н., профессор, главный научный сотрудник лаборатории физики прочности,* Институт физики прочности и материаловедения Сибирского отделения РАН
ORCID: 0000-0002-5741-7574
E-mail: dvi@ispms.ru

Вадим Владимирович Горбатенко, *к.ф.-м.н., старший научный сотрудник лаборатории физики прочности,* Институт физики прочности и материаловедения Сибирского отделения РАН
ORCID: 0000-0001-6464-6159
E-mail: gvv@ispms.ru

Лидия Владиславовна Данилова, *к.ф.-м.н., младший научный сотрудник лаборатории физики прочности,* Институт физики прочности и материаловедения Сибирского отделения РАН
ORCID: 0000-0002-4124-0516
E-mail: dlv@ispms.ru

Анна Валентиновна Бочкарева, *к.т.н., научный сотрудник лаборатории физики прочности,* Институт физики прочности и материаловедения Сибирского отделения РАН
ORCID: 0000-0002-3140-5292
E-mail: avb@ispms.ru

Dina V. Orlova, *Cand. Sci. (Phys.-Math.), Research Associate of the Laboratory of Strength Physics,* Institute of Strength Physics and Materials Science, Siberian Branch of the Russian Academy of Sciences
ORCID: 0000-0003-0068-2542
E-mail: dvo@ispms.ru

Vladimir I. Danilov, *Dr. Sci. (Phys.-Math.), Prof., Chief Researcher of the Laboratory of Strength Physics,* Institute of Strength Physics and Materials Science, Siberian Branch of the Russian Academy of Sciences
ORCID: 0000-0002-5741-7574
E-mail: dvi@ispms.ru

Vadim V. Gorbatenko, *Cand. Sci. (Phys.-Math.), Senior Researcher of the Laboratory of Strength Physics,* Institute of Strength Physics and Materials Science, Siberian Branch of the Russian Academy of Sciences
ORCID: 0000-0001-6464-6159
E-mail: gvv@ispms.ru

Lidiya V. Danilova, *Cand. Sci. (Phys.-Math.), Junior Researcher of the Laboratory of Strength Physics,* Institute of Strength Physics and Materials Science, Siberian Branch of the Russian Academy of Sciences
ORCID: 0000-0002-4124-0516
E-mail: dlv@ispms.ru

Anna V. Bochkareva, *Cand. Sci. (Eng.), Research Associate of the Laboratory of Strength Physics,* Institute of Strength Physics and Materials Science, Siberian Branch of the Russian Academy of Sciences
ORCID: 0000-0002-3140-5292
E-mail: avb@ispms.ru

Вклад авторов / Contribution of the Authors

Д. В. Орлова – анализ и обсуждение экспериментальных результатов, написание первичного варианта рукописи.
В. И. Данилов – формирование идеи, утверждение окончательного варианта рукописи.
В. В. Горбатенко – проведение механических испытаний, регистрация эволюции картин локализованной пластичности, анализ и обсуждение хронограмм.
Л. В. Данилова – математическая обработка экспериментальных данных, построение и анализ корреляционных зависимостей.
А. В. Бочкарева – проведение экспериментальных исследований, анализ данных по ширине и скорости деформационного фронта.

D. V. Orlova – analysis and discussion of experimental results, writing the draft version of the manuscript.
V. I. Danilov – formation of the article main concept, revising final version of the manuscript.
V. V. Gorbatenko – carrying out mechanical tests, registration of evolution of localized plasticity patterns, analysis and discussion of chronograms.
L. V. Danilova – mathematical processing of experimental data, construction and analysis of correlation dependencies.
A. V. Bochkareva – conducting experiments, analysis of width and rate of the deformation front.

Поступила в редакцию 27.02.2024
После доработки 12.03.2024
Принята к публикации 18.04.2024

Received 27.02.2024
Revised 12.03.2024
Accepted 18.04.2024

SUPERDUTY STEEL / **СТАЛИ ОСОБОГО НАЗНАЧЕНИЯ**

UDC 620.192.63
DOI 10.17073/0368-0797-2024-3-332-339

Original article
Оригинальная статья

Determination of hydrogen influence on microhardness and microstructure characteristics of aviation alloys

D. V. Saulin, K. G. Kuzminykh, V. Z. Poilov

Perm National Research Polytechnic University (29 Komsomolskii Ave., Perm 614990, Russian Federation)

sdv_perm@mail.ru

Abstract. This paper presents results of the studies of hydrogen exposure duration influence on the characteristics of two aviation alloys at atmospheric pressure and room temperature. First alloy (alloy *1*) was obtained by hot isostatic pressing, and was used for the manufacture of gas turbine rotor discs. Second alloy (alloy *2*) was obtained by directional crystallization, and was used for the manufacture of gas turbine blades. It was determined that microhardness of the samples increased during 1000 h of hydrogen exposure duration. The relative increase of the microhardness was insignificant, and for the sample of alloy *1* it was 2.5 %, and for the sample of alloy *2* – 2 %. Correlation analysis of the XRD diagram parameters indicated positive and negative statistically significant relationships correlation between XRD diagrams peaks parameters, hydrogen exposure duration and microhardness of the samples. It was revealed that XRD diagrams peaks of alloy *1* were broadened and their heights increased during hydrogenation, which can be associated with a decrease of dislocations in the grains and their local accumulation at the grains boundaries. Conterwise, XRD diagrams peaks of alloy *2* were narrowed, which can indicate an increase of dislocations in the material grain structure. XRD diagrams processing demonstrated that the crystallite size and dislocation density for alloy *1* decreased with a delay from the hydrogenation start, but for alloy *2* these parameters monotonically increased, and it corresponds to microhardness changes trends of the samples during hydrogenation.

Keywords: hydrogen, aviation alloys, microhardness, correlation analysis, XRD diagram, peak width, dislocation density, crystallite size

Acknowledgements: The results were obtained while fulfilling the state assignment of the Ministry of Science and Higher Education of the Russian Federation for fundamental scientific research (project FSNM-2023-0004).

For citation: Saulin D.V., Kuzminykh K.G., Poilov V.Z. Determination of hydrogen influence on microhardness and microstructure characteristics of aviation alloys. *Izvestiya. Ferrous Metallurgy*. 2024;67(3):332–339. https://doi.org/10.17073/0368-0797-2024-3-332-339

Определение влияния водорода на изменение микротвердости и характеристик микроструктуры образцов авиационных сплавов

Д. В. Саулин, К. Г. Кузьминых, В. З. Пойлов

Пермский национальный исследовательский политехнический университет (Россия, 614990, Пермь, Комсомольский пр., 29)

sdv_perm@mail.ru

Аннотация. В работе представлены результаты исследований влияния длительности воздействия водорода при атмосферном давлении и комнатной температуре на образцы двух авиационных сплавов. Один сплав (сплав *1*) получен методом горячего изостатического прессования и используется для изготовления дисков ротора газовых турбин. Другой сплав (сплав *2*) получен методом направленной кристаллизации и используется для изготовления лопаток газовых турбин. Установлено, что в ходе воздействия водорода на образцы сплавов в течение 1000 ч микротвердость образцов увеличивается, но при этом относительное увеличение микротвердости невелико, составляя 2,5 % для образца сплава *1* и 2 % для образца из сплава *2*. Корреляционный анализ параметров дифрактограмм показал наличие положительных и отрицательных корреляционных статистически значимых связей между параметрами пиков дифрактограмм, длительностью воздействия водорода и микротвердостью образцов. У сплава *1* в процессе наводороживания наблюдается снижение ширины и увеличение высоты пиков дифрактограммы, что может быть связано со снижением количества дислокаций в зернах или их локальным накоплением на границах зерен материала. Напротив, у сплава *2* происходит расширение пиков, что может свидетельствовать об увеличении количества дислокаций в структуре зерен материала. Расчеты показали, что в процессе наводороживания размер кристаллита и плотность

дислокаций у сплава *1* снижаются, но с задержкой по времени от начала процесса, а у сплава *2* монотонно увеличиваются, что соответствует тенденциям изменения микротвердости образцов в процессе наводороживания.

Ключевые слова: водород, авиационные сплавы, микротвердость, корреляционный анализ, дифрактограмма, ширина пиков, плотность дислокаций, размер кристаллитов

Благодарности: Работа выполнена в рамках государственного задания Министерства науки и высшего образования Российской Федерации на проведение фундаментальных научных исследований (проект FSNM-2023-0004).

Для цитирования: Саулин Д.В., Кузьминых К.Г., Пойлов В.З. Определение влияния водорода на изменение микротвердости и характеристик микроструктуры образцов авиационных сплавов. *Известия вузов. Черная металлургия*. 2024;67(3):332–339. https://doi.org/10.17073/0368-0797-2024-3-332-339

Introduction

One of corrosion types accompanied by the destruction of metals and alloys is hydrogen corrosion. Its characteristic feature is that products of interaction between hydrogen and alloy elements, gas phase or alloy structure defects form inside the alloy causing microcracks. The stronger and harder the alloy, the more pronounced is the issue of hydrogen embrittlement, and a hydrogen concentration of a few ppmw in the material is often sufficient to seriously alter the material properties [1].

Hydrogen embrittlement is known to be a process leading to reduced metal viscosity and plasticity caused by the presence of atomic hydrogen. For hydrogen embrittlement to start within the metal structure, hydrogen should diffuse inside it. As known, the rate of hydrogen diffusion in metals depends on concentration of the diffusing agent, temperature, pressure, and crystal structure[1] [2]. For example, in body-centered cubic (BCC) lattices of metals, the hydrogen diffusion coefficient is usually four to five orders of magnitude higher than in face-centered cubic (FCC) lattices or hexagonal close-packed (HCP) ones. However, there are exceptions, such as Pd (FCC) and Co (HCP) metals, which have diffusion coefficient values several orders of magnitude larger than most other metals with BCC and HCP lattices.

If we exclude the processes of hydride formation or hydrogen interaction with carbides, the hydrogen saturation of alloys is usually divided into types related to the features and mechanisms of hydrogen interaction with the metal crystal lattice and its grains, which help to explain the features of hydrogen embrittlement processes. These mechanisms form the basis of the best-known micromechanical models of hydrogen-material interactions: HEDE, HELP, AIDE and HESIV [2 – 5]. There are also combined hydrogen embrittlement models, however, most researchers opt for HEDE and HELP. Thus, the authors of [6 – 8] note that HELP (hydrogen-enhanced localized plasticity) mechanism is likely to proceed simultaneously with HEDE (hydrogen-enhanced decohesion), i.e., hydrogen causes hardening and softening of the material at the same time. Meanwhile, quantitative measurement of the local distribution of hydrogen concentrations in alloys is a serious challenge yet to be solved, which hampers researchers to fully verify the models including hydrogen diffusion.

According to findings of the study presented in [9], the relationship between plasticity and hydrogen-induced fracture mechanism, in addition to changing plasticity and accelerating evolution of metal microstructure, also leads to local high concentrations of hydrogen and a local stress state. The conditions under which cracks emerge due to hydrogen embrittlement are determined by dislocation processes enhanced and accelerated in the presence of hydrogen.

The theory of "hydrogen traps" is also intriguing. Thus, the authors of [10] describe the interaction of hydrogen with defects in the crystal lattice, classify hydrogen traps into reversible, irreversible, and mixed based on their energy levels and demonstrate the impact of hydrogen traps on the hydrogen diffusion coefficient. Regarding diffusive mobility of hydrogen in steel, the authors of [11] investigated the impact of diffusively mobile hydrogen on the plasticity of aircraft steel intended for power parts and assemblies of aviation equipment. The authors note that it is not the total hydrogen content in the metal that determines hydrogen embrittlement. Steel plasticity considerably reduces due to diffusion-mobile hydrogen only, as it has low binding energy with defects in the crystal lattice and gradually moves to the zone of maximum stresses.

As to changes in the metal microstructure in the presence of hydrogen, the paper [12] discusses the HEDE and HELP mechanisms of fatigue crack formation. Moreover, the HELP mechanism considers that hydrogen facilitates movement of dislocations (defects in the crystal lattice) inside the metal grains. In this case, dislocations can accumulate both inside the metal grains and at the grain boundaries, resulting in changing width of XRD diagrams peaks. The broadening XRD diagrams peaks will indicate a more uniform distribution of dislocations (defects) across the grains. On the contrary, when XRD diagrams peaks narrow, the number of dislocations (defects) in the grains will decrease, at the same time, the accumulation of dislocations at the grain boundary may be observed. The Scherrer formula can be used to calculate

[1] Hydrogen Embrittlement. NASA Technical Memorandum. URL: https://ntrs.nasa.gov/api/citations/20160005654/downloads/20160005654.pdf

the dependence of the crystallite size on the variation of the XRD diagrams peaks width [12; 13] and the Williamson-Hall method – to the value of the average relative lattice deformation and dislocation density [14 – 16].

Due to the fact that in the presence of hydrogen, defects in the metal structure can sooner or later lead to cracks and destruction of the metal, the main objective of the work is to determine the effect of a hydrogen atmosphere on the microstructure of aircraft alloys at room temperature and atmospheric pressure.

Characteristics of initial materials

The samples of aircraft alloys, which are widely used to manufacture gas turbines, served as initials materials:

– sample of alloy *1* containing Ni, Co, Cr, Al, Ti, Mo, Nb, W, similar to VV750P alloy described in the [17], obtained by hot isostatic pressing and used to manufacture gas turbine rotor disks, for example, the PD-14 engine.

– sample of alloy *2* containing Ni, Al, Co, Cr, W, Ta, Re, similar to alloy ZhS32 described in [18], obtained by the method of directional crystallization and used to manufacture gas turbine blades.

Hydrogen used for hydrogenation of the samples was obtained using a TsvetChrome-50AV hydrogen generator.

Methods of the experiment and analysis, study parameters

The effect of hydrogen on alloy samples was studied at room temperature and atmospheric pressure. The alloy samples were placed in a sealed glass container filled with pure hydrogen obtained in the hydrogen generator and held at room temperature for a given time, their characteristics (microhardness and phase composition) were periodically monitored. The samples were held in hydrogen medium for more than 1000 h.

The Vickers hardness of the samples was measured using a Q60N, Qness hardness tester with a load of 9.807 N (1 kgf). As microhardness of the samples' surface is not heterogeneous, all periodic measurements of microhardness in the course of hydrogenation were performed in the zones of previous measurements, and there were minimum 12 such zones. The measurement results were then processed, anomalous values were discarded and the average value of the sample surface microhardness was determined.

The crystal structure of the alloys was investigated using XRD7000 *X*-ray diffractometer, Shimadzu (CuK_α radiation, $\lambda = 1.5406$ Å). The XRD diagrams were recorded when the samples were rotating, at tube voltage of 30 kV, current of 30 mA, scanning speed of 1°/min with a step of 0.02°. The XRD diagrams were processed using XRD 6000/7000 Ver. 5.21 software.

Results and discussion

Fig. 1 shows the changing microhardness of the samples during hydrogenation at room temperature. We can see that the average microhardness of the sample of alloy *1* is higher than that of the sample of alloy *2*. In this case, during hydrogenation microhardness in the samples of both alloys *1* and *2* slightly increases and it changes the most during the first 400 – 500 h. During 1000 h of hydrogen exposure at room temperature, the microhardness in the sample of alloy *1* changed by about 2.5 %, and that in the sample of alloy *2* – by 2 %. It should be noted that the dispersion of microhardness values in both cases is very large.

We conducted correlation analysis to test the hypothesis that microhardness of alloy samples depends on the duration of the hydrogenation process. The coefficients of correlation between the samples microhardness and duration of hydrogenation were calculated in MS Excel. The calculation showed a positive correlation between the process duration and the samples microhardness. It was found that the correlation coefficient is 0.775 at $R_{cr} = 0.482$ for alloy *1* and 0.556 at $R_{cr} = 0.553$ for alloy *2*, that is correlation coefficients are statistically significant.

According to the XRD diagrams, the sample of alloy *1* has a cubic structure *Pm*-3*m* and contains four main (by decreasing intensity) peaks: 43.60 (*hkl* = 111), 50.50 (*hkl* = 200), 74.60 (*hkl* = 220) and 90.40 (*hkl* = 311), while the sample of alloy *2* has a close-packed cubic face-centered structure *Fm*-3*m* (cubooctahedron) and contains five main (by decreasing intensity) peaks: 43.60 (*hkl* = 111), 50.60 (*hkl* = 200), 40.60 (*hkl* = 110), 90.40 (*hkl* = 311) and 74.60 (*hkl* = 220).

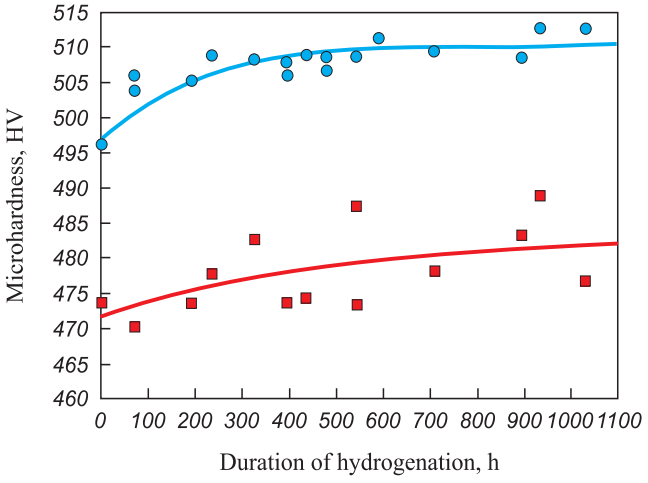

Fig. 1. Change in microhardness of the samples during hydrogenation at room temperature:
● – alloy *1*; ■ – alloy *2*

Рис. 1. Изменение микротвердости образцов в процессе наводороживания при комнатной температуре:
● – сплав *1*; ■ – сплав *2*

To determine the influence of hydrogenation on the structure of alloys, we conducted a correlation analysis of the XRD diagram parameters recorded for alloy samples at different durations of hydrogen exposure. As XRD diagrams feature different number of peaks, for the correlation analysis, we selected three of them with the same *hkl* index: 111, 200 and 311.

We used the following values as XRD diagram parameters for the correlation analysis:

– lattice spacing (*d*), Å;

– peak intensity (*I*), imp.;

– peak full width at half maximum (FWHW), deg;

– integral intensity or peak area (*S*), impulses per degree;

– duration of sample exposure to hydrogen (τ), h;

– values of current average Vickers microhardness of the sample, HV.

Table 1 presents the results of the correlation analysis for the sample of alloy *1*. The correlation coefficients in absolute value exceeding the critical correlation coefficient (R_{cr} = 0.621), i.e., statistically significant ones, are highlighted in bold and underlined.

The analysis of the calculation results shows that for all peaks there is a negative correlation between the hydrogenation duration and the peaks width, i.e., in the course of hydrogenation, all peaks narrow. We should also note the negative correlation between intensity of the peak with *hkl*: 200 and its width and positive correlation between the peak intensity and the process duration or hardness.

Thus, the correlation analysis shows that as the hydrogenation duration increases, so does the microhardness in the sample of alloy *1*, while the peaks narrow, which can be interpreted as a decrease in the number of defects in the material grain structure or the local arrangement of dislocations, for example, at the grain boundary, which can subsequently lead to the structure fracture along the grain boundaries [19; 20].

Table 2 presents the results of the correlation analysis for the sample of alloy *2*. The correlation coefficients in absolute value exceeding the critical correlation coefficient (R_{cr} = 0.669), i.e., statistically significant ones, are highlighted in bold and underlined.

The calculation results show that alloy *2*, unlike alloy *1*, features a positive correlation between the dura-

Table 1. **Correlation coefficients of XRD diagram parameters for alloy *1***

Таблица 1. **Коэффициенты корреляции параметров дифрактограмм образца сплава *1***

Parameters	τ, h	*d*, Å	*I*, imp.	FWHW, deg	*S*, imp.·deg	*HV*
Peak with *hkl*: 111						
τ, ч	1	–0.206	0.230	**–0.880**	–0.209	–
d, Å		1	–0.108	0.388	0.395	0.325
I, imp.			1	–0.318	0.549	0.263
FWHW, deg				1	0.446	–0.576
S, imp.deg					1	0.147
HV						1
Peak with *hkl*: 200						
τ, ч	1	–0.202	**0.644**	**–0.696**	0.239	–
d, Å		1	0.419	0.362	0.370	0.356
I, imp.			1	**–0.649**	0.331	**0.817**
FWHW, deg				1	–0.096	–0.516
S, imp.deg					1	**0.622**
HV						1
Peak with *hkl*: 311						
τ, ч	1	–0.237	0.210	**–0.721**	**–0.892**	–
d, Å		1	–0,606	0.595	0.010	0.260
I, imp.			1	–0.531	–0.134	0.132
FWHW, deg				1	**0.626**	–0.357
S, imp.deg					1	**–0.694**
HV						1

tion of hydrogen exposure and the width of the peak with *hkl*: 111, but negative correlation between the exposure duration and peak intensity, i.e., with increasing duration of hydrogen exposure, the peak widens and its intensity drops. The peaks with *hkl*: 200 and 311 also demonstrate a negative correlation between the peaks' width and their intensity. There is a statistically significant correlation between microhardness and XRD diagram parameters only for the peak with *hkl*: 311. With increasing microhardness, the intensity of this peak drops and the peak area expands. In addition, the peak with *hkl*: 200 of alloy *2* shows a negative correlation between the lattice spacing value and the peak width, which was not the case for alloy *1*.

Thus, with increasing duration of hydrogen exposure, the microhardness of the sample enhances, but the intensity of some peaks drops (*hkl*: 111 and 311) when these peaks show a significant negative correlation between the peak width and its intensity. The peak with *hkl*: 111, in contrast to the peak with the same *hkl* of alloy 1, features a positive correlation between the process duration and the peak width, which can be interpreted as an increase in the number of dislocations (defects) in the material grain structure.

We used the Scherrer formula to calculate the crystallite size and the Williamson-Hall method to determine the lattice characteristics and dislocation density from the XRD diagram parameters. Figs. 2 and 3 demonstrate the results of calculating the change in the average crystallite size and dislocation density during hydrogenation.

The graphs show that the average crystallite size of alloy *1* shrinks (by more than 30 %) during the process, while that of alloy *2* increases (by less than 25 %). Meanwhile, the crystallite size of alloy *1* remains almost constant during 400 h of hydrogen exposure and then begins to reduce, while the crystallite size of alloy *2* increases. Similar dependencies are observed for the change in dislocation density (Fig. 3). The dislocation density of alloy *1* drops to almost zero values with a delay of 400 h, while for alloy *2*, this value increases.

According to the graphs in Fig. 3, microhardness in the sample of alloy *1* obtained by hot isostatic pressing mostly changes during the first 400 – 500 h, while subsequent changes are very slight. Thus, it can be concluded that exposure of alloy *1* to hydrogen for 400 – 500 h at room temperature and atmospheric pressure leads to hydrogen accumulation in the sample of alloy *1*, its microhardness enhancing, while its the microstructure remaining the same. At further saturation of the sample with hydrogen, the alloy microstructure alters practically without any changes in its hardness. For alloy *2* obtained

Table 2. **Correlation coefficients of XRD diagram parameters for alloy *2***

Таблица 2. **Коэффициенты корреляции параметров дифрактограмм образца сплава *2***

Parameters	τ, h	*d*, Å	*I*, imp.	FWHW, deg	*S*, imp.·deg	*HV*
Peak with *hkl*: 111						
τ, ч	1	0.079	**–0.860**	**0.873**	–0.455	–
d, Å		1	–0.035	0.448	–0.359	–0.080
I, imp.			1	**–0.743**	0.617	–0.630
FWHW, deg				1	–0.380	0.384
S, imp.deg					1	–0.105
HV						1
Peak with *hkl*: 200						
τ, ч	1	0.653	**–0.812**	0.169	–0.301	–
d, Å		1	–0.302	**–0.681**	–0.259	0.098
I, imp.			1	–0.467	0.537	–0.586
FWHW, deg				1	–0.176	0.337
S, imp.deg					1	–0.435
HV						1
Peak with *hkl*: 311						
τ, ч	1	–0.077	–0.269	0.119	**0.771**	–
d, Å		1	0.102	–0.068	–0.039	–0.150
I, imp.			1	**–0.839**	–0.221	**–0.677**
FWHW, deg				1	0.383	0.588
S, imp.deg					1	**0.681**
HV						1

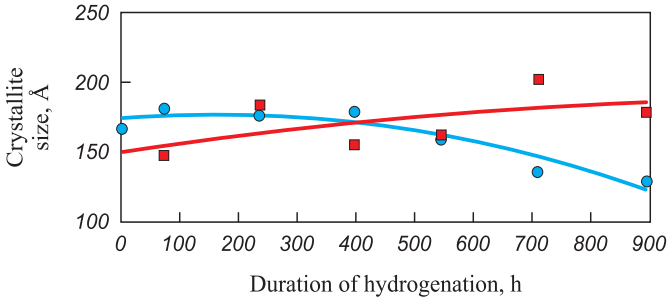

Fig. 2. Effect of hydrogen exposure duration on crystallite size:
● – alloy *1*; ■ – alloy *2*

Рис. 2. Влияние длительности воздействия водорода на изменение размеров кристаллитов:
● – сплав *1*; ■ – сплав *2*

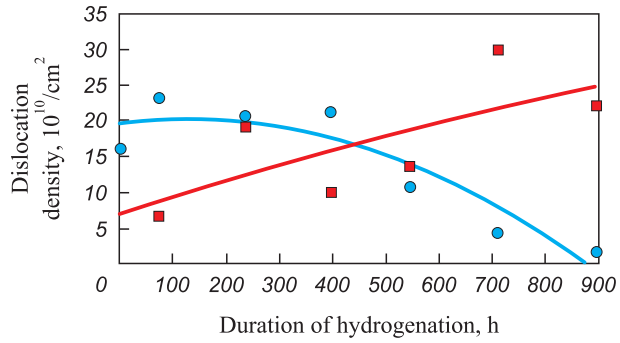

Fig. 3. Effect of hydrogen exposure duration on dislocation density:
● – alloy *1*; ■ – alloy *2*

Рис. 3. Влияние длительности воздействия водорода на изменение плотности дислокаций:
● – сплав *1*; ■ – сплав *2*

by directional crystallization, the metal hardness and microstructure change continuously when exposed to hydrogen.

Conclusions

The investigation revealed that as alloy samples are exposed to hydrogen for 1000 h, the samples microhardness increases, its relative growth in the sample of alloy *1* reaching 2.5 %, and in the sample of alloy *2* amounting to 2 %. The correlation analysis of the change in XRD diagram parameters during hydrogenation of alloy samples indicated positive and negative statistically significant relationships correlation between XRD diagram peak parameters, hydrogen exposure duration and microhardness of the samples. It was found that alloy *1*, being exposed to hydrogen, features narrowing and lengthening of XRD diagram peaks, which may indicate a decrease in the number of dislocations (defects) in the grains or their local accumulation at the grain boundaries of the material. On the contrary, alloy *2*, being exposed to hydrogen, features some widening of XRD diagram peaks, which can be indicative of increased dislocations in the material grain structure. The calculations of the effective crystallite size and average dislocation density indicated that during hydrogenation.There was a delayed decrease in both crystallite size and dislocation density for alloy *1*. In contrast, these parameters increased monotonically for alloy *2*. These findings align with the observed trends in microhardness changes during hydrogenation for both alloys.

References / Список литературы

1. Sun B., Lu W., Gault B., Ding R., Makineni S.K., Wan D., Wu C.-H., Chen H., Ponge D., Raabe D. Chemical heterogeneity enhances hydrogen resistance in high-strength steels. *Nature Materials*. 2021;20:1629–1634. https://doi.org/10.1038/s41563-021-01050-y
2. Gonzalez M.S., Hernandez I.R. Review: Hydrogen embrittlement of metals and alloys in combustion engines. *Tecnología en Marcha*. 2018;31(2):3–13. http://dx.doi.org/10.18845/tm.v31i2.3620
3. Djukic M.B., Zeravcic V.S., Bakic G.M., Sedmak A., Rajicic B. Hydrogen damage of steels: A case study and hydrogen embrittlement model. *Engineering Failure Analysis*. 2015;58–2:485–498. https://doi.org/10.1016/j.engfailanal.2015.05.017
4. Traidia A., Chatzidouros E., Jouiad M. Review of hydrogen-assisted cracking models for application to service lifetime prediction and challenges in the oil and gas industry. *Corrosion Reviews*. 2018;36(4):323–347. https://doi.org/10.1515/corrrev-2017-0079
5. Bruck S., Schippl V., Schwarz M., Christ H.-J., Fritzen C.-P., Weihe S. Hydrogen embrittlement mechanism in fatigue behavior of austenitic and martensitic stainless steels. *Metals*. 2018;8(5):339. https://doi.org/10.3390/met8050339
6. Djukic M.B., Bakic G.M., Zeravcic V.S., Sedmak A., Rajicic B. Review: The synergistic action and interplay of hydrogen embrittlement mechanisms in steels and iron: Localized plasticity and decohesion. *Engineering Fracture Mechanics*. 2019;216:106528. https://doi.org/10.1016/j.engfracmech.2019.106528
7. Sergeev N.N., Sergeev A.N., Kutepov S.N., Gvozdev A.E., Ageev E.V. A review of theoretical concepts of hydrogen cracking in metals and alloys. *Proceedings of the Southwest State University*. 2017;21(3):6–33. (In Russ.). https://doi.org/10.21869/2223-1560-2017-21-3-6-33

   Сергеев Н.Н., Сергеев А.Н., Кутепов С.Н., Гвоздев А.Е., Агеев Е.В. Анализ теоретических представлений о механизмах водородного растрескивания металлов и сплавов. *Известия Юго-Западного государственного университета*. 2017;21(3):6–33. https://doi.org/10.21869/2223-1560-2017-21-3-6-33
8. Yakovlev Yu.A., Polyanskii V.A., Sedova Yu.S., Belyaev A.K. Models of hydrogen influence on the mechanical properties of metals and alloys. *PNRPU Mechanics Bulletin*. 2020;(3):136–160. (In Russ.). https://doi.org/10.15593/perm.mech/2020.3.13

   Яковлев Ю.А., Полянский В.А., Седова Ю.С., Беляев А.К. Модели влияния водорода на механические свойства металлов и сплавов. *Вестник Пермского национального исследовательского политехнического университета.*

Механика. 2020;(3):136–160.
https://doi.org/10.15593/perm.mech/2020.3.13

9. Robertson I.M., Sofronis P., Nagao A., Martin M.L., Wang S., Gross D.W., Nygren K.E. Hydrogen embrittlement understood. *Metallurgical and Materials Transactions A*. 2015;46:2323–2341.
https://doi.org/10.1007/s11661-015-2836-1
10. Sergeev N.N., Kutepov S.N. On the interaction of hydrogen with lattice defects in metals and alloys. *Izvestiya Tul'skogo gosudarstvennogo universiteta. Tekhnicheskie nauki*. 2017;(4):131–141. (In Russ.).

Сергеев Н.Н., Кутепов С.Н. О взаимодействии водорода с дефектами кристаллической решетки в металлах и сплавах. *Известия Тульского государственного университета. Технические науки*. 2017;(4):131–141.
11. Voznesenskaya N.M., Tonysheva O.A., Leonov A.V., Dul'nev K.V. Hydrogen influence on high-strength corrosion-resistant steel VNS65-Sh properties and ways of elimination of hydrogen embrittlement. *Proceedings of VIAM*. 2018;(10):3–9. (In Russ.). https://doi.org/10.18577/2307-6046-2018-0-10-3-9

Вознесенская Н.М., Тонышева О.А., Леонов А.В., Дульнев К.В. Влияние водорода на свойства высокопрочной коррозионной стали ВНС65-Ш (18Х13Н4К4С2АМ3-Ш) и пути устранения водородной хрупкости. *Труды ВИАМ*. 2018;(10):3–9.
https://doi.org/10.18577/2307-6046-2018-0-10-3-9
12. Connolly M., Martin M., Bradley P., Lauria D., Slifka A., Amaro R., Looney C., Park J.-S. In situ high energy X-ray diffraction measurement of strain and dislocation density ahead of crack tips grown in hydrogen. *Acta Materialia*. 2019;180:272–286.
https://doi.org/10.1016/j.actamat.2019.09.020
13. Chaki S.H., Malek T.J., Chaudhary M.D., Tailor J.P., Deshpande M.P. Magnetite Fe_3O_4 nanoparticles synthesis by wet chemical reduction and their characterization. *Advances in Natural Sciences: Nanoscience and Nanotechnology*. 2015;6(3):035009.
https://doi.org/10.1088/2043-6262/6/3/035009
14. Pushkarev S.S., Grekhov M.M., Zenchenko N.V. X-Ray diffraction analysis of features of the crystal structure of $GaN/Al_{0.32}Ga_{0.68}N$ HEMT-heterostructures by the Williamson–Hall method. *Semiconductors*. 2018;52(6):734–738.
https://doi.org/10.1134/s1063782618060209
15. Wang L., Cheng X., Peng H., Zhao P.W., Cai Z.X. Effect of tempering temperature on hydrogen embrittlement in V-containing low alloy high strength steel. *Materials Letters*. 2021;302:130327.
https://doi.org/10.1016/j.matlet.2021.130327
16. Mote V., Purushotham Y., Dole B. Williamson-Hall analysis in estimation of lattice strain in nanometer-sized ZnO particles. *Journal of Theoretical and Applied Physics*. 2012;6:6.
https://doi.org/10.1186/2251-7235-6-6
17. Volkov A.M., Vostrikov A.V., Bakradze M.M. Development principles and alloying features of P/M Ni-base superalloys for jet-engine disks application. *Proceedings of VIAM*. 2016;(8):2. (In Russ.).
http://dx.doi.org/ 10.18577/2307-6046-2016-0-8-2-2

Волков А.М., Востриков А.В., Бакрадзе М.М. Принципы создания и особенности легирования гранулируемых жаропрочных никелевых сплавов для дисков ГТД. *Труды ВИАМ*. 2016;(8):2.
http://dx.doi.org/10.18577/2307-6046-2016-0-8-2-2
18. Kolyadov E.V., Rassokhina L.I., Visik E.M., Gerasimov V.V., Filonova E.V. Study of single crystal turbine blades made of ZhS32 alloy with a promising scheme of cooling. *Zavodskaya laboratoriya. Diagnostika materialov*. 2018;84(10):35–40. (In Russ.).
https://doi.org/10.26896/1028-6861-2018-84-10-35-40

Колядов Е.В., Рассохина Л.И., Висик Е.М., Герасимов В.В., Филонова Е.В. Исследование монокристаллических рабочих турбинных лопаток из сплава ЖС32 с перспективной схемой охлаждения. *Заводская лаборатория. Диагностика материалов*. 2018;84(10):35–40.
https://doi.org/10.26896/1028-6861-2018-84-10-35-40
19. Nagao A., Dadfarnia M., Somerday B.P., Sofronis P., Ritchie R.O. Hydrogen-enhanced-plasticity mediated decohesion for hydrogen-induced intergranular and "quasi-cleavage" fracture of lath martensitic steels. *Journal of the Mechanics and Physics of Solids*. 2018;112:403–430.
https://doi.org/10.1016/j.jmps.2017.12.016
20. Nagao A., Smith C.D., Dadfarnia V, Sofronis P., Robertson I.M. The role of hydrogen in hydrogen embrittlement fracture of lath martensitic steel. *Acta Materialia*. 2012;60(13–14):5182–5189.
https://doi.org/10.1016/j.actamat.2012.06.040

Information about the Authors / Сведения об авторах

Dmitrii V. Saulin, *Cand. Sci. (Eng.), Assist. Prof. of the Chair "Chemical Engineering",* Perm National Research Polytechnic University
ORCID: 0009-0009-0228-7379
E-mail: sdv_perm@mail.ru

Konstantin G. Kuzminykh, *Senior Lecturer of the Chair "Chemical Engineering",* Perm National Research Polytechnic University
E-mail: kgkuz@mail.ru

Vladimir Z. Poilov, *Dr. Sci. (Eng.), Prof. of the Chair "Chemical Engineering", Head of CUC "Center for High-tech Chemical Technologies and Physico-Chemical Research",* Perm National Research Polytechnic University
E-mail: vladimirpoilov@mail.ru

Дмитрий Владимирович Саулин, *к.т.н., доцент кафедры «Химические технологии»,* Пермский национальный исследовательский политехнический университет
ORCID: 0009-0009-0228-7379
E-mail: sdv_perm@mail.ru

Константин Геннадьевич Кузьминых, *старший преподаватель кафедры «Химические технологии»,* Пермский национальный исследовательский политехнический университет
E-mail: kgkuz@mail.ru

Владимир Зотович Пойлов, *д.т.н., профессор кафедры «Химические технологии», руководитель ЦКП «Центр наукоемких химических технологий и физико-химических исследований»,* Пермский национальный исследовательский политехнический университет
E-mail: vladimirpoilov@mail.ru

Contribution of the Authors / Вклад авторов

D. V. Saulin – analysis of literary data, conducting experiments, analysis of results, writing the text.

K. G. Kuzminykh – analysis of literary data, conducting experiments, analysis of results, writing the text.

V. Z. Poilov – scientific guidance, discussion of results, writing the text.

Д. В. Саулин – анализ литературных данных, проведение экспериментальной части, анализ результатов экспериментов, написание статьи.

К. Г. Кузьминых – анализ литературных данных, проведение экспериментальной части, анализ результатов экспериментов, написание статьи.

В. З. Пойлов – научное руководство, обсуждение результатов экспериментов, написание статьи.

Received 25.10.2023
Revised 11.12.2023
Accepted 28.03.2024

Поступила в редакцию 20.10.2023
После доработки 11.12.2023
Принята к публикации 28.03.2024

SUPERDUTY STEEL / **СТАЛИ ОСОБОГО НАЗНАЧЕНИЯ**

UDC 669.018.8
DOI 10.17073/0368-0797-2024-3-340-350

Original article
Оригинальная статья

Problems of selection of corrosion-resistant steels and alloys in oil and gas industry for operating conditions

A. S. Fedorov ✉, **V. S. Karasev, E. L. Alekseeva, A. A. Al'khimenko, N. O. Shaposhnikov**

Peter the Great St. Petersburg Polytechnic University (29 Politekhnicheskaya Str., St. Petersburg 195251, Russian Federation)

✉ fedorov_as@spbstu.ru

Abstract. Corrosion-resistant steels and alloys have a number of unique properties. This allows them to be used in various industries. Despite their name, they are to some extent subject to various types of corrosion and corrosion-mechanical damage. This article discusses cases of corrosion damage of products made of corrosion-resistant steels and alloys in the oil and gas industry. The reasons of material failure can be incorrect exploitation of material, low-quality material of products, and incorrect selection of material for operating conditions. For each group of failure causes the examples from open sources and from the practice of the team of authors of this work are considered. The paper substantiates the importance of preliminary laboratory studies of corrosion-resistant materials and their testing with simulation of environmental factors. It is necessary for reasonable choice under specific operating conditions. It is shown that in practice the reasonable choice of corrosion-resistant materials is not always given due attention, so the seemingly economically favorable solutions may turn out to be incorrect. The main focus is made on the practical side of the issue in order to avoid such problems in the future. The relevance of the work is confirmed by the recent acute problem of substitution of foreign steel grades.

Keywords: corrosion-resistant steels and alloys, reasonable selection, causes of failure, operating conditions, incorrect operation, laboratory tests, physical simulation

Acknowledgements: The research was supported by the Ministry of Science and Higher Education of the Russian Federation under the World Class Research Centre Program: Advanced Digital Technologies (Agreement No. 075-15-2020-311 dated 20.04.2022).

For citation: Fedorov A.S., Karasev V.S., Alekseeva E.L., Al'khimenko A.A., Shaposhnikov N.O. Problems of selection of corrosion-resistant steels and alloys in oil and gas industry for operating conditions. *Izvestiya. Ferrous Metallurgy*. 2024;67(3):340–350. https://doi.org/10.17073/0368-0797-2024-3-340-350

Проблемы подбора коррозионностойких сталей и сплавов в нефтегазовой отрасли под условия эксплуатации

А. С. Федоров ✉, **В. С. Карасев, Е. Л. Алексеева, А. А. Альхименко, Н. О. Шапошников**

Санкт-Петербургский политехнический университет Петра Великого (Россия, 195251, Санкт-Петербург, ул. Политехническая, 29)

✉ fedorov_as@spbstu.ru

Аннотация. Коррозионностойкие стали и сплавы обладают рядом уникальных свойств, позволяющих использовать их в различных отраслях промышленности. Однако, несмотря на свое название, они в той или иной мере подвержены различным видам коррозионных и коррозионно-механических повреждений. В данной работе рассматриваются случаи коррозионного разрушения изделий из коррозионностойких сталей и сплавов в нефтегазовой отрасли. Установлено, что причинами разрушения могут стать как некорректная эксплуатация и некачественный материал изделий, так и некорректный подбор материала под условия эксплуатации. Для каждой группы причин отказа рассмотрены примеры из открытых источников и из практики коллектива авторов работы. Обоснована важность проведения предварительных лабораторных исследований коррозионностойких материалов и их испытаний с воспроизведением факторов среды для обоснованного выбора под конкретные условия эксплуатации. Показано, что на практике обоснованному выбору коррозионностойких материалов не всегда уделяется должное внимание, поэтому кажущиеся на первый взгляд экономически выгодными решения могут оказаться некорректными. Основной фокус сделан на практической стороне вопроса для того, чтобы в будущем избежать подобных проблем. Актуальность работы подтверждается остро стоящей в последнее время проблемой замещения зарубежных марок сталей.

Ключевые слова: коррозионностойкие стали и сплавы, обоснованный выбор, причины разрушений, условия эксплуатации, некорректная эксплуатация, лабораторные испытания, физическое моделирование

Благодарности: Исследование выполнено при финансовой поддержке Министерства науки и высшего образования Российской Федерации в рамках программы Исследовательского центра мирового уровня: Передовые цифровые технологии (соглашение № 075-15-2022-311 от 20.04.2022).

Для цитирования: Федоров А.С., Карасев В.С., Алексеева Е.Л., Альхименко А.А., Шапошников Н.О. Проблемы подбора коррозионностойких сталей и сплавов в нефтегазовой отрасли под условия эксплуатации. *Известия вузов. Черная металлургия*. 2024;67(3):340–350. https://doi.org/10.17073/0368-0797-2024-3-340-350

Introduction

Corrosion-resistant materials play a significant role in various industrial sectors [1 – 4]. Possessing enhanced corrosion resistance combined with the required mechanical properties [5 – 7], corrosion-resistant materials are used in aggressive environments where longevity without loss of operational characteristics is essential [8; 9]. Historically, the high cost of corrosion-resistant materials limited their use. However, over time, the understanding of the advantages of corrosion-resistant materials has led to their increasingly widespread use, particularly through the optimization of composition and properties for application in specific environments in critical components and structures [10 – 12]. At present, corrosion-resistant steels and alloys are used for more critical, expensive, and complex equipment where the potential risks, costs, or benefits outweigh the material's cost.

For the domestic metallurgical industry, the issue of producing import-substituting grades of corrosion-resistant steels and alloys is currently pressing. Russia accounts for 0.4 % of global corrosion-resistant steel production, with the volume of products produced satisfying no more than 25 % of the total domestic consumption of steel in various industries [13 – 15]. In 2021, 120,000 tonnes of corrosion-resistant steel were produced in Russia, while 463,000 tonnes were imported from abroad. Moreover, domestic equivalents do not always meet the end user's requirements for physical, mechanical, and corrosion properties.

A significant problem is that the domestic regulatory and technical documentation (RTD), containing requirements for the production technology and quality assessment of corrosion-resistant steels and alloys, is either outdated with minimal product requirements or entirely absent.

The relevance of this study lies in the emergence of numerous requests for import substitution, selection, and comparative evaluation of the properties of stainless steels and alloys for the implementation of domestic products, equipment, and technologies. Additionally, it draws on data from open sources and the many years of experience in failure analysis by the Scientific and Technological Complex "New Technologies and materials" at Peter the Great St. Petersburg Polytechnic University. It is also important to note that discussions on the topic of failures and, moreover, their open analysis is a very contentious issue, as it leads to the search for culprits and punishment. However, in this work, the authors focused on the scientific or practical side of the issue to avoid similar problems in the future.

Review of failures

Conducting laboratory tests and research is an integral part of the justified selection of materials for specified operating conditions or their range [16 – 18]. In laboratory conditions, it is possible to carry out both standard tests according to existing methodologies (GOST, ASTM, ISO, DIN, etc.) and research work simulating aggressive environments close to real objects.

As numerous examples from open sources and the authors' extensive practice show, the choice of a particular material depending on operating conditions can often be incorrect [19 – 22]. Additionally, factors such as installation conditions, technological impacts [23 – 25], interactions with other materials [26 – 28], changes in operating conditions, and metallurgical quality [29 – 31] may not be taken into account. All these factors lead to failures and serious economic and environmental consequences.

Tables 1 – 3 provide an overview of failures of various products made from corrosion-resistant materials in the oil and gas industry and show the causes of these failures. Analysis of the sources revealed that cases of failures can be grouped into three categories: incorrect operation of the material, low-quality material of the products, and incorrect selection of material for the operating conditions. Among the cases of incorrect operation, those where the condition of the material was compromised during installation on-site – such as during welding work in the construction of structures made from corrosion-resistant steels – were also included.

Let us examine in detail the most interesting cases of damage and the methods for resolving the problems from each category.

Incorrect operation of the material. Consider an example from open sources. The authors of [21] analyzed the causes of corrosion damage in the rectification column of a cellulose acetate production plant, made from duplex

Table 1. **Overview of damage to corrosion-resistant materials. Incorrect exploitation of material**

Таблица 1. **Обзор разрушений коррозионностойких материалов. Некорректная эксплуатация материала**

No.	Material	Product	Failure/Causes	Source
1	UNS S32760 0.025 % C – 25 % Cr – 7.5 % Ni – 3.8 % Mo – 0.25 % N – – 0.57 % Cu – 0.5 % W	Welded oil transportation pipe	The pipe failed after one month of operation due to pitting in the heat-affected zone (HAZ) caused by the formation of σ-phase in an amount of 8 vol. % during the pre-welding heating process.	[20]
2	UNS S31803 0.016 % C – 22.4 % Cr – – 5.8 % Ni – 3.1 % Mo – – 0.17 % N – 0.55 % Si	Rectification column	The material exhibited a high rate of general corrosion after just a few months of use. The column operated in an oxygen-free environment with an excess of sulphuric acid in the liquid, which prevented the formation of a stable passive film on the steel surface.	[21]
3	UNS S32750 0.020 % C – 24.2 % Cr – – 8.7 % Ni – 3.8 % Mo – – 0.22 % N – 0.5 % Si – – 0.1 % Cu – 0.38 % Mn	Welded high-pressure vessel	Stress corrosion cracking (SCC) occurred in the heat-affected zone (HAZ). During welding, σ-phase formed in the HAZ in an amount of 2 vol. %. The operational environment was saturated with chlorides (~220 ppm), and the operating temperature was 110 °C. Crevice corrosion contributed to the propagation of SCC along the ferrite-austenite boundaries.	[22]

Table 2. **Overview of damage to corrosion-resistant materials. Low-quality material**

Таблица 2. **Обзор разрушений коррозионностойких материалов. Некачественный материал изделий**

No.	Material	Product	Failure/Causes	Source
1	UNS S32900 0.040 % C – 25 % Cr – 4 % Ni – – 1.5 % Mo – 0.5 % Si – 0.5 % Mn	Stem of a double-disc shut-off valve	The stem of a double-disc shut-off valve failed after 30 years of operation in an environment containing hydrogen sulphide (pH = 4, operating temperature 128 °C) due to sulphide stress corrosion cracking (SSCC). The SSCC crack predominantly propagated in the ferrite and along the ferrite-austenite boundary due to the presence of the σ-phase. Although the stem operated for 30 years, it could have lasted longer with properly conducted heat treatment.	[23]
2	UNS S32304 0.020 % C – 23.7 % Cr – – 4.2 % Ni – 0.3 % Mo – – 0.09 % N – 0.67 % Si – – 0.31 % Cu – 1.4 % Mn	Welded flexible pipe	The pipe experienced intergranular corrosion, leading to cracks in the welds. The cause of this was an excess of ferrite (~70 %) in the weld and the additional presence of unfavorable chromium nitrides at the ferrite-austenite boundaries. The excessive ferrite content resulted from the low linear energy values used during the welding process.	[24]

Table 2 (continutation). **Overview of damage to corrosion-resistant materials. Low-quality material**

Таблица 2 (продолжение). **Обзор разрушений коррозионностойких материалов. Некачественный материал изделий**

No.	Material	Product	Failure/Causes	Source
3	AISI 304 0.052 % C – 17.1 % Cr – 8.1 % Ni – 0.1 % Mo – 0.36 % Si – 1.02 % Mn	Convective pipe for geothermal water	Improper heat treatment before putting the pipe into operation led to sensitisation, which increases susceptibility to intergranular cracking. Residual stresses arising during production also contributed to the failure process. The presence of chlorides in the working environment caused SCC cracks to appear. In the initial stage, SCC cracks propagated along the austenite grain boundaries, then they transformed into a coexisting mode of intergranular and transgranular cracking. The authors attribute the pipe failure to the synergistic effect of sensitisation, the presence of chlorides, and residual stresses.	[25]
4	14Cr17N2 0.135 % C – 16.8 % Cr – – 1.66 % Ni – 0.51 % Si – – 0.58 % Mn	Flange of shut-off valve	The flange exhibited structural heterogeneity and a high content of chromium carbides along the grain boundaries. In addition to isolated pitting and localized corrosion damage, intergranular failure of the metal surface was observed. The poor metallurgical quality of the flange was exacerbated by active corrosion processes in an aggressive environment containing chlorides. As a result, the steel from this production is unsuitable for operation in seawater conditions.	STC "New Technologies and materials"
5	AISI 904L 0.011 % C – 20.7 % Cr – – 23.2 % Ni – 4.2 % Mo – – 0.32 % Si – 1.46 % Cu – – 1.16 % Mn	Steel plate	In this case, the cause of intergranular corrosion was the presence of excess phases located along the boundaries of the austenite grains in the base metal and in the interdendritic spaces of the weld joint, as well as micropores that served as concentrators for the propagation of intergranular corrosion cracks.	STC "New Technologies and materials"
6	EN 1.4469 (GX2CrNiMoN26-7-4) 0.020 % C – 27.3 % Cr – – 7.5 % Ni –4 % Mo – 0.67 % Si – 0.55 % Cu – 0.59 % Mn – – 0.2 % N – 0.05 % Ti	Cast components of centrifugal pumps	The main reason for the reduced resistance to crevice corrosion was the presence of grain boundary σ-phase precipitates (6.7 vol. %), which deplete the solid solution of alloying elements responsible for corrosion resistance, such as chromium and molybdenum.	STC "New Technologies and materials"
7	07Cr16Ni6 0.040 % C – 15.2 % Cr – 6.6 % Ni – 0.64 % Si – 0.16 % Cu – 0.49 % Mn	First stage impeller of the rotor	The cause of the failure was the presence of structural heterogeneity and the precipitation of carbides at the phase boundaries. These factors led to the failure of the impeller through the mechanism of stress corrosion cracking (SCC).	STC "New Technologies and materials"

Table 3. **Overview of damage to corrosion-resistant materials. Incorrect selection of material for operating conditions**

Таблица 3. **Обзор разрушений коррозионностойких материалов. Некорректный подбор материала под условия эксплуатации**

No.	Material	Product	Failure/Causes	Source
1	42CrMN (AISI 4130) 0.30 % C – 1 % Cr – 0.2 % Mo – – 0.25 % Si – 0.5 % Mn	Key	The occurrence of contact corrosion at the point of contact between the key and the valve stem led to the failure, resulting in the release of the pumped fluid into the environment.	[26]
	22Cr (DSS) 0.03 % C – 22.5 % Cr – 5.5 % Ni – – 3 % Mo – 1 % Mn	Valve stem		
2	AISI 410 0.07 % C – 13 % Cr – 0.5 % Ni – – 0.3 % Mo – 0.2 % Si – 0.5 % Mn	Steam turbine blades	The predominant mechanism is fatigue failure caused by changing operating conditions of the blades in the incoming steam. The presence of corrosion pits and intergranular cracks contributed to the activation of corrosion fatigue. Cyclic loading at high temperatures led to the rapid growth and propagation of cracks.	[27]
3	Super 13Cr 0.03 % C – 13 % Cr – 6 % Ni – – 1.7 % Mo – 0.3 % Si – 0.1 % Cu – – 0.7 % Mn – 0.09 % N	Pipeline of Resak A-6 Well in Malaysia	Intergranular cracks were found on all fracture surfaces of the extracted components. The presence of oxygen, CO_2, and H_2S in the $CaCl_2$ salt solution was the most likely cause of the failure. Laboratory test results showed that this steel is susceptible to SCC in the operational environment at the reservoir water temperature of the well.	[28]
4	12Cr18Ni9 (AISI 304) 0.05 % C – 18.1 % Cr – 8.1 % Ni – – 0.05 % Mo – 0.5 % Si – – 0.05 % Cu – 1.22 % Mn	Heat exchanger elements of the low-temperature natural gas separation unit	According to the approved project documentation, the material for the heat exchanger unit should have been 12Cr18Ni10T (AISI 321). However, the research revealed a substitution of this steel grade with 12Cr18Ni9 (AISI 304). The primary cause of the failure was a violation of the project documentation requirements regarding the unsanctioned change of the steel grade. This led to the incorrect selection of the welding mode, which caused the activation of the metal in the heat-affected zone of the non-stabilized titanium steel, resulting in through pitting under the influence of the corrosive environment.	STC "New Technologies and materials"
5	05Х16Н4Д2Б 0.020 % C – 13 % Cr – 4 % Ni – – 0.18 % Si – 2.1 % Cu – – 0.32 % Mn	Pump shaft	The hardness of this material did not match the quality certificate and did not meet the requirements of the NACE MR0175 standard. During laboratory tests for SCC resistance, failure occurred in all cases within the first day of testing.	STC "New Technologies and materials"

steel UNS S31803. The process fluid was an aqueous solution of 80 % acetic acid, which was separated by rectification. Due to the incomplete neutralisation of sulphuric acid in the process fluid used as a catalyst for ester hydrolysis, the column operated in a reducing environment, preventing the formation of a stable passive film on the metal surface.

To solve this problem, the authors proposed modifying the composition of the process fluid. By adding hydrogen peroxide under laboratory conditions, they created oxidizing conditions that promoted the formation of a stable passive film. Based on the results of laboratory studies, hydrogen peroxide was continuously added to the operating column. This approach proved successful in stopping corrosion processes until the next scheduled maintenance shutdown.

Low-quality material of the products. Consider a case from the authors' practice involving intergranular corrosion, using AISI 904L steel plate as an example. Before putting the material into operation, acceptance tests for resistance to intergranular corrosion (IGC) were required. The tests were conducted according to GOST 6032 – 2017 using the weight loss method in a boiling aqueous solution of ferric sulfate ($Fe_2(SO_4)_3 \cdot 9H_2O$) and sulphuric acid (H_2SO_4) in a flask with a reflux condenser. The duration of exposure in the boiling solution was 48 h. Upon completion of the tests, samples were bent at a 90° angle to assess the cracking of the base metal and the welded joint. Figs. 1, *a* and *b* show intergranular cracks in the base metal and the weld metal.

In this case, the cause of intergranular corrosion was the presence of excess phases located along the boundaries of the austenitic grains of the base metal and in the interdendritic spaces of the welded joint, as well as micro-voids that served as stress concentrators for the propagation of IGC cracks. Thus, laboratory tests established that the material of this production is prone to IGC. Introducing this plate into operation poses a high risk of subsequent cracking.

Incorrect selection of material for operating conditions. Consider the failure of heat exchanger elements in a low-temperature natural gas separation unit due to through pitting corrosion in the weld area, based on the authors' practice (see Fig. 2). According to the approved project documentation, the material for this unit should have been steel 12Cr18Ni10T (AISI 321) with a titanium content of 0.4 to 1.0 wt. %. However, investigations revealed a substitution of the steel grade with 12Cr18Ni9 (AISI 304). In terms of pitting corrosion resistance, 12Cr18Ni10T and 12Cr18Ni9 steels are similar in their corrosion properties [32; 33]. However, in the case of welding non-stabilized steels, the corrosion resistance of the weld and the heat-affected zone can be significantly lower than that of the base metal [34].

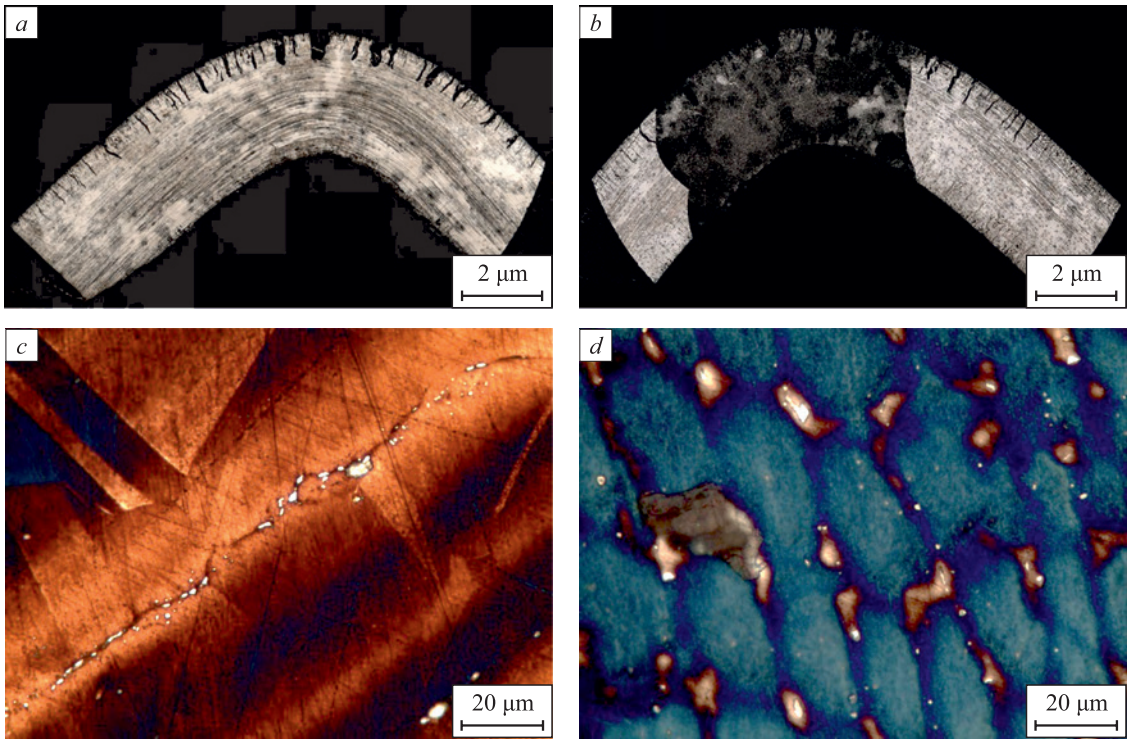

Fig. 1. Intergranular cracks in the base metal (*a*) and in the welded joint (*b*), and images of excess phases in the base metal (*c*) and in the welded joint (*d*)

Рис 1. Межкристаллитные трещины в основном металле (*a*) и в сварном соединении (*b*), а также изображения избыточных фаз в основном металле (*c*) и в сварном соединении (*d*)

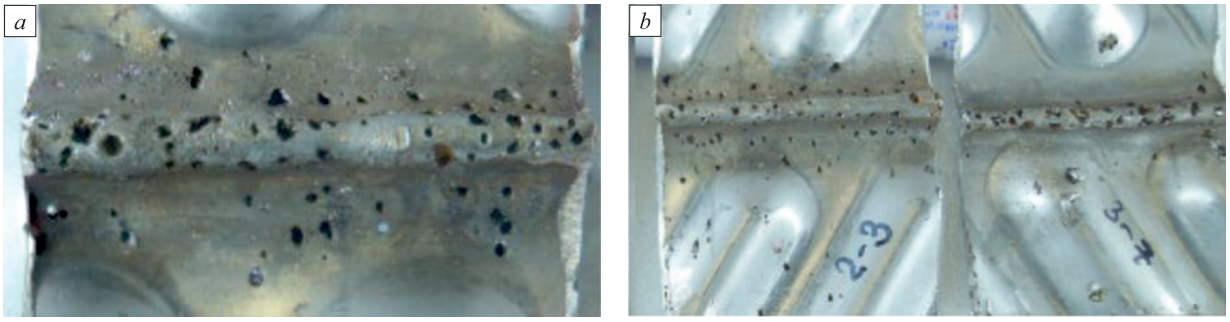

Fig. 2. Appearance of corrosion damage in the area of welded joint of heat-exchange elements of low-temperature natural gas separation unit

Рис. 2. Внешний вид коррозионных поражений в области сварного соединения теплообменных элементов аппарата низкотемпературной сепарации природного газа

The presence of titanium ensures the formation of favorable TiC carbides instead of undesirable $Cr_{23}C_6$ carbides, which reduce corrosion resistance.

Thus, the primary cause of the through defects in this case was the violation of the project documentation requirements regarding the unsanctioned change of the steel grade. This led to the incorrect selection of the welding mode, which caused activation of the metal in the heat-affected zone of the non-stabilized titanium steel, resulting in through pitting under the influence of the corrosive environment.

Results and discussion

The relatively small number of examined failures raises a broad spectrum of issues related to the production of high-quality corrosion-resistant steels and alloys, the selection of materials for operating conditions, the incompleteness of existing RTD, and the qualifications of specialists.

The issue of the quality of corrosion-resistant materials is extensive and requires the development and implementation of new RTD that describes quality requirements. This is a long-term and meticulous task; nevertheless, there are successful examples of such developments in domestic practice [35 – 38]. It is worth noting that currently, the only document in the oil and gas industry related to the selection and operation of corrosion-resistant steels is NACE MR0175, Part 3, which has not been harmonized with GOST. Moreover, this document only pertains to hydrogen sulphide-containing environments, while the evaluation of the possibility of using steels in CO_2-containing environments is becoming increasingly relevant [39].

Incorrect material selection is linked to the lack of selection methodologies and proper corrosion resistance assessment techniques. Material selection guidelines are usually developed within companies and are subject to internal policies. However, the relatively new Institute of Oil and Gas Technological Initiatives ("INTI") can gradually address such issues. The testing methodologies being developed to assess the corrosion resistance of materials should consider the reproduction of aggressive operating conditions on the sites.

At the Scientific and Technological Complex "New Technologies and materials", there is a substantial testing base of various stands and installations, allowing materials to be tested under conditions as close to operating conditions as possible, including flow parameters. The authors' team designed and manufactured autoclave installations of various volumes (Fig. 3, *a*), allowing tests to be conducted at elevated pressure and temperature in both static and dynamic conditions [40]. Tests involving supercritical fluids are also conducted in autoclaves.

The aggressiveness of the environment can manifest not only through the presence of corrosion-active agents but also through abrasive particles leading to abrasive wear. The combined influence of these two factors can significantly exacerbate the material degradation process. Their combined effect can be simulated using closed "flow-loop" stands, which also consider thermobaric parameters and fluid flow impact (Fig. 3, *b*).

However, conducting tests where many environmental parameters are controlled requires a lot of time and resources. Therefore, databases are created using the results of numerous tests, considering parameters determined on the stand, which are then used in a mathematical model to develop a digital twin.

The review of issues related to the justified selection of corrosion-resistant steels and alloys in the oil and gas industry highlights important aspects related to their operation in aggressive environments.

In the oil and gas industry, materials face aggressive environments, high temperatures, cyclic loads, and mechanical stresses. In practice, justified selection of corrosion-resistant materials does not always receive adequate attention, so seemingly economically advantageous solutions can turn out to be incorrect. This can lead to serious problems and additional costs for replacement

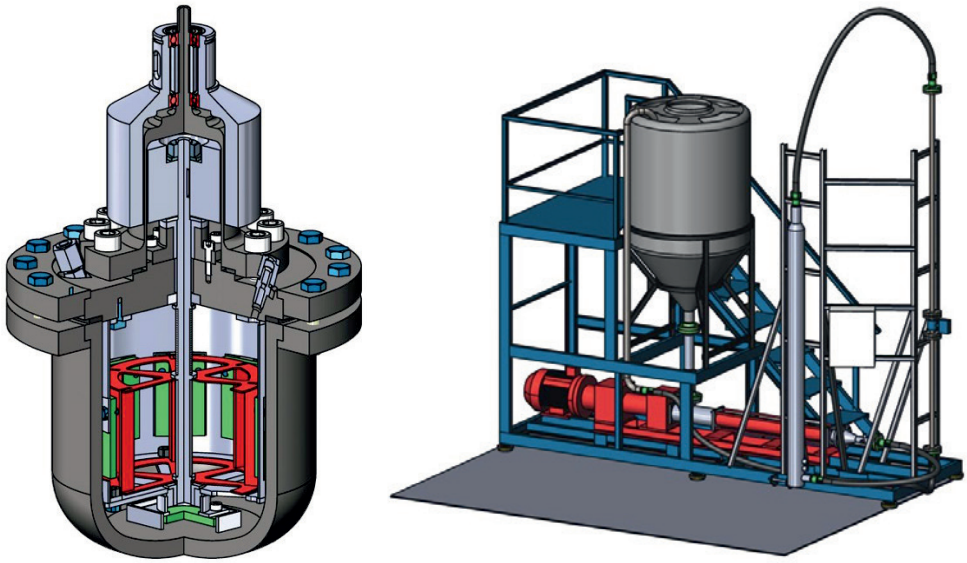

a *b*

Fig. 3. Test facility for physical modelling with reproduction of aggressive operating conditions: dynamic autoclave with rotation (*a*); corrosion-erosion bench (*b*)

Рис. 3. Испытательная база для проведения физического моделирования с воспроизведением агрессивных условий эксплуатации: динамический автоклав с вращением (*a*); коррозионно-эрозионный стенд (*b*)

or major repairs. For successful application of corrosion-resistant materials, preliminary laboratory studies must be conducted to recreate environmental factors to confirm the material's quality and corrosion resistance under specific operating conditions. Effective solutions require close cooperation between engineers, scientists, researchers, and manufacturers.

Conclusions

A review of the causes of failures of products made from corrosion-resistant materials in the oil and gas industry has been conducted. It has been established that the causes of material failure can be incorrect operating conditions, poor-quality materials, and incorrect selection of materials for the operating conditions. Examples from open sources and the authors' practice have been considered for each group of failure causes. The importance of conducting preliminary laboratory studies of corrosion-resistant materials and their testing with the simulation of environmental factors for a justified choice under specific operating conditions has been substantiated. The approaches used by the authors' team for conducting physical modelling of environmental factors with the recreation of real conditions, including flow parameters, have been demonstrated.

References / Список литературы

1. Kablov E.N. Materials for aerospace engineering. *Vse materialy. Entsiklopedicheskii spravochnik*. 2007;(5):7–27. (In Russ.).

   Каблов Е.Н. Материалы для авиакосмической техники. *Все материалы. Энциклопедический справочник*. 2007;(5):7–27.
2. Galkin M.P., Brodov A.A. Modern requirements for production of special steels and alloys. In: *XV Int. Congress of Steelmakers*. 2018:23–26. (In Russ.)

   Галкин М.П., Бродов А.А. Современные требования к производству специальных сталей и сплавов. *XV Международный конгресс сталеплавильщиков*. 2018:23–26.
3. Omura K., Kunioka S., Furukawa M. Product development on market trends of stainless steel and its future prospects. *Nippon Steel Technical Report*. 2010;99:9–19.
4. Gardner L. The use of stainless steel in structures. *Progress in Structural Engineering and Materials*. 2005;7(2):45–55. https://doi.org/10.1002/pse.190
5. Gol'dshtein M.I., Grachev S.V., Veksler Yu.G. Special Steels: Textbook for Universities. Moscow: MISIS; 1999:408. (In Russ.).

   Гольдштейн М.И., Грачев С.В., Векслер Ю.Г. Специальные стали: учебник для вузов. Москва: МИСИС; 1999:408.
6. Tomashov N.D., Chernova G.P. Corrosion Theory and Corrosion-Resistant Structural Alloys: Textbook for Universities. Moscow: Metallurgiya; 1993:416. (In Russ.).

   Томашов Н.Д., Чернова Г.П. Теория коррозии и коррозионностойкие конструкционные сплавы: Учебное пособие для вузов. Москва: Металлургия; 1993:416.
7. Fedorov A., Zhitenev A., Strekalovskaya D. Effect of heat treatment on the microstructure and corrosion properties of cast duplex stainless steels. *E3S Web of Conferences*. 2021; 225:01003. https://doi.org/10.1051/e3sconf/202122501003
8. Reck B.K., Rotter V.S. Comparing growth rates of nickel and stainless steel use in the early 2000s. *Journal of Industrial Ecology*. 2012;16(4):518–528. https://doi.org/10.1111/j.1530-9290.2012.00499.x

9. Zhitenev A.I., Fedorov A.S., Kovalev P.V., Strekalovskaya D.A., Al'khimenko A.A. Cast structure and properties of duplex stainless steels. *Izvestiya. Ferrous Metallurgy*. 2022;65(5):323–332. (In Russ.).
https://doi.org/10.17073/0368-0797-2022-5-323-332

Житенев А.И., Федоров А.С., Ковалев П.В., Стрекаловская Д.А., Альхименко А.А. Литая структура и свойства дуплексных нержавеющих сталей. *Известия вузов. Черная металлургия*. 2022;65(5):323–332.
https://doi.org/10.17073/0368-0797-2022-5-323-332

10. Hassel T., Maier H.J., Alkhimenko A., Davydov A., Shaposhnikov N., Turichin G., Klimova O. Investigation of the mechanical properties and corrosion behaviour of hybrid L80 Type 1 and duplex steel joints produced by magnetically impelled arc butt welding. *Journal of Advanced Joining Processes*. 2022;5:100109. https://doi.org/10.1016/j.jajp.2022.100109

11. Alekseeva E.L., Ermakov B.S., Gyulikhandanov E.L., Alkhimenko A.A., Lapechenkov A.A., Galata L. Influence of heat treatment on the corrosive and strength properties of the EP718 dispersion-hardening nickel alloy. *Russian Journal of Non-Ferrous Metals*. 2022;63:63–70.
https://doi.org/10.3103/S1067821222010035

12. Alekseeva E.L., Alkhimenko A.A., Kovalev M.A., Shaposhnikov N.O., Shishkova M.L., Devyaterikova N.A., Breki A.D., Kolmakov A.G., Gvozdev A.E., Kutepov S.N. The evaluation of the corrosion properties of steel two-layer oil well tubing for oil extraction. *Inorgamic Materials: Applied Research*. 2022;13:52–58.
https://doi.org/10.1134/S207511332201004X

13. Sedukhin V.V. Improvement of chemical composition and technology of smelting duplex steel alloyed with nitrogen in an open induction furnace: Cand. Tech. Sci. Diss. South Ural State University; 2022. (In Russ.).

Седухин В.В. Совершенствование химического состава и технологии выплавки дуплексной марки стали, легированной азотом, в открытой индукционной печи: Диссертация … кандидата технических наук. Южно-Уральский государственный университет; 2022.

14. Gowthaman P.S., Jeyakumar S., Saravanan B.A. Machinability and tool wear mechanism of Duplex stainless steel – A review. *Materials Today: Proceedings*. 2020;26(2):1423–1429. https://doi.org/10.1016/j.matpr.2020.02.295

15. Baddoo N.R. Stainless steel in construction: A review of research, applications, challenges and opportunities. *Journal of Constructional Steel Research*. 2008;64(11):1199–1206. https://doi.org/10.1016/j.jcsr.2008.07.011

16. Da Costa E.M., Dedavid B.A., Dos Santos C.A., Lopes N.F., Fraccaro C., Pagartanidis T., Lovatto L.P. Crevice corrosion on stainless steels in oil and gas industry: A review of techniques for evaluation, critical environmental factors and dissolved oxygen. *Engineering Failure Analysis*. 2022;144:106955. https://doi.org/10.1016/j.engfailanal.2022.106955

17. Craig B.D., Smith L. Corrosion Resistant Alloys (CRAs) in the Oil and Gas Industry – Selection Guidelines Update. 3rd ed. Nickel Institute Technical Series; 2011:12.

18. Hill R., Perez A.L. New steels and corrosion-resistant alloys. *Trends in Oil and Gas Corrosion Research and Technologies*. 2017:613–626.
https://doi.org/10.1016/B978-0-08-101105-8.00026-7

19. Machuca L.L., Pojtanabuntoeng T., Salgar-Chaparro S., Suarez E., Kinsella B., Darwin A. MIC Investigation of stainless steel seal ring corrosion failure in a floating production storage and offloading (FPSO) vessel. In: *Failure Analysis of Microbiologically Influenced Corrosion*. CRC Press; 2021:225–249.

20. Smiderle J., Pardal J.M., Tavares S.S.M., Vidal A.C.N. Premature failure of superduplex stainless steel pipe by pitting in sea water environment. *Engineering Failure Analysis*. 2014;46:134–139.
https://doi.org/10.1016/j.engfailanal.2014.08.001

21. Colombo A., Trasatti S.P. Corrosion of an UNS S31803 distillation column for acetic acid recovery. *Engineering Failure Analysis*. 2015;55:317–326.
https://doi.org/10.1016/j.engfailanal.2015.07.017

22. Linton V.M., Laycock N.J., Thomsen S.J., Klumpers A. Failure of a super duplex stainless steel reaction vessel. *Engineering Failure Analysis*. 2004;11(2):243–256.
https://doi.org/10.1016/j.engfailanal.2003.05.011

23. Corleto C.R., Argade G.R. Failure analysis of dissimilar weld in heat exchanger. *Case Studies in Engineering Failure Analysis*. 2017;9:27–34.
https://doi.org/10.1016/j.csefa.2017.05.003

24. Tavares S.S.M., Scandian C., Pardal J.M., Luz T.S., Da Silva F.J. Failure analysis of duplex stainless steel weld used in flexible pipes in off shore oil production. *Engineering Failure Analysis*. 2010;17(6);1500–1506.
https://doi.org/10.1016/j.engfailanal.2010.05.012

25. Liu M., Ni Z., Du C., Liu Z., Sun M., Fan E., Li X. Failure investigation of a 304 stainless steel geothermal tube. *Engineering Failure Analysis*. 2021;129:105694.
https://doi.org/10.1016/j.engfailanal.2021.105694

26. Sotoodeh K. A review and analysis of industrial valve material failures due to corrosion and proposals for prevention measures based on industrial experiences in the offshore sector of the oil and gas industry. *Journal of Failure Analysis and Prevention*. 2021;21:261–267.
https://doi.org/10.1007/s11668-020-01064-9

27. Rivaz A., Anijdan S.M., Moazami-Goudarzi M. Failure analysis and damage causes of a steam turbine blade of 410 martensitic stainless steel after 165,000 h of working. *Engineering Failure Analysis*. 2021;113:104557.
https://doi.org/10.1016/j.engfailanal.2020.104557

28. Ueda M., Nakamura K., Hudson N., Ibrahim M.Z., Selamat K., Chen P. Corrosion behavior of super 13Cr martensitic stainless steels in completion fluids. In: *CORROSIOn 2003*. OnePetro; 2003.

29. Park J.H., Kang Y. Inclusions in stainless steels – A review. *Steel Research International*. 2017;88(12):1700130.
https://doi.org/10.1002/srin.201700130

30. Fedorov A., Zhitenev A., Karasev V., Alkhimenko A., Kovalev P. Development of a methodology for the quality management of duplex stainless steels. *Materials*. 2022;15(17);6008.
https://doi.org/10.3390/ma15176008

31. Mancini S., di Nunzio P.E., Notargiacomo S., Langellotto L. Defect reduction and quality optimization through the modelling of plastic deformation and metallurgical evolution. *Materials Science Forum.* 2021;1016:846–851.
https://doi.org/10.4028/www.scientific.net/MSF.1016.846

32. Rozenfel'd I.L. Corrosion and Protection of Metals. Moscow: Metallurgiya; 1969:448. (In Russ.).

Розенфельд И.Л. Коррозия и защита металлов. Москва: Металлургия; 1969:448.

33. Groysman A. Corrosion for Everybody. Springer Science Business Media B.V.; 2010:382.

34. Lippol'd D.S., Koteki D.D. Metallurgy of Welding and Weldability of Stainless Steels. St. Petersburg: Izd-vo Politekhn. un-ta; 2011:467. (In Russ.).

Липпольд Д.С., Котеки Д.Д. Металлургия сварки и свариваемость нержавеющих сталей. Санкт-Петербург: Издательство Политехнического университета; 2011:467.

35. Petrov N.G. On MTK tasks 543/TC 214 "Protection of products and materials from corrosion, aging and bio-damage" and development of regulatory documents for anticorrosive protection. In: *Gas Transmission Systems: Present and Future (GTS-2023). Abstracts of the IX Int. Sci. and Tech. Conf. Kazan*; 2023:76–77. (In Russ.).

Петров Н.Г. О задачах МТК 543/ТК 214 «Защита изделий и материалов от коррозии, старения и биоповреждений» и разработке нормативных документов противокоррозионной защиты. *Газотранспортные системы: настоящее и будущее (ГТС-2023). Тезисы IX Международной научно-технической конференции. Казань*; 2023:76–77.

36. Kazakov A.A., Zhitenev A.I., Salynova M.A. Extension of ASTM E2283 standard practice for the assessment of large exogenous nonmetallic inclusions in super duty steels. *CIS Iron and Steel Review*. 2019;18:20–26. https://doi.org/10.17580/cisisr.2019.02.01

37. Kazakov A.A., Zhitenev A.I., Kolpishon E.Yu., Salynova M.A. Quantitative assessment of non-metallic inclusions for forgings from super-large ingots. *Chernye metally*. 2018;(12):50–56. (In Russ.).

Казаков А.А., Житенев А.И., Колпишон Э.Ю., Салынова М.А. Количественная оценка неметаллических включений для поковок из сверхкрупных слитков. *Черные металлы*. 2018;(12):50–56.

38. Kazakov A.A., Kiselev D.V., Kazakova E.I. Quantitative methods for assessing the microstructure of steel and alloys for revising outdated GOST standards. *Lit'e i metallurgiya*. 2021;(2):42–48. (In Russ.). https://doi.org/10.21122/1683-6065-2021-2-42-48

Казаков А.А., Киселев Д.В., Казакова Е.И. Количественные методы оценки микроструктуры стали и сплавов для пересмотра устаревших ГОСТ. *Литье и металлургия*. 2021;(2):42–48. https://doi.org/10.21122/1683-6065-2021-2-42-48

39. Fedorov A.S., Alekseeva E.L., Al'khimenko A.A., Shaposhnikov N.O., Kovalev M.A. Study of the effect of test parameters on the assessment of steel resistance to carbon dioxide corrosion. *Zavodskaya laboratoriya. Diagnostika materialov*. 2021;87(12):36–41. (In Russ.). https://doi.org/10.26896/1028-6861-2021-87-12-42-47

Федоров А.С., Алексеева Е.Л., Альхименко А.А., Шапошников Н.О., Ковалев М.А. Исследование влияния параметров испытаний на оценку стойкости сталей к углекислотной коррозии. *Заводская лаборатория. Диагностика материалов*. 2021;87(12):36–41. https://doi.org/10.26896/1028-6861-2021-87-12-42-47

40. Kruk P., Golubev I., Shaposhnikov N., Shinder J., Kotov D. The effect of the operation of downhole equipment on the processes of corrosive wear (by the example inflow control devices of nozzle type). *Materials*. 2022;15(19):6731. https://doi.org/10.3390/ma15196731

Information about the Authors / Сведения об авторах

Aleksandr S. Fedorov, *Engineer of the Scientific and Technological Complex "New Technologies and Materials",* Peter the Great St. Petersburg Polytechnic University
ORCID: 0000-0003-2571-060X
E-mail: fedorov_as@spbstu.ru

Vladimir S. Karasev, *Engineer of the Scientific and Educational Center "Severstal-Polytech",* Peter the Great St. Petersburg Polytechnic University
ORCID: 0009-0006-9622-7243
E-mail: karasev_vs@spbstu.ru

Ekaterina L. Alekseeva, *Cand. Sci. (Eng.), Leading Engineer, Head of the Laboratory of the Scientific and Technological Complex "New Technologies and Materials",* Peter the Great St. Petersburg Polytechnic University
E-mail: alekseeva_el@spbstu.ru

Aleksei A. Al'khimenko, *Director of the Scientific and Technological Complex "New Technologies and Materials",* Peter the Great St. Petersburg Polytechnic University
ORCID: 0000-0001-6701-1765
E-mail: a.alkhimenko@spbstu.ru

Nikita O. Shaposhnikov, *Executive Director of the Scientific and Technological Complex "New Technologies and Materials",* Peter the Great St. Petersburg Polytechnic University
E-mail: shaposhnikovno@gmail.com

Александр Сергеевич Федоров, *инженер Научно-технологического комплекса «Новые технологии и материалы»,* Санкт-Петербургский политехнический университет Петра Великого
ORCID: 0000-0003-2571-060X
E-mail: fedorov_as@spbstu.ru

Владимир Сергеевич Карасев, *инженер Научно-образовательного центра «Северсталь-Политех»,* Санкт-Петербургский политехнический университет Петра Великого
ORCID: 0009-0006-9622-7243
E-mail: karasev_vs@spbstu.ru

Екатерина Леонидовна Алексеева, *к.т.н., ведущий инженер, заведующий лабораторией Научно-технологического комплекса «Новые технологии и материалы»,* Санкт-Петербургский политехнический университет Петра Великого
E-mail: alekseeva_el@spbstu.ru

Алексей Александрович Альхименко, *директор Научно-технологического комплекса «Новые технологии и материалы»,* Санкт-Петербургский политехнический университет Петра Великого
ORCID: 0000-0001-6701-1765
E-mail: a.alkhimenko@spbstu.ru

Никита Олегович Шапошников, *исполнительный директор Научно-технологического комплекса «Новые технологии и материалы» центра НТИ,* Санкт-Петербургский политехнический университет Петра Великого
E-mail: shaposhnikovno@gmail.com

Contribution of the Authors

A. S. Fedorov – formation of the main research idea, development of the work methodology, analysis of research results.
V. S. Karasev – development of the work methodology, analysis of research results.
E. L. Alekseeva – formation of the main research idea, setting the tasks.

A. A. Al'khimenko – concept formation, scientific guidance.

N. O. Shaposhnikov – research plan development, scientific guidance.

Вклад авторов

А. С. Федоров – формирование основной идеи исследований, разработка методологии работы, анализ результатов исследований.
В. С. Карасев – разработка методологии работы, анализ результатов исследований.
Е. Л. Алексеева – формирование основной идеи исследований, постановка целей и задач работы.
А. А. Альхименко – формирование концепции, научное руководство.
Н. О. Шапошников – разработка плана исследований, научное руководство.

Received 11.09.2023
Revised 03.11.2023
Accepted 11.12.2023

Поступила в редакцию 11.09.2023
После доработки 03.11.2023
Принята к публикации 11.12.2023

PHYSICO-CHEMICAL BASICS OF METALLURGICAL PROCESSES / ФИЗИКО-ХИМИЧЕСКИЕ ОСНОВЫ МЕТАЛЛУРГИЧЕСКИХ ПРОЦЕССОВ

UDC 669.187.28.539.55
DOI 10.17073/0368-0797-2024-3-351-359

Original article
Оригинальная статья

Thermodynamic modeling of interphase distribution of chromium and boron in slags of AOD reduction period

A. A. Babenko, V. I. Zhuchkov, N. I. Kel', **A. G. Upolovnikova, R. R. Shartdinov**

Institute of Metallurgy of the Ural Branch of the Russian Academy of Sciences (101 Amundsen Str., Yekaterinburg 620016, Russian Federation)

dunnington@mail.ru

Abstract. The paper presents the results of a thermodynamic modeling of the chromium and boron reduction from slags of reduction period of argon-oxygen decarburization (AOD) by a complex reducing agent containing silicon and aluminum. Using the simplex lattice method, an experiment planning matrix is constructed containing 16 compositions of the oxide system $CaO–SiO_2$ – (3 – 6 %) B_2O_3 – 12 % Cr_2O_3 – 3 % Al_2O_3 – 8 % MgO of variable basicity 1.0 – 2.5. The results of thermodynamic modeling are graphically presented in form of dependence of equilibrium distribution of chromium and boron on the slag composition at temperatures of 1600 and 1700 °C. The constructed diagrams make it possible to quantify the influence of the temperature, basicity and B_2O_3 in the slag on equilibrium interphase distribution of chromium and boron. It is established that increasing the slag basicity from 1.0 to 2.5 improves the process of chromium reduction, but restores the boron stability. With an increase in B_2O_3 content in the slag, a slight deterioration of chromium reduction process occurs, while the boron content in the metal increases. With a simultaneous increase in basicity up to 2.5 and a decrease in boron oxide in the slag from 5 to 3 %, the interphase distribution coefficient of chromium is reduced to $1.5 \cdot 10^{-3}$. Changing the process temperature from 1600 to 1700 °C does not have a negative effect on the process of chromium reduction, but worsens the boron reduction conditions. Based on analysis of the formed slag phases and thermodynamics of the reactions of their formation, it is established that chromium is mainly reduced by aliminum with only partial development of silicothermy. The residual silicon content reduces boron, thereby limiting its concentration in the metal. The results of high-temperature experiments showed high correspondence with the results of thermodynamic studies.

Keywords: stainless steel, argon-oxygen decarburization (AOD), reduction period, thermodynamic modeling, chromium, boron, interphase distribution

Acknowledgements: The work was carried out according to the state assignment for IMET UB RAS.

For citation: Babenko A.A., Zhuchkov V.I., Kel' I.N., Upolovnikova A.G., Shartdinov R.R. Thermodynamic modeling of interphase distribution of chromium and boron in slags of AOD reduction period. *Izvestiya. Ferrous Metallurgy*. 2024;67(3):351–359.
https://doi.org/10.17073/0368-0797-2024-3-351-359

Термодинамическое моделирование межфазного распределения хрома и бора в шлаках восстановительного периода АКР-процесса

А. А. Бабенко, В. И. Жучков, И. Н. Кель, **А. Г. Уполовникова, Р. Р. Шартдинов**

Институт металлургии Уральского отделения РАН (Россия, 620016, Екатеринбург, ул. Амудсена, 101)

dunnington@mail.ru

Аннотация. В работе приведены результаты термодинамического моделирования процесса восстановления хрома и бора из шлаков восстановительного периода аргонокислородного рафинирования комплексным восстановителем, содержащим кремний и алюминий. При помощи симплекс решетчатого метода построена матрица планирования эксперимента, содержащая 16 составов оксидной системы $CaO–SiO_2$ – (3 – 6 %) B_2O_3 – 12 % Cr_2O_3 – 3 % Al_2O_3 – 8 % MgO переменной основности 1,0 – 2,5. Результаты термодинамического моделирования представлены графически в виде диаграмм зависимости равновесного распределения хрома и бора от состава шлака при температурах 1600 и 1700 °C. Построенные диаграммы позволили количественно оценить влияние температуры, основности и содержания

B_2O_3 на равновесное межфазное распределение хрома и бора. Установлено, что повышение основности шлака с 1,0 до 2,5 улучшает процесс восстановления хрома, но ухудшает восстановление бора. При увеличении содержания B_2O_3 в шлаке происходит незначительное ухудшение процесса восстановления хрома, при этом увеличивается содержание бора в металле. При одновременном повышении основности до 2,5 и снижении содержания оксида бора в шлаке с 5 до 3 % коэффициент межфазного распределения хрома снижается до $1{,}5 \cdot 10^{-3}$. Изменение температуры процесса с 1600 до 1700 °С не оказывает существенного влияния на процесс восстановления хрома, однако ухудшает условия восстановления бора. На основе анализа фаз формируемого шлака и термодинамики реакций их образования установлено, что восстановление хрома протекает в основном за счет алюминия с частичным развитием силикотермических реакций. Остаточное содержание кремния восстанавливает бор, чем объясняется его низкая концентрация в металле. Результаты проведенных высокотемпературных экспериментов показали высокую согласованность с результатом термодинамического моделирования.

Ключевые слова: нержавеющая сталь, аргонокислородное рафинирование, восстановительный период, термодинамическое моделирование, хром, бор, межфазное распределение

Благодарности: Исследование выполнено за счет государственного задания ИМЕТ УрО РАН.

Для цитирования: Бабенко А.А., Жучков В.И., Кель И.Н., Уполовникова А.Г., Шартдинов Р.Р. Термодинамическое моделирование межфазного распределения хрома и бора в шлаках восстановительного периода АКР-процесса. *Известия вузов. Черная металлургия*. 2024;67(3):351–359. https://doi.org/10.17073/0368-0797-2024-3-351-359

Introduction

Stainless steel is an absolutely essential part of a modern economy – the annually growing volumes of its consumption and a wide range of applications from medical products [1] to structural materials prove this statement[1]. Stainless steel is so popular because it is resistant to corrosion in various aggressive environments as an oxide layer, with a high concentration of chromium (12 wt. % and higher), forms on the metal surface, which prevents the steel from contacting air oxygen [2 – 4]. Despite the obvious advantages of stainless steel, the domestic production volumes are modest and the demand for this steel is covered by imports [5].

Currently, the main method of producing low-carbon stainless steel is the duplex process with smelting carbonaceous semi-product (1.5 – 2.0 wt. % C) in an arc furnace followed by treatment in the argon-oxygen decarburization (AOD) unit [6; 7]. The AOD process includes two periods: oxidation and reduction. During the oxidation period, the carbonaceous semi-product of stainless steel is decarbonized by blowing a mixture of oxygen and argon through it. When the carbon concentration in the metal drops to 0.03 wt. % or less, the reduction period of melting begins, during which the bath of the unit is purged with nothing but argon, and lime, ferroalloys (ferrosilicon, ferrosilicochrome) and calcium fluoride are added [8].

As a result of chromium oxidation by oxygen, the concentration of Cr_2O_3 in the slag increases, which negatively affects the technological processes occurring in the reduction period of melting, the intensity of their development being limited by the viscosity of the formed oxide system. According to [9], Cr_2O_3 usually has low solubility (5 %) in $CaO–SiO_2–Al_2O_3–MgO$ based slags, which increases their melting point and, consequently, viscosity. Therefore, calcium fluoride (CaF_2) is used to reduce the viscosity of slags in the reduction period of melting. The use of this flux has the following downsides: it is environmentally unfriendly as volatile carcinogenic fluorine compounds are formed, physical properties of the formed slags are inconsistent and the effect of silicate decomposition of solid slags persists during storage. Therefore, it is reasonable to explore other liquefying additives to replace calcium fluoride, for example, pegmatite [10], Al_2O_3 [11] or B_2O_3 [12]. Although the use of Al_2O_3 prevents the formation of volatile fluoride compounds, according to [11], the refining ability of the slag deteriorates. As such, its use is limited. Therefore, the boron-containing material is a reasonable choice as it is an inexpensive, available and environmentally friendly fluxing material.

Although B_2O_3 is an acidic oxide and facilitates polymerization [13], it helps to reduce slag viscosity by changing the structural components of the melt mesh. Adding B_2O_3 to the slag helps to improve kinetics of chromium reduction and metal desulfurization [14; 15]. Hardening characteristics of low-carbon steel are to improve and the aging effect is to reduce [17] due to expected partial reduction of boron by silicon and aluminum dissolved in the steel, followed by its transfer to the metal, in addition to the slag liquefying with boron oxide [17].

Practically no domestic or foreign researchers have explored the effectiveness of the interphase distribution of chromium and boron during their reduction by a complex ferroalloy containing aluminum and silicon.

The paper presents the results of thermodynamic modeling of equilibrium interphase distribution of chromium and boron reduced by silicon and aluminum from the $CaO–SiO_2–B_2O_3–Al_2O_3–Cr_2O_3–MgO$ oxide system by aluminum ferrosilicon, a complex ferroalloy.

Materials and methods

We performed thermodynamic modeling of the equilibrium interphase distribution of chromium and

[1] Stainless Steel in Figures 2019. URL: http://www.worldstainless.org/Files/issf/non-image-files/PDF/ISSF_Stainless_Steel_in_Figures_2019_English_public_version.pdf (accessed on 27.03.2023)

boron reduced by silicon and aluminum of the complex reducing agent (aluminum ferrosilicon) from the $CaO-SiO_2-B_2O_3-Al_2O_3-Cr_2O_3-MgO$ oxide system using the HSC Chemistry 6.12 software package. This software is based on the calculating equilibrium compositions and the amount of resulting products, using the Gibbs energy minimization algorithm.

Thermodynamic modeling was performed for the temperatures of 1600 and 1700 °C. The mass of the working medium was 115 kg (100 kg of metal and 15 kg of slag) with the gas phase (N_2) volume of 2.24 m^3 and the system pressure of 0.098 MPa. The amount of the reducing agent is 0.89 kg. The interphase distribution coefficients of chromium and boron were obtained by their concentration ratios in the slag and metal ($L_B = (B_2O_3)/[B]$ and $L_{Cr} = (Cr_2O_3)/[Cr]$).

The oxide system composition corresponds to 16 points of the local simplex plan and is presented in Table 1. In addition to calcium, silicon and boron oxides, all slags include chromium, magnesium and aluminum oxides in the amount of 12, 8 and 3 %, respectively. The metal part is represented by stainless steel containing, %: 16.0 Cr; 0.03 C; 0.28 Si; 0.010 S; 1.46 Mn; 6.98 Ni; 0.01 Al; the rest is Fe and aluminum ferrosilicon (AFS), a complex alloy containing, %: 55.8 Si; 18.8 Al; 25.4 Fe.

The results of thermodynamic modeling are presented by approximating mathematical models in the form of a reduced polynomial of the third degree, which describe the influence of the slag composition of the studied oxide system on the interphase distribution coefficients of chromium and boron at temperatures of 1600 and 1700 °C [18]. The adequacy of the constructed mathematical models was tested by three control points, not included in the experiment planning matrix, using *t*-criterion at the significance level of 0.01.

Figs. 1 and 2 graphically present the results of mathematical modeling in the form of composition – property diagrams. The solid lines show isolines of the equilibrium interphase distribution of chromium and boron, while thin lines reflect the basicity of the slag (CaO/SiO_2) with its value indicated.

Along with thermodynamic modeling of the equilibrium interphase distribution of chromium and boron, we conducted high-temperature experimental studies using an electric resistance furnace in magnesia crucibles in an argon current at 1600 °C. The low-carbon stainless steel was held for 30 min under slag in the points used for local simplex. The temperature was measured using a BP5/20 tungsten thermocouple. Metal samples were prepared from chips of AISI 304 stainless steel and steel ST3SP, as well as the slag from two base points Y_1 and Y_3 (Table 1). We took the test charge of ground metal and slag in the quantities of 75 and 50 g to achieve the maximum phase contact surface and to exclude the influence

Table 1. **Composition of slag in 16 points of the local simplex plan**

Таблица 1. **Состав шлака 16 точек плана локального симплекса**

Slag index	Slag composition						
	in pseudocomponent coordinates, unit fractions				in coordinates of initial components, wt. %		
	X_1	X_2	X_3	X_4	CaO	SiO_2	B_2O_3
Y_1	1.00	0	0	0	37.00	37.00	3
Y_2	0	1.00	0	0	52.86	21.14	3
Y_3	0	0	1.00	0	50.71	20.29	6
Y_4	0	0	0	1.00	35.50	35.50	6
Y_{12}	0.67	0.33	0	0	42.29	31.71	3
Y_{13}	0.33	0.67	0	0	47.57	26.43	3
Y_{21}	0	0.67	0.33	0	52.14	20.86	4
Y_{22}	0	0.33	0.67	0	51.43	20.57	5
Y_{31}	0	0	0.67	0.33	45.64	25.36	6
Y_{32}	0	0	0.33	0.67	40.57	30.43	6
Y_{41}	0.33	0	0	0.67	36.00	36.00	5
Y_{42}	0.67	0	0	0.33	36.50	36.50	4
Y_{121}	0.67	0	0.33	0	41.57	31.43	4
Y_{122}	0.33	0	0.33	0.33	41.07	30.93	5
Y_{131}	0.33	0.33	0.33	0	46.86	26.14	4
Y_{132}	0.33	0	0.67	0	46.14	25.86	5

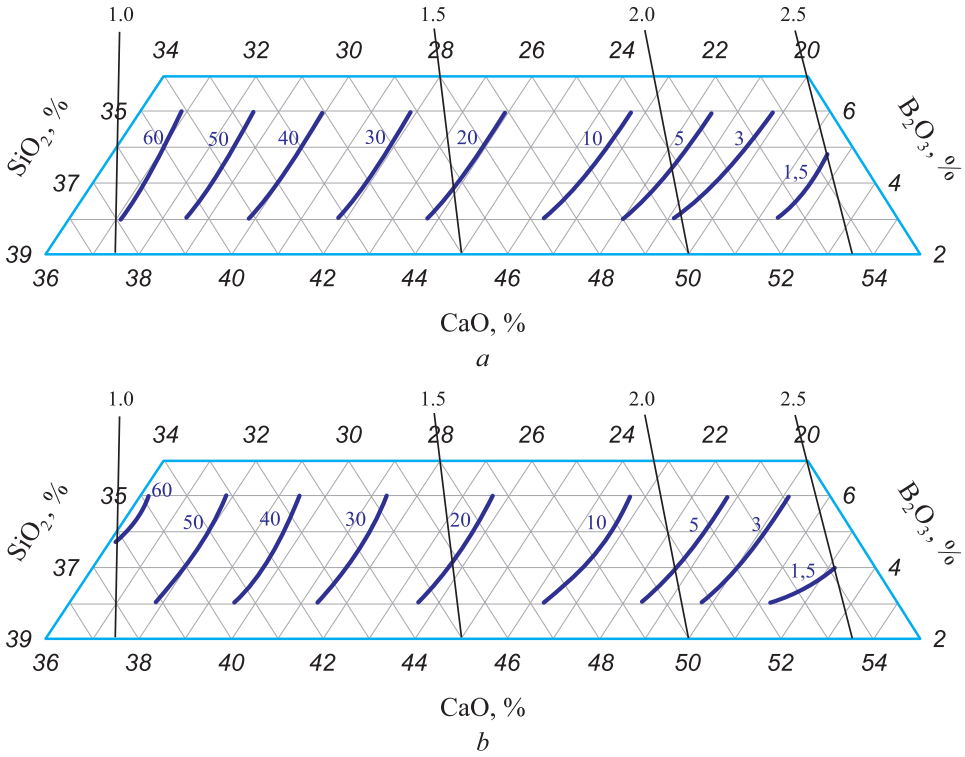

Fig. 1. Dependence of the coefficient of equilibrium interphase distribution of chromium on the slag chemical composition at 1600 (*a*) and 1700 °C (*b*)

Рис. 1. Зависимость коэффициента равновесного межфазного распределения хрома от химического состава шлака при 1600 (*a*) и 1700 °C (*b*)

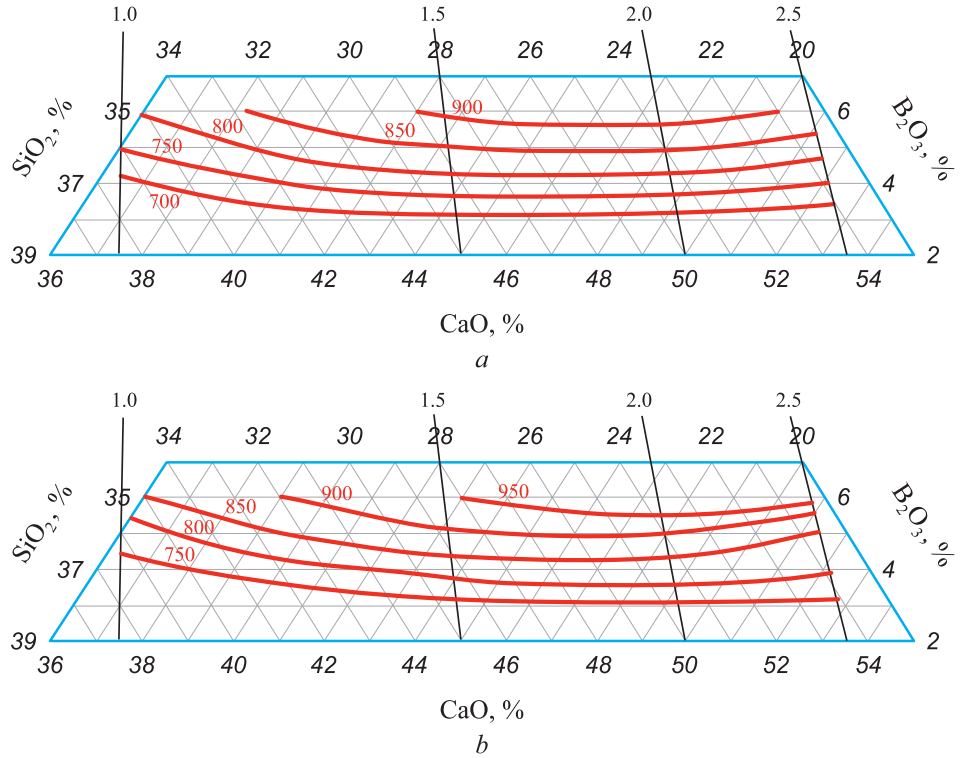

Fig. 2. Dependence of the coefficient of equilibrium interphase distribution of boron on the slag chemical composition at 1600 (*a*) and 1700 °C (*b*)

Рис. 2. Зависимость коэффициента равновесного межфазного распределения бора от химического состава шлака при 1600 (*a*) и 1700 °C (*b*)

of the mass of metal and slag phases on the interphase distribution coefficients of chromium and boron [19].

Results and discussion

Table 2 and Figs. 1, 2 present the results of thermodynamic modeling of the equilibrium interphase distribution of chromium and boron depending on the basicity of the slags of the studied oxide system and temperature.

With the slag basicity ranging from 1.0 to 1.5 and the boron oxide concentration varying from 3 to 6 wt. %, the interphase distribution coefficient of chromium dropped from $60 \cdot 10^{-3}$ to $20 \cdot 10^{-3}$ at 1600 °C (Fig. 1, *a*). The increase in the slags basicity to 2.5, with the boron oxide concentration changing from 5 to 3 %, results in drop of the interphase distribution coefficient of chromium to $1.5 \cdot 10^{-3}$, which is indicative of more effective chromium reduction due to growing basicity of formed slags. The increase in boron oxide concentration comes with a slight deterioration of the chromium reduction process. The rise in the B_2O_3 content in the slag from 3 to 6 % is accompanied (for example, at basicity of 2.0) by an increase in the equilibrium interphase distribution coefficient of chromium from $3 \cdot 10^{-3}$ to $5 \cdot 10^{-3}$ at a temperature of 1600 °C (Fig. 1, *a*). The temperature rise from 1600 to 1700 °C has a slight impact on the interphase distribution coefficient of chromium (Table 2). At 1700 °C in the considered range of basicity and boron oxide content, it remains at the level ranging from $60 \cdot 10^{-3}$ to $1.5 \cdot 10^{-3}$ (Fig. 1, *b*).

With the basicity of formed slags ranging from 1.0 to 2.5, as the boron oxide concentration rises from 3 to 6 %, the equilibrium interphase distribution coefficient of boron increases from 700 to 900 (Fig. 2, *a*). We can clearly observe the influence of boron oxide on the equilibrium interphase distribution coefficient, while the impact of basicity is weak. For example, in the basicity range of 1.5 – 2.5, the equilibrium interphase distribution coefficient of boron is 900, its oxide concentration ranging from 5.7 to 6.0 %. The decrease of boron oxide concentration to 5.0 – 5.3 % in the considered basicity range causes the drop of the equilibrium interphase distribution coefficient of boron to 850. The behavior of the equilibrium interphase distribution coefficient of boron follows a similar pattern when the boron oxide concentration reaches 3.0 – 3.4 %.

The process temperature rising to 1700 °C leads to a slight increase in L_B by 50 units and deteriorates the process of boron reduction (Fig. 2, *b*).

The positive impact of basicity of formed slags in the studied range of the chemical composition on the chromium and boron reduction can be qualitatively explained in terms of the phase composition formation (Table 3) and thermodynamics of reactions of chromium and boron reduction by aluminum and silicon (Table 4).

Table 2. **Interfacial distribution coefficient of chromium and boron**

Таблица 2. **Коэффициент равновесного межфазного распределения хрома и бора**

Slag index	Basicity (CaO/SiO_2)	1600 °C		1700 °C	
		$L_{Cr} \cdot 10^{-3}$	L_B	$L_{Cr} \cdot 10^{-3}$	L_B
Y_1	1.0	60.28	619.114	56.26	642.657
Y_2	2.5	0.90	654.000	0.98	724.683
Y_3	2.5	2.16	887.343	2.31	983.439
Y_4	1.0	69.43	796.648	64.95	845.092
Y_{12}	1.3	27.53	677.126	25.63	710.389
Y_{13}	1.8	6.71	685.229	7.21	733.197
Y_{21}	2.5	1.19	745.779	1.48	802.996
Y_{22}	2.5	1.60	822.055	1.95	845.092
Y_{31}	1.8	12.89	922.397	12.85	976.023
Y_{32}	1.3	36.95	885.245	33.96	921.957
Y_{41}	1.0	66.68	751.965	60.48	777.277
Y_{42}	1.0	63.46	694.136	57.51	719.056
Y_{121}	1.3	31.45	762.105	29.07	797.220
Y_{122}	1.3	34.20	830.599	31.51	866.934
Y_{131}	1.8	8.73	780.574	9.09	831.897
Y_{132}	1.8	11.07	858.519	11.22	911.182

According to the results of thermodynamic modeling (Table 3), the composition of chromium-containing phases of low-base slag Y_1 is represented mainly by Cr_2O_3 and $CaO·Cr_2O_3$ phases, the number of which decreases in the process of chromium reduction from 8.1 and 5.4 % to 0.7 and 0.4 %, respectively. At the same time, the process of chromium reduction by silicon mainly occurs following the reactions (1) and (2) (Table 4), which is confirmed by the increase in content of SiO_2 and $CaSiO_3$ in the final slag from 4.8 and 18.8 % to 5.8 and 20.6 %, respectively (Table 3). The reduction of chromium by aluminum occurs following the reactions (6) and (7) (Table 4), which is confirmed by the increase in the content of the products of these reactions Al_2O_3 and $CaO·Al_2O_3$ from 0.8 and 0.3 % to 1.2 and 0.4 % (Table 3).

The reduction of chromium from low-base slag Y_4 (basicity of 1.0) occurs following the same reactions as for slag Y_1. Low-base slags are characterized by reduction of chromium mainly by aluminum as a result of reactions (6) and (7) with partial development of silicothermic reactions (1) and (2) (Table 4), which is attributed to the higher negative ΔG value of aluminothermic reactions compared to silicothermic ones.

In the highly basic slag Y_2 (basicity of 2.5) in the presence of a large amount of free CaO, the reduction of chromium by silicon is more active (reactions (2) – (4))

Table 3. **Slag phases involved in reduction of chromium and boron at 1600 °C**

Таблица 3. **Фазы шлака, участвующие в процессе восстановления хрома и бора при температуре 1600 °С**

Phase, %	Slag							
	Y_1		Y_2		Y_3		Y_4	
	before	after	before	after	before	after	before	after
Cr_2O_3	8.1	0.7	1.0	0.002	1.6	0.007	8.7	0.9
$CaO·Cr_2O_3$	5.4	0.4	15.1	0.020	14.2	0.040	4.5	0.4
$Ca_2B_2O_5$	4.4	4.2	2.8	3.4	7.5	9.0	7.9	7.6
$Ca_3B_2O_6$	0.5	0.4	15.1	5.6	10.2	8.1	0.6	0.6
Al_2O_3	0.8	1.2	0.3	0.6	0.4	0.8	0.8	1.3
$CaO·Al_2O_3$	0.3	0.4	2.1	3.1	1.6	2.3	0.2	0.3
CaO	0.2	0.2	5.0	3.4	2.7	1.8	0.2	0.2
SiO_2	4.8	5.8	0	0.1	0.1	0.2	6.0	6.9
$CaSiO_3$	18.8	20.6	3.2	5.0	4.3	6.8	17.9	19.4
$2CaO·SiO_2$	8.9	9.0	33.7	37.2	26.4	27.9	6.5	6.6
$3CaO·2SiO_2$	10.0	10.8	6.1	11.0	6.9	11.9	6.7	7.2

Table 4. **Change in Gibbs energy during reduction of chromium and boron from oxides at 1600 °C**

Таблица 4. **Изменение энергии Гиббса реакций восстановления хрома и бора из оксидов при 1600 °С**

Number	Chemical reactions	ΔG_{1600}, kJ
Chromium reduction		
(1)	$Cr_2O_3 + 1.5Si = 2Cr + 1.5SiO_2$	–210.95
(2)	$Cr_2O_3 + 1.5Si + 1.5CaO = 1.5\ CaSiO_3 + 2Cr$	–347.82
(3)	$1.3Cr_2O_3 + 2Si + 3CaO = 3CaO·2SiO_2 + 2.7Cr$	–542.60
(4)	$Cr_2O_3 + 1.5Si + 3CaO = 1.5·2CaO·SiO_2 + 2Cr$	–441.64
(5)	$CaO·Cr_2O_3 + 1.5Si = 2Cr + CaO + 1.5SiO_2$	–141.83
(6)	$Cr_2O_3 + 2Al = Al_2O_3 + 2Cr$	–421.04
(7)	$CaO·Cr_2O_3 + 2Al = CaO·Al_2O_3 + 2Cr$	–408.11
Boron reduction		
(8)	$Ca_2B_2O_5 + 2Al = 2CaO·Al_2O_3 + 2B$	–50.148
(9)	$Ca_3B_2O_6 + 2Al = 3CaO·Al_2O_3 + 2B$	–78.91
(10)	$Ca_3B_2O_6 + 1{,}5Si = 1.5·2CaO·SiO_2 + 2B$	–12.79

(Table 4). Due to the slag high basicity, the content of $CaO \cdot Cr_2O_3$ in Y_2 is much higher than in low-base Y_1. Therefore, a considerable amount of this phase is reduced by aluminum following the reaction (7) (Table 4). It should be noted that after chromium reduction, the chromium-containing phases are present in negligible amounts, i.e., the content of Cr_2O_3 drops from 1.0 to 0.002 % and that of $CaO \cdot Cr_2O_3$ – from 15.1 to 0.02 % (Table 3). Similarly, chromium is reduced from the high-base slag Y_3.

Boron is insignificantly reduced from the slag as the change of Gibbs free energy of its reduction by aluminum and silicon from calcium borates is minimal, therefore, the transition of boron to metal for all studied slag compositions following the reactions (8) – (10) is insignificant (Table 4).

We conducted high-temperature experimental studies to verify if the results of thermodynamic modeling of the chromium and boron interphase distribution are adequate. The experiment showed that the Cr_2O_3 content in the slag at 1600 °C is 0.96 wt. %, which corresponds to the interphase distribution coefficient of $49.8 \cdot 10^{-3}$. The interphase distribution of boron reaches 648 with a residual B_2O_3 content in the slag of 3.89 wt. %. In general, the experimental results are close to the thermodynamic modeling, the kinetic factors accounting for the difference between them.

Conclusions

The thermodynamic modeling enabled us to obtain new data, based on which we constructed approximating mathematical models of the composition – property relation with graphical representation in the form of diagrams showing the equilibrium interphase distribution of chromium and boron depending on the process temperature, B_2O_3 content and basicity of the studied oxide system. Based on the plotted diagrams, we conducted quantitative evaluation of the impact that the above-mentioned factors had on the equilibrium interphase distribution of chromium and boron.

It was found that the increase in the basicity of the oxide system from 1.0 to 2.5, other conditions being equal, favorably affects the completeness of chromium reduction. At the same time, the increase in boron oxide concentration is accompanied by a slight decrease of the chromium reduction. The process temperature rise has no significant effect on the chromium reduction, but negatively affects the reduction of boron. It was determined that chromium is mostly reduced by aluminum with partial development of silicothermic reactions. The performed high-temperature experiment confirmed the results of thermodynamic modeling.

References / Список литературы

1. Illarionov A.G., Grib S.V., Yurovskikh A.S., Volokitina E.A., Gilev M.V., Azorina T.S. Usage of metal materials for medical implants. *Bulletin of the Ivanovo Medical Academy*. 2017;22(4):46–50. (In Russ.).

   Илларионов А.Г., Гриб С.В., Юровских А.С., Волокитина Е.А., Гилев М.В., Азорина Т.С. Применение металлических материалов для медицинских имплантатов. *Вестник Ивановской медицинской академии*. 2017;22(4):46–50.

2. Bel'tyukov E.A., Shartdinov R.R., Lobanova L.A., etc. Effect of boron on the properties of stainless steels. In: *Ural School of Young Metallurgists: materials of the XXI Int. Sci. and Tech. Ural School-Seminar of Metallurgists-Young Scientists, February 07–11, 2022*. Yekaterinburg: UrFU; 2022:394–399. (In Russ.).

   Бельтюков Е.А., Шартдинов Р.Р., Лобанова Л.А. и др. Влияние бора на свойства нержавеющих сталей. В кн.: *Уральская школа молодых металловедов: материалы XXI Международной научно-технической Уральской школы-семинара металловедов – молодых ученых 07–11 февраля 2022, Екатеринбург*. Екатеринбург: Издательство Уральского университета; 2022:394–399.

3. Capitan M.J., Lefebvre S., Traverse A., Paúl A., Odriozola J.A. Anomalous scattering study of oxide scales formed at 1173 K on surface modified stainless steel. *Journal of Materials Chemistry*. 1998;8(10):2293–2298. https://doi.org/10.1039/A802233J

4. Wei D.B., Huang J.X., Zhang A.W., Jiang Z.Y., Tieu A.K., Shi X., Jiao S.H., Qu X.Y. Study on the oxidation of stainless steels 304 and 304L in humid air and the friction during hot rolling. *Wear*. 2009;267(9-10):1741–1745. https://doi.org/10.1016/j.wear.2008.11.030

5. Gribkov A.A., Brodov A.A. Present and future of Russian market of stainless steel. *Ferrous Metallurgy. Bulletin of Scientific, Technical and Economic Information*. 2021;77(2):193–199. (In Russ.). https://doi.org/10.32339/0135-5910-2021-2-193-199

   Грибков А.А., Бродов А.А. Настоящее и будущее рынка нержавеющей стали России. *Черная металлургия. Бюллетень научно-технической и экономической информации*. 2021;77(2):193–199. https://doi.org/10.32339/0135-5910-2021-2-193-199

6. Tokovoi O.K. Argon-Oxygen Decarburization of Stainless Steel: Monograph. Chelyabinsk: SUSU; 2015:250. (In Russ.).

   Токовой О.К. Аргонокислородное рафинирование нержавеющей стали: Монография. Челябинск: Издательский центр ЮУрГУ; 2015:250.

7. Cai J., Li J. Decarburization and chromium conservation model in AOD refining process of 304 stainless steel. In: *12th Int. Symp. on High-Temperature Metallurgical Processing. The Minerals, Metals & Materials Series*. Springer: Cham; 2022:71-80. https://doi.org/10.1007/978-3-030-92388-4_7

8. Povolotskii D.Ya., Gudim Yu.A. Production of Stainless Steel. Chelyabinsk: SUSU; 1988:236. (In Russ.).

   Поволоцкий Д.Я., Гудим Ю.А. Производство нержавеющей стали. Челябинск: Издательство ЮУрГУ; 1988:236.

9. Kornievskii V.N., Panchenko A.I., Logozinskii I.N., etc. Development of technology for ladle-furnace processing of electric steel using pegmatite as a substitute for fluorspar. *Sovremennaya elektrometallurgiya*. 2015;(4):38–46. (In Russ.).

   Корниевский В.Н., Панченко А.И., Логозинский И.Н. и др. Разработка технологии внепечной обработки элект-

ростали с применением пегматита как заменителя плавикового шпата. *Современная электрометаллургия*. 2015;(4):38–46.

10. Morii L., Kumura Sh., Mori H., Shinkai M., Sakuma H. Development of new refining process for manufacture of stainless steel. *DENKI-SEIKO*. 1993;64(1):4–12. https://doi.org/10.4262/denkiseiko.64.4

11. Hongming W., Tingwang Z., Hua Z. Effect of B_2O_3 on melting temperature, viscosity and desulfurization capacity of CaO-based refining flux. *ISIJ International*. 2011;51(5): 702–708. http://dx.doi.org/10.2355/isijinternational.51.702

12. Forsbacka L. Experimental study and modelling of viscosity of chromium containing slags: Dr. Tech. Sci. Diss, Helsinki; 2007:88.

13. Wu T., Zhang Y., Yuan F., An Z. Effects of the Cr_2O_3 content on the viscosity of CaO-SiO_2-10 Pct Al_2O_3-Cr_2O_3 quaternary slag. *Metallurgical and Materials Transactions B*. 2018;49:1719–1731. https://doi.org/10.1007/s11663-018-1258-z

14. Akberdin A.A., Kireeva G.M., Kim A.S. Physical properties of boron-containing blast furnace slags. *Kompleksnoe ispol'zovanie mineral'nogo syr'ya*. 1996;(3):27–31. (In Russ.).

Акбердин А.А., Киреева Г.М., Ким А.С. Физические свойства борсодержащих доменных шлаков. *Комплексное использование минерального сырья*. 1996;(3):27–31.

15. Babenko A.A., Zhuchkov V.I., Upolovnikova A.G., Kel' I.N. Study of the viscosity of slags of CaO – SiO_2 – B_2O_3 – 25 % Al_2O_3 – 8 % MgO system. *Izvestiya. Ferrous Metallurgy*. 2017;60(10):820–825. (In Russ.). https://doi.org/10.17073/0368-0797-2017-10-820-825

Бабенко А.А., Жучков В.И., Уполовникова А.Г., Кель И.Н. Изучение вязкости шлаков системы CaO – SiO_2 – B_2O_3 – 25 % Al_2O_3 – 8 % MgO. *Известия вузов. Черная металлургия*. 2017;60(10):820–825. https://doi.org/10.17073/0368-0797-2017-10-820-825

16. Mills K.C., Yuan L., Li Z., Zhang G.H., Chou K.C. A review of the factors affecting the thermophysical properties of silicate slags. *High Temperature Materials and Processes*. 2012;31(4–5):301–321. https://doi.org/10.1515/htmp-2012-0097

17. Nazyuta L.Yu., Tikhonyuk L.S., Kostyrya I.N., etc. Features of microalloying with boron in the smelting of low-alloy structural steels. *Metall i lit'e Ukrainy*. 2018;298–299(3–4): 18–27. (In Russ.).

Назюта Л.Ю., Тихонюк Л.С., Костыря И.Н. и др. Особенности микролегирования бором при выплавке низколегированных конструкционных сталей. *Металл и литье Украины*. 2018;298–299(3–4):18–27.

18. Kim V.A., Nikolai EH.N., Akberdin A.A., etc. Planning an Experiment when Studying the Physical and Chemical Properties of Metallurgical Slags: A Methodological Manual. Alma-Ata: Nauka; 1989:116. (In Russ.).

Ким В.А., Николай Э.Н., Акбердин А.А. и др. Планирование эксперимента при исследовании физико-химических свойств металлургических шлаков: Методическое пособие. Алма-Ата: Наука; 1989:116.

19. Boronenkov V.N., Zinigrad M.I., Leont'ev L.I., etc. Modeling of the Structure, Properties and Processes of Interphase Interaction in the Metal-Oxide Melt-Gas System. Yekaterinburg: UB RAS; 2010:452. (In Russ.).

Бороненков В.Н., Зиниград М.И., Леонтьев Л.И. и др. Моделирование структуры, свойств и процессов межфазного взаимодействия в системе металл-оксидный расплав-газ. Екатеринбург: УрО РАН; 2010:452.

Information about the Authors / Сведения об авторах

Anatoly A. Babenko, *Dr. Sci. (Eng.), Prof., Chief Researcher, Head of the Department of Ferrous Metallurgy,* Institute of Metallurgy, Ural Branch of the Russian Academy of Sciences
ORCID: 0000-0003-0734-6162
E-mail: babenko251@gmail.com

Vladimir I. Zhuchkov, *Dr. Sci. (Eng.), Prof., Chief Researcher of the Laboratory of Steel and Ferroalloys,* Institute of Metallurgy, Ural Branch of the Russian Academy of Science
E-mail: ntm2000@mail.ru

Il'ya N. Kel', *Cand. Sci. (Eng.), Senior Researcher of the Laboratory of Steel and Ferroalloys,* Institute of Metallurgy, Ural Branch of the Russian Academy of Sciences
ORCID: 0000-0001-6411-6932
E-mail: dunnington@mail.ru

Alena G. Upolovnikova, *Cand. Sci. (Eng.), Senior Researcher of the Laboratory of Steel and Ferroalloys,* Institute of Metallurgy, Ural Branch of the Russian Academy of Sciences
ORCID: 0000-0002-6698-5565
E-mail: upol.ru@mail.ru

Ruslan R. Shartdinov, *Junior Researcher of the Laboratory of Steel and Ferroalloys,* Institute of Metallurgy, Ural Branch of the Russian Academy of Sciences
ORCID: 0000-0003-0852-1161
E-mail: rr.shartdinov@gmail.com

Анатолий Алексеевич Бабенко, *д.т.н., профессор, главный научный сотрудник, руководитель отдела черной металлургии,* Институт металлургии Уральского отделения РАН
ORCID: 0000-0003-0734-6162
E-mail: babenko251@gmail.com

Владимир Иванович Жучков, *д.т.н., профессор, главный научный сотрудник лаборатории стали и ферросплавов,* Институт металлургии Уральского отделения РАН
E-mail: ntm2000@mail.ru

Илья Николаевич Кель, *к.т.н., старший научный сотрудник лаборатории стали и ферросплавов,* Институт металлургии Уральского отделения РАН
ORCID: 0000-0001-6411-6932
E-mail: dunnington@mail.ru

Алена Геннадьевна Уполовникова, *к.т.н., старший научный сотрудник лаборатории стали и ферросплавов,* Институт металлургии Уральского отделения РАН
ORCID: 0000-0002-6698-5565
E-mail: upol.ru@mail.ru

Руслан Рафикович Шартдинов, *младший научный сотрудник лаборатории стали и ферросплавов,* Институт металлургии Уральского отделения РАН
ORCID: 0000-0003-0852-1161
E-mail: rr.shartdinov@gmail.com

Contribution of the Authors

A. A. Babenko – development and proposal of an experiment planning matrix, discussion and analysis of results, editing the text.

V. I. Zhuchkov – discussion and analysis of results, editing the text.

I. N. Kel' – thermodynamic modeling, writing the text.

A. G. Upolovnikova – data visualization, editing the text.

R. R. Shartdinov – writing the text, preparing the samples for *X*-ray phase analysis.

Вклад авторов

А. А. Бабенко – разработка и предложение матрицы планирования эксперимента, обсуждение и анализ полученных данных, редактирование текста.

В. И. Жучков – обсуждение и анализ полученных данных, редактирование текста.

И. Н. Кель – проведение термодинамического моделирования, написание текста.

А. Г. Уполовникова – визуализация данных, редактирование текста.

Р. Р. Шартдинов – написание текста, подготовка проб для рентгенофазового анализа.

Received 25.10.2023
Revised 31.10.2023
Accepted 28.03.2024

Поступила в редакцию 25.10.2023
После доработки 31.10.2023
Принята к публикации 28.03.2024

PHYSICO-CHEMICAL BASICS OF METALLURGICAL PROCESSES / **ФИЗИКО-ХИМИЧЕСКИЕ ОСНОВЫ МЕТАЛЛУРГИЧЕСКИХ ПРОЦЕССОВ**

UDC 621.785.532:536.46
DOI 10.17073/0368-0797-2024-3-360-365

Original article
Оригинальная статья

PHYSICAL AND CHEMICAL PROCESSES DURING NITRIDING OF CHROMIUM FERROSILICON BY FILTRATION COMBUSTION

K. A. Bolgaru[1], A. A. Reger[1] ✉, V. I. Vereshchagin[2], A. A. Akulinkin[1]

[1] **Tomsk Scientific Center of the Siberian Branch of the Russian Academy of Sciences** (10/4 Akademicheskii Ave., Tomsk 634055, Russian Federation)
[2] **National Research Tomsk Polytechnic University** (30 Lenina Ave., Tomsk 634050, Russian Federation)

✉ regerwork1@gmail.com

Abstract. In this paper, the nitriding of chromium ferrosilicon is carried out in the combustion mode under the condition of natural nitrogen filtration. The authors studied the effect of the key parameters (pressure of gaseous nitrogen, diameter and dispersity of starting samples) on the maximum temperature and combustion of the starting powder mixture based on chromium ferrosilicon. The combustion synthesis of chromium ferrosilicon proceeds steadily in the stationary mode with formation of a macrohomogeneous nitrided composition which, according to the results of *X*-ray phase analysis, contains two nitride phases - chromium nitride and silicon nitride. Interaction of the initial powder with gaseous nitrogen in the filtration combustion mode proceeds by the following probable chemical reaction: $3CrSi_2 + 3Si + 3FeSi_2 + 11.5N_2 = 3CrN + 5Si_3N_4 + 3Fe$. Increasing the diameter of the starting samples slightly affects the amount of absorbed nitrogen and slows the propagation of the combustion wave front. An increase in the pressure of gaseous nitrogen increases the amount of absorbed nitrogen and the combustion rate. Increasing the dispersity of the starting powder increases the amount of absorbed nitrogen and the combustion rate. It was found that the combustion reaction is not possible with a dense initial sample. The maximum combustion temperature, depending on the nitriding conditions, varies between 2400 and 2650 °C and increases with increasing gaseous nitrogen pressure, diameter of the initial samples and dispersion of chromium ferrosilicon powder. It is possible to realise nitriding of chrome ferrosilicon in the combustion mode at the pressure of gaseous nitrogen not less than 3 MPa, diameter of initial samples not less than 3.5 cm and size of initial particles not more than 100 μm. Optimal parameters of nitriding are gaseous nitrogen pressure of 5 MPa, diameter of samples 5 cm, size of initial particles less than 100 μm and bulk density of samples (2.23 g/cm^3).

Keywords: self-propagating high-temperature synthesis, combustion synthesis, nitriding, nitrides, ferroalloy, powder metallurgy

For citation: Bolgaru K.A., Reger A.A., Vereshchagin V.I., Akulinkin A.A. Physical and chemical processes during nitriding of chromium ferrosilicon by filtration combustion. *Izvestiya. Ferrous Metallurgy*. 2024;67(3):360–365. https://doi.org/10.17073/0368-0797-2024-3-360-365

ФИЗИКО-ХИМИЧЕСКИЕ ПРОЦЕССЫ АЗОТИРОВАНИЯ ФЕРРОСИЛИКОХРОМА В РЕЖИМЕ ФИЛЬТРАЦИОННОГО ГОРЕНИЯ

К. А. Болгару[1], А. А. Регер[1] ✉, В. И. Верещагин[2], А. А. Акулинкин[1]

[1] **Томский научный центр Сибирского отделения РАН** (Россия, 634055, Томск, Академический пр., 10/4)
[2] **Национальный исследовательский Томский политехнический университет** (Россия, 634050, Томск, пр. Ленина, 30)

✉ regerwork1@gmail.com

Аннотация. В работе изучены процессы азотирования ферросиликохрома в режиме горения в условиях естественной фильтрации азота и представлены результаты исследования влияния основных параметров синтеза (давление газообразного азота, диаметр образцов и размер исходных частиц) на максимальную температуру и процесс горения исходной порошковой шихты. Горение ферросиликохрома протекает устойчиво в стационарном режиме с образованием макрооднородной азотированной композиции, которая по результатам рентгенофазового анализа содержит в своём составе две нитридные фазы – нитрид хрома и нитрид кремния. Взаимодействие исходного порошка с газообразным азотом в режиме фильтрационного горения протекает по следующей вероятной химической реакции: $3CrSi_2 + 3Si + 3FeSi_2 + 11,5N_2 = 3CrN + 5Si_3N_4 + 3Fe$. Увеличение диаметра исходных образцов незначительно влияет на количество поглощеного азота и приводит к замедлению продвижения фронта волны горения. При повышении давления газообразного реагента наблюдается увеличение количества поглощенного азота и скорости горения. Более тонкое измельчение исходного порошка позволяет увеличить количество поглощенного азота и скорость горения. Определено, что при уплотнении исходного образца реализовать реакцию горения невозможно. Максимальная температура горения в зависимости от условий азотирования изменяется в пределах от 2400 до 2650 °C и повышается при увеличении давления газообразного азота, диаметра исходных образцов и дисперсности порошка ферросиликохрома. Реализовать азоти-

рование ферросиликохрома в режиме горения возможно при давлении газообразного азота не менее 3 МПа, диаметре исходных образцов не менее 3,5 см и размере исходных частиц не более 100 мкм. Оптимальными параметрами азотирования ферросиликохрома является давление газообразного азота 5 МПа, диаметр образцов 5 см, размер исходных частиц менее 100 мкм и насыпная плотность порошка 2,23 г/см^3.

Ключевые слова: самораспространяющийся высокотемпературный синтез, фильтрационное горение, азотирование, нитриды, ферросплав, порошковая металлургия

Для цитирования: Болгару К.А., Регер А.А., Верещагин В.И., Акулинкин А.А. Физико-химические процессы азотирования ферросиликохрома в режиме фильтрационного горения. *Известия вузов. Черная металлургия*. 2024;67(3):360–365.
https://doi.org/10.17073/0368-0797-2024-3-360-365

Introduction

The method of self-propagating high-temperature synthesis (SHS) is based on highly exothermic reactions that occur in the form of a combustion wave in a self-propagating mode. The SHS method has undeniable advantages: energy efficiency, short synthesis time, environmental friendliness, and simplicity of equipment [1 – 3].

Currently, a large number of materials, particularly nitrides, have been obtained by the filtration SHS method in a nitrogen environment [4 – 6]. Several nitride materials possess unique physicochemical properties [7 – 9]. They can be used in the production of gas turbine components [10], heat-dissipating radiators [11], cutting tools [12; 13], photocatalysts [14], semiconductors [15], and so on.

The most promising application in the filtration SHS method is the use of accessible and relatively inexpensive ferroalloys. Using ferroalloys in SHS processes can produce nitride material at a relatively low cost without losing product quality [16; 17]. Iron, which is part of the ferroalloys, has a catalytic effect on the nitriding process of other elements included in the initial mixture [18]. Thus, iron increases the intensity and depth of nitriding of the initial material. There is a considerable amount of work dedicated to the filtration combustion of simple ferroalloys. The patterns of nitriding of ferrosilicon [19 – 21], as well as the filtration combustion of ferrochrome and ferrovanadium [22], have been thoroughly studied. The study [23] investigated the combustion of industrial ferrotitanium in nitrogen. The monograph [24] described the nitriding of ferroboron and ferroniobium in a combustion mode.

However, the use of complex ferroalloys in filtration combustion processes is interesting and little studied. Complex ferroalloys are alloys of iron with two or more elements. At present, SHS combustion of ferro-silicoaluminium [25] and ferro-aluminum-silicon-zirconium [2] has been studied.

The aim of this work was to study the combustion processes of chromium ferrosilicon in a self-propagating mode under conditions of natural nitrogen filtration to obtain a nitride-containing composite material based on chromium nitride and silicon nitride.

Materials and methods

Chromium ferrosilicon (CFS) was used as the starting material. *X*-ray phase analysis showed that this ferroalloy is multiphase and contains $CrSi_2$, Si, and $FeSi_2$ (Fig. 1). According to the chemical analysis, the composition of CFS is as follows (wt. %): 49.4 Si, 29.7 Cr, 20.7 Fe, and the rest are oxides. For nitriding in the self-propagating mode, the initial CFS was ground in a ball mill and dried in a vacuum drying oven at a temperature of 150 °C for 3 h.

Nitriding of the initial CFS was carried out in a constant pressure setup with a volume of 3 liters. For the synthesis, the initial powder mixture was placed in a gas-permeable container mounted on a non-conductive stand. An igniting composition was poured over the initial charge. A coil was connected to the igniting composition to conduct an electric pulse from a transformer. After the electric pulse was applied, the combustion reaction of the igniting composition was initiated. Then, the heat released as a result of the combustion of the igniting composition initiated the combustion reaction of the initial CFS powder. After the combustion wave front passed and complete cooling occurred, the unreacted nitrogen was vented, and the nitrided samples were removed for further physicochemical studies.

The phase composition was studied using a Shimadzu XRD-6000 diffractometer. The oxygen and nitrogen contents were determined using a LEKO-ONH 836 instrument. The maximum combustion temperature was measured using the thermocouple method with tungsten-rhenium thermocouples (WRe5-WRe20) on an LA20USB.

Results and discussion

Combustion of chromium ferrosilicon proceeds in a stationary mode. The nitrided samples obtained based

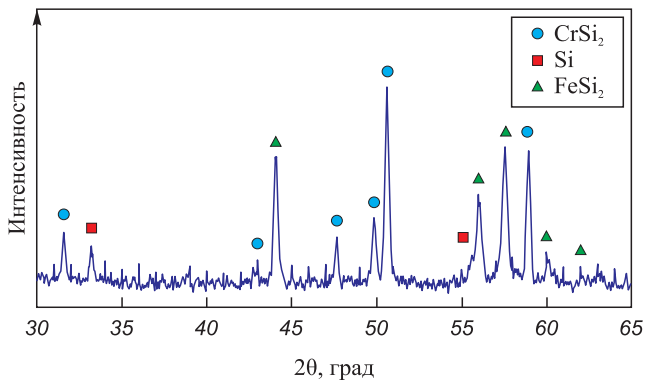

Fig. 1. *X*-ray diffraction pattern of chromium ferrosilicon

Рис. 1. Рентгеновская дифрактограмма ферросиликохрома

on CFS are macrohomogeneous. An image of the nitrided CFS is shown in Fig. 2.

The probable chemical reactions of the interaction of the initial charge based on CFS with nitrogen are given below:

$$3CrSi_2 + 5.5N_2 = 3CrN + 2Si_3N_4; \quad (1)$$

$$3Si + 2N_2 = Si_3N_4; \quad (2)$$

$$3FeSi_2 + 4N_2 = 2Si_3N_4 + 3Fe. \quad (3)$$

The overall chemical reaction equation is as follows:

$$3CrSi_2 + 3Si + 3FeSi_2 + 11.5N_2 = \\ = 3CrN + 5Si_3N_4 + 3Fe. \quad (4)$$

Reaction (4) corresponds to the complete nitriding of the initial CFS (with a conversion degree of 1). Due to the rapid processes of SHS, the initial charge is in the reaction zone for a relatively short time and does not fully react with nitrogen. It is theoretically calculated that the maximum amount of absorbed nitrogen by chromium ferrosilicon is 28.99 %.

The nitrided CFS product is a multiphase material containing β-Si_3N_4, α-Fe, CrN, Cr and $CrSi_2$. The presence of Cr and $CrSi_2$ indicates the incomplete nitriding reaction of the initial powder (Fig. 3).

Parameters such as the pressure of the gaseous reactant, sample diameter, particle size, and density of the initial material significantly influence the maximum temperature, process, and feasibility of filtration combustion in a self-propagating mode.

Fig. 2. Sample of nitrided chromium ferrosilicon

Рис. 2. Образец азотированного ферросиликохрома

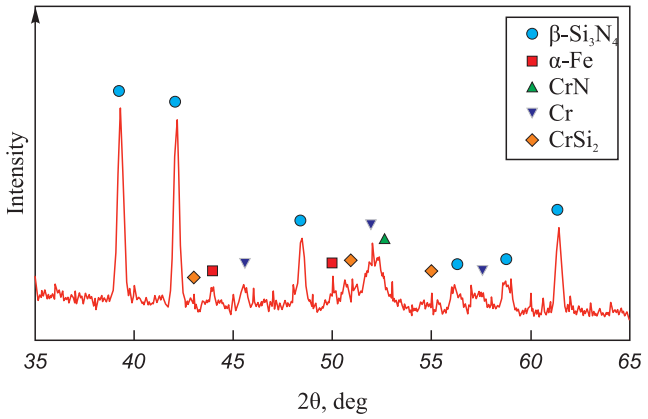

Fig. 3. *X*-ray diffraction pattern of nitrided chromium ferrosilicon

Рис. 3. Рентгеновская дифрактограмма азотированного ферросиликохрома

Fig. 4 shows the dependence of the amount of absorbed nitrogen and the combustion rate on the diameter of the initial samples. The influence of the diameter was studied in the range of 35 to 65 mm. Combustion of CFS can be initiated with initial sample diameters of at least 35 mm. Increasing the diameter slightly affects the amount of absorbed nitrogen and leads to a decrease in the combustion rate from 0.11 to 0.021 mm/s. This slight change in the amount of absorbed nitrogen is due to the increased difficulty of nitrogen filtration reaching the reaction zone as the diameter increases. At the same time, due to the slowdown in the combustion wave front, the residence time of the initial CFS particles in the reaction zone increases. The slowdown of the combustion wave front is related to the increased volume of the powder mixture, which

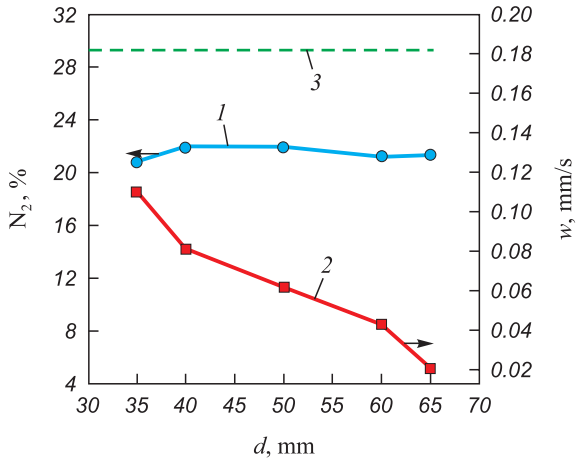

Fig. 4. Dependence of the content of absorbed nitrogen (*1*) and combustion rate (*2*) on diameter of the starting samples (*3* – theoretically calculated maximum amount of absorbed nitrogen) at P = 5 MPa, D > 100 μm and ρ = 2.23 g/cm^3

Рис. 4. Зависимость количества поглощенного азота (*1*) и скорости горения (*2*) от диаметра образцов (*3* – теоретически рассчитанное максимальное количество поглощенного азота) при P = 5 МПа, D > 100 мкм и ρ = 2,23 г/см^3

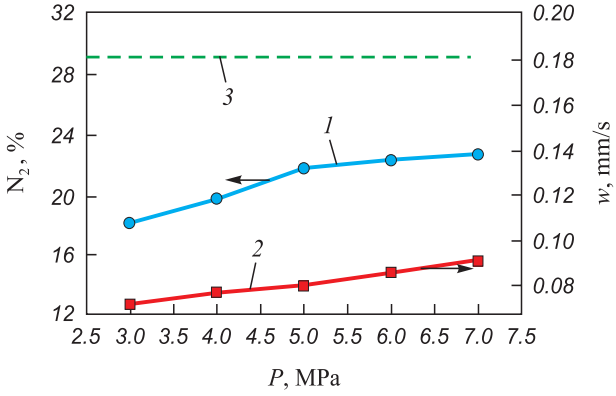

Fig. 5. Dependence of the content of absorbed nitrogen (*1*) and combustion rate (*2*) on pressure of gaseous nitrogen (*3* – theoretically calculated maximum amount of absorbed nitrogen) at d = 50 mm, ρ = 2.23 g/cm^3 and D > 100 μm

Рис. 5. Зависимость количества поглощенного азота (*1*) и скорости горения (*2*) ферросиликохрома от давления газообразного азота (*3* – теоретически рассчитанное максимальное количество поглощенного азота) при d = 50 мм, ρ = 2,23 г/см^3 и D > 100 мкм

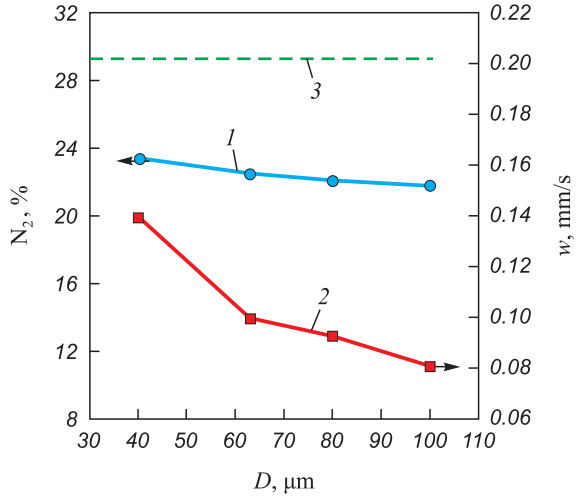

Fig. 6. Dependence of the content of absorbed nitrogen (*1*) and combustion rate (*2*) on dispersity of the starting powder (*3* – theoretically calculated maximum amount of absorbed nitrogen) at d = 50 mm, P = 5 MPa and ρ = 2.23 g/cm^3

Рис. 6. Зависимость количества поглощенного азота (*1*) и скорости горения (*2*) от дисперсности порошка ферросиликохрома (*3* – теоретически рассчитанное максимальное количество поглощенного азота) при d = 50, P = 5 МПа и ρ = 2,23 г/см^3

requires a large amount of heat for heating. When changing the diameter, the maximum amount of absorbed nitrogen was about 22 %, which is 6.99 % less than the theoretically calculated amount of nitrogen absorption. As the diameter of the initial powder mixture increases, the maximum combustion temperature of CFS changes from 2400 to 2650 °C.

In a laboratory setup with a volume of 3 liters, it is preferable to implement combustion of samples with a diameter of 50 mm.

Increasing the pressure accelerates the filtration of gaseous nitrogen and, accordingly, increases the concentration of the reagent gas in the chemical reaction zone. Combustion of CFS at a nitrogen pressure of less than 3 MPa could not be achieved. Increasing the pressure of gaseous nitrogen leads to an increase in the amount of absorbed nitrogen from 18.3 to 22.8 % and the combustion rate from 0.073 to 0.092 mm/s. In the nitrogen pressure range from 5 to 7 MPa, the change in the amount of absorbed nitrogen becomes less pronounced. Increasing the nitrogen pressure above 7 MPa is not advisable because, at 5 MPa, the influence of pressure on the combustion process becomes insignificant (Fig. 5). When implementing CFS combustion at a pressure of 7 MPa, the sample contains 6.29 % less nitrogen than the theoretically calculated value. As the pressure of gaseous nitrogen increases from 3 to 7 MPa, the maximum combustion temperature rises from 2350 to 2600 °C.

Combustion of CFS with particle sizes greater than 100 μm and without fine fractions (less than 63 μm) could not be achieved. As the particle size of the initial material decreases, the amount of absorbed nitrogen increases from 21.9 to 23.5 % and the combustion rate from 0.081 to 0.140 mm/s. The increase in the dispersity of the initial material leads to an increase in the specific surface area capable of reacting (Fig. 6). The reduction in particle size of CFS results in an increase in the maximum temperature from 2400 to 2490 °C.

The increase in the density of the initial powder mixture was achieved by pressing the initial powder into tablets with a diameter and height of 40 mm in molds. Combustion of the pressed powder, which retains the shape of the tablet (ρ = 2.52 g/cm^3), could not be achieved. Therefore, only samples with a bulk density (2.23 g/cm^3) were used.

Conclusions

The combustion of chromium ferrosilicon proceeds in a stationary mode, resulting in homogeneous nitrided samples without melt droplets or cracks.

Increasing the diameter leads to a decrease in the combustion rate from 0.11 to 0.021 mm/s and slightly affects the amount of absorbed nitrogen. Increasing the nitrogen pressure results in an increase in the amount of absorbed nitrogen (18.3 – 22.8 %) and the combustion rate (0.073 – 0.092 mm/s) of chromium ferrosilicon. Reducing the dispersity of the initial material allows for an increase in the amount of absorbed nitrogen from 21.9 to 23.5 % and the combustion rate from 0.081 to 0.140 mm/s. A slight increase in the density of the initial powder prevents achieving the combustion reaction of chromium ferrosilicon in a nitrogen environment.

The maximum combustion temperature increases with a rise in gaseous nitrogen pressure from 3 to 7 MPa (from 2350 to 2600 °C), the diameter of the initial samples from

35 to 65 mm (from 2400 to 2650 °C), and a decrease in the particle size of the initial charge from less than 100 to less than 40 μm (from 2400 to 2490 °C).

Stable combustion in the self-propagating mode of chromium ferrosilicon powder samples is possible at a nitrogen pressure of at least 3 MPa, a sample diameter of at least 3.5 cm, a particle size of less than 100 μm with the presence of fine fractions (less than 63 μm), and a sample density not exceeding 2.23 g/cm^3. It is optimal to carry out nitriding of the initial chromium ferrosilicon under conditions of natural nitrogen filtration at a pressure of 5 MPa, a sample diameter of 5 cm, a particle size of the initial material less than 100 μm, and a bulk sample density of 2.23 g/cm^3.

The product of chromium ferrosilicon nitriding contains β-Si_3N_4, CrN, α-Fe, Cr and $CrSi_2$. The presence Cr and $CrSi_2$ indicates the incomplete nitriding reaction of the initial chromium ferrosilicon. The nitrogen saturation is 21.9 %, which is 7.09 % less than the theoretically calculated maximum amount of absorbed nitrogen.

References / Список литературы

1. Chukhlomina L.N., Vitushkina O.G. SHS nitriding of ferrosilicon with ilmenite. *ChemChemTech*. 2011;54(5):105–108. (In Russ.).

   Чухломина Л.Н., Витушкина О.Г. СВС-азотирование ферросилиция в присутствии ильменита. *Известия вузов. Серия: Химия и химическая технология*. 2011;54(5):105–108.
2. Bolgaru K.A., Vereshchagin V.I., Reger A.A. Synthesis of composite of silicon nitride, aluminium nitride, zirconium nitride from complex ferroalloy – ferro-aluminium-silicon-zirconium by nitriding in combustion mode. *ChemChemTech*. 2021;64(7):68–74. (In Russ.). https://doi.org/10.6060/ivkkt.20216407.6362

   Болгару К.А., Верещагин В.И., Регер А.А. Синтез композиции нитридов кремния, алюминия и циркония азотированием в режиме горения сложного ферросплава – ферроалюмосиликоциркония. *Известия вузов. Серия: Химия и химическая технология*. 2021;64(7):68–74. https://doi.org/10.6060/ivkkt.20216407.6362
3. Amosov A.P., Borovinskaya I.P., Merzhanov A.G. Powder Technology of Self-Propagating High-Temperature Synthesis of Materials. Moscow: Mashinostroenie. 2007:567.

   Амосов А.П., Боровинская И.П., Мержанов А.Г. Порошковая технология самораспространяющегося высокотемпературного синтеза материалов. Москва: Машиностроение; 2007:567.
4. Won H.I., Won C.W., Nersisyan H.H., Yoon K.S. Salt-assisted combustion synthesis of silicon nitride with high α-phase content. *Journal of Alloys and Compounds*. 2010;496(1-2):656–659. https://doi.org/10.1016/j.jallcom.2010.02.157
5. Yeh C.L., Liu E.W. Combustion synthesis of chromium nitrides by SHS of Cr powder compacts under nitrogen pressures. *Journal of Alloys and Compounds*. 2006;426(1-2):131–135. https://doi.org/10.1016/j.jallcom.2006.01.082
6. Yeh C.L., Chuang H.C. Experimental studies on self-propagating combustion synthesis of niobium nitride. *Ceramics International*. 2004;30(5):733–743. https://doi.org/10.1016/j.ceramint.2003.10.001
7. Zhang J., Ge Y., Tian Z., Sun S., Cui W., Liu G., Chen K. Combustion synthesis of α-Si_3N_4 with green additives. *Ceramics International*. 2019;45(5):6594–6596. https://doi.org/10.1016/j.ceramint.2018.12.147
8. Zhang Y., He X., Han J., Du S. Combustion synthesis of hexagonal boron–nitride-based ceramics. *Journal of Materials Processing Technology*. 2001;116(2-3):161–164. https://doi.org/10.1016/S0924-0136(01)01023-8
9. Chen Y.X., Li J.T., Du J.S. Cost effective combustion synthesis of silicon nitride. *Materials Research Bulletin*. 2008;43(6):1598–1606. https://doi.org/10.1016/j.materresbull.2007.06.051
10. Won H.I., Won C.W., Nersisyan H.H., Yoon K.S. Salt-assisted combustion synthesis of silicon nitride with high α-phase content. *Journal of Alloys and Compounds*. 2010;496(1–2):656–659. https://doi.org/10.1016/j.jallcom.2010.02.157
11. Juang R.C., Chen C.C. Combustion synthesis of hexagonal aluminum nitride crystal by aluminum carbides. *Materials Science and Engineering: A*. 2007;458(1–2):210–215. https://doi.org/10.1016/j.msea.2007.01.004
12. Fang S. Morphological study of a cubic boron nitride (CBN) cutting tool and characterization of its wear scenarios in abrasive machining process. *Ceramics International*. 2020;46(11B):19491–19498. https://doi.org/10.1016/j.ceramint.2020.04.302
13. Sugihara T., Nishimoto Y., Enomoto T. Development of a novel cubic boron nitride cutting tool with a textured flank face for high-speed machining of Inconel 718. *Precision Engineering*. 2017;48:75–82. https://doi.org/10.1016/j.precisioneng.2016.11.007
14. Akulinkin A., Bolgaru K., Reger A. Facile synthesis of porous g-C_3N_4/β-SiAlON material with visible light photocatalytic activity. *Materials Letters*. 2021;305:130788. https://doi.org/10.1016/j.matlet.2021.130788
15. Hua Q., Ma B., Hu W. Aluminum, gallium, and indium nitrides. *Encyclopedia of Materials: Technical Ceramics and Glasses*. 2021;3:74–83. https://doi.org/10.1016/B978-0-12-803581-8.12065-X
16. Ziatdinov M.Kh. From the history of nitrided ferroalloys. *Izvestiya. Ferrous Metallurgy*. 2020;63(10):773–781. (In Russ.). https://doi.org/10.17073/0368-0797-2020-10-773-781

    Зиатдинов М.Х. Из истории азотированных ферросплавов. *Известия вузов. Черная металлургия*. 2020;63(10):773–781. https://doi.org/10.17073/0368-0797-2020-10-773-781
17. Manashev I.R., Gavrilova T.O., Shatokhin I.M., Ziatdinov M.Kh., Leont'ev L.I. Utilization of dispersed waste of ferroalloy production on the basis of metallurgical SHS-process. *Izvestiya. Ferrous Metallurgy*. 2020;63(8):591–599. (In Russ.). https://doi.org/10.17073/0368-0797-2020-8-591-599

    Манашев И.Р., Гаврилова Т.О., Шатохин И.М., Зиатдинов М.Х., Леонтьев Л.И. Утилизация дисперсных отходов ферросплавного производства на базе металлургического СВС-процесса. *Известия вузов. Черная металлургия*. 2020;63(8):591–599. https://doi.org/10.17073/0368-0797-2020-8-591-599

18. Zhang M., Chen Z., Huang J., Wang S., Xiong Q., Feng Z., Liu Q., Sun Z., Li X. In situ nitriding reaction formation of β-Sialon with fibers using transition metal catalysts. *Ceramics International*. 2019;45(17A):21923–21930. https://doi.org/10.1016/j.ceramint.2019.07.204

19. Chukhlomina L.N., Maksimov Yu.M., Kitler V.D., Vitushkina O.G. Mechanism and features of nitriding of ferrosilicon in the combustion regime. *Combustion, Explosion, Shock Waves*. 2006;42(3):309–316. https://doi.org/10.1007/s10573-006-0056-0

20. Ma C., Li Y., Chen J., Zhu S., Li B. Cost-effective manufacture and synthesis mechanism of ferrosilicon nitride porous ceramic with interlocking structure. *Ceramics International*. 2021;47(4):5265–5272. https://doi.org/10.1016/j.ceramint.2020.10.107

21. Ziatdinov M.Kh., Shatokhin I.M. Self-propagating high-temperature synthesis of ferrosilicon nitride. *Steel in Translation*. 2008;38(1):39–44. https://doi.org/10.3103/S0967091208010130

22. Ziatdinov M.Kh., Shatokhin I.M., Leont'ev L.I. SHS technology of composition ferroalloys. Part I. Metallurgical SHS process. Synthesis of ferrovanadium and ferrochromium nitrides. *Izvestiya. Ferrous Metallurgy*. 2018;61(5):339–347. (In Russ.). https://doi.org/10.17073/0368-0797-2018-5-339-347

Зиатдинов М.Х., Шатохин И.М., Леонтьев Л.И. Технология СВС композиционных ферросплавов часть 1. Металлургический СВС процесс. Синтез нитридов феррованадия и феррохрома. *Известия вузов. Черная металлургия*. 2018;61(5):339–347. https://doi.org/10.17073/0368-0797-2018-5-339-347

23. Glazunov A.A., Maksimov Yu.M., Chukhlomina L.N., Braverman B.Sh., Avramchik A. N. Combustion of ferrotitanium in nitrogen. *Combustion, Explosion, and Shock Waves*. 2020;56(2):137–141. https://doi.org/10.1134/S0010508220020033

24. Chukhlomina L.N., Maksimov Yu.M., Vereshchagin V.I. Self-Propagating High–Temperature Synthesis of Composites Nitride-Based Materials. Novosibirsk: Nayka; 2012:260. (In Russ.).

Чухломина Л.Н., Максимов Ю.М., Верещагин В.И. Самораспространяющейся высокотемпературный синтез композиционных нитридсодержащих керамических материалов. Новосибирск: Наука; 2012:260.

25. Bolgaru K., Reger A., Vereshchagin V., Akulinkin A. Combustion synthesis of porous ceramic β-Si_3N_4-based composites with the use of ferroalloys. *Ceramics International*. 2021;47(24):34765–4773. https://doi.org/10.1016/j.ceramint.2021.09.015

Information about the Authors / Сведения об авторах

Konstantin A. Bolgaru, *Cand. Sci. (Eng.), Senior Researcher,* Tomsk Scientific Center of the Siberian Branch of the Russian Academy of Sciences
ORCID: 0000-0001-6772-8192
E-mail: kbolgaru2008@yandex.ru

Константин Александрович Болгару, *к.т.н., старший научный сотрудник,* Томский научный центр Сибирского отделения РАН
ORCID: 0000-0001-6772-8192
E-mail: kbolgaru2008@yandex.ru

Anton A. Reger, *Junior Researcher,* Tomsk Scientific Center of the Siberian Branch of the Russian Academy of Sciences
ORCID: 0000-0001-5269-8576
E-mail: regerwork1@gmail.com

Антон Андреевич Регер, *младший научный сотрудник,* Томский научный центр Сибирского отделения РАН
ORCID: 0000-0001-5269-8576
E-mail: regerwork1@gmail.com

Vladimir I. Vereshchagin, *Dr. Sci. (Eng.), Prof.,* National Research Tomsk Polytechnic University
E-mail: vver@tpu.ru

Владимир Иванович Верещагин, *д.т.н., профессор,* Национальный исследовательский Томский политехнический университет
E-mail: vver@tpu.ru

Aleksandr A. Akulinkin, *Junior Researcher,* Tomsk Scientific Center of the Siberian Branch of the Russian Academy of Sciences
ORCID: 0000-0002-7020-969X
E-mail: akulinkinalex@gmail.com

Александр Александрович Акулинкин, *младший научный сотрудник,* Томский научный центр Сибирского отделения РАН
ORCID: 0000-0002-7020-969X
E-mail: akulinkinalex@gmail.com

Contribution of the Authors / Вклад авторов

K. A. Bolgaru – scientific guidance, formation of goals and objectives, writing and revision of the text, correction of conclusions.
A. A. Reger – writing the text, conducting synthesis, analysis of the obtained data, visualization.
V. I. Vereshchagin – scientific guidance, writing and revision of the text, correction of conclusions.
A. A. Akulinkin – conducting physicochemical analysis, data processing.

К. А. Болгару – научное руководство, формирование целей и задач, написание статьи, доработка текста, корректировка выводов.
А. А. Регер – написание статьи, проведение синтеза, анализ полученных данных, визуализация.
В. И. Верещагин – научное руководство, написание статьи, доработка текста, корректировка выводов.
А. А. Акулинкин – проведение физико-химических анализов, обработка данных.

Received 13.10.2023
Revised 13.11.2023
Accepted 28.03.2024

Поступила в редакцию 13.10.2023
После доработки 13.11.2023
Принята к публикации 28.03.2024

INNOVATION IN METALLURGICAL INDUSTRIAL AND LABORATORY EQUIPMENT, TECHNOLOGIES AND MATERIALS

ИННОВАЦИИ В МЕТАЛЛУРГИЧЕСКОМ ПРОМЫШЛЕННОМ И ЛАБОРАТОРНОМ ОБОРУДОВАНИИ, ТЕХНОЛОГИЯХ И МАТЕРИАЛАХ

UDC 621.771.25
DOI 10.17073/0368-0797-2024-3-366-368

Short Report
Краткое сообщение

Determination of longitudinal stability of strip in rolling cage – non-drive dividing device system

A. R. Fastykovskii ✉, **V. A. Vakhrolomeev, A. G. Nikitin**

Siberian State Industrial University (42 Kirova Str., Novokuznetsk, Kemerovo Region – Kuzbass 654007, Russian Federation)

✉ omd@sibsiu.ru

Abstract. In modern industrial and civil construction, various rolled metal products are used in greater volumes. The largest share of them is occupied by rebar profiles produced at small-grade mills. The ever-growing demand for rebar rolling requires an increase in production volumes. The most promising technology in this regard is rolling – separation, which, with relatively low material costs, allows operating rolling mills to significantly increase the production volume of rebar profiles while reducing energy consumption. However, despite the obvious advantages of rolling – separation technology using non-drive dividing devices, it is very difficult to correctly determine the rational modes of conducting the process taking into account the peculiarities of production and equipment layout, which is due to insufficient theoretical knowledge. One of the main problems is determination of the permissible distance in the rolling cage – non-drive dividing device system. The conducted studies allowed us to propose a dependence for determining the maximum permissible distance in the rolling cage – non-drive dividing device system for reasons of longitudinal stability of the strip, taking into account the size and shape of cross-section of the split articulated profile, the nature of pinching, and the backstretch stress. It was experimentally established that when determining the permissible distance between rolling cage and non-drive dividing device, it is advisable to take the length reduction coefficient equal to 0.7.

Keywords: reinforcing profiles, rolling – separation, stability condition, permissible distance, length reduction coefficient

For citation: Fastykovskii A.R., Vakhrolomeev V.A., Nikitin A.G. Determination of longitudinal stability of strip in rolling cage – non-drive dividing device system. *Izvestiya. Ferrous Metallurgy*. 2024;67(3):366–368. https://doi.org/10.17073/0368-0797-2024-3-366-368

Определение продольной устойчивости полосы в системе прокатная клеть – неприводное делительное устройство

А. Р. Фастыковский ✉, **В. А. Вахроломеев, А. Г. Никитин**

Сибирский государственный индустриальный университет (Россия, 654007, Кемеровская область – Кузбасс, Новокузнецк, ул. Кирова, 42)

✉ omd@sibsiu.ru

Аннотация. В современном промышленном и гражданском строительстве в больших объемах используется различный металлопрокат, наибольшую долю в котором занимают арматурные профили, производимые на мелкосортных станах. Постоянно растущая потребность в арматурном прокате требует повышения объемов производства. Наиболее перспективна в этом плане технология прокатки – разделения, которая при относительно небольших материальных затратах позволяет на действующих прокатных станах существенно повысить объем производства арматурных профилей при снижении энергозатрат. Однако, несмотря на очевидные преимущества технологии прокатки – разделения с использованием неприводных делительных устройств, большие затруднения вызывает правильное определение рациональных режимов ведения процесса с учетом особенностей производства и компоновки оборудования, что связано с недостаточной теоретической изученностью. Одной из основных проблем является определение допустимого расстояния в системе прокатная клеть – неприводное делительное устройство. Проведенные исследования позволили предложить зависимость для определения максимально допустимого расстояния в системе прокатная клеть – неприводное делительное устройство из соображений продольной устойчивости полосы с учетом размера и формы поперечного сечения разделяемого сочлененного профиля, характера защемления, напряжения подпора. Экспериментально установлено, что при определении допустимого расстояния между прокатной клетью и неприводным делительным устройством коэффициент приведения длины целесообразно принимать равным 0,7.

Ключевые слова: арматурные профили, прокатка – разделение, условие устойчивости, допустимое расстояние, коэффициент приведения длины

Для цитирования: Фастыковский А.Р., Вахроломеев В.А., Никитин А.Г. Определение продольной устойчивости полосы в системе прокатная клеть – неприводное делительное устройство. *Известия вузов. Черная металлургия*. 2024;67(3):366–368.
https://doi.org/10.17073/0368-0797-2024-3-366-368

Modern realities are characterized by the active growth in industrial and civil construction. Advanced construction technologies increasingly rely on the use of prefabricated structures made of reinforced concrete and metal products [1 – 3]. The constantly rising demand for construction metal products necessitates solutions that offer a short payback period, low costs for production re-equipment, and a significant increase in productivity. The rolling – separation technology meets all these requirements [4; 5]. Currently, the rolling – separation technology is developing in two directions, distinguished by where the longitudinal dividing occurs: either within the rolls of the rolling mill, which simultaneously forms and divides the articulated profile, or in a separate stand-alone non-driven dividing device. On most modern rolling mills, the second method is preferred, as separating the operations of forming the articulated profile and subsequent longitudinal separation in a separate stand-alone non-driven device significantly simplifies equipment setup [6 – 9]. However, this arrangement can lead to a potential loss of natural longitudinal stability if the distance between the rolling mill and the non-driven dividing device is chosen incorrectly. Currently, this issue is addressed through trial and error, which results in increased defective products and unforeseen downtime of the primary rolling equipment.

The use of 3D simulation methods does not allow for the assessment of the permissible distance that ensures natural longitudinal stability [10]. To evaluate the risk of losing longitudinal stability of the strip and to determine the critical distance between the rolling mill and the non-driven dividing device, a dependency obtained using the well-known Euler's formula [11] is proposed:

$$l_{max} = \frac{\pi\sqrt{Ei^2_{min}}}{\sqrt{\sigma_2 k}} \text{ at } \frac{\sigma_2}{\sigma_s} \le 1,$$

where l_{max} is the maximum permissible distance between the rolling mill, which forms the articulated profile, and the non-driven dividing device, ensuring longitudinal stability; E is the modulus of elasticity of the first kind, MPa; k is the coefficient of length reduction; i_{min} is the minimum radius of the section inertia; σ_2 is the support stress necessary for longitudinal division by the non-driven dividing device; σ_s is the resistance to deformation of the material being divided.

As can be seen from the presented dependency, the magnitude of the maximum permissible distance depends on the support stress necessary for longitudinal separation, the shape, and the area of the cross-section of the articulated profile, which are characterized by the minimum radius of inertia, the modulus of elasticity of the first kind, and the coefficient of length reduction. Among the factors considered, the coefficient of length reduction has a significant impact, varying from 0.5 to 2.0 depending on the nature of the clamping [11].

To determine the coefficient of length reduction during the implementation of the rolling – separation process, laboratory experiments were conducted. These experiments compared the critical force corresponding to the moment of loss of stability, obtained both theoretically using Euler's equation and experimentally. The experimental and theoretical data obtained with coefficients of length reduction of 0.5 and 0.7 are shown in the figure.

According to the obtained data, when determining the natural longitudinal stability of the strip in the rolling mill – non-driven dividing device system, a coefficient of length reduction equal to 0.7 is required to achieve values closer to the experimental data. With a coefficient of length reduction of 0.7, the calculated data are 10 – 15 % less than the experimental data. In practical use, this provides a margin of safety when determining the permissible distance in the rolling mill–non-driven dividing device system.

Conclusions

A dependency has been derived that enables the estimation of the maximum permissible distance between the rolling mill stand and the non-driven dividing device,

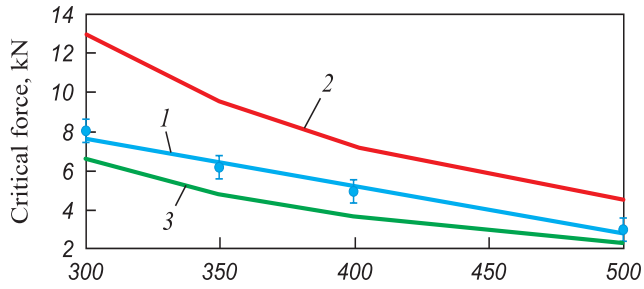

Dependence of critical force on the distance between the source of deformation and the place of pinching:
1 – experimental results; *2* and *3* – calculated values according to the Euler formula with a length reduction coefficient of 0.5 and 0.7

Зависимость критической силы от расстояния между очагом деформации и местом защемления:
1 – экспериментальные результаты; *2* и *3* – расчетные значения по формуле Эйлера при коэффициенте приведения длины 0,5 и 0,7

ensuring the longitudinal stability of the strip during the implementation of the rolling–separation technology. Experimentally, it has been established that the length conversion coefficient for the rolling–separation technology using a non-driven dividing device should reasonably be taken as 0.7.

References / Список литературы

1. You Y.-J., Park Y.-H., Kim H.-Y., Park J.-S. Hybrid effect on tensile properties of FRP rods with various material compositions. *Composite Structures*. 2007;80(1):117–122. https://doi.org/10.1016/j.compstruct.2006.04.065
2. Liu J., Wang F., Zhou H., Wang E., Cao P. Study on shear strength of glass fiber-reinforced polymer (GFRP) rebar concrete piles with circular cross-sections. *China Civil Engineering Journal*. 2016;(9):103–109.
3. Yazdanbakhsh A., Bank L.C., Chen C. Use of recycled FRP reinforcing bar in concrete as coarse aggregate and its impact on the mechanical properties of concrete. *Construction and Building Materials*. 2016;121(6):278–284. https://doi.org/10.1016/j.conbuildmat.2016.05.165
4. Danchenko V., Dyja H., Lesik L., Mashkin L., Milenin A. Technologia i modelowanie procesów walcowania w wykrojach. In: *Politechnika Częstochowska, Prace Dydaktyczne Wydziału Inżynierii Procesowej, Materiałowej i Fizyki Stosowanej, Seria: Metalurgia*. 2002;(28):326-328:417–418.
5. Michałowski M., Turczyn S., Nowakowski A. Analiza płynięcia metalu w wykrojach rozcinających stosowanych do walcowania prętów żebrowanych. *Hutnik – Wiadomości Hutnicze*. 2002;69(8-9):342–345.
6. Efimov O.Yu., Chinokalov V.Ya., Fastykovskii A.R., Kopylov I.V. Use of rolling–separation technology at mill 250-1. *Stal'*. 2008;(4):78–80.

   Ефимов О.Ю., Чинокалов В.Я., Фастыковский А.Р., Копылов И.В. Использование технологии прокатки – разделения на стане 250-1. *Сталь*. 2008;(4):78–80.
7. Fastykovskii A.R. On the issue of longitudinal strip separation by non-drive devices in the rolling mill flow. *Proizvodstvo prokata*. 2009;(3):4–9.

   Фастыковский А.Р. К вопросу продольного разделения полосы неприводными устройствами в потоке прокатного стана. *Производство проката*. 2009;(3):4–9.
8. Matsuo G., Suzuki M. The latest technology of multi – slit rolling. *SEAISI Quaterly*. 1995(3):49–58.
9. Slednev V.P. Paired Rolling of Section Profiles. Moscow: Metallurgiya; 1988;167.

   Следнев В.П. Спаренная прокатка сортовых профилей. Москва: Металлургия; 1988;167.
10. Wisselink H.H., Huetink J. 3D FEM simulation of stationary metal forming processes with applications to slitting and rolling. *Journal of Materials Processing Technology*. 2004;148(3):328–341. https://doi.org/10.1016/j.jmatprotec.2004.02.036
11. Astanin V.G. Resistance of Materials. Moscow: Yurait; 2023;438.

    Атанин В.Г. Сопротивление материалов. Москва: Изд-во Юрайт; 2023;438.

Information about the Authors / Сведения об авторах

Andrei R. Fastykovskii, *Dr. Sci. (Eng.), Prof. of the Chair "Metal Forming and Metal Science. OJSC "EVRAZ ZSMK",* Siberian State Industrial University
ORCID: 0000-0001-9259-9038
E-mail: omd@sibsiu.ru

Vladimir A. Vakhrolomeev, *Postgraduate of the Chair "Metal Forming and Metal Science. OJSC "EVRAZ ZSMK",* Siberian State Industrial University
E-mail: wladimir170581@mail.ru

Aleksandr G. Nikitin, *Dr. Sci. (Tech.), Professor of the Chair of Mechanics and Machine Engineering,* Siberian State Industrial University
ORCID: 0000-0001-9198-6386
E-mail: nikitin1601@yandex.ru

Андрей Ростиславович Фастыковский, *д.т.н., профессор кафедры «Обработка металлов давлением и материаловедения. ЕВРАЗ ЗСМК»,* Сибирский государственный индустриальный университет
ORCID: 0000-0001-9259-9038
E-mail: omd@sibsiu.ru

Владимир Анатольевич Вахроломеев, *аспирант кафедры «Обработка металлов давлением и материаловедения. ЕВРАЗ ЗСМК»,* Сибирский государственный индустриальный университет
E-mail: wladimir170581@mail.ru

Александр Григорьевич Никитин, *д.т.н., профессор кафедры механики и машиностроения,* Сибирский государственный индустриальный университет
ORCID: 0000-0001-9198-6386
E-mail: nikitin1601@yandex.ru

Contribution of the Authors / Вклад авторов

A. R. Fastykovskii – formation of the basic concept, formulation of conclusions, scientific guidance.
V. A. Vakhrolomeev – performing the experiments, writing the text.

A. G. Nikitin – revision of the text, correction of conclusions, discussion of the experiments.

А. Р. Фастыковский – формирование основной концепции, формулирование выводов, научное руководство.
В. А. Вахроломеев – выполнение экспериментальной части работы, написание текста.
А. Г. Никитин – доработка текста, корректировка выводов, обсуждение экспериментальной части.

Received 27.12.2023
Revised 15.01.2024
Accepted 16.01.2024

Поступила в редакцию 27.12.2023
После доработки 15.01.2024
Принята к публикации 16.01.2024

UDC 621.78.013
DOI 10.17073/0368-0797-2024-3-369-376

Original article
Оригинальная статья

Mathematical modeling of slab heating in a furnace with walking beams due to their curvature

A. V. Vargin ✉, **I. A. Levitskii**

National University of Science and Technology "MISIS" (4 Leninskii Ave., Moscow 119049, Russian Federation)

✉ mr.vargin@yandex.ru

Abstract. Slab heating before hot rolling process is necessary for obtaining required metal ductility. The most effective for this purpose are furnaces with walking beams that provide heat supply to all sides of the slab. However, the places of slabs lower surfaces, contacting with water-cooled beams, are shielded from the radiation of the furnace lower heating zones and give the heat to the beams. Previously, the authors developed and programmatically implemented a mathematical model of slab heating in a furnace with walking beams, based on the numerical solution by finite difference method of the three-dimensional heat conduction problem with piecewise defined boundary conditions on the slab bottom surface. In this model, for the open zones of the slab bottom surface, boundary conditions were similar to those on the top surface, and for the zones of contact with the beams were set effective boundary conditions assuming duration of this contact. In this paper, the model was modified to take into account the curvature of the beams and to recalculate the configuration of zones with different boundary conditions on the slab bottom surface for each position of the slab along the furnace. By variant calculations at different values of heat transfer intensity from the slab bottom surfaces to the beams it was determined that curvature of a single beam can significantly change the characteristic of the corresponding "cold" spot, but it practically does not affect the general characteristic of the slab heating non-uniformity. If all fixed beams are subjected to curvature, the final temperature difference across the slab is significantly reduced due to an increase in its minimum temperature. It was found that the influence of beam curvature on the temperature field at the end of heating process is higher the more intensive the heat transfer to the beams is.

Keywords: mathematical modeling, slab heating, furnace with walking beams, curvature of beams

For citation: Vargin A.V., Levitskii I.A. Mathematical modeling of slab heating in a furnace with walking beams due to their curvature. *Izvestiya. Ferrous Metallurgy*. 2024;67(3):369–376. https://doi.org/10.17073/0368-0797-2024-3-369-376

Математическое моделирование нагрева сляба в печи с шагающими балками с учетом их кривизны

А. В. Варгин ✉, **И. А. Левицкий**

Национальный исследовательский технологический университет «МИСИС» (Россия, 119049, Москва, Ленинский пр., 4)

✉ mr.vargin@yandex.ru

Аннотация. Нагрев слябов перед горячей прокаткой необходим для придания металлу требуемых пластических свойств. Наиболее эффективны для этого печи с шагающими балками, обеспечивающие подачу теплоты со всех сторон сляба. Однако области нижних поверхностей слябов, контактирующие с водоохлаждаемыми балками, экранированы от излучения нижних зон обогрева печи и отдают теплоту балкам. Ранее авторами была разработана и программно реализована математическая модель нагрева сляба в печи с шагающими балками, основанная на численном решении методом конечных разностей трехмерной задачи теплопроводности с кусочно-определенными граничными условиями на нижней поверхности сляба. В этой модели для открытых областей нижней поверхности сляба задавались граничные условия, аналогичные условиям на верхней поверхности, а для областей контакта с балками – эффективные граничные условия, учитывающие продолжительность этого контакта. В данной работе модель нагрева сляба модифицирована, она позволяет учитывать кривизну балок и пересчитывать конфигурацию областей с различными граничными условиями на нижней поверхности сляба для каждого положения его вдоль печи. Вариантными расчетами при различных значениях интенсивности теплоотвода от нижних поверхностей сляба к балкам получено, что искривление одиночной балки может существенно изменить характеристику соответствующего «холодного» пятна,

но оно практически не влияет на общую характеристику неравномерности нагрева сляба. Однако если искривлению подвергнуть все неподвижные балки, то существенно сокращается итоговый перепад по слябу вследствие увеличения его минимальной температуры. Установлено, что влияние кривизны балок на температурное поле в конце нагрева тем больше, чем интенсивнее теплоотвод к балкам.

Ключевые слова: математическое моделирование, нагрев сляба, печь с шагающими балками, кривизна балок

Для цитирования: Варгин А.В., Левицкий И.А. Математическое моделирование нагрева сляба в печи с шагающими балками с учетом их кривизны. *Известия вузов. Черная металлургия*. 2024;67(3):369–376. https://doi.org/10.17073/0368-0797-2024-3-369-376

Introduction

The furnaces with walking beams, which provide a comprehensive heat supply to the slab surfaces, are considered to be the most advanced units used for heating slabs before rolling in the hot-rolled sheet production [1]. Usually such a scheme of heat supply is called four-sided because (as confirmed by experience and calculations) heat supply to the end surfaces of slabs affects the temperature field of nothing but small sections of slabs adjacent to these surfaces, and the length of slabs in sheet rolling is many times greater than their other dimensions. However, although these furnaces have a lower heating zone, the conditions of heat supply to the upper and lower surfaces of the heated slabs are different. The slab transportation system includes fixed and movable beams, partially shielding the zones of the slab lower surface that are in contact with them from the combustion products of the lower heating zones, and also partially transferring heat to the elements of the beam cooling system in the places of contact.

As a result, "cold spots" emerge on the lower surface of slabs, the effect of which reaches out to the slabs upper surface, not only their inner horizontal sections. One of the ways to reduce the described inhomogeneity of the temperature field is to give some curvature to the fixed beams of the transportation system. However, no comprehensive quantity-related studies of this effect have been conducted.

Expensive modern equipment is required to explore the above-mentioned factors by experiment [2], which is not easy in industrial conditions. Therefore, an investigational study is usually conducted at the first stage of the research (to obtain primary information about the target of research) and at its last stage (to verify the recommendations made). The main part of the investigation is usually conducted by mathematical modeling of the processes occurring in the furnace working space. Different models of metal heating in the reheating furnaces [3] can be classified into statistical [4; 5], analytical [6] and numerical ones [7 – 10]. In rare cases, inverse heat conduction problems are addressed, along with direct ones [6; 11]. Optimization problems are also solved using mathematical models of furnace processes [11 – 15] that take advantage of modern CFD simulation software [16; 17].

The authors of [18] propose a two-dimensional model of slab heating in a pusher type furnace, the distinguishing feature of which is the joint solution of the heat conduction problem for the slab to be heated and for the section of the support tube (water-cooled skid). However, in this model, the tube is directed along the slab, so (given that the model is two-dimensional) the length of the "cold spot" can only be traced in the direction of the slab width.

The authors of [19] propose a three-dimensional model of slab heating in a furnace with time-varying boundary conditions simulating slab passage through different process zones of a pusher-type furnace. The peculiarity of this model is the possibility to set piecewise defined boundary conditions on the slab bottom surface, these conditions being different for the areas of this surface contact with beams and open areas of the slab bottom surface.

The purpose of this work is to further develop the mathematical model of slab heating in a furnace with walking beams (taking into account the impact of these beams on the heating process), considering the influence of the possible curvature of the transportation system beams on the slab temperature, and the use of this model for numerical experiments.

Research methods

The developed model is a three-dimensional trasient heat conduction problem in the Cartesian coordinate system for a parallelepiped-shaped computational domain without internal heat sources, with temperature-dependent thermophysical characteristics and asymmetric time-varying boundary conditions of the third kind [19].

This differential problem has no analytical solution; therefore, it has to be solved numerically, using the finite difference method (balance method) [7; 19; 20].

This method involves the introduction of discrete time $t_k = k\Delta t$ ($k = 1, 2, ...$) with a constant step Δt and discrete coordinates: $x_i = i\Delta x$ ($i = 0, 1, 2, ..., n_x$); $y_j = j\Delta y$ ($j = 0, 1, 2, ..., n_y$); $z_l = l\Delta z$ ($l = 0, 1, 2, ..., n_z$), which for this simple geometry also change with constant steps Δx, Δy and Δz. The values n_x, n_y and n_z are called the number of workpiece divisions along each of the coordinate directions.

As the computational grid is introduced, the entire calculation domain is divided into elementary volumes,

the number of which is equal to $(n_x + 1)(n_y + 1)(n_z + 1)$. Each of these volumes contains one node of the spatial grid determined by three indexes (i, j, l). At each time step, the elementary heat balance equations are recorded for each elementary volume, forming a quasi-linear system of equations with respect to the nodal temperature values at the end of the time step. The general solution methods are inadvisable in this case (due to the sparsity structure of the coefficient matrix), therefore iterative methods are more effective [19; 20], as they enable to discard huge auxiliary matrices.

We chose boundary conditions of the third kind in the model due to their stabilizing influence on the convergence of the iterative algorithm used for solving the three-dimensional heat conduction problem.

In accordance with these boundary conditions, the relationship between the heat flux density q_w on the boundary surface (e.g., on the slab top surface) and its temperature T_w is described by the Newton-Richman formula:

$$q_w = \alpha(T_0 - T_w), \quad (1)$$

where T_0 is the temperature of the heating medium, K; α is the heat transfer coefficient, W/(m^2·K).

The thermal influence of the transportation system beams on the thermal conditions on the slab bottom surface is taken into account by dividing the slab bottom surface into rectangular areas and setting different boundary conditions for these areas. These rectangular areas can be of three types with respect to the problem under consideration:

– always open parts of the surface;

– parts of the surface in contact with fixed beams;

– parts of the surface in contact with movable beams (when the slab is lifted or moved).

For always open areas of the lower surface, the boundary conditions are similar to those on the slab upper surface (1), the only difference is that the values of the heating medium temperature and heat transfer coefficient may not be the same. For the remaining areas, this condition is true only when there is no contact with the beams. However, during the periods of contact with the beams, an expression like (1) can also be formally used for the corresponding areas. In this case, the temperature of the steam-water mixture circulating in the beam cooling system should be used as the medium temperature, and some conditional coefficient of heat transfer k, W/(m^2·K), from the corresponding area of the slab bottom surface to this cooling medium, should be used as the heat transfer coefficient. The value of this coefficient depends on the design of the transportation system, and it is an external (set) parameter in this model [7; 19].

The slab transportation cycle consists of separate stages (slab lifting, forward movement, slab lowering, movable beams return operations). When their duration is known (as well as the time for slab removal from the furnace, the time for putting slabs along the furnace and the transportation system valve rod travel), one can set the boundary conditions for each zone of the slab bottom surface at any given time. However, this approach requires calculation with a time step of no more than 1 s, which can significantly increase the duration of the calculation procedure. In the present work, as in [19], a more time-saving approach is applied, according to which, for each contact zone, weighted average boundary conditions of the type (1) are set, with the effective heat transfer coefficient and the effective temperature of the medium. At the same time, the contribution to the effective values of the individual periods characteristics is proportional to their duration.

In [19], the division of the slab bottom surface into areas of different types does not change during the slab heating process, which corresponds to straight beams. A special feature of the present work is that the curvature of beams can be set by representing their centerline as a sinusoid for which the amplitude (mm) and period (m) are set. When the amplitude value is set to zero, the beams are considered straight. When the amplitude (curvature) is set different from zero, the slab longitudinal coordinate relative to the furnace entrance section is calculated at each time step, and then the deviation of the boundaries of intersection with the slab relative to the initial value is calculated for each beam (movable and fixed). This modified slab-beam contact zone is still considered rectangular (due to the relatively small curvature and width of the beam), but its boundaries along the slab are shifted, and the algorithm proposed in this paper adjusts these boundaries at each computational time step.

The created mathematical model is implemented in the visual development environment Builder C++ version 6.0. Fig. 1 shows the start window of the calculation program, in which the curvature characteristics in the form of sinusoid amplitude and its period (default values shown in Fig. 1 correspond to straight beams) can be set for all beams (in addition to their position, width, coefficient of heat transfer to the cooling medium and temperature of this medium).

In the “Mode” tab (in Fig. 1 it is closed), the values of the heating medium temperature and heat transfer coefficients on each slab face by heating stages are set for the corresponding technological zones. As mentioned above, these values for all slab faces are used directly, and at the bottom face, they are applied unchanged to the open zones only, while for the beam contact zones, these values are used to calculate the effective heat transfer coefficients and the effective medium temperature.

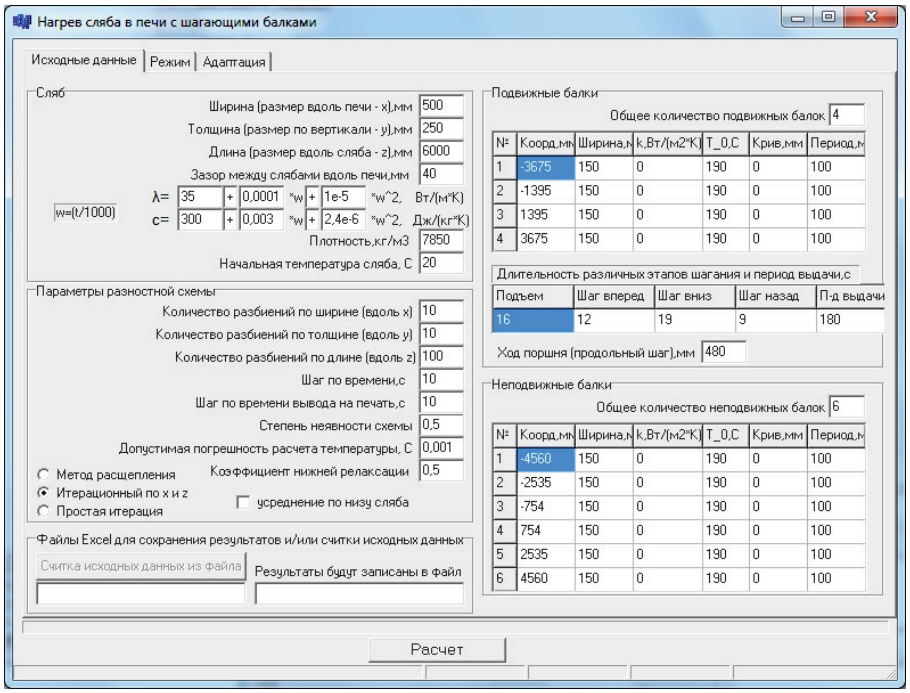

Fig. 1. Input data for modeling

Рис. 1. Исходные данные для моделирования

Research results

Fig. 2 shows the temperature variation along the longitudinal axis of the slab bottom surface, with dimensions 250×500×6000 mm, heated in a furnace equipped with four fixed (axes are indicated by a green line) and two movable (axes are indicated by a blue line) beams. The results are obtained for three values of intensity of heat transfer to the beams:

– k = 0 W/(m^2·K), corresponds to the case when the shielding effect of beams only is taken into account;

– k = 100 W/(m^2·K), approximately corresponds to the actual rider designs;

– k = 50 W/(m^2·K), corresponds to intermediate values.

For the next series of calculations, the curvature of one of the fixed beams was modeled according to Fig. 3. The curvature was described by a sinusoid with an amplitude of 200 mm and a period of 5 m (the curvature parameters corresponded to the maximum practically feasible values). Fig. 4 shows the results of slab heating simulation under these conditions.

In the case of zero heat transfer intensity (Fig. 4, *a*), the influence of beam curvature is practically imperceptible. However, as the intensity of heat transfer to the beams increases, the temperature profile becomes noticeably asymmetrical (Fig. 4, *b* compared to Fig. 2, *b* and Fig. 4, *c* compared to Fig. 2, *c*).

At the same time, the overall heating characteristics will remain essentially the same as for heating straight

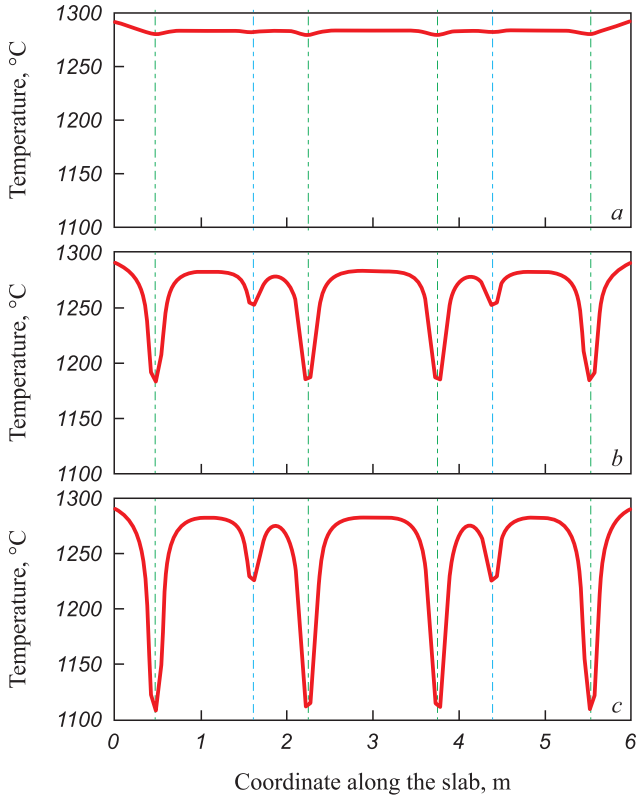

Fig. 2. Temperature change along longitudinal axis of the slab lower surface at different intensity of heat transfer to the beams: *a* – k = 0 W/(m^2·K); *b* – k = 50 W/(m^2·K); *c* – k = 100 W/(m^2·K)

Рис. 2. Изменение температуры вдоль продольной оси нижней поверхности сляба при различной интенсивности теплоотвода к балкам:
a – k = 0 Вт/(м^2·К); *b* – k = 50 Вт/(м^2·К); *c* – k = 100 Вт/(м^2·К)

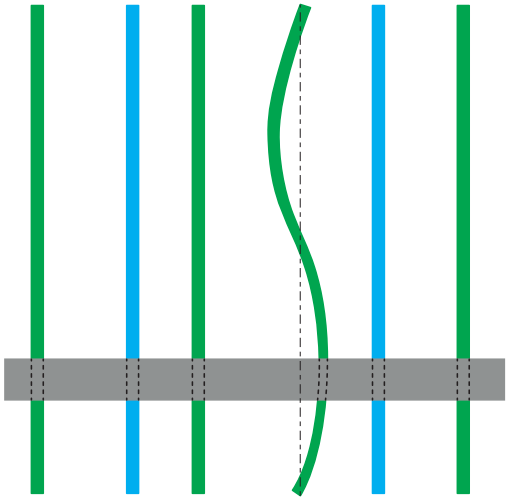

Fig. 3. Layout of the slab in relation to the furnace beams when one fixed beam is curved:
– fixed beams; – movable beams; – slab

Рис. 3. Схема расположения сляба относительно балок печи при искривлении одной неподвижной балки:
– неподвижные балки; – подвижные балки; – сляб

beams (see the Table). In the Table, the "minimum" and "maximum" columns contain the minimum and maximum temperature values throughout the slab at the end of the heating cycle, the "difference" column presents the difference between them, and the "average" column indicates the slab bulk temperature at the end of the heating cycle.

Fig. 5 shows the temperature profile along the longitudinal axis of the slab bottom surface for the case when all fixed beams are curved.

DISCUSSION OF THE RESEARCH RESULTS

The results obtained revealed that for fixed beams the "spot" of impact is deeper (i.e. "cooler") than for movable beams. This is because at given values of the slab width, removal period and transportation mechanism

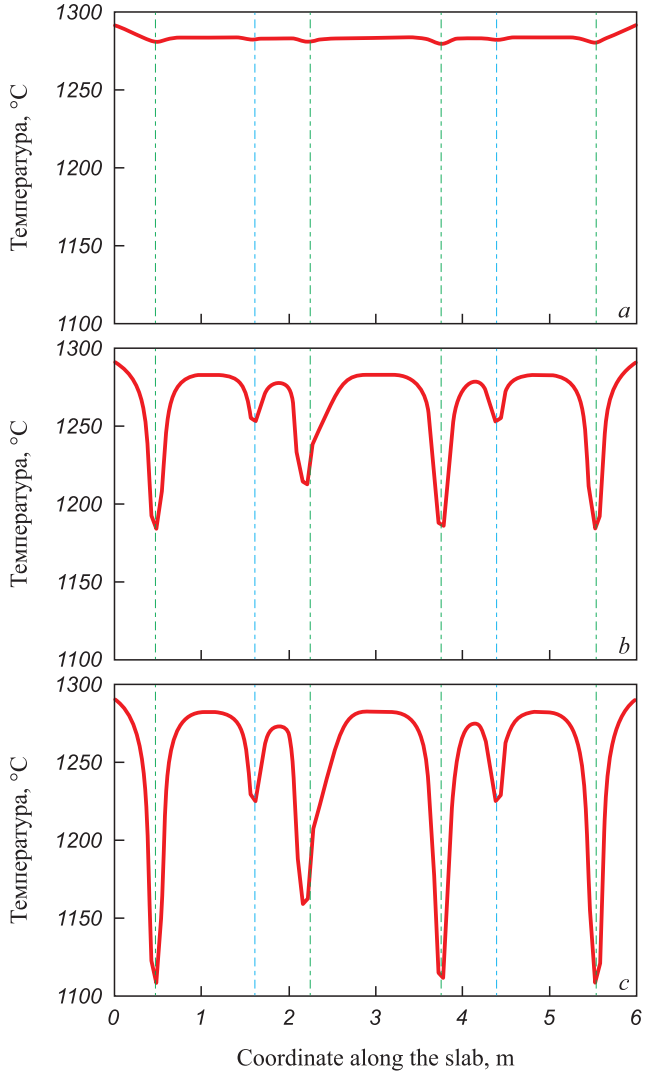

Fig. 4. Temperature change along longitudinal axis of the slab lower surface at different intensity of heat transfer to the beams when one beam is curved:
a – k = 0 W/(m^2·K); *b* – k = 50 W/(m^2·K); *c* – k = 100 W/(m^2·K)

Рис. 4. Изменение температуры вдоль продольной оси нижней поверхности сляба при различной интенсивности теплоотвода к балкам при искривлении одной из балок:
a – k = 0 Вт/(м^2·K); *b* – k = 50 Вт/(м^2·K); *c* – k = 100 Вт/(м^2·K)

Extreme values of the final slab temperature for different variants

Экстремальные значения конечной температуры сляба для различных вариантов

Variant description	k, W/(m^2·K)	Temperature index, °C			
		minimum	average	maximum	difference
Straight beams	0	1278.1	1286.0	1292.0	14.3
Straight beams	50	1183.0	1278.8	1291.5	108.5
Straight beams	100	1107.3	1273.3	1291.0	184.0
One beam is curved	0	1277.7	1286.0	1292.0	14.3
One beam is curved	50	1183.0	1278.9	1291.5	108.5
One beam is curved	100	1107.3	1273.3	1291.3	184.0
All the fixed beams are curved	100	1152.6	1273.5	1291.2	138.6

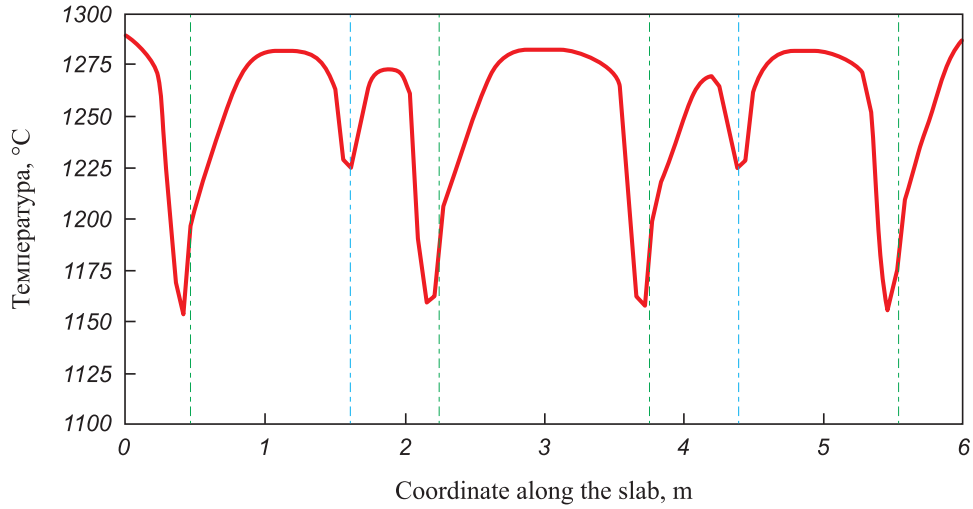

Fig. 5. Temperature change along longitudinal axis of the slab lower surface at k = 100 W/(m^2·K) when all fixed beams are curved

Рис. 5. Изменение температуры вдоль продольной оси нижней поверхности сляба при k = 100 Вт/(м^2·К) при искривлении всех неподвижных балок

parameters, the contact time of slab bottom surface areas with fixed beams is longer than with movable beams.

Fig. 2 shows that when heat is transferred from the slabs to the beams, the lower surface temperature is much more inhomogeneous than when this surface is just shielded from the radiation of the lower heating zones combustion products. The curvature of a single beam can significantly change the characteristic of the corresponding "cold" spot, and this effect enhances as the heat transfer to the beams increases (Fig. 4, *b*, *c*). However, it has little or no effect on the general characteristic of the slab heating non-uniformity (see the Table), as when the beam curves, the slab surface contact area does not change, but only takes more time. However, if all fixed beams are subjected to curvature, the final difference across the slab is significantly reduced due to an increase in its minimum temperature, which leads to enhanced homogeneity of the slab temperature field.

Conclusions

The mathematical model of slab heating in a furnace with walking beams, earlier developed and programmatically implemented by the authors, that took into account the impact of these beams on the slab bottom surface, was modified by adding the possibility of considering the curvature of the beams.

We simulated heating of a 250×500×6000 mm slab for a furnace equipped with four fixed and two movable beams under standard mode with different intensity of heat transfer to the beams (the beams being straight or curved).

It is found that the intensity of heat transfer to the beams significantly affects both the level of the slab temperature field and its homogeneity.

The variant calculations showed that the curvature of only one beam changes the local characteristics of the corresponding "cold" spot, practically not affecting the minimum, maximum and bulk values of the slab temperature, while the curvature of all beams (of at least one type) increases the minimum slab temperature and homogeneity of the slab temperature field as a whole. Moreover, the more intensive the heat transfer to the beams is, the higher the impact of the beam curvature on the temperature field at the end of heating (in particular, on its homogeneity).

References / Список литературы

1. Gusovskшш V.L., Lifshits A.E. Methods of Calculation of Heating and Thermal Furnaces: Training and Reference Book. Moscow: Teplotechnik; 2004:400. (In Russ.).

   Гусовский В.Л., Лифшиц А.Е. Методики расчета нагревательных и термических печей: Учебно-справочное издание. Москва: Теплотехник; 2004:400.
2. Ulanovskii A.A., Taake M., Belen'kii A.M., Bursin A.N., Chibizova S.I. Using a Phoenix TM autonomous automated system for monitoring temperature field of metal heated in metallurgical furnaces. *Chernye Metally*. 2019;(9):54–60. (In Russ.).

   Улановский А.А., Тааке М., Беленький А.М., Бурсин А.Н., Чибизова С.И. Использование автономной автоматизированной системы фирмы Phoenix TM для мониторинга температурного поля нагреваемого металла в металлургических печах. *Черные металлы*. 2019;(9):54–60.
3. Singh V.K., Talukdar P. Comparisons of different heat transfer models of a walking beam type reheat furnace. *International Communications in Heat and Mass Transfer*. 2013; 47:20–26.
   https://doi.org/10.1016/j.icheatmasstransfer.2013.06.004

4. Belen'kii A.M., Bogatova M.Zh., Chibizova S.I. Statistical modeling of metal heating in furnaces with walking beams. *Chernye Metally*. 2021;(8):32–37. (In Russ.). https://doi.org/10.17580/chm.2021.08.06

Беленький А.М., Богатова М.Ж., Чибизова С.И. Статическое моделирование нагрева металла в печах с шагающими балками. *Черные металлы*. 2021;(8):32–37. https://doi.org/10.17580/chm.2021.08.06

5. Bogatova M.Zh., Chibizova S.I. Statistical modeling of temperature operating modes of heating furnaces for hot strip mills. *Izvestiya. Ferrous Metallurgy*. 2021;64(5):374–381. (In Russ.). https://doi.org/10.17073/0368-0797-2021-5-374-381

Богатова М.Ж., Чибизова С.И. Статистическое моделирование температурных режимов работы нагревательных печей листовых станов горячей прокатки. *Известия вузов. Черная металлургия*. 2021;64(5):374–381. https://doi.org/10.17073/0368-0797-2021-5-374-381

6. Levitskii I.A. The linear heat conduction problem for bodies with a regular shape under boundary conditions of the third kind. *Chernye Metally*. 2019;(10):67–72. (In Russ.).

Левицкий И.А. Линейная задача теплопроводности для тел правильной формы при граничных условиях третьего рода. *Черные металлы*. 2019;(10):67–72.

7. Abdukodirov I.B. Mathematical model of slab heating in a furnace with walking beams: Mag. Diss. Moscow; 2020:68. (In Russ.).

Абдукодиров И.Б. Математическая модель нагрева сляба в печи с шагающими балками: Диссертация магистра: 22.04.02: Москва; 2020:68.

8. Han S.H., Chang D., Kim C.Y. A numerical analysis of slab heating characteristics in a walking beam type reheating furnace. *International Journal of Heat and Mass Transfer*. 2010;53(19–20):3855–3861. https://doi.org/10.1016/j.ijheatmasstransfer.2010.05.002

9. Kurnosov V.V., Levitskii I.A., Pribytkov I.A. Massive billets different rates heating in batch furnaces study. *Izvestiya. Ferrous Metallurgy*. 2012;55(9):27–31. (In Russ.). https://doi.org/10.17073/0368-0797-2012-9-27-31

Курносов В.В., Левицкий И.А., Прибытков И.А. Исследование нагрева массивных заготовок с различными скоростями в печах периодического действия. *Известия вузов. Черная металлургия*. 2012;55(9):27–31. https://doi.org/10.17073/0368-0797-2012-9-27-31

10. Landfahrer M., Schluck C. Numerical and experimental investigation of scale formation on steel tubes in a real-size reheating furnace. *International Journal of Heat and Mass Transfer*. 2019;129:460–467. https://doi.org/10.1016/j.ijheatmasstransfer.2018.09.110

11. Kurnosov V.V., Levitskii I.A. Mathematic simulation of workpieces heating with variable thermal characteristics and thermal condition, corresponding to a given heating curve. *Izvestiya. Ferrous Metallurgy*. 2012;55(7):19–22. (In Russ.). https://doi.org/10.17073/0368-0797-2012-7-19-22

Курносов В.В., Левицкий И.А. Математическое моделирование нагрева заготовок с переменными теплофизическими характеристиками и теплового режима, соответствующего заданному графику нагрева. *Известия вузов. Черная металлургия*. 2012;55(7):19–22. https://doi.org/10.17073/0368-0797-2012-7-19-22

12. Jang J.-Y., Huang J.-B. Optimization of a slab heating pattern for minimum energy consumption in a walking-beam type reheating furnace. *Applied Thermal Engineering*. 2015;85:313–321. https://doi.org/10.1016/J.APPLTHERMALENG.2015.04.029

13. Tang G., Wu B., Bai D., Wang Y., Bodnar R., Zhou C.Q. Modeling of the slab heating process in a walking beam reheating furnace for process optimization. *International Journal of Heat and Mass Transfer*. 2017;113:1142–1151. https://doi.org/10.1016/j.ijheatmasstransfer.2017.06.026

14. Ding J.G., Kong L.P., Guo J.H., Song M.X., Jiao Z.J. Multi-objective optimization of slab heating process in walking beam reheating furnace based on particle swarm optimization algorithm. *Steel Research International*. 2021;92(3): 2000382. https://doi.org/10.1002/srin.202000382

15. Tang L., Liu J., Rong A., Yang Z. An effective heuristic algorithm to minimize stack shuffles in selecting steel slabs from the slab yard for heating and rolling. *Journal of the Operational Research Society*. 2001;52(10):1091–1097. https://doi.org/10.1057/palgrave.jors.2601143

16. Tang G., Wu B., Wang Y., Bodnar R., Zhou C. CFD modeling and validation of a dynamic slab heating process in an industrial walking beam reheating furnace. *Applied Thermal Engineering*. 2018;132:779–789. https://doi.org/10.1016/j.applthermaleng.2018.01.017

17. Mayr B., Prieler R., Demuth M., Moderer L., Hochenauer C. CFD analysis of a pusher type reheating furnace and the billet heating characteristic. *Applied Thermal Engineering*. 2017;115:986–994. https://doi.org/10.1016/j.applthermaleng.2017.01.028

18. Druzhinin G.M., Samoilovich Yu.A., Popov E.V. Ways to reduce the thermal heterogeneity of massive steel slabs by heating in through the heating furnaces. *Izvestiya. Ferrous Metallurgy*. 2013;56(7):27–32. (In Russ.). https://doi.org/10.17073/0368-0797-2013-7-27-32

Дружинин Г.М., Самойлович Ю.А., Попов Е.В. Способы снижения термической неоднородности массивных стальных слябов при нагреве в методических нагревательных печах. *Известия вузов. Черная металлургия*. 2013;56(7):27–32. https://doi.org/10.17073/0368-0797-2013-7-27-32

19. Abdukodirov I.B., Vargin A.V., Levitskii I.A. Simulation of slab heating in a walking beam furnace. *Izvestiya. Ferrous Metallurgy*. 2023;65(11):112–118. https://doi.org/10.17073/0368-0797-2023-1-112-118

Абдукодиров И.Б., Варгин А.В., Левицкий И.А. Математическая модель нагрева сляба в печи с шагающими балками. *Известия вузов. Черная металлургия*. 2023;66(1):112–118. https://doi.org/10.17073/0368-0797-2023-1-112-118

20. Arutyunov V.A., Bukhmirov V.V., Krupennikov S.A. Mathematical Modeling of Industrial Furnaces Thermal Operation. Moscow: Metallurgiya; 1990:239. (In Russ.).

Арутюнов В.А., Бухмиров В.В., Крупенников С.А. Математическое моделирование тепловой работы промышленных печей. Москва: Металлургия; 1990:239.

Сведения об авторах / Information about the Authors

Александр Вячеславович Варгин, *аспирант кафедры энергоэффективных и ресурсосберегающих промышленных технологий,* Национальный исследовательский технологический университет «МИСИС»
ORCID: 0000-0001-8657-8716
E-mail: mr.vargin@yandex.ru

Игорь Анисимович Левицкий, *к.т.н., доцент кафедры энергоэффективных и ресурсосберегающих промышленных технологий,* Национальный исследовательский технологический университет «МИСИС»
ORCID: 0000-0002-9345-3628
E-mail: lewwwis@mail.ru

Aleksandr V. Vargin, *Postgraduate of the Chair "Energy-Efficient and Resource-Saving Industrial Technologies",* National University of Science and Technology "MISIS"
ORCID: 0000-0001-8657-8716
E-mail: mr.vargin@yandex.ru

Igor' A. Levitskii, *Cand. Sci. (Eng.), Assist. Prof. of the Chair "Energy-Efficient and Resource-Saving Industrial Technologies",* National University of Science and Technology "MISIS"
ORCID: 0000-0002-9345-3628
E-mail: lewwwis@mail.ru

Поступила в редакцию 14.09.2023
После доработки 08.01.2024
Принята к публикации 28.02.2024

Received 14.09.2023
Revised 08.01.2024
Accepted 28.02.2024

Над номером работали:

Л.И. Леонтьев, *главный редактор*

Е.В. Протопопов, *заместитель главного редактора*

Е.А. Ивани, *ответственный секретарь*

Л.П. Бащенко, *заместитель ответственного секретаря*

Е.Ю. Потапова, *заместитель главного редактора по развитию*

О.А. Долицкая, *научный редактор*

Е.М. Запольская, *ведущий редактор*

А.О. Гашникова, *ведущий редактор*

В.В. Расенець, *верстка, иллюстрации*

Г.Ю. Острогорская, *менеджер по работе с клиентами*

Подписано в печать 20.06.2024. Формат 60×90 $^{1}/_{8}$. Бум. офсетная № 1.
Печать цифровая. Усл. печ. л. 15,25. Заказ 19999. Цена свободная.

Отпечатано в типографии Издательского Дома МИСИС.
119049, Москва, Ленинский пр-кт, д. 4, стр. 1.
Тел./факс: +7 (499) 236-76-17

Development and implementation of technological measures to extend the campaign of blast furnace No. 5 of PJSC Severstal

Energy saving model for related processes in steelmaking

Ways to improve the properties of high-entropy alloys Cantor CoCrFeNiMn and CoCrFeNiAl

Calculations of the phase composition of austenitic high-nitrogen welding wire and study of a welded joint made from it

Effect of heat treatment on structure of austenitic steel 07Cr25Ni13 obtained by WAAM

Grain boundary migration and mechanical properties altering in Fe – 10Ni – 20Cr alloy under irradiation

Nitrogen diffusion along the layer boundaries after nitriding of multilayer materials

Kinetics of deformation fronts during serrated Lüders deformation in α-iron at high temperature

Determination of hydrogen influence on microhardness and microstructure characteristics of aviation alloys

Problems of selection of corrosion-resistant steels and alloys in oil and gas industry for operating conditions

Thermodynamic modeling of interphase distribution of chromium and boron in slags of AOD reduction period

Physical and chemical processes during nitriding of chromium ferrosilicon by filtration combustion

Determination of longitudinal stability of strip in rolling cage – non-drive dividing device system

Mathematical modeling of slab heating in a furnace with walking beams due to their curvature

Зарегистрирован Федеральной службой по надзору в сфере связи, информационных технологий и массовых коммуникаций. Свидетельство о регистрации ПИ № ФС77-35456.

Подписной индекс 70383.